Topics in Current Chemistry 359

Pierangelo Metrangolo
Giuseppe Resnati *Editors*

Halogen Bonding II

Impact on Materials Chemistry and Life Sciences

Springer

359
Topics in Current Chemistry

Aims and Scope

The series Topics in Current Chemistry presents critical reviews of the present and future trends in modern chemical research. The scope of coverage includes all areas of chemical science including the interfaces with related disciplines such as biology, medicine and materials science.

The goal of each thematic volume is to give the non-specialist reader, whether at the university or in industry, a comprehensive overview of an area where new insights are emerging that are of interest to larger scientific audience.

Thus each review within the volume critically surveys one aspect of that topic and places it within the context of the volume as a whole. The most significant developments of the last 5 to 10 years should be presented. A description of the laboratory procedures involved is often useful to the reader. The coverage should not be exhaustive in data, but should rather be conceptual, concentrating on the methodological thinking that will allow the non-specialist reader to understand the information presented.

Discussion of possible future research directions in the area is welcome.

Review articles for the individual volumes are invited by the volume editors.

Readership: research chemists at universities or in industry, graduate students.

More information about this series at
http://www.springer.com/series/128

Pierangelo Metrangolo • Giuseppe Resnati
Editors

Halogen Bonding II

Impact on Materials Chemistry and Life Sciences

With contributions by

H. Ajani · A.-C.C. Carlsson · G. Cavallo · P. Deepa · M. Erdélyi · M. Fourmigué · M. Haukka · P. Hobza · S.M. Huber · W.J. Jin · M.H. Kolář · J. Lieffrig · P. Metrangolo · X. Pang · A. Pecina · A. Priimagi · G. Resnati · K. Rissanen · M. Saccone · S. Schindler · M.S. Taylor · A.X. Veiga

Springer

Editors
Pierangelo Metrangolo
Dipartimento di Chimica, Materiali
e Ingegneria Chimica "Giulio Natta"
Politecnico di Milano
Milano, Italy

Giuseppe Resnati
Dipartimento di Chimica, Materiali
e Ingegneria Chimica "Giulio Natta"
Politecnico di Milano
Milano, Italy

ISSN 0340-1022 ISSN 1436-5049 (electronic)
Topics in Current Chemistry
ISBN 978-3-319-15731-3 ISBN 978-3-319-15732-0 (eBook)
DOI 10.1007/978-3-319-15732-0

Library of Congress Control Number: 2007936673

Springer Cham Heidelberg New York Dordrecht London

Printed on acid-free paper

Springer International Publishing AG Switzerland is part of Springer Science+Business Media (www.springer.com)

Preface

Typically, halogen atoms in haloorganics are considered as sites of high electron density because of their high electronegativity. Consistent with this well-established understanding, it is commonly accepted that halogen atoms can form attractive interactions by functioning as an electron-donor site (nucleophilic site). In fact, halogen atoms can work as hydrogen-bond acceptors and some cases of these interactions were recognized as early as the 1920s [1–4]. Halogen atoms of halocarbons also function as an electron-donor site when interacting with other elements, e.g., when entering the first coordination sphere of alkali metal cations[1] or alkaline earth metal cations.

However, the electron density in covalently bound halogens is anisotropically distributed [5–7]. There is a region of higher electron density, which forms a negative belt orthogonal to the covalent bond involving the halogen atom, and a region of lower electron density, which generates a cap on the elongation of the covalent bond (the so-called σ-hole) where the electrostatic potential is frequently positive (mainly in the heavier halogens). (This description of the distribution of the electron density holds for halogen atoms forming one covalent bond. For a discussion of polyvalent halogens see [8, 9].) This region can form attractive interactions with electron-rich sites but the general ability of halogen atoms to function as the electron acceptor site (electrophilic site) in attractive interactions has been fully recognized only recently. In 2009 the International Union of Pure and Applied Chemistry (IUPAC) started a project aiming "to take a comprehensive look at intermolecular interactions involving halogens as electrophilic species and classify them" [10]. An IUPAC Recommendation defining these interactions as halogen bonds [11] was delivered in 2013 when the project was concluded: This definition

[1] A CSD search (CSD version 5.34, November 2012 plus one update, ConQuest version 1.15) for Y···X-C short contacts (Y=Li^+, Na^+, K^+, Rb^+, Cs^+ and X=Cl, Br, I) gave 140 hits and 296 counts, and revealed that the median value of the Y···X-C angle is 103.08° (only structures with Y···C > 3.0 Å were considered). Cations enter the most negative region of the halogen atom (i.e., the belt orthogonal to the X–C bond), thus confirming that the halogen atom is working as the nucleophile.

states that "A halogen bond occurs when there is evidence of a net attractive interaction between an electrophilic region associated with a halogen atom in a molecular entity and a nucleophilic region in another, or the same, molecular entity." The IUPAC definition categorizes unambiguously an interaction responsible for the formation of adducts described as early as 1814 but which had been overlooked for decades. It developed into a routinely used tool to direct self-assembly phenomena only after its effectiveness in crystal engineering was demonstrated in the mid-1990s [12].

More recently, the unique features of halogen bonding, such as directionality, tunable interaction strength, hydrophobicity, and large donor atom size, have contributed to the realization of a totally new class of functional materials based on halogen bonding.

The unique features of the halogen bond described above arise from the concerted action of polarization and dispersion energies as demonstrated by P. Hobza et al. in the first chapter of this book. In the second chapter, M. S. Taylor examines the interactions between anions and electron-deficient, covalently-bound halogens, which lead to the realization of powerful examples of selective and high-affinity anion receptors through halogen bonding, including implementations in polar, protic media. Studies in solution on the nature of the elusive halonium ions in three-center halogen-bonded complexes are reviewed by M. Erdélyi et al. in the third chapter, where they highlight that charged halogen-bonded complexes possess significant charge transfer characteristics. Halogen-bonded complexes involving halonium ions in the solid state are also the focus of the research described by K. Rissanen et al. in the fourth chapter of this book.

M. Fourmigué et al., instead, reviewed in the fifth chapter how to organize organic radicals in the solid state through halogen bonding in order to design new molecular magnets and conductors, while W. J. Jin et al. have reviewed in the sixth chapter the exploitation of halogen bonding and the heavy atom effect of halogen atoms to obtain powerful phosphorescent organic materials. M. Saccone et al. describe in the seventh chapter the construction of supramolecular azobenzene-containing materials formed by halogen bonding, which show superior performances compared to analogous hydrogen-bonded materials.

The last chapter by S. M. Huber et al. closes the second volume of this book with a survey of applications of halogen bonds in organic synthesis and organocatalysis.

Although halogen bond-based functional materials design is still in its infancy, we foresee a bright future for this field. We expect that materials designed based on halogen bonding could lead to new applications in, for example, biomimetics, optics/photonics, functional surfaces, and photoswitchable supramolecules.

Milan, Italy Pierangelo Metrangolo and Giuseppe Resnati

References

1. Hantzsch A (1915) Die Chromoisomerie der p-dioxy-terephthalsäure derivate als phenol-enol-isomerie. Chem Ber 48:797–816
2. Nakamoto K, Margoshes M, Rundle RE (1955) Stretching frequencies as a function of distances in hydrogen bonds. J Am Chem Soc 77:6480–6486
3. Schleyer PR, West R (1959) Comparison of covalently bonded electro-negative atoms as proton acceptor groups in hydrogen bonding. J Am Chem Soc 81:3164–3165
4. Metrangolo P, Resnati G (2013) Metal-bound halogen atoms in crystal engineering. Chem Commun 49:1783−1785
5. Metrangolo P, Resnati G (eds) (2008) Halogen bonding: fundamentals and applications. Structure and bonding series, vol. 126. Springer-Verlag, Berlin Heidelberg
6. Murray JS, Lane P, Politzer P (2009) Expansion of the σ-hole concept. J Mol Model 15:723–729
7. Politzer P, Murray JS, Clark T (2013) Halogen bonding and other σ-hole interactions: a perspective. Phys Chem Chem Phys 15:11178–11189
8. O'Hair RAJ, Williams CM, Clark T (2010) Neighboring group stabilization by sigma-holes. J Mol Model 16:559–565
9. Wang W (2011) Halogen bond involving hypervalent halogen: CSD search and theoretical study. J Phys Chem A 115:9294–9299
10. Project no. 2009-032-1-100. Categorizing halogen bonding and other noncovalent interactions involving halogen atoms. http://www.iupac.org/nc/home/projects/project-db/project-details.html?tx_wfqbe_pi1%5Bproject_nr%5D=2009-032-1-100; (2010) Chem Int 32(2):20–21
11. Desiraju GR, Ho PS, Kloo L, Legon AC, Marquardt R, Metrangolo P, Politzer P, Resnati G, Rissanen K (2013) Definition of the halogen bond (IUPAC Recommendations 2013). Pure Appl Chem 35:1711–1713
12. Metrangolo P, Resnati G (2001) Halogen bonding: a paradigm in supramolecular chemistry. Chem Eur J 7:2511–2519

Contents

Top Curr Chem (2015) 359: 1–26
DOI: 10.1007/128_2014_606

Published online: 20 March 2015

Characteristics of a σ-Hole and the Nature of a Halogen Bond

Michal H. Kolář, Palanisamy Deepa, Haresh Ajani, Adam Pecina, and Pavel Hobza

Abstract The nature of halogen bonding in 128 complexes was investigated using advanced quantum mechanical calculations. First, isolated halogen donors were studied and their σ-holes were described in terms of size and magnitude. Later, both partners in the complex were considered and their interaction was described in terms of DFT-SAPT decomposition. The whole set of complexes under study was split into two categories on the basis of their stabilisation energy. The first subset with 38 complexes possesses stabilisation energies in the range 7–32 kcal/mol, while the second subset with 90 complexes has stabilisation energies smaller than 7 kcal/mol. The first subset is characterised by small intermolecular distances (less than 2.5 Å) and a significant contraction of van der Waals (vdW) distance (sum of vdW radii). Here the polarisation/electrostatic energy is dominant, mostly followed

The online version of this chapter (doi:10.1007/128_2014_606) contains supplementary material, which is available to authorized users.

M.H. Kolář
Institute of Organic Chemistry and Biochemistry, Academy of Sciences of the Czech Republic, Flemingovo nám. 2, 166 10 Prague 6, Czech Republic

Institute for Advanced Simulations (IAS-5), Forschungszentrum Jülich GmbH, 52428 Jülich, Germany

Computational Biophysics, German Research School for Simulation Sciences GmbH, 52428 Jülich, Germany

P. Deepa, H. Ajani, and A. Pecina
Institute of Organic Chemistry and Biochemistry, Academy of Sciences of the Czech Republic, Flemingovo nám. 2, 166 10 Prague 6, Czech Republic

P. Hobza (✉)
Institute of Organic Chemistry and Biochemistry, Academy of Sciences of the Czech Republic, Flemingovo nám. 2, 166 10 Prague 6, Czech Republic

Department of Physical Chemistry, Regional Centre of Advanced Technologies and Materials, Palacky University, 771 46 Olomouc, Czech Republic
e-mail: pavel.hobza@uochb.cas.cz

by induction and dispersion energies. The importance of induction energy reflects the charge-transfer character of the respective halogen bonds. Intermolecular distances in the second subset are large and the respective contraction of vdW distance upon the formation of a halogen bond is much smaller. Here the dispersion energy is mostly dominant, followed by polarisation and induction energies. Considering the whole set of complexes, we conclude that the characteristic features of their halogen bonds arise from the concerted action of polarisation and dispersion energies and neither of these energies can be considered as dominant. Finally, the magnitude of the σ-hole and DFT-SAPT stabilisation energy correlates only weakly within the whole set of complexes.

Keywords CCSD(T) • DFT-SAPT • Dispersion energy • Electrostatic potential • Halogen bond • Noncovalent interactions • σ-Hole • σ-Hole magnitude • σ-Hole size

Contents

1 Introduction

The family of noncovalent interactions [1] has recently been augmented by a new type of bonding between a Lewis acid and a Lewis base where the Lewis base is an electron donor (O, N, S, P, . . .) and the Lewis acid is an atom which simultaneously contains an area of positive and negative electrostatic potential (ESP). The area of positive ESP, called the σ-hole [2–4], originates in an unequal occupation of valence orbitals. It was originally found on halogens but later also recognised on atoms of groups IV, V and VI. The bonds are referred to as halogen bonds, chalcogen and pnicogen bonds or, in general, σ-hole bonds [5].

For the σ-hole bonds, the σ-hole of the electron acceptor (i.e. Lewis acid) seems to be a key concept, although it concerns only one of the two interacting partners. To elucidate the complete picture of σ-hole bonding, it is inevitable to analyse the contributions to the total stabilisation energy of the entire complex as well. The text below focuses on both the analysis of electron acceptors in halogen bonds and, in more detail, on electron acceptor–donor pairs.

The stabilisation of an X–Y···D halogen bond, where Y is Cl, Br or I, X is an electronegative atom (mostly another halogen) or carbon and D is an electron donor (O, N, S, ...), is explained elegantly by the existence of a positive σ-hole. Energetically, the X–Y···D halogen bond is similar to the X–H···D hydrogen bond (H-bond). Following the reliable CCSD(T)/CBS calculations of the stabilisation energy, the most stable halogen-bonded complex (iodobenzene···trimethylamine) from the X40 dataset [6] (complexes containing halogens) amounts to 5.8 kcal/mol, and this stabilisation energy is comparable to the stabilisation of strong H-bonds. Much larger stabilisation energies were, however, calculated (at the same theoretical level) for complexes of small halogen donors, e.g. 17.1 and 15.3 kcal/mol for $FI\cdots NH_3$ and $FBr\cdots NH_3$, respectively [7]. Similarly, large stabilisation energies (8.0 and 15.0 kcal/mol) were also calculated (again at the same theoretical level) for the crystals of the complexes of the large organic molecules 1,3-dithiole-2-thione-4-carboxylic acid (DTCA) and 1,4-diazabicyclo[2.2.2]octane (DABCO) with diiodine I_2 [8]. Where do these large stabilisation energies come from? Is the nature of stabilisation in these complexes the same as in the previously mentioned ones?

The attraction in halogen-bonded complexes was originally assigned to electrostatic attraction between the positive σ-hole and a lone pair of the electron donor, which is reflected in a recently published IUPAC definition of halogen bond [9]. In our recent paper [10], however, we have pointed out the important role of dispersion interaction, which is easily explained by the fact that, in any halogen bond, two atoms with high polarisability (the halogen and electron donors) are located close to each other (closer than the sum of van der Waals (vdW) radii). In ten different halogen-bonded complexes investigated [10] by the symmetry-adapted perturbation theory (SAPT), the dispersion energy was dominant in eight cases while only in two cases was the electrostatic term slightly larger than the dispersion one. This is in contradiction to the previously mentioned definition of the halogen bond [9], which states that 'the forces involved in the formation of the halogen bond are primarily electrostatic'. Is it because of the fact that the complexes investigated in [10] were not typical halogen-bonded ones? Nevertheless, the list of the complexes studied (benzene···X_2, X=F, Cl, Br; formaldehyde···X, X=chloroform, halothane, enfurane, isofurane; bromomethanol dimer) justifies our choice.

This chapter is organised as follows. First, attention is paid to the characterisation of isolated halogen donors. Their σ-holes are described in terms of size and magnitude. These properties have recently been introduced to characterise such a rather complicated three-dimension object as the σ-hole [11]. In the second part of the chapter, both interacting partners are studied in terms of the SAPT decomposition of their total stabilisation energy. An extended set of SAPT decompositions calculated consistently at the same theoretical level is provided for different types of halogen-bonded complexes: ranging from weak/moderate complexes formed by standard electron donors (e.g. water, ammonia, formaldehyde, dimethyl ether or trimethylammonia) and standard halogen donors (e.g. halobenzenes or substituted halobenzenes) to strong halogen-bonded complexes with a significant charge transfer. An attempt is made to combine approaches to monomers and complexes to provide novel insight into halogen bonding.

2 Methods

2.1 Isolated Subsystems

The *magnitude* of the σ-hole was defined by Kolář et al. [11] as the value of the most positive (or the least negative) electrostatic potential (ESP) localised at the halogen boundary. The most positive ESP had been used previously to characterise σ-holes but the nomenclature was rather confusing. Further, the *size* of the σ-hole was defined as the spatial extent of the region of positive ESP on the halogen boundary. Such spatial characteristics were shown to be indications for attractive interaction: in [11], we concluded that the channel of attraction of the halogen bond, understood as an angular range with a positive total stabilisation energy with either hydrogen fluoride or argon atoms, is well reflected in the size of the σ-hole.

When limited to aromatic molecules with the C_{2v} symmetry point group, the size was initially defined in terms of the angular properties of the ESP profile (see [11] for details). The extension for non-symmetric cases has recently been provided [12]. The size was generalised as an area of positive ESP lying on the boundary of the halogen atom, defined arbitrarily as an isosurface of 0.001 e/bohr [3] electron density [13]. The area has to be refined to have an approximately rounded boundary, since the shape of positive ESP may be quite complicated for non-symmetric molecules [12].

The magnitude and size were calculated for all of the halogenated subsystems. Prior to the ESP calculations, all of the molecules were energy minimised. Both the minimisation and the ESP calculations were done at the PBE0/aug-cc-pVDZ level with the pseudopotentials on bromine and iodine atoms [14–17]. The calculations were performed in the Gaussian09 program package [18].

2.2 SAPT Decomposition

The SAPT method [19] provides an exact decomposition of the total interaction energies into various components of the first and second perturbation order. The DFT version of the SAPT (DFT-SAPT) [20–28] allows for the treatment of extended complexes (up to about 40 atoms) and the total interaction energy is decomposed into polarisation/electrostatic (E^{POL}), induction (E^{I}), dispersion (E^{D}) and exchange-repulsion (E^{ER}) terms. Here, the E^{I} and E^{D} terms include their exchange parts and induction energy further includes the δHF term, which accounts for higher than second-order terms covered by the Hartree–Fock approach. It should be mentioned that SAPT decomposition does not include the charge transfer energy, which is the energy stabilising complexes between electron donor (small ionisation potential) and electron acceptor (small electron affinity). This energy is covered in the induction energy and thus it contains not only the classical induction

energy term (permanent multipole/induced multipole) but also charge transfer (electron donor/electron acceptor) energy.

The greatest improvement of the DFT-SAPT method over the original SAPT is the acceleration of the calculations by one order of magnitude. The intramolecular treatment is conducted using the DFT and therefore suffers from inaccurate energies of the virtual orbitals. This drawback is corrected for in advance of the actual SAPT treatment by a gradient-controlled shift procedure, which uses the difference between the exact vertical ionisation potential (IP) and the energy of the (HOMO) [24]. In this work, PBE0/aug-cc-pVTZ and PBE0/aug-cc-pVDZ calculations were carried out to obtain the IP respective HOMO values and intermolecular terms were described by aug-cc-pVDZ and aug-cc-pVTZ basis sets. Bromine and iodine atoms were treated by pseudopotentials to describe relativistic effects of inner-core electrons correctly.

All the post Hartree–Fock calculations (including DFT-SAPT) were carried out using the Molpro 2010 package [29]. The DFT calculations were done utilising the Turbomole 6.3 package [30].

2.3 Complexes

Our goal was to collect a large set of halogen-bonded complexes of different size and origin. The common feature of all these complexes is the presence of halogen or dihalogen bonds [31, 32]. While in the halogen bond the halogen (Cl, Br or I) covalently bound to an electronegative atom or carbon is in contact with an electron donor (O, N, S, ...); in the case of the dihalogen bond one halogen atom is in contact with another halogen.

First, the complexes where the benchmark CCSD(T) stabilisation energies are known were utilised; in all these studies the complex geometry was determined at a lower theoretical level, mostly at DFT with an empirical dispersion correction [33] (DFT-D). We studied 18 complexes from our X40 dataset [6] (Table 2), 46 complexes from the XB51 dataset [7] (Table 3), 11 complexes from our previous papers [34–36] (Table 4) and 13 complexes from [37] (Table 5). Second, in the following halogen-bonded complexes, the stabilisation energy as well as the complex geometry were calculated at MP2 or DFT-D levels. Table 6 summarises eight complexes [38] of crystal motifs which were taken from the Cambridge Structure Database. Table 7 contains 15 complexes from [39] for which the binding free energy in nonpolar solvent was measured. Finally, Table 8 contains 17 structures of organic crystals, taken from [40–45]. Altogether, 128 halogen-bonded complexes were investigated. Structures of all investigated complexes are collected in the Electronic Supplementary Material Figs. S1, S2, S3, S4, S5, S6 and S7.

The structure of each of the halogen-bonded complexes was taken from the original references without any additional optimisation. For most of the complexes, the DFT-D (B97-D3/def2-QZVP) calculations [46] were also performed. All

interaction energies were corrected for the basis set superposition error (BSSE) utilising counterpoise correction [47].

As mentioned above, DFT-SAPT calculations were performed using the aug-cc-pVDZ and aug-cc-pVTZ basis sets. When passing to the larger basis set, all the SAPT energy terms remain practically unchanged with the exception of dispersion energy, which is underestimated with the smaller basis. This ratio was evaluated for 18 complexes from the X40 dataset and was used for scaling the aug-cc-pVDZ dispersion energy of the remaining complexes for which the DFT-SAPT/aug-cc-pVTZ calculation would be prohibitively expensive. For even larger crystal structures, for which the SAPT/aug-cc-pVDZ calculations of dispersion energy would be impractical, the dispersion and exchange-dispersion terms were approximated by an empirical atom-atom dumped dispersion term [48]. The ratio of the empirical dispersion energy and aug-cc-pVTZ perturbation dispersion energy evaluated again for 18 complexes from the X40 dataset was used for scaling the empirical dispersion energy for extended halogen-bonded complexes.

3 Results and Discussion

3.1 Halogenated Molecules

The properties of the subsystems, the magnitude and size of the σ-hole and the energy of the lowest unoccupied molecular orbital (LUMO) are shown in Table 1. The magnitude and size correlate well, with the correlation coefficient R being 0.86. This agrees with the previously presented dependence. Furthermore, the magnitude and size both increase with the atomic number of the halogen atom, which is also a well-known trend. All the molecules possess a positive σ-hole with the exception of H_3CCl, which has a slightly negative V_{max} of −0.0001 a.u. The most positive σ-hole can be found in FI, where two effects are combined, both increasing the magnitude of the σ-hole (activating the halogen for the halogen bond). These effects are the presence of a heavy halogen atom along with a strong electron withdrawing chemical group in its vicinity. Indeed, a comparison of, e.g. H_3CBr with F_3CBr or BzI with C_6F_5I reveals that the presence of fluorine atoms increases both the magnitude and the size of the σ-hole on iodine [2, 49]. In dihalogen molecules, the activation of the halogen participating in a halogen bond increases with the decreasing atomic number of the second halogen (iodine σ-hole magnitude IBr<ICl<IF). Hence, the fluorine has a positive σ-hole with a size of about 6 Å^2 when bound to another fluorine. The magnitude and size of its σ-hole are comparable with, e.g. H_3CI.

The magnitude and LUMO energy anticorrelate with $R = -0.76$. This means that strong electron acceptors (i.e. molecules with the most negative LUMO energy) have more positive σ-holes.

Table 1 The magnitude (in a.u.) and size (in Å^2) of the σ-holes of halogenated monomers and the energies of the lowest unoccupied molecular orbital (LUMO) (in a.u.)

Molecule	Magnitude	Size	LUMO
F_2	0.025	6.0	−0.134
Cl_2	0.042	10.7	−0.128
ClF	0.062	13.7	−0.127
ClF_3	0.069	13.6	−0.162
H_3CCl	0.000	0.0	−0.006
F_3CCl	0.032	12.3	−0.009
C_2H_3Cl	0.008	2.5	−0.016
C_2HCl	0.034	11.4	−0.001
C_6H_5Cl	0.007	2.1	−0.025
C_6Cl_6	0.026	8.6	−0.062
$C_6H_2OHCl_3$	0.018	5.8	−0.045
Br_2	0.052	12.5	−0.140
BrF	0.083	14.4	−0.136
BrF_3	0.090	15.6	−0.163
H_3CBr	0.013	3.3	−0.017
F_3CBr	0.042	14.2	−0.042
C_2H_3Br	0.020	5.6	−0.018
C_2HBr	0.049	13.7	−0.020
C_6H_5Br	0.019	5.2	−0.025
C_6Br_6	0.036	10.5	−0.085
$BrC_4H_2NO_2$	0.055	11.7	−0.114
CH_2BrOH	0.013	3.4	−0.019
$C_7F_4O_2HBr$	0.023	8.0	−0.064
I_2	0.056	9.7	−0.144
IF	0.097	17.3	−0.140
ICl	0.074	17.1	−0.140
IBr	0.066	16.5	−0.142
ICN	0.081	16.7	−0.077
H_3CI	0.022	6.5	−0.038
F_3CI	0.050	17.6	−0.073
C_2H_3I	0.028	8.6	−0.031
C_2HI	0.058	16.5	−0.043
C_6H_5I	0.027	8.1	−0.034
C_6F_5I	0.052	17.0	−0.071
C_4F_9I	0.050	19.2	−0.081
$INC_4H_2O_2$	0.068	15.0	−0.111
$HO_2C_7F_4I$	0.053	19.2	−0.082
TFIB	0.051	16.2	−0.074

3.2 Complexes

Tables 2, 3, 4, 5, 6, 7 and 8 summarise the energy characteristics of all complexes investigated and also show the Y···D and Δr distances, i.e. the distance between

Table 2 DFT-SAPT interaction energies (in kcal/mol) and Y···D/Δ*r* distances (Å) for halogen-bonded complexes from the X40 dataset [6]

No.	Basis	Complex	CCSDT/CBS	DFT-SAPT						Y···D/Δ*r*[a]	P:I:D[b]	Q[c]	Q[d]
			Δ*E*	E_{tot}	E_1^{Pol}	E_1^{Ex}	E_2^{Ind}	E_2^{Disp}	$E_2^{Disp.\ empirical}$				
1	aVDZ	$H_3CCl\cdots OCH_2$	−1.17	−0.79	−1.13	2.34	−0.36	−1.64	−1.38	3.30/0.03	0.7:0.2:1	1.18	1.40
	aVTZ			−1.07	−1.11	2.36	−0.38	−1.94			0.6:0.2:1		
2	aVDZ	$H_3CBr\cdots OCH_2$	−1.72	−1.44	−2.26	3.39	−0.48	−2.09	−1.94	3.17/0.2	1.1:0.2:1	1.19	1.28
	aVTZ			−1.79	−2.19	3.40	−0.50	−2.49			0.9:0.2:1		
3	aVDZ	$H_3CI\cdots OCH_2$	−2.38	−2.18	−3.66	4.78	−0.88	−2.41	−2.48	3.21/0.29	1.5:0.4:1	1.23	1.19
	aVTZ			−2.63	−3.53	4.79	−0.94	−2.96			1.2:0.3:1		
4	aVDZ	$F_3CCl\cdots OCH_2$	−2.25	−1.60	−2.92	3.99	−0.71	−1.97	−1.61	2.98/0.29	1.5:0.4:1	1.17	1.44
	aVTZ			−1.87	−2.83	3.99	−0.72	−2.31			1.2:0.3:1		
5	aVDZ	$F_3CBr\cdots OCH_2$	−3.1	−2.75	−4.66	5.29	−0.98	−2.41	−2.21	2.95/0.42	1.9:0.4:1	1.20	1.31
	aVTZ			−3.09	−4.50	5.27	−0.97	−2.88			1.6:0.3:1		
6	aVDZ	$F_3CI\cdots OCH_2$	−4.08	−3.86	−6.65	7.39	−1.78	−2.82	−2.89	3.01/0.49	2.4:0.6:1	1.23	1.20
	aVTZ			−4.35	−6.43	7.38	−1.83	−3.47			1.9:0.5:1		
7	aVDZ	$C_6H_5Cl\cdots OC_3H_6$	−1.49	−0.93	−1.55	3.64	−0.60	−2.42	−1.93	3.12/0.15	0.6:0.2:1	1.12	1.41
	aVTZ			−1.18	−1.49	3.62	−0.60	−2.71			0.5:0.2:1		
8	aVDZ	$C_6H_5Br\cdots OC_3H_6$	−2.43	−2.32	−3.39	5.03	−0.88	−3.08	−2.71	3.07/0.3	1.1:0.3:1	1.14	1.13
	aVTZ			−2.65	−3.29	5.02	−0.89	−3.50			0.9:0.3:1		
9	aVDZ	$C_6H_5I\cdots OC_3H_6$	−3.46	−3.71	−5.44	7.07	−1.80	−3.54	−3.44	3.09/0.41	1.5:0.5:1	1.18	1.03
	aVTZ			−4.18	−5.27	7.04	−1.82	−4.14			1.3:0.4:1		
10	aVDZ	$C_6H_5Cl\cdots NC_3H_9$	−2.11	−1.37	−3.37	6.27	−1.03	−3.24	−2.72	3.06/0.24	1.0:0.3:1	1.11	1.33
	aVTZ			−1.68	−3.26	6.21	−1.03	−3.61			0.9:0.3:1		
11	aVDZ	$C_6H_5Br\cdots NC_3H_9$	−3.78	−3.78	−7.47	9.69	−1.33	−4.67	−4.45	2.97/0.43	1.6:0.3:1	1.13	1.19
	aVTZ			−4.26	−7.27	9.58	−1.30	−5.28			1.4:1:1		
12	aVDZ	$C_6H_5I\cdots NC_3H_9$	−5.81	−6.74	−12.91	15.72	−3.39	−6.16	−6.61	2.97/0.56	2.0:0.6:1	1.06	0.98
	aVTZ			−7.02	−12.76	15.65	−3.42	−6.50			2.0:0.5:1		

13	aVDZ	$C_6H_5Br\cdots SHCH_3$	−2.32	2.00	−3.20	4.63	−0.34	−3.09	−2.62	3.54/0.11	1.0:0.1:1	1.15	1.36
	aVTZ			−2.41	−3.12	4.60	−0.33	−3.56			0.9:0.1:1		
14	aVDZ	$C_6H_5I\cdots SHCH_3$	−3.08	−2.70	−5.06	6.55	−0.57	−3.63	−3.37	3.56/0.22	1.4:0.2:1	1.05	1.13
	aVTZ			−2.83	−4.99	6.54	−0.57	−3.81			1.3:0.1:1		
15	aVDZ	$H_3CBr\cdots Bz$	−1.81	−1.47	−1.21	3.14	−0.13	−3.28	−3.41	3.55	0.4:0.04:1	1.13	1.09
	aVTZ			−1.88	−1.14	3.09	−0.12	−3.7			0.0:0.03:1		
16	aVDZ	$H_3CI\cdots Bz$	−2.48	−2.04	−1.99	3.89	−0.15	−3.79	−4.45	3.66	0.5:0.04:1	1.18	1.00
	aVTZ			−2.31	−2.21	4.55	−0.19	−4.46			0.5:0.04:1		
17	aVDZ	$F_3CBr\cdots Bz$	−3.11	−2.74	−2.60	4.09	−0.46	−3.78	−4.14	3.46	0.7:0.1:1	1.13	1.03
	aVTZ			−3.12	−2.60	4.16	−0.44	−4.27			0.6:0.1:1		
18	aVDZ	$F_3CI\cdots Bz$	−3.91	−3.29	−3.68	5.45	−0.63	−4.43	−5.38	3.53	0.8:0.1:1	1.16	0.95
	aVTZ			−4.78	−3.61	5.53	−1.59	−5.12			0.7:0.3:1		

[a]Δr is the difference of the distance between halogen and electron donor (Y···D) and the sum of the respective vdW radii
[b]Ratio of polarisation, induction and dispersion energies
[c]Ratio of dispersion energies determined with aug-cc-pVTZ and aug-cc-pVDZ basis sets
[d]Ratio of dispersion energies determined with SAPT/aug-cc-pVTZ and empirical dispersion energy

Table 3 DFT-SAPT/aVTZ-PP interaction energies (in kcal/mol) and Y···D (Å) for the XB51 dataset [7]

No.	Complex	CCSDT/CBS	DFT-SAPT						
		ΔE	E_{tot}	E_1^{Pol}	E_1^{Ex}	E_2^{Ind}	E_2^{Disp}	Y···D/Δr^a	P:I:D[b]
1	HCN···ICF_3	3.61	−3.78	−5.49	5.84	−1.38	−2.76	3.1/0.43	2.0:0.5:1
2	HCN···BrF	7.53	−8.24	−14.76	17.22	−5.41	−5.30	2.52/0.88	2.8:1.0:1
3	HCN···ClF	4.81	−4.08	−8.30	11.54	−3.62	−3.70	2.61/0.69	2.2:1.0:1
4	HCN···$BrO_2C_4H_2N$	4.32	−4.28	−6.76	7.60	−1.76	−3.35	2.81/0.59	2.0:0.5:1
5	HCN···I $NC_4H_2O_2$	5.91	−6.39	−9.78	10.82	−3.21	−4.22	2.86/0.67	2.3:0.8:1
6	HCN···BrC_6H_5	1.15	−1.10	−1.54	2.76	−0.47	−1.85	3.18/0.22	0.8:0.3:1
7	HCN···IC_6H_5	1.87	−1.93	−2.73	3.88	−0.81	−2.28	3.25/0.28	1.2:0.4:1
8	H_3N···ICF_3	5.88	−6.94	−12.03	12.06	−2.90	−4.07	2.99/0.54	3.0:0.7:1
9	H_3N···BrF	15.30	−19.60	−39.14	43.48	−15.20	−8.74	2.35/1.05	4.5:1.7:1
10	H_3N···ClF	10.54	−9.59	−28.31	42.61	−16.49	−7.40	2.34/0.96	3.8:2.2:1
11	H_3N···$BrC_4H_2NO_2$	8.02	−8.91	−17.52	18.54	−4.56	−5.36	2.66/0.74	3.3:0.9:1
12	H_3N···$IC_4H_2NO_2$	10.99	−14.25	−25.37	26.16	−8.30	−6.74	2.69/0.84	3.8:1.2:1
13	H_3N···BrC_6H_5	2.02	−2.13	−3.92	5.02	−0.74	−2.46	3.13/0.27	1.6:0.3:1
14	H_3N···IC_6H_5	3.33	−3.79	−6.53	7.34	−1.42	−3.18	3.17/0.36	2.1:0.4:1
15	HCP···ICF_3	0.89	−0.83	−0.85	2.45	−0.34	−2.09	3.72/0.06	0.4:1.7:1
16	HCP···BrF	2.07	−2.24	−3.25	7.62	−2.50	−4.11	3.08/0.57	0.8:0.6:1
17	HCP···ClF	1.16	−0.86	−1.71	5.57	−1.93	−2.79	3.16/0.39	0.6:0.7:1
18	HCP···$BrC_4H_2O_2N$	1.19	−1.04	−1.20	3.21	−0.53	−2.52	3.41/0.24	0.5:0.2:1
19	HCP···$IC_4H_2O_2N$	1.53	−1.43	−1.58	4.12	−0.94	−3.03	3.49/0.29	0.5:0.3:1
20	HCP···BrC_6H_5	0.85	−0.78	−0.82	2.02	−0.08	−1.90	3.63/0.02	0.4:0.04:1
21	HCP···IC_6H_5	0.92	−0.89	−0.94	2.36	−0.16	−2.15	3.76/0.02	0.4:0.07:1
22	Br_2···FC_2H	0.74	−0.51	−0.28	0.88	−0.12	−0.99	3.19/0.01	0.3:0.1:1
23	Br_2···FCH_3	3.61	−2.62	−4.28	5.58	−1.07	−2.85	2.81/0.39	1.5:0.4:1
24	Br_2···NCH	2.87	−3.68	−5.79	6.80	−1.65	−3.04	2.86/0.54	1.9:0.5:1

25	$Br_2\cdots NH_3$	5.95	−8.45	−16.83	18.97	−5.25	−5.34	2.66/0.74	3.1:1:1
26	$Br_2\cdots OCH_2$	4.41	−4.22	−7.48	9.40	−2.27	−3.87	2.75/0.62	1.9:0.6:1
27	$Br_2\cdots OPH_3$	7.29	−6.09	−10.76	13.04	−3.44	−4.93	2.68/0.69	2.2:0.7:1
28	$Br_2\cdots PCH$	1.18	−1.06	−1.19	3.07	−0.59	−2.35	3.44/0.21	0.5:0.3:1
29	$Br_2\cdots NC_5H_5$	9.00	−10.89	−19.97	24.15	−7.60	−7.47	2.57/0.83	2.7:1.0:1
30	$FI\cdots FC_2H$	0.29	−0.29	−0.02	0.28	−0.03	−0.52	3.02/0.31	0.04:0.06:1
31	$FI\cdots FCH_3$	9.33	−6.29	−9.95	11.60	−3.72	−4.22	2.66/0.67	2.4:0.9:1
32	$FI\cdots NCH$	5.97	−11.24	−18.37	20.97	−7.72	−6.13	2.61/0.92	3.0:1.3:1
33	$FI\cdots NH_3$	13.36	−23.82	−40.62	41.56	−16.07	−8.68	2.5/1.03	4.7:1.9:1
34	$FI\cdots OCH_2$	9.94	−11.66	−18.81	21.74	−8.43	−6.15	2.57/0.93	3.1:1.4:1
35	$FI\cdots OPH_3$	17.11	−16.13	−27.19	30.47	−11.39	−8.02	2.5/1.0	3.4:1.4:1
36	$FI\cdots PCH$	2.74	−2.68	−4.13	9.50	−3.39	−4.66	3.17/0.61	0.9:0.7:1
37	$FI\cdots NC_6H_5$	17.66	−31.50	−47.19	51.80	−24.25	−11.85	2.42/1.11	3.9:2.0:1
38	$H_3CI\cdots FC_2H$	0.50	−0.38	−0.30	1.05	−0.09	−1.04	3.39/0.06	0.3:0.09:1
39	$H_3CI\cdots FCH_3$	1.70	−1.69	−2.50	3.86	−0.59	−2.46	3.18/0.15	1.0:0.2:1
40	$H_3CI\cdots LiH$	3.62	−3.50	−8.13	9.06	−0.54	−3.89	2.74/1.06	2.1:0.1:1
41	$H_3CI\cdots NCH$	1.42	−1.60	−2.28	3.44	−0.68	−2.08	3.28/0.25	1.1:0.3:1
42	$H_2CI\cdots NH_3$	2.73	−3.34	−5.72	6.48	−1.19	−2.91	3.21/0.32	1.9:0.4:1
43	$H_3CI\cdots OCH_2$	2.39	−2.48	−3.83	5.35	−0.98	−3.03	3.17/0.33	1.3:0.3:1
44	$H_3CI\cdots OPH_3$	3.34	−3.57	−5.63	7.56	−1.50	−4.00	3.14/0.36	1.4:0.4:1
45	$H_3CI\cdots PCH$	0.85	−0.84	−0.91	2.23	−0.15	−2.01	3.77/0.01	0.5:0.08:1
46	$H_3CI\cdots NC_5H_5$	3.61	−5.01	−6.83	8.32	−2.23	−4.28	3.11/0.42	1.6:0.5:1

[a]Δr is the difference of the distance between halogen and electron donor (Y···D) and the sum of the respective vdW radii
[b]The ratio of polarisation, induction and dispersion energies

Table 4 DFT-SAPT/aug-cc-pVTZ interaction energies (in kcal/mol) and Y···D (Å) for halogen-bonded complexes

No.	Complex	CCSDT/CBS	DFT-SAPT					Y···D/Δr[a]	P:I:D[b]	Ref.[c]
		ΔE	E_{tot}	E_1^{Pol}	E_1^{Ex}	E_2^{Ind}	E_2^{Disp}			
1	F_2···Bz	−1.19	−1.22	−0.96	2.08	−0.49	−1.77	–	0.5:0.3:1	[34]
2	Cl_2···Bz	−2.86	−3.14	−3.17	6.52	−1.73	−4.53	–	0.7:0.4:1	[34]
3	Br_2···Bz	−3.66	−4.23	−5.01	9.83	−2.87	−5.85	–	0.9:0.5:1	[34]
4	CH_2BrOH···CH_2BrOH(Br–O)	−1.48	−1.56	−2.48	4.30	−0.50	−2.88	3.1/0.27	0.9:0.2:1	[35]
5	CH_2BrOH···CH_2BrOH(Br–Br)	−1.22	−1.44	−0.98	1.94	−0.31	−2.09	3.8/0.1	0.5:0.1:1	[35]
6	Trimethylbenzene···Br_2	−4.23	−4.89	−4.04	7.31	−1.50	−6.34	–	0.6:0.2:1	[34]
7	Hexamethylbenzene···Br_2	−5.66	−6.06	−5.43	9.60	−2.07	−7.79	–	0.8:0.3:1	[34]
8	I_2···I_2	−2.95	−3.44	−3.61	5.58	−1.09	−4.32	3.7/0.26	0.8:0.3:1	[36]
9	Br_2···Br_2	−2.28	−2.47	−2.53	4.27	−0.76	−3.45	3.4/0.3	0.7:0.2:1	[36]
10	Cl_2···Cl_2	−1.33	−1.20	−1.27	3.02	−0.63	−2.32	3.3/0.2	0.5:0.3:1	[36]
11	F_2···F_2	−0.39	−0.33	−0.17	0.46	−0.04	−0.58	2.9/0.2	0.3:0.1:1	[36]

[a]Δr is the difference of the distance between halogen and electron donor (Y···D) and the sum of the respective vdW radii
[b]Ratio of polarisation, induction and dispersion energies
[c]Structures from [34–36]

Table 5 DFT-SAPT/aVTZ-PP interaction energies (in kcal/mol) and Y···D (Å) for halogen-bonded complexes [37]

No.	Complex	CCSD(T)/CBS	DFT-SAPT						
		ΔE	E_{tot}	E_1^{Pol}	E_1^{Ex}	E_2^{Ind}	E_2^{Disp}	Y···D/Δr[a]	P:I:D[b]
1	$C_2H_3Cl\cdots OCH_2$	−1.49	−0.98	−0.93	1.96	−0.30	−1.70	3.53/0.26	0.5:0.1:1
2	$C_2HCl\cdots OH_2$	−2.08	−1.97	−2.25	2.61	−0.49	−1.84	3.07/0.2	1.1:0.3:1
3	$C_2HCl\cdots OCH_2$	−2.34	−1.69	−2.07	2.18	−0.42	−1.39	3.11/0.16	1.5:0.3:1
4	$C_2H_3Cl\cdots NH_3$	−0.89	−0.78	−1.04	2.10	−0.40	−1.44	3.33/0.03	0.7:0.3:1
5	$C_2HCl\cdots NH_3$	−2.65	−1.80	−2.68	3.16	−0.58	−1.71	3.20/0.1	1.6:0.3:1
6	$C_2H_3Br\cdots OH_2$	−1.36	−1.05	−0.85	1.19	−0.22	−1.17	3.36/0.01	0.7:0.2:1
7	$C_2H_3Br\cdots OCH_2$	−2.16	−1.04	−0.66	1.08	−0.25	−1.21	3.36/0.01	0.5:0.2:1
8	$C_2HBr\cdots OH_2$	−3.0	−3.68	−4.60	5.0	−1.18	−2.90	2.96/0.41	1.6:0.4:1
9	$C_2HBr\cdots OCH_2$	−3.37	−2.93	−4.17	4.11	−0.67	−2.2	2.99/0.38	1.9:0.3:1
10	$C_2H_3Br\cdots NH_3$	−1.87	−2.09	−2.84	3.34	−0.52	−2.13	3.24/0.16	1.3:0.2:1
11	$C_2HBr\cdots NH_3$	−4.12	−3.74	−5.14	4.71	−0.76	−2.55	3.10/0.3	2.0:0.3:1
12	$C_2H_3I\cdots OH_2$	−2.51	−1.56	−1.79	2.29	−0.41	−1.64	3.15/0.35	1.1:0.3:1
13	$C_2HI\cdots OH_2$	−4.38	−4.27	−6.15	5.80	−1.27	−2.66	3.06/0.44	2.3:0.5:1

[a]Δr is the difference of the distance between halogen and electron donor (Y···D) and the sum of the respective vdW radii
[b]Ratio of polarisation, induction and dispersion energies

Table 6 MP2/aug-cc-pVDZ, DFT-SAPT/aVTZ-PP interaction energies (in kcal/mol) and Y···D (Å) for crystal motifs [38]

No.	Complex	MP2/aug-cc-pVDZ	DFT-SAPT					Y···D/Δr[a]	P:I:D[b]
		ΔE	E_{tot}	E_1^{Pol}	E_1^{Ex}	E_2^{Ind}	E_2^{Disp}		
1	$CH_3CN\cdots BrF$	−8.85	−11.33	−19.05	22.22	−7.94	−6.56	2.46/0.94	2.9:1.2:1
2	$CH_3CN\cdots ClF$	−6.13	−5.62	−11.05	15.38	−5.44	−4.5	2.54/0.76	2.5:1.1:1
3	$CH_3CN\cdots BrF_3$	−9.30	−10.89	−16.45	17.10	−6.07	−5.46	2.61/0.79	3.0:1.1:1
4	$CH_3CN\cdots ClF_3$	−7.52	−6.31	−12.45	16.43	−5.47	−4.82	2.58/0.72	2.6:1.1:1
5	$CO\cdots BrF_3$	−1.25	−1.92	−2.09	2.91	−0.85	−1.88	2.97/0.4	1.1:0.5:1
6	$CO\cdots ClF_3$	−1.19	−1.30	−1.73	2.91	−0.69	−1.78	2.91/0.36	1.0:0.4:1
7	$CO\cdots BrF$	−1.27	−1.85	−1.97	2.81	−0.78	−1.91	2.90/0.47	1.0:0.4:1
8	$CO\cdots ClF$	−1.02	−1.14	−1.42	2.39	−0.57	−1.54	2.88/0.39	0.9:0.4:1

[a]Δr is the difference of the distance between halogen and electron donor (Y···D) and the sum of the respective vdW radii
[b]Ratio of polarisation, induction and dispersion energies

Table 7 DFT-SAPT/aVDZ-PP interaction energies and Y···D (Å) for halogen-bonded complexes [39]

No.	Complex	DFT-D[a]	DFT-SAPT							
		ΔE	E_{tot}	E_1^{Pol}	E_1^{Ex}	E_2^{Ind}	E_2^{Disp}	Y···D/Δr[b]	P:I:D[c]	E_{tot}[d]
1	ICN···NC_5H_5		−13.57	−20.73	20.73	−7.73	−6.72	2.77/0.76	3.1:1.2:1	−14.45
2	IBr···NC_5H_5		−21.32	−37.45	43.80	−18.68	−10.34	2.53/1.0	3.6:1.8:1	−22.67
3	ICl···NC_5H_5		−24.33	−41.08	46.84	−20.78	−10.70	2.49/1.04	3.8:1.9:1	−25.72
4	I_2···NC_5H_5		−16.99	−31.76	38.29	−15.56	−9.61	2.59/0.94	3.3:1.6:1	−18.64
5	I_2···NC_7H_{13}	−18.74	−25.44	−50.02	60.53	−23.30	−14.54	2.48/1.05	3.4:1.6:1	−27.33
6	I_2···OSC_2H_6	−9.39	−12.57	−22.44	27.22	−10.22	−8.20	2.62/0.88	2.7:1.2:1	−13.64
7	I_2···OPC_3H_9	−9.34	−13.49	−23.18	26.89	−10.24	−8.00	2.62/0.88	2.9:1.3:1	−14.53
8	I_2···NC_6H_{15}	−18.75	−25.20	−46.63	57.85	−22.21	−16.34	2.55/0.95	2.9:1.1:1	−27.33
9	C_4F_9I···OSC_2H_6	−5.01	−9.24	−14.44	15.97	−5.27	−6.38	3.75/0.25	2.3:0.8:1	−10.12
10	C_4F_9I···NC_6H_{15}	−11.14	−14.31	−24.34	29.43	−9.11	−11.83	2.81/0.72	2.4:0.9:1	−15.85
11	C_4F_9I···NC_7H_{13}	−10.05	−15.43	−29.12	33.80	−10.73	−10.79	2.69/0.84	2.7:1.0:1	−16.84
12	C_4F_9I···OPC_3H_9	−5.67	−10.30	−15.46	16.08	−5.53	−6.21	3.56/0.06	2.5:0.9:1	−11.12
13	C_6F_5I···OSC_2H_6	−4.93	−9.31	−14.14	15.44	−5.03	−6.42	2.80/0.7	2.2:0.8:1	−10.15
14	C_6F_5I···NC_6H_{15}	−10.91	−14.35	−23.75	28.44	−8.64	−11.96	2.81/0.72	2.3:0.8:1	−15.91
15	C_6F_5I···NC_7H_{13}	−10.79	−14.85	−27.82	31.94	−9.73	−10.63	2.70/0.83	2.6:0.9:1	−16.24

[a]DFT-D calculations at B97-D3/def2-QZVP level

[b]Δr is the difference of the distance between halogen and electron donor (Y···D) and the sum of the respective vdW radii

[c]Ratio of polarisation, induction and dispersion energies

[d]aug-cc-pVDZ: dispersion energy is multiplied by a factor of 1.15. This was determined as the mean value of the ratio of dispersion energies calculated at aug-cc-pVTZ to aug-cc-pVDZ levels (cf. Table 2)

Table 8 DFT-SAPT/aVDZ-PP interaction energies (kcal/mol) and Y···D (Å) for crystal structures

No.	Complex	DFT-D[a]	DFT-SAPT					X···Y/Δr[b]	P:I:D[c]	E^{a}_{tot}	Ref.
		ΔE	E_{tot}	E_1^{Pol}	E_1^{Ex}	E_2^{Ind}	E_2^{Disp}				
1	I_2···DABCO		−24.19	−65.36	83.02	−26.94	−17.15[d]	2.36/1.17	3.8:1.6:1	−26.43	[6]
2	I_2···DTCA		−5.98	−42.06	59.00	−11.82	−12.78[d]	2.73/1.05	3.3:0.9:1	−7.66	[6]
3	C_6Cl_6···C_6Cl_6		−2.1	−1.2	–	−0.1	−4.37[d]	–	0.3:0.02:1	−2.67	[25]
4	C_6Br_6···C_6Br_6		−2.9	−2.3	–	−0.3	−6.10[d]	–	0.4:0.05:1	−3.70	[25]
5	C_4N_3 H_4Br···$C_7F_4O_2HBr$	−4.44	−4.83	−7.58	9.34	−1.77	−5.59[d]	2.89/0.50	1.4:0.3:1	−5.60	[27]
6	$C_6F_4I_2$···$I_2F_4C_6$	−7.03	−7.59	−10.11	11.59	−3.31	−6.85[e]	3.01/0.32 4.06/0.73	1.5:0.5:1	−8.68	[28]
7	$C_7F_4O_2HBr$···$NBrC_4N_3H_2$	−4.44	−4.56	−7.58	9.38	−1.78	−5.45[e]	2.90/0.5 4.03/0.33	1.4:0.3:1	−5.43	
8	1,2-TFIB···TMO	−8.06	−6.47	−16.24	20.35	−3.05	−8.97[e]	3.170.61	1.8:0.4:1	−7.91	[27, 28]
9	1,2-TFIB···TMO	−10.07	−11.87	−19.86	23.34	−6.55	−10.46[e]	3.97/0.44	1.9:0.6:1	−13.53	[27]
10	2-Mercapto-1-methylimidazole···1,2-TFIB	−8.97	−6.78	−12.09	12.58	−2.54	−5.63[e]	3.31/0.47	2.1:0.5:1	−7.68	[30]
11	4,4′-Bipyridine···1,2-TFIB	−7.08	−7.77	−12.70	14.89	−4.35	−6.68[e]	2.91/0.62	1.9:0.7:1	−8.84	[28]
12	1,2-TFIB···TMO	−7.42	−6.28	−10.05	12.20	−2.21	−7.40[e]	3.39/0.39	1.4:0.3:1	−7.46	[27, 28]
13	1,2-TFIB···1,2-TFIB	−2.50	−3.04	−2.22	3.47	−0.43	−4.61[e]	4.01/0.05 3.55/0.22	0.5:0.09:1	−3.79	[28]

14	(3,4,5-Trichlorophenol)$_2$	−1.78	−1.03	−2.00	4.49	−0.41	−3.70[e]	3.11/0.16	0.5:0.1:1	−1.62	[31]
15	1,2-TFIB···1,2-TFIB-(A)	−2.38	−3.17	−2.33	3.87	−0.39	−5.14[e]	3.26/0.7	0.5:0.08:1	−3.99	[27, 28]
16	1,2-TFIB···1,2-TFIB-(B)	−6.21	−7.25	−5.25	9.19	−0.79	−12.34[e]	3.74/0.22	0.4:0.06:1	−9.23	[27, 28]
17	1,2-TFIB···1,2-TFIB-(C)	−1.23	−1.81	−1.39	2.88	−0.30	−3.56[e]	3.43/0.1 3.50/0.17	0.4:0.08:1	−2.37	[27, 28]

[a]DFT-D calculations at B97-D3/def2-QZVP level
[b]Δr is the difference between the X···Y distance and the van der Waals distance
[c]Ratio of polarisation, induction and dispersion energies
[d]aug-cc-pVDZ: dispersion energy is multiplied by a factor of 1.15. This was determined as the mean value of the ratio of dispersion energies calculated at aug-cc-pVTZ to aug-cc-pVDZ levels (cf. Table 2)
[e]Empirical dispersion energy is multiplied by a factor of 1.19. This was determined as the mean value of the ratio of dispersion energies calculated with aug-cc-pVTZ to E^{D}_{empir}

the halogen and the electron donor and the difference between this distance and the sum of the respective vdW radii.

Table 2 collects 18 complexes from the X40 dataset, for which the benchmark CCSD(T)/CBS energies were determined. For all these complexes, DFT-SAPT calculations were performed with both smaller (aug-cc-pVDZ) and larger (aug-cc-pVTZ) basis sets. The aug-cc-pVTZ DFT-SAPT total energies agree better with the CCSD(T)/CBS benchmark energies than the aug-cc-pVDZ ones. The average relative differences amount to 16% and 11%, respectively. The aug-cc-pVTZ DFT-SAPT total energies vary between −1.07 and −7.02 kcal/mol, but the stabilisation energies for most (12) complexes lie in a narrower interval, between 2 and 5 kcal/mol. Following expectations, the largest stabilisation energy was found for complexes containing heavy halogens and trimethylammonium as an electron donor. A comparison of the single energy terms showed that the first-order polarisation and exchange-repulsion, and the second-order induction energies determined with both basis sets are very similar and deviate by less than a few per cent. Dispersion energy is different, and here the aug-cc-pVTZ values are systematically larger than those calculated with the aug-cc-pVDZ basis set, on average by 15% (the largest difference, 23%, was found for the $F_3CI\cdots OCH_2$ complex and the smallest, 5%, for the $BzI\cdots SHCH_3$ complex). This value was used for scaling the dispersion energy calculated with a smaller aug-cc-pVDZ basis set. Only the aug-cc-pVTZ values are utilised in the subsequent discussion.

Investigating the aug-cc-pVTZ single energies, we found that in most (10) cases the dispersion energy is the largest (the most negative), followed by polarisation and induction energies. Only in eight complexes is the polarisation energy larger than the dispersion energy, but the difference is not large (on relative average by 30%). Induction energy is, in all 18 complexes, systematically the smallest, which indicates that with these complexes the charge transfer does not play an important role. All of the Y···D distances are shorter than the sum of the respective vdW radii (vdW distance), which amounts to 3.27, 3.37, 3.50, 3.30, 3.40, 3.53, 3.55, 3.65, 3.78, 2.70, 3.50, 3.70 and 3.96 Å for Cl···O, Br···O, I···O, Cl···N, Br···N, I···N, Cl···S, Br···S, I···S, F···F, Cl···Cl, Br···Br and I···I, respectively. The shortest distances (2.95 and 2.97 Å) were found for the complexes of trifluorobromomethane with formaldehyde and bromo- and iodobenzene with trimethylammonium and the longest distance (3.66 Å) for iodomethane···benzene. The largest contractions of the vdW distance (0.56, 0.49 and 0.43 Å, respectively) were detected for $BzI\cdots NC_3H_9$, $F_3CI\cdots OCH_2$ and $BzBr\cdots NC_3H_9$ complexes. Following expectations, the stabilisation energies of these complexes are among the largest.

Table 3 collects energies for 46 complexes of the XB51 dataset. As in the previous case, the DFT-SAPT/aug-cc-pVTZ total energies agree well with the CCSD(T)/CBS stabilisation energies. The average relative difference (18%) is larger than given previously but still reasonable. In the present case, the DFT-SAPT total energies lie in the broader interval, between −0.51 and −31.5 kcal/mol. The largest DFT-SAPT total energy in the Table 2 amounted to −7.02 kcal/mol. We (arbitrarily) consider this value to be the border between weak and medium, and

strong halogen-bonded complexes. A total of 34 complexes in this table have their stabilisation energies in the range 0.51–7.0 kcal/mol while 12 complexes are characterised by even more favourable stabilisation energy (in the range 7.0–31.5 kcal/mol). Only 14 of the 34 weaker complexes have the dispersion energy larger than the polarisation energy. In the remaining 20 cases, the polarisation is dominant. The dominant stabilisation in the 12 strongest complexes originates in polarisation energy, which is, in all cases, followed by induction energy. Dispersion energy is systematically the smallest one here. Such a combination of these three stabilisation energies (polarisation > induction > dispersion) is unique and was not detected in either the 18 complexes collected in the Table 2 or in the 34 weaker complexes in Table 3. Investigating these complexes, we immediately realise that the large induction energy cannot originate in classical permanent dipole-induced dipole induction energy but rather in charge-transfer energy. This is confirmed by the negative values of the LUMO of these electron acceptors (cf. Table 1), which indicates that they are exceptionally good electron acceptors. All of these strong complexes possess short Y···D distances, even below 2.5 Å. As in the previous case, the largest contractions of the vdW distances (1.11, 1.05 and 1.03 Å, respectively) were found for the strongest complexes, $FI\cdots NC_6H_5$, $H_3N\cdots BrF$ and $FI\cdots NH_3$. It should be noted that the contractions of the vdW distances are in the present case about twice as large as those in the Table 2. Similarly, the stabilisation energies are also much larger in the present complexes. It is apparent that the contractions of the vdW distances of more than 1 Å are connected with large stabilisation energies of more than 20 kcal/mol.

Table 4 collects 11 halogen-bonded complexes which differ from those previously investigated. Four of them are dihalogen dimers possessing a dihalogen bond, another five are complexes of benzene (or methylated benzene) with dihalogen (all having a X···π halogen bond) and, finally, the last two are halogen-bonded and dihalogen-bonded structures of bromomethanol dimer. In this case, the agreement between CCSD(T)/CBS stabilisation energies and DFT-SAPT total energies is comparable with previous cases (the average relative error amounts to 11%). DFT-SAPT stabilisation energies are moderate and are similar to those in Table 2 and part of Table 3 and are in the range of 0.3–6.1 kcal/mol. In all 11 cases, the dispersion energy is dominant and the induction energy is systematically the smallest. Evidently, none of these complexes correspond to the charge-transfer type, and thus all Y···D distances are larger than 2.9 Å. In all of these complexes, the contraction of the vdW distance is only small (less than 0.3 Å).

The complexes shown in Table 5 represent typical model halogen-bonded complexes between standard electron donors (OH_2, NH_3, and OCH_2) and halogen donors (halogen alkenes and alkynes). These complexes are characterised by a modest stabilisation energy between 0.78 and 4.27 kcal/mol and by relatively large halogen-bond lengths (more than 2.96 Å). DFT-SAPT total energies agree moderately with the CCSD(T) benchmark data (the average relative error is larger than previously and amounts to 22%). For complexes 1, 4, 6 and 7 belonging to the weakest group, the dispersion energy is dominant. For the nine remaining complexes, the first order polarisation energy is the largest (the most negative) energy

term. Induction energy is systematically the smallest here. The largest contractions of the vdW distances (0.44 and 0.41 Å, respectively) were again found for the strongest complexes (iodo- and bromomethane with water), and these contractions and stabilisation energies basically agree with those from Table 2.

For the complexes from Table 6, the benchmark CCSD(T) calculations are not available and the DFT-SAPT/aug-cc-pVTZ values are clearly more reliable than the MP2 ones. BrF, ClF, BrF_3 and ClF_3 are the halogen donors, whereas the CH_3CN and CO molecules are used as electron donors. Evidently, the strongest complexes, with a stabilisation energy of more than 10 kcal/mol, are formed between the CH_3CN electron donor and the BrF and BrF_3 electron acceptors (halogen donors). Table 1 shows that BrF_3 is the best electron acceptor (with the lowest LUMO) and BrF is still a very good electron acceptor. The chloro- analogues of these two acceptors exhibit relatively low LUMO values and are thus good acceptors as well. The two strongest complexes with a stabilisation energy of more than 10.9 kcal/mol have dominant polarisation energy followed by induction and dispersion terms. As mentioned above, such a decomposition is characteristic for strong charge-transfer halogen-bonded complexes. The six remaining complexes, with stabilisation energy in the range of 1.1 and 6.3 kcal/mol, belong to weaker halogen-bonded complexes. Here, the polarisation energy is four times more dominant and the dispersion energy twice, and in two cases the induction energy is larger than the dispersion energy. The intermolecular distances are in agreement with the stabilisation energies: for the four most stable ones the distance is short (below 2.61 Å) while in all the remaining cases it is considerably longer. The contractions of vdW distances in these complexes are also among the largest (0.72–0.94 Å).

Several complexes in Table 7 are too large and the DFT-SAPT calculations with the aug-cc-pVTZ basis set would be computationally inaccessible for them. Thus for all of the complexes from Table 7 we have used the smaller, aug-cc-pVDZ basis set, and the resulting dispersion energy was scaled by a factor of 1.15, which had been determined as the average ratio between dispersion energies at aug-cc-pVTZ and aug-cc-pVDZ levels (cf. Table 2). The resulting DFT-SAPT stabilisation energies are very large (between 10.1 and 27.3 kcal/mol) and are much larger than the DFT-D ones. Evidently, the former energies are more reliable. The decomposition of the total DFT-SAPT energy is in line with these values and the polarisation energy is systematically dominant. In eight cases the polarisation energy is followed by the induction energy, which proves the importance of the role of the charge transfer, and these complexes are mostly more stable than the others. In these complexes, the contraction of the vdW distance is very large (about 1 Å or even more) and also here it is valid that a contraction of about 1 Å is connected with a large stabilisation energy of more than 20 kcal/mol. In the remaining seven, mostly weaker complexes, the role of the induction and dispersion energies is reversed, but the polarisation energy remains dominant. The intermolecular distances here are in accord with the total energies and are larger than in the previous case.

Several crystal structures from Table 8 are even larger than those in Table 7 with as many as 32 atoms. Hence, even DFT-SAPT/aug-cc-pVDZ calculations would be

prohibitively expensive. Since SAPT decomposition is necessary for the assignment of the role of electrostatic, induction and dispersion energies (and thus the nature of binding) in extended complexes as well, a hybrid DFT-SAPT method was used here. All the energy terms with the exception of the dispersion one were evaluated using the aug-cc-pVDZ basis set while the dispersion energy was determined empirically (see the original paper [47]). These empirical dispersion energies were scaled by 1.19, which is the average ratio between DFT-SAPT/aug-cc-pVTZ and empirical dispersion energy determined for 18 complexes from Table 2. The dispersion energy for the complexes from Table 8 was thus scaled by 1.15 (complexes 1–6) or by 1.19 (complexes 7–17). Five complexes from Table 8 belong to a group of strongly stable halogen-bonded complexes with a stabilisation energy larger than 7 kcal/mol and in four (out of five) cases the polarisation energy is dominant. The dispersion energy is dominant in only one complex. Among these five complexes, the induction energy is mostly the smallest one and only in one case is the induction term larger than the dispersion term. This concerns the most stable complex (complex 1), having diiodine as an electron acceptor and DABCO as an electron donor. Diiodine is a very good electron acceptor (see Table 1), which is manifested by a large charge-transfer energy and, consequently, induction energy. In this case, the induction term is considerably larger than the dispersion energy and, further, the dominant (polarisation) term is the largest among all 128 complexes investigated. In this group of complexes, the intermolecular distances are all about 3 Å with the exception of diiodine-containing complexes, where the distance is well below 2.8 Å, and the contraction of the vdW distance is the largest (more than 1 Å). The second group of twelve complexes possesses stabilisation energies in the range of 1.5–6.8 kcal/mol and thus belongs among the weak/moderate halogen-bonded complexes. In eight out of twelve cases, the dispersion energy is dominant and only in two cases does the polarisation represent the largest attractive term. The induction energy is systematically the smallest one. All intermolecular distances are rather large and the respective contractions of the vdW distance are small or moderate.

Summarising results from previous tables, we can state that all of the halogen-bonded complexes investigated can be split into two different classes. The 38 complexes in the first group are the strongest with total stabilisation energy larger than 7 kcal/mol. Relatively small intermolecular distances (even below 2.4 Å) and a significant contraction of the vdW distance (up to 1.2 Å) are connected with the important role of induction energy, which is here mostly (in 21 cases) larger than the dispersion energy. In these complexes, the polarisation (electrostatic) energy is almost systematically dominant and only in one complex is the dispersion energy the largest. The second group of 90 less stable halogen-bonded complexes have stabilisation energies between 0.3 and 7 kcal/mol. Their intermolecular distances are contracted much less upon the formation of halogen bonds (mostly less than 0.5 Å; only in diatomic halogen donors could the contraction be larger). In 48 complexes out of the second group (53%), the dispersion energy is dominant, followed by the polarisation and the induction energies. In the rest of the complexes (47%), the polarisation energy is dominant, followed by the dispersion and induction

terms, and only in two cases is the induction energy larger than the dispersion energy.

The electrostatic terms in halogen and hydrogen bonds should be more or less comparable. The contribution of the dispersion energy to the stability of the halogen bond is much larger than that of the hydrogen bond. This is clearly caused by the fact that in the halogen bond two heavy atoms (the halogen and electron donors) with high polarisability are in close contact, while in the case of the hydrogen bond it is only the light hydrogen and electron donor which are close together. To demonstrate the importance of this contact atom pair, we evaluated, besides the total (empirical) dispersion energy, the contribution to the dispersion energy coming from this atom pair. In the case of 14 complexes from Table 2 (complexes with benzene were omitted), the contact atom pair dispersion energy forms on average 39% of the total dispersion energy. This ratio even increased (40%) when eight extended complexes from Table 8 were considered.

In the previous studies, it was demonstrated that the strength of halogen bonding in isolated complexes is proportional to the maximum of the ESP on the halogen [50]. In biological systems, however, this relation may not be so straightforward, because other effects such as solvation/desolvation come into play and the maximum of ESP is related to enthalpy changes rather than to free energies [51, 52]. Here we attempt to relate the properties of monomers, i.e. σ-holes, with the properties of complexes.

Surprisingly enough, the magnitude of the σ-hole correlates weakly with the stabilisation energy, with the correlation coefficient R being 0.52. The dependence of the stabilisation energy on the magnitude of the σ-hole is shown in Fig. 1. Of course, both interacting partners affect the stabilisation of a complex. However, the

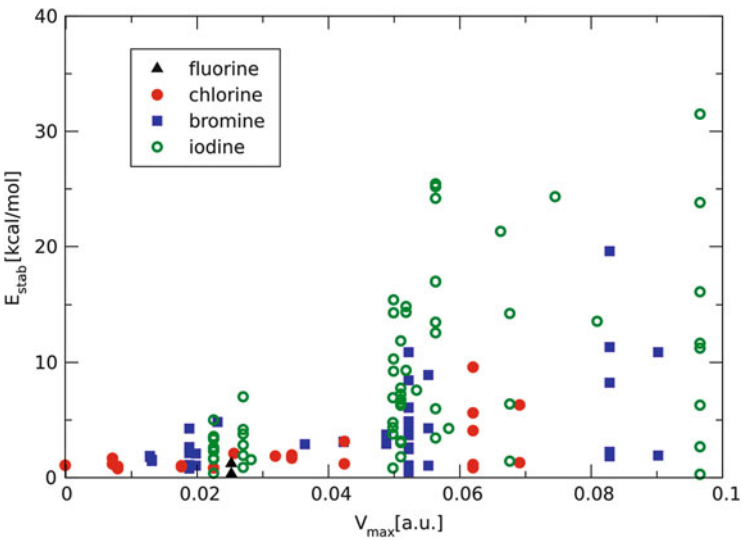

Fig. 1 The dependence of the stabilisation energy E_{stab} on the magnitude of the σ-hole V_{max}

points are spread in a triangular region with columns, distinguishing various halogenated monomers. When selecting the most stable complex of particular halogenated monomers, the correlation between the monomer's magnitude of σ-holes and the stabilisation energy increases to $R = 0.77$. Therefore, it seems that the magnitude of the σ-hole tells us something about the ability of a monomer to create a halogen bond but cannot provide the complete picture on halogen bonding. Indeed, when comparing complexes with the same electron donor, a strong correlation should be expected [50].

When the total stabilisation energy depends on both interacting molecules, the same should be true about the components of stabilisation energy. We did not observe any relation between the magnitudes of the σ-hole and the polarisation or induction terms of DFT-SAPT decomposition, most likely because of the large effect of the electron donor.

4 Conclusions

The analysis of electron acceptors (halogenated molecules) revealed a correlation between the extreme of ESP and the spatial extent of the positive region on top of the halogen boundary. The magnitude and size of a halogen σ-hole suggest a possible strength of the halogen bond in noncovalent complexes.

It was shown that all halogen-bonded complexes investigated could be split into two groups on the basis of their stabilisation energies. The complexes in the first group are stronger (their stabilisation energy is larger than 7 kcal/mol) and can be characterised as halogen-bonded complexes with a strong charge-transfer contribution. In practically all cases in this class, the polarisation (electrostatic) term is dominant and the induction term is mostly the second most important term, reflecting the important role of charge-transfer energy. The second class of halogen-bonded complexes is characterised by weaker stabilisation energies (below 7 kcal/mol) and represents rather standard halogen-bonded complexes. In this class of complexes, the dispersion energy is mostly dominant. In the whole set of 128 halogen-bonded complexes investigated, the polarisation (electrostatic) energy is dominant in 62% while in the remaining 38% it is the dispersion energy, which represents the dominant attractive term. We can thus state that the concerted action of polarisation and dispersion energies is responsible for the characteristic properties of halogen bonding. The electrostatic interaction between the positive σ-hole and the negative electron donor is responsible not only for the stability but also for the high directionality of the bond, while dispersion energy is responsible for its high stability. A dominant role is played by the contact atom pair (the halogen and electron donors), which contributes as much as 40% of the total dispersion energy. This significant contribution, which is characteristic for the halogen bond, is a consequence of two factors: first, the attractive electrostatic interaction between the halogen positive σ-hole and the negative electron donor and, second, the lower exchange-repulsion between the two subsystems, which is

also manifested as so-called polar flattening [53]. The recent IUPAC definition [9] of the halogen bond states that 'the forces involved in the formation of the halogen bond are primarily electrostatic, but polarisation, charge-transfer and dispersion contributions all play an important role'. A question thus arises as to whether the definition is sufficiently accurate and describes the unique phenomenon of the σ-hole of halogen bonding satisfactorily and fully.

Acknowledgements This work was part of the Research Project RVO: 61388963 of the Institute of Organic Chemistry and Biochemistry, Academy of Sciences of the Czech Republic. It was also supported by the Czech Science Foundation [P208/12/G016] and the operational program Research and Development for Innovations of the European Social Fund (CZ 1.05/2.1.00/03/0058). MHK acknowledges the kind support provided by the Alexander von Humboldt Foundation.

References

1. Hobza P, Müller Dethlef K (2009) Non-covalent interactions. Royal Society of Chemistry, Cambridge
2. Clark T, Hennemann M, Murray JS, Politzer P (2007) J Mol Model 13:291–296
3. Politzer P, Murray JS, Clark T (2013) Phys Chem Chem Phys 15:11178–11189
4. Politzer P, Murray JS (2013) ChemPhysChem 14:278–294
5. Murray J, Lane P, Politzer P (2009) J Mol Model 15:723–729
6. Řezáč J, Riley KE, Hobza P (2012) J Chem Theory Comput 8:4285–4292
7. Kozuch S, Martin JML (2013) J Chem Theory Comput 9:1918–1931
8. Deepa P, Sedlak R, Hobza P (2014) Phys Chem Chem Phys 16:6679
9. Desiraju GR, Ho PS, Kloo L, Legon AC, Marguardt R, Metrangolo P, Politzer P, Resnati G, Rissanen K (2013) IUPAC definition of halogen bond. Pure Appl Chem 8:1711–1713
10. Riley KE, Hobza P (2013) Phys Chem Chem Phys 15:17742
11. Kolář M, Hostaš J, Hobza P (2014) Phys Chem Chem Phys 16:9987
12. Kolář M, Carloni P, Hobza P (2014) Phys Chem Chem Phys 16:19111
13. Bader RFW, Carroll MT, Cheeseman JR, Chang C (1987) J Am Chem Soc 109:7968–7979
14. Dunning TH Jr (1989) J Chem Phys 90:1007
15. Woon DE, Dunning TH Jr (1993) J Chem Phys 98:1358
16. Adamo C, Barone V (1999) J Chem Phys 110:6158–6169
17. Peterson KA, Figgen D, Goll E, Stoll H, Dolg M (2003) J Chem Phys 119:11113
18. Frisch MJ, Trucks GW, Schlegel HB, Scuseria GE, Robb MA, Cheeseman JR, Scalmani G, Barone V, Mennucci B, Petersson GA, Nakatsuji H, Caricato M, Li X, Hratchian HP, Izmaylov AF, Bloino J, Zheng G, Sonnenberg JL, Hada M, Ehara M, Toyota K, Fukuda R, Hasegawa J, Ishida M, Nakajima T, Honda Y, Kitao O, Nakai H, Vreven T, Montgomery JA Jr, Peralta JE, Ogliaro F, Bearpark M, Heyd JJ, Brothers E, Kudin KN, Staroverov VN, Kobayashi R, Normand J, Raghavachari K, Rendell A, Burant JC, Iyengar SS, Tomasi J, Cossi M, Rega N, Millam JM, Klene M, Knox JE, Cross JB, Bakken V, Adamo C, Jaramillo J, Gomperts R, Stratmann RE, Yazyev O, Austin AJ, Cammi R, Pomelli C, Ochterski JW, Martin RL, Morokuma K, Zakrzewski VG, Voth GA, Salvador P, Dannenberg JJ, Dapprich S, Daniels AD, Farkas Ö, Foresman JB, Ortiz JV, Cioslowski J, Fox DJ (2009) Gaussian 09, revision D.01. Gaussian, Inc., Wallingford
19. Jeziorski B, Moszynski R, Szalewicz K (1994) Chem Rev 94:1887–1930
20. Hesselmann A, Jansen G (2002) Chem Phys Lett 357:464–470
21. Hesselmann A, Jansen G (2002) Chem Phys Lett 362:319–325

22. Misquitta AJ, Szalewicz K (2002) Chem Phys Lett 357:301–306
23. Jansen G, Hesselmann A (2001) J Phys Chem A 105:11156–11157
24. Hesselmann A, Jansen G (2003) Chem Phys Lett 367:778–784
25. Hesselmann A, Jansen G, Schütz M (2005) J Chem Phys 122:014103–014119
26. Hesselmann A, Jansen G, Schütz M (2006) J Am Chem Soc 128:11730–11731
27. Podeszwa R, Bukowski R, Szalewicz K (2006) J Phys Chem A 110:10345–10354
28. Williams HL, Chabalowski CF (2001) J Phys Chem A 105:646–659
29. Werner H-J, Knowles PJ, Manby FR, Schuetz M, Celani P, Knizia G, Korona T, Lindh R, Mitrushenkov A, Rauhut G, Adler TB, Amos RD, Bernhardsson A, Berning A, Cooper DLO, Deegan MJ, Dobbyn AJ, Eckert F, Goll F, Hampel C, Hesselmann A, Hetzer G, Hrenar T, Jansen G, Koeppl C, Liu Y, Lloyd AW, Mata RA, May AJ, McNicholas SJ, Meyer W, Mura ME, Nicklass A, Palmieri P, Pflueger K, Pitzer K, Reiher M, Shiozaki T, Stoll H, Stone AJ, Tarroni R, Thorsteinsson T, Wang M, Wolf A (2010) MOLPRO, version 2010.1, a package of ab initio programs. See http://www.molpro.net
30. TURBOMOLE V6.3 2011, a development of the University of Karlsruhe and the Forschungszentrum Karlsruhe GmbH, 1989–2007, TURBOMOLE GmbH, since 2007; http://www.turbomole.com
31. Price SL, Stone AJ, Lucas J, Rowland RS, Thornley AE (1994) J Am Chem Soc 116:4910–4918
32. Awwadi FF, Willett RD, Peterson KA, Twamley B (2006) Chem Eur J 12:8952–8960
33. Grimme S, Antony J, Ehrlich S, Krieg H (2010) J Chem Phys 132:154104
34. Munusamy E, Sedlak R, Hobza P (2011) ChemPhysChem 12:3253
35. Riley KE, Řezáč J, Hobza P (2013) J Mol Model 19:2879
36. Sedlak R, Deepa P, Hobza P (2014) J Phys Chem A 118:3846–3855
37. Lu YX, Fan J-C, Zaho W-N, Jiang Y-J, Yu Q-S (2009) J Comput Chem 30:725
38. Wang W (2011) J Phys Chem A 115:9294–9299
39. Chudzinski MG, Taylor MS (2012) J Org Chem 77:3483–3491
40. Trnka J, Sedlak R, Kolář M, Hobza P (2013) J Phys Chem A 117:4331–4337
41. Mukherjee A, Desiraju GR (2011) Cryst Growth Des 11:3735–3739
42. Cincic D, Friscic T, Jones W (2008) J Am Chem Soc 130:7524–7525
43. Cauliez P, Polo V, Roisnel T, Llusar R, Fourmigue M (2010) CrystEngComm 12:558–566
44. Cincic D, Friscic T, Jones W (2011) CrystEngComm 13:3224–3231
45. Jay JI, Padgett CW, Walsh RDB, Hanks TW, Pennington WT (2001) Cryst Growth Des 1:501–507
46. Zhao Y, Truhlar DG (2008) Theor Chem Acc 120:215–241
47. Boys SF, Bernardi F (2007) Mol Phys 19:553–566
48. Hesselmann A (2011) J Phys Chem A 115:11321–11330
49. Riley K, Murray J, Fanfrlík J, Řezáč J, Solá R, Concha M, Ramos F, Politzer P (2011) J Mol Model 17:3309–3318
50. Riley KE, Murray JS, Politzer P, Concha MC, Hobza P (2008) J Chem Theory Comput 5:155–163
51. Hardegger LA, Kuhn B, Spinnler B, Anselm L, Ecabert R, Stihle M, Gsell B, Thoma R, Diez J, Benz J, Plancher J-M, Hartmann G, Banner DW, Haap W, Diederich F (2011) Angew Chem Int Ed 50:314–318
52. Fanfrlík J, Kolář M, Kamlar M, Hurný D, Ruiz FX, Cousido-Siah A, Mitschler A, Řezáč J, Munusamy E, Lepšík M, Matějíček P, Veselý J, Podjarny A, Hobza P (2013) ACS Chem Biol 8:2484–2492
53. El Kerdawy A, Murray JS, Politzer P, Bleiziffer P, Heßelmann A, Görling A, Clark T (2013) J Chem Theory Comput 9:2264–2275

Top Curr Chem (2015) 359: 27–48
DOI: 10.1007/128_2014_588

Published online: 12 December 2014

Anion Recognition in Solution via Halogen Bonding

Mark S. Taylor

Abstract An overview of the interactions between anions and electron-deficient, covalently bound halogens is presented. It might be anticipated that species such as halides and oxoanions would be good acceptors of halogen bonds because of their relatively high charge densities and nucleophilicities. The stabilities of the trihalide anions X_3^- provide a clear indication that this is indeed the case. The thermodynamics of formation of the trihalides, and of analogous complexes between anions and monodentate haloorganics in organic solvent, are discussed in detail. Although the incorporation of multiple interacting groups to achieve high guest affinity has been a key principle of supramolecular chemistry for decades, it is only recently that multidentate halogen bond donors capable of anion recognition have been reported. This contribution highlights the range of architectures that have been employed as the basis for multidentate halogen bond donor design. Examples of selective and high-affinity anion recognition through halogen bonding, including implementations in polar, protic media, are discussed.

Keywords Anion recognition · Halogen bonding · Molecular recognition · Noncovalent interactions · Supramolecular chemistry

Contents

M.S. Taylor (✉)
Department of Chemistry, University of Toronto, 80 St. George Street, Toronto, ON, Canada, M5S 3H6
e-mail: mtaylor@chem.utoronto.ca

Abbreviations

Ac	Acetyl
Ar	Aryl
B3LYP	Becke 3-parameter Lee–Yang–Parr functional
Bu	Butyl
Bz	Benzoyl
Cy	Cyclohexyl
DFT	Density functional theory
DMSO	Dimethyl sulfoxide
Et	Ethyl
H	Enthalpy
K_a	Association constant
M	Mole per liter
Me	Methyl
Mes	Mesityl
MP2	Second-order Møller–Plesset perturbation theory
NMR	Nuclear magnetic resonance
Ph	Phenyl
Pr	Propyl
S	Enthalpy
T	Temperature
t-Bu	*tert*-Butyl
Tf	Trifluoromethanesulfonyl (triflyl)
THF	Tetrahydrofuran
Ts	Tosyl, 4-toluenesulfonyl
UV–vis	Ultraviolet–visible
X	Generic halogen substituent

1 Introduction

The varied sizes, shapes, charge distributions, and basicities of anions provide an interesting set of challenges for the design of selective receptors. Research on anion recognition chemistry can be traced back to the late 1960s and 1970s [1–3], and the field remains a topical and active one [4]. The prospects of gaining insight into the thermodynamics of noncovalent interactions and solvation/desolvation phenomena, and of developing new tools for anion analysis, separation, and sequestration

continue to motivate research in this area. Synthetic anion transporters [5] and anion-binding catalysts [6] represent another set of emerging applications.

The majority of synthetic anion receptors developed to date interact with their guests through hydrogen bonding, ion-pairing, or Lewis acid–base interactions. The fact that halogen bonding is a directional interaction which requires a relatively electron-rich acceptor species suggests that it is worthy of consideration as a basis for anion receptor design, but it is only recently that systematic attempts to develop multidentate halogen bond donors capable of anion binding have been reported. In a relatively short period of time, it has become clear that halogen bonding can be employed to achieve high-affinity anion recognition, and hints that it may offer unique features and opportunities in this regard have begun to emerge.

This chapter provides an overview of the interactions between anions and halogen bond donors in the solution phase. Section 2 deals with monodentate halogen bond donors, and includes a discussion of the well-characterized trihalide anions as well as the weaker interactions between anions and haloorganics. Because pronounced solvent effects often complicate the interpretation of anion binding data, the available gas-phase thermochemical data are discussed for comparison with the solution-phase results. Incorporating multiple haloorganic donor groups into appropriate architectures allows for enhanced affinity caused by the chelate effect: multidentate receptors of this type are discussed in Sect. 3. Another useful strategy for increasing affinity is the use of cationic halogen bond donors, which benefit from a Coulombic contribution to their interactions with anions. Section 4 outlines the utility of such donors for anion recognition, including systems that function in polar, protic media. Finally, Sect. 5 describes receptors that bind to anionic guests through combinations of halogen bonding and halogen bonding.

2 Interactions of Anions with Monodentate Halogen Bond Donors

2.1 Molecular Halogen or Interhalogen Donors

Interactions between anions and halogens X_2 or interhalogens X–Y are among the most widely studied and extensively characterized subclasses of halogen bonds. The trihalides X_3^- and mixed trihalides X_2Y^- are familiar, textbook examples: it was in the context of these species that the concepts of hypervalency and 3-center, 4-electron bonding were elucidated [7, 8]. Numerous computational investigations of their molecular and electronic structures have been undertaken [9–12], along with detailed experimental studies. Their geometries have been probed by crystallography: the reported structural data for triiodide (I_3^-) salts reveal a pronounced preference for the linear geometry, although the bond distances and degree of symmetry vary significantly as a function of local environment in the solid state [13].

Table 1 Equilibrium constants for the formation of trihalide ions in solution ($X^- + X_2 \rightarrow X_3^-$)

Solvent	Anion	K_a (M^{-1})
Water	Cl_3^-	0.19
	Br_3^-	16
	I_3^-	7.2×10^2
Acetonitrile	Cl_3^-	10^{10}
	Br_3^-	10^7
	I_3^-	4.0×10^6
Acetone	Cl_3^-	$>10^{12}$
	Br_3^-	2.0×10^9
	I_3^-	2.0×10^8
Nitromethane	Cl_3^-	$>10^{13}$
	Br_3^-	2.0×10^7
	I_3^-	5.0×10^6

Structural and thermodynamic data for isolated trihalide ions in the gas phase are also available. Flowing afterglow–tandem mass spectrometry has been employed to determine the bond strengths for I_3^-, Br_3^-, Cl_3^-, and F_3^- [14, 15]. The gas-phase bond enthalpies at 298 K for these four ions are $DH^{298}(X_2\text{–}X^-) = 126$, 127, 100, and 101 kJ/mol, respectively, with the values for I_3^- and Br_3^- being among the highest halogen bond energies reported to date. Although Cl_3^- and F_3^- possess weaker bonds than the heavier trihalides, the fact that this drop-off is not precipitous has been used as an argument against bonding models involving a key role for d orbitals. The data for trifluoride anion constitute a rare example of a thermodynamically characterized halogen bond involving covalently bound fluorine as a donor site [16]. Trifluoride can be observed at low temperature in an inert gas matrix but is unstable in solution.

Equilibrium constants for the formation of trihalides (i.e., $K_a = [X_3^-]/[X_2][X^-]$) in a wide range of solvents have been reported. Spectrophotometric titrations and voltammetry are among the methods employed for these determinations. Whereas the association constants in water parallel the trend in gas-phase bond enthalpy ($I_3^- > Br_3^- > Cl_3^-$), this trend is reversed in organic solvents (Table 1) [17, 18]. The results highlight the often dominant contribution of solvation energies to the overall thermodynamics of anion–molecule interactions in solution [19].

2.2 *Monodentate Haloorganic Donors*

Interactions of anions with uncharged, organic halogen bond donors, while generally less favorable than those involving molecular halogens as donors, have been documented experimentally in numerous studies. In the solid state, short contacts between anions and halogenated organics are relatively common [20, 21]. The preference for a 180° $A^-\cdots X\text{–}C$ angle which is a general feature of halogen bonding is evident in these structures, along with a lengthening of the C–X bond

Table 2 Experimental and calculated (B3LYP/6-311 + G(3df)-LANL2DZ) enthalpies of interaction between halides and halotrifluoromethanes in the gas phase at 298 K

Complex	ΔH (experiment, kJ/mol)	ΔH (calculated, kJ/mol)
$Cl^- \cdots BrCF_3$	−69.0	−62.3
$Br^- \cdots BrCF_3$	−58.2	−52.3
$Cl^- \cdots ICF_3$	−98.7	−90.0

upon anion complexation in the majority of instances. However, variations in the number and arrangement of donor groups around each anionic acceptor give rise to diverse architectures. When anions capable of accepting more than one halogen bond (such as halides, which often interact with two or three donors in the solid state) are combined with multidentate donors, two- or three-dimensional networks are formed. Metrangolo and co-workers have used the solid-state halogen bonding of anions to achieve the separation of mixtures of α,ω-diiodoperfluoroalkanes of varying length into individual components [22]. Such methods are desirable because the telomerization process used for production-scale synthesis of α,ω-diiodoperfluoroalkanes generally results in a distribution of chain lengths. Size matching between an α,ω-bis(trimethylammonium)-functionalized alkane $Me_3N^+(CH_2)_{m+6}NMe_3^+$ and the halogen-bonded "superanion" $I^- \cdots I(CF_2)_mI \cdots I^-$ resulted in selective co-crystallization, enabling the isolation of an α,ω-diiodoperfluoroalkane of given length.

Complexes of anions with haloorganics have been characterized in the gas phase. Using pulsed-ionization high-pressure mass spectrometry, Bogdanov and McMahon determined the enthalpies of complexation for several halide–halotrifluoromethane adducts [23]. Their experimental data, along with enthalpies of interaction calculated at the B3LYP/6-311 + G(3df) level of theory (using the LANL2DZ basis set for iodine), are assembled in Table 2. Trends that can be inferred from the experimental data include the higher acceptor ability of the charge-dense chloride relative to bromide, and the higher halogen bond donor ability of ICF_3 relative to $BrCF_3$. A comparison of the enthalpies of interaction of bromide with Br_2 (−127 kJ/mol, previous section) and $BrCF_3$ (−58.2 kJ/mol) emphasizes the higher halogen bond donor ability of the molecular halogens relative to haloorganics. The correspondence between experimental and computational data from Table 2 is quite good, considering that the B3LYP functional might not be expected to account fully for contributions of dispersion to the halogen bonding interactions.

Interactions between iodoperfluorooctane $C_8F_{17}I$ and anions have been studied in the gas phase using blackbody infrared radiative dissociation (BIRD) [24]. Values of the critical dissociation energy E_0 were determined by master equation modeling of the BIRD data to be 100 ± 7 and 81.5 ± 6 kJ/mol, respectively, for the $Br^- \cdots IC_8F_{17}$ and $I^- \cdots IC_8F_{17}$ complexes. The preferred binding of the more charge-dense Br^- over I^- is consistent with the data from Table 2, and is in line with the trend of calculated energies of interaction between the halides and iodoperfluorobutane at the B3LYP and MP2 levels of theory [25].

Table 3 Association constants K_a for interactions between $Bu_4N^+Br^-$ and monodentate organic halogen bond donors in organic solvent

Donor	Solvent	K_a (M^{-1})	References
Bromine-based donors			
Br_3CH	CH_2Cl_2	0.33	[28]
Br_3CCO_2H	CH_2Cl_2	0.8	[28]
Br_3CF	CH_2Cl_2	1.0	[28]
$Br_3CCOCBr_3$	CH_2Cl_2	2.4	[28]
Br_4C	CH_2Cl_2[a]	2.8	[26]
Br_3CNO_2	CH_2Cl_2	8.5	[28]
Br_3CCN	CH_2Cl_2	9.9	[28]
BrCN	CH_2Cl_2	21	[28]
Iodine-based donors			
$I_2C{=}CI_2$	Acetonitrile	57	[30]
$I(CF_2)_2I$	Acetonitrile	67	[29]
IC_6F_5	Acetone	1.0×10^2	[25]
IC_8F_{17}	Acetone	1.0×10^3	[25]

[a]Pr_4N^+ salt used

Several types of monodentate, organic halogen bond donor interact favorably enough with anions to enable determinations of binding constants in organic solvent. For certain donors, changes in UV–vis spectra accompany addition of anionic acceptors, enabling spectrophotometric titrations: for example, for electron-deficient bromomethanes, anion complexation is often signaled by the appearance of a low-energy charge transfer band [26–30]. In the case of fluorinated donors, upfield changes in ^{19}F chemical shift of nearby fluorine substituents are characteristic of halogen bonding, and permit determinations of binding constants by nuclear magnetic resonance (NMR) titrations [25, 31]. Representative data for interactions of tetraalkylammonium bromides with diverse classes of bromo- and iodo-based monodentate organic donors are assembled in Table 3. Enthalpies and entropies of interaction of bromide with the bromine-based donors have been determined by van't Hoff plot analysis: the entropies of interaction are negative, and show relatively little variation across the series of donors examined (values of $T\Delta S$ ranging from -1.7 to -9.2 kJ/mol were determined) [28]. For a subset of donors, association constants with a range of anions have been reported; data of this type are assembled in Table 4.

A detailed analysis of trends in the thermodynamic and spectral data for bromocarbon–bromide complexes has been conducted [28]. The authors noted a linear correlation between the frequencies of the charge-transfer bands for the complexes and the energies of the lowest unoccupied molecular orbitals of the acceptors, in agreement with Mulliken's theory of charge-transfer interactions [32]. The anion–molecule adducts were modeled by computation at several levels of theory, including DFT (with the ωB97X-D, M06-2X and B97-1 functionals) and MP2 methods. Correlations between experimental free energies of binding and calculated electronic interaction energies were noted, and time-dependent DFT (TD-DFT) calculations provided simulated spectra for the complexes which were

Table 4 Association constants K_a for interactions between $R_4N^+X^-$ and monodentate organic halogen bond donors in organic solvent

Complex	Solvent/counterion	K_a (M^{-1})	References
$Cl^-\cdots Br_4C$	CH_2Cl_2/Pr_4N^+	3.0	[26]
$Br^-\cdots Br_4C$	CH_2Cl_2/Pr_4N^+	2.8	[26]
$I^-\cdots Br_4C$	CH_2Cl_2/Pr_4N^+	3.2	[26]
$SCN^-\cdots Br_4C$	CH_2Cl_2/Bu_4N^+	0.8	[27]
$Cl^-\cdots IC_6F_5$	Acetone/Bu_4N^+	1.5×10^2	[25]
$Br^-\cdots IC_6F_5$	Acetone/Bu_4N^+	1.0×10^2	[25]
$I^-\cdots IC_6F_5$	Acetone/Bu_4N^+	44	[25]
$TsO^-\cdots IC_6F_5$	Acetone/Bu_4N^+	<5	[25]
$NO_3^-\cdots IC_6F_5$	Acetone/Bu_4N^+	<5	[25]
$Cl^-\cdots IC_8F_{17}$	Acetone/Bu_4N^+	2.2×10^3	[25]
$Br^-\cdots IC_8F_{17}$	Acetone/Bu_4N^+	1.0×10^3	[25]
$I^-\cdots IC_8F_{17}$	Acetone/Bu_4N^+	3.3×10^2	[25]

in reasonably good agreement with the experimental data. Natural bond orbital analysis was used to approximate the extent of charge transfer ΔQ upon binding, along with the stabilization energy E_{CT} resulting from orbital mixing. The results suggested a significant contribution of orbital interactions to the formation of this class of halogen-bonded complexes. A trend is not evident from the free energies of interaction of Cl^-, Br^-, and I^- with CBr_4 (Table 4), in contrast to the gas-phase data for $BrCF_3$ and the solution-phase data for iodoperfluoroorganic donors (see below).

Iodoperfluoroorganics interact favorably with halide ions in acetone or acetonitrile solvent, as probed by ^{19}F NMR titrations [25, 31] or UV–vis spectroscopy [29] (Table 3). The superior donor ability of iodoperfluorooctane relative to iodoperfluorobenzene which can be inferred from the binding constants with Br^- also holds for uncharged acceptors [33]. The data in Table 4 reveal a preference for interactions with the lighter halides ($K_a(Cl^-) > K_a(Br^-) > K_a(I^-)$), in accordance with gas-phase thermodynamic data and computational modeling. The association constant between $Bu_4N^+Cl^-$ and $C_8F_{17}I$ is solvent-dependent: K_a values of 1.3×10^2, 32, and 31 M–1 were determined in acetone, DMSO, and dichloromethane, respectively [25]. The halogen bond donor ability of tetraiodoethylene towards bromide is similar to those of the fluorinated organics discussed above. This observation may be consistent with computational studies, suggesting that polarizable iodo substituents can enhance halogen bond donor ability to a greater extent than might be expected based on electrostatic trends alone [34].

Anion binding by iodoperfluoroalkanes and -arenes underlies the ability of these compounds to facilitate the transport of anions across lipid bilayers, apparently by a cooperative mechanism involving complexes of higher than 1:1 stoichiometry [35]. Compounds having multiple C–I bonds – as components of ditopic ion transporters [36] or rigid-rod scaffolds [37] – also show interesting activities in this

regard. This application of halogen bonding is discussed in detail in the chapter authored by S. Matile in this volume.

3 Multidentate Halogen Bond Donors as Anion Receptors

The chelate effect is among the key principles of supramolecular chemistry, and a multitude of examples illustrate how high-affinity anion recognition can be achieved by arranging multiple hydrogen bond donor groups into an appropriate orientation using a pre-organized scaffold [38]. The first reported study of anion binding by a receptor bearing multiple halogen bond donor groups was carried out by Metrangolo and co-workers [39]. Ion-pair complexation was targeted in the design of podand **1a**: the receptor was expected to interact with alkali metal cations through its tris(2-alkoxyethyl)amine moiety and with anions by halogen bonding with its iodoperfluorophenoxy groups (Fig. 1). Compound **1b**, having a fluorine substituent in place of the iodo group, was prepared as a control to probe the importance of halogen bonding. Evidence for ion-pair complexation by **1a** was obtained by electrospray ionization mass spectrometry (ESI-MS), which revealed mass/charge ratios corresponding to $[\mathbf{1a} + \mathrm{M}]^+$ and $[\mathbf{1a} + \mathrm{Cl}]^-$ from samples prepared by mixing **1a** with alkali metal salts MCl. The association constant with NaI in $CDCl_3$ was determined to be 2.6×10^5 M^{-1} by NMR spectroscopy, using a competitive binding assay. A value of 1.3×10^4 M^{-1} was found for the **1b**–NaI association constant under these conditions, suggesting that halogen bonding stabilizes the **1a**–NaI complex by roughly 7 kJ/mol. The magnitude of this effect suggests that, in solution, only one of the iodoperfluorophenoxy groups of **1a** interacts with iodide via halogen bonding. The solid-state structure of the NaI adduct, determined by X-ray crystallography, was consistent with this type of binding mode.

Attempts to design receptors that orient multiple iodoperfluoroorganic groups appropriately for bi- or tridentate halogen bonding with an anionic guest have been focused largely on *ortho*-substituted iodoperfluorobenzene moieties. Taylor and co-workers have investigated several scaffolds and linking strategies (Fig. 2). Ethynylene- and butadiynylene-linked receptors **2a** and **2b** were accessed using controlled Sonogashira coupling of 1,2-dioodotetrafluorobenzene as a key step, albeit in modest yield to due challenging separations of byproducts of

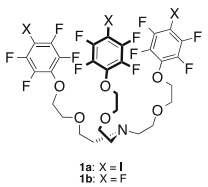

Fig. 1 Ion-pair receptors **1a** and **1b**

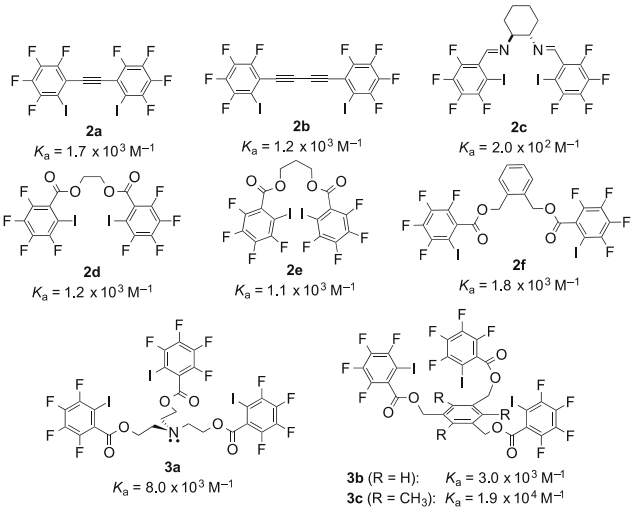

Fig. 2 Bis- and tris(iodoperfluoroarene) anion receptors **2a**–**3c**. Association constants K_a with $Bu_4N^+Cl^-$ (acetone, 295 K) are listed

similar polarity. On the other hand, 2-iodotetrafluorobenzaldehyde and 2-iodotetrafluorobenzoic acid proved to be useful building blocks for the construction of multidentate receptors by high-yielding imine formation (**2c**) or esterification reactions (**2d**–**2f**, **3a**–**3c**). Association constants with $Bu_4N^+Cl^-$, as determined by ^{19}F NMR titrations in acetone solvent, are assembled in Fig. 2 [25, 31]. The binding data suggest that these receptors indeed act as multidentate halogen bond donors towards chloride: K_a values for bis(iodoperfluorenes) **2a**–**2f** are up to an order of magnitude higher than that of C_6F_5I (see the previous section), and another increase in K_a of roughly an order of magnitude was obtained for tris (iodoperfluoroarene) **3c**. Job plot analysis was consistent with a 1:1 complexation mode, which was further supported by computational modeling of the **2a**–Cl^-, **2b**–Cl^-, and **3c**–Cl^- adducts. However, when co-crystallized with $Bu_4N^+I^-$, **2b** was found to form zigzag-type chains in the solid state [40]. The higher chloride affinity of hexasubstituted **3c** relative to trisubstituted **3b** is consistent with a beneficial preorganizing role for the methyl groups of **3c** [41].

Solvent effects on the **3c**–Cl^- interaction have been investigated [25]. The association constant was found to be lower in halogenated solvents than in acetonitrile: K_a values of 31 and 6 M^{-1} were determined in CH_2Cl_2 and $CHCl_3$, respectively. The magnitude and direction of this effect are higher than would be predicted based on solvent polarity alone. It may be that the halogenated solvents are acting as competitive hydrogen and/or halogen bond donors towards chloride. Acetone and DMSO, solvents capable of acting as oxygen-centered Lewis bases, gave rise to association constants of 5.0×10^3 and 13 M^{-1}, respectively.

Association constants between **3c** and a range of anions are assembled in Table 5. The relative affinities of the halides ($Cl^- > Br^- > I^-$) and the preferred binding of halides over oxoanions such as toluenesulfonate, nitrate, and bisulfate were

Table 5 Association constants K_a for interactions between $Bu_4N^+X^-$ and tridentate halogen bond donor **3c** (acetone, 295 K)

Anion X^-	K_a (M^{-1})
Cl^-	1.9×10^4
Br^-	3.8×10^3
I^-	7.6×10^2
TsO^-	10
NO_3^-	<10
HSO_4^-	<10

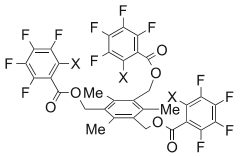

4a: X = F
4b: X = H
4c: X = Br

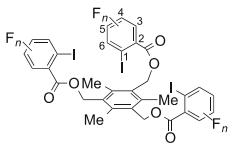

5a: 3-F **6a**: 3,4-F_2 **7**: 4,5,6-F_3
5b: 4-F **6b**: 3,6-F_2
5c: 5-F **6c**: 4,5-F_2

Fig. 3 Derivatives of receptor **3c** varying in the donor group and number/position of fluorine substituents

Table 6 Association constants K_a for interactions of receptors **4a**–**7** with $Bu_4N^+Cl^-$ (acetone, 295 K)

Receptor	K_a (M^{-1})
4a	<5
4b	<5
4c	<10
5a	18
5b	3
5c	7
6a	38
6b	2.2×10^2
6c	15
7	2.8×10^2

consistent with the data for the monodentate donor C_6F_5I (see above) and for bidentate **2b**. Receptor decomposition prevented determination of association constants with more basic anions such as acetate, dihydrogenphosphate, and fluoride. It should be noted that, for bidentate **2f**, the gas-phase critical dissociation energies E_0 (as determined based on data from BIRD experiments – see above) decreased in the order $E_0(NO_2^-) > E_0(I^-) > E_0(TsO^-, HSO_4^-)$ [24]. This result – in particular, the altered 'order' of binding to iodide and nitrate in the gas phase vs acetone solvent – points to a role for solvent in the unusual anion selectivity of the iodoperfluorobenzoate-based multidentate halogen bond donors.

Derivatives of receptor **3c** that bear other substituents in place of the crucial 2-iodo donor group have been prepared (Fig. 3, Table 6). Perfluorinated control **4a** did not interact to a measurable extent with $Bu_4N^+Cl^-$ under these conditions, suggesting that the complexation of Cl^- by **3c** is driven by halogen bonding and not anion–arene interactions [42, 43]. Receptor **4b**, in which the iodo substituent is

replaced by hydrogen, could potentially interact with anions through C–H···X^- hydrogen bonding, but showed no measurable chloride affinity in acetone solvent. The attenuated halogen bond donor ability of the lighter halogens is evident in the low association constant of tris(bromoperfluorobenzoate) **4c**. The effects of varying the number and position of fluoro substituents on the tris(iodobenzoate) receptor have also been investigated (**5a**–**5c**, **6a**–**6c**, and **7**). Removal of fluoro substituents had a dramatic, deleterious effect on halogen bond donor ability: the association constants of monofluorinated **5a**–**5c** for $Bu_4N^+Cl^-$ in acetone were found to be 3–4 orders of magnitude lower than that of **3c**. Obtaining quantitative data for interactions of weak halogen bond donor group of this type would be challenging without the chelate effect of the tridentate receptor. A linear free energy relationship between $\log(K_a)$ and the calculated electrostatic potential at iodine was noted for this series of receptors varying in fluorine substitution. This observation is consistent with the 'σ-hole' model of halogen bonding [44], and is in line with trends expected based on computation [45].

Huber and co-workers have reported the synthesis and anion-binding properties of iodinated perfluorotriaryls **8a** and **8b** (Fig. 4) [46]. Association constants with tetrabutylammonium chloride and bromide were determined by isothermal titration calorimetry (ITC) in THF solvent. The ITC data were consistent with a 1:1 binding stoichiometry, and indicated that binding is enthalpically driven under these conditions, with only a minor entropic contribution ($-5.1 < T\Delta S < +2.4$ kJ/mol). The halide affinities of these neutral, bidentate halogen bond donors are remarkably high. The solid-state structure of the **8b**–Cl^- complex (tris(dimethylamino) cyclopropenium countercation) showed the expected bifurcated halogen bond in which one iodine group from each diiodotrifluorophenyl group interacts with chloride. Receptors **8a** and **8b** proved to be active catalysts for the reaction of 1-chloroisochroman with silyl ketene acetals, presumably by a mechanism involving chloride abstraction by the multidentate halogen bond donor. This type of halogen bond-promoted reactivity is discussed by Huber and co-workers in another chapter of this volume.

A picket-fence zinc(II) porphyrin bearing four halogen bond-donor iodotriazole groups has been synthesized by Beer and co-workers (Fig. 5) [47]. Halogen bond donor **9a** and control **9b**, which lacks the iodo substituent, were prepared from an azidoacetate-substituted Zn(II) porphyrin by copper-catalyzed Huisgen cycloadditions. Addition of anions to **9a** and **9b** was accompanied by a bathochromic shift of the Soret band in the UV–vis spectrum, probably signaling axial ligation to the Zn(II) porphyrin. Association constants determined from the concentration

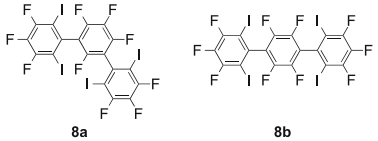

8a
$K_a(Cl^-) = 1.8 \times 10^4\ M^{-1}$
$K_a(Br^-) = 1.3 \times 10^4\ M^{-1}$

8b
$K_a(Cl^-) = 7.5 \times 10^4\ M^{-1}$
$K_a(Br^-) = 6.2 \times 10^4\ M^{-1}$

Fig. 4 Iodinated perfluorotriaryl anion receptors **8a** and **8b**. Association constants K_a with $Bu_4N^+X^-$ (THF, 303 K) are listed

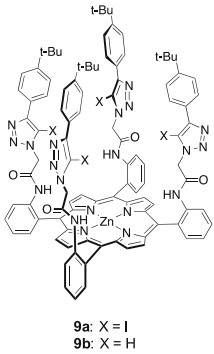

Fig. 5 Structures of iodotriazole-functionalized picket-fence Zn (II) porphyrin **9a** and control receptor **9b**

Table 7 Association constants K_a for interactions between halogen bond-donor porphyrin **9a** or control receptor **9b** with tetrabutylammonium salts $Bu_4N^+X^-$ (chloroform, 293 K)

Receptor	Anion X^-	K_a (M^{-1})
9a	Cl^-	3.6×10^3
9a	Br^-	1.1×10^3
9a	I^-	3.0×10^2
9a	AcO^-	2.6×10^5
9a	$H_2PO_4^-$	$>10^6$
9a	SO_4^{2-}	$>10^6$
9b	Cl^-	2.6×10^3
9b	Br^-	6.8×10^2
9b	I^-	1.5×10^2
9b	AcO^-	3.4×10^5
9b	$H_2PO_4^-$	$>10^6$
9b	SO_4^{2-}	$>10^6$

dependence of this spectral change are assembled in Table 7. For control receptor **9b**, a downfield shift in the ^{1}H NMR signal corresponding to the triazole CH hydrogen was observed upon anion addition, consistent with C–H$\cdots$X$^-$ hydrogen bonding. Either UV–vis spectroscopy or ^{1}H NMR could thus be employed to determine association constants of anions with this receptor. Table 7 indicates that both **9a** and **9b** interact most favorably with relatively basic anions, although the preference for dihydrogenphosphate over acetate runs counter to this trend and may reflect discrimination based on guest shape. A comparison of the binding data for the two receptors suggests that the halogen bond donor groups enhance the binding of halides over oxoanions, in accord with other studies (see above). Solvent effects on the anion affinities of **9a** and **9b** were also probed. These were particularly pronounced for halogen bond donor **9a**: the **9a**–Cl^- association constant was roughly 75-fold higher in acetonitrile than in chloroform, whereas the **9b**–Cl^- association constant varied by only 13-fold in these two solvents.

4 Anion Recognition with Cationic Halogen Bond Donors

Hydrogen bond-donating anion receptors that function in competitive solvents (i.e., polar, protic media such as water) frequently make use of cationic donor sites such as ammonium or guanidinium groups, thus benefiting from a favorable Coulombic attraction to their guests [48]. Similarly, cationic halogen bond donor groups have proved to be useful for achieving anion recognition in polar solvents. Key initial steps in this direction were reported by Beer and co-workers, who showed that chloride–haloimidazolium halogen bonding could be used to template the formation of a pseudorotaxane [49], and then extended this concept to develop an iodotriazolium-based rotaxane capable of binding to halides in a ternary chloroform/methanol/water mixture [50]. These systems involve anion binding through the combined action of halogen and hydrogen bond donor groups, and are discussed in the next section.

Building on this foundation, the Beer group designed bromoimidazoliophane $\mathbf{10a}^{2+} \cdot 2PF_6^-$ as a bidentate, charge-assisted halogen bond donor (Fig. 6) [51]. Because of restricted rotation about the C–C bonds of the macrocycle, $\mathbf{10a}^{2+} \cdot 2Br^-$ was synthesized as a mixture of *syn* and *anti* conformers, which were separated by recrystallization. Imidazoliophane $\mathbf{10b}^{2+} \cdot 2PF_6^-$, which was synthesized to gauge the contribution of halogen bonding to the anion affinity of $\mathbf{10a}^{2+}$, did not show this atropisomerism, presumably because of the reduced steric demand of the imidazolium groups lacking the bromo substituent. In the solid state, both the *syn* and *anti* isomers of $\mathbf{10a}^{2+}$ formed halogen-bonded complexes with Br^-, with bidentate complexation being observed for the former and 1:1 imidazolium–anion interactions in the latter. Association constants for anion binding by *syn*-$\mathbf{10a}^{2+} \cdot 2PF_6^-$ and $\mathbf{10b}^{2+} \cdot 2PF_6^-$ were determined by ^{1}H NMR titrations in a 9:1 CD_3OD/D_2O solvent mixture (Table 8). The high affinities of the halogen

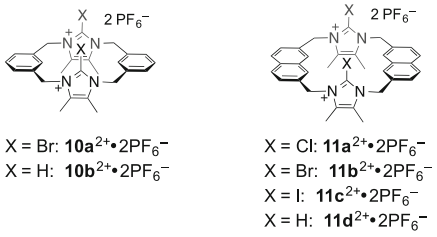

Fig. 6 Bidentate haloimidazoliophane receptors $\mathbf{10a}^{2+} \cdot 2PF_6^-$ and $\mathbf{11a}^{2+}$–$\mathbf{11c}^{2+} \cdot 2PF_6^-$, and non-halogenated control imidazoliophanes $\mathbf{10a}^{2+} \cdot 2PF_6^-$ and $\mathbf{11d}^{2+} \cdot 2PF_6^-$

Table 8 Association constants K_a for interactions between bromoimidazoliophane $\mathbf{10a}^{2+} \cdot 2PF_6^-$ or control imidazoliophane $\mathbf{10b}^{2+} \cdot 2PF_6^-$ with tetrabutylammonium salts $Bu_4N^+X^-$ (9:1 CD_3OD/D_2O, 293 K)

Anion	K_a with $\mathbf{10a}^{2+} \cdot 2PF_6^-$ (M^{-1})	K_a with $\mathbf{10b}^{2+} \cdot 2PF_6^-$ (M^{-1})
Cl^-	<10	1.3×10^2
Br^-	8.9×10^2	1.3×10^2
I^-	1.8×10^2	1.0×10^2

bond donor for Br^- and I^- in this competitive solvent are noteworthy, as are the clear differences in the anion recognition properties of $\mathbf{10a}^{2+}$ and $\mathbf{10b}^{2+}$. It is probable that the rigid structure of $\mathbf{10a}^{2+}$ contributes to the selective binding of Br^- over Cl^- and I^-.

Related haloimidazoliophane structures $\mathbf{11a}^{2+}$–$\mathbf{11c}^{2+}$ having a naphthyl-based linker in place of *m*-xylylene group of $\mathbf{10a}^{2+}$ have been explored by the Beer group (Fig. 6) [52]. It was anticipated that this change of linker group could not only alter the dimensions of the macrocycle but also give rise to emissive behavior which would allow for the prospect of a fluorescence-based response to anion binding. The rates of *syn/anti* conformational interconversion – akin to the process described above for $\mathbf{10a}^{2+}$ – varied according to the size of the imidazolium substituent X, decreasing in the order X = H > Cl > Br > I. For iodoimidazolium $\mathbf{11c}^{2+}$, bond rotation was sufficiently slow at room temperature to allow for isolation of the *syn* and *anti* isomers. Solid-state structures of the $\mathbf{11c}^{2+} \cdot Br^- \cdot PF_6^-$ and $\mathbf{11c}^{2+} \cdot I^- \cdot PF_6^-$ complexes revealed a 2:2 receptor:anion complexation mode rather than the 1:1 bidentate coordination observed for $\mathbf{10a}^{2+}$. Solution-phase interactions of $\mathbf{11b}^{2+}$ and $\mathbf{11c}^{2+}$ with anions were probed by fluorescence spectroscopy, taking advantage of the increase in quantum yield and the appearance of a new, red-shifted feature in the emission spectrum upon anion binding. Of the anions investigated (F^-, Cl^-, Br^-, I^-, NO_3^-, $H_2PO_4^-$, SO_4^{2-}, BzO^-, and AcO^-), only bromide and iodide gave rise to fluorescence responses from which association constants could be inferred (Table 9). The high halide affinities of these receptors, and their abilities to signal binding by a fluorescence change, are significant results, as is the apparent size-matching effect which gives rise to the preference of $\mathbf{11b}^{2+}$ for iodide and $\mathbf{11c}^{2+}$ for bromide. Diffusion-ordered NMR spectroscopy (DOSY) suggested that, in solution, 1:1 receptor:halide complexes predominated, rather than the 2:2 complexes observed by X-ray crystallography. Neither the imidazolium $\mathbf{11d}^{2+}$ nor the chloroimidazolium $\mathbf{11a}^{2+}$ showed emission responses upon anion addition, although ^{1}H NMR could be used to determine association constants of 19, 85, and 80 M^{-1} for the $\mathbf{11d}^{2+}$–Cl^-, $\mathbf{11d}^{2+}$–Br^-, and $\mathbf{11d}^{2+}$–I^- complexes, respectively.

Metrangolo and co-workers have studied the interactions of anions with receptors $\mathbf{12a}^+ \cdot I^-$ and $\mathbf{12b}^+ \cdot I^-$, each bearing a single haloimidazolium moiety (Fig. 7) [53]. Association constants were determined by ^{1}H NMR titrations with tetrabutylammonium salts $Bu_4N^+X^-$ in d_6-DMSO, and compared to those of the corresponding imidazolium $\mathbf{12c}^+ \cdot I^-$ lacking the halo substituent (Table 10). Whereas bromoimidazolium $\mathbf{12b}^+$ showed no evidence of anion binding under

Table 9 Association constants K_a for interactions between bromoimidazoliophane $\mathbf{11b}^{2+} \cdot 2PF_6^-$ or iodoimidazoliophane $\mathbf{11c}^{2+} \cdot 2PF_6^-$ with tetrabutylammonium salts $Bu_4N^+X^-$ (9:1 CH_3OH/H_2O, 293 K)

Anion	K_a with $\mathbf{11b}^{2+} \cdot 2PF_6^-$ (M^{-1})	K_a with $\mathbf{11c}^{2+} \cdot 2PF_6^-$ (M^{-1})
Br^-	2.88×10^4	9.55×10^5
I^-	6.31×10^5	3.71×10^4

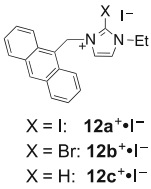

Fig. 7 Iodoimidazolium $\mathbf{12a}^+ \cdot I^-$, bromoimidazolium $\mathbf{12b}^+ \cdot I^-$, and control imidazolium $\mathbf{12c}^+ \cdot I^-$

Table 10 Association constants K_a for interactions between receptors $\mathbf{12a}^+ \cdot I^-$ or $\mathbf{12c}^+ \cdot I^-$ with tetrabutylammonium salts $Bu_4N^+X^-$ (d_6-DMSO, 300 K)

Anion	K_a with $\mathbf{12a}^+ \cdot I^-(M^{-1})$	K_a with $\mathbf{12c}^+ \cdot I^-(M^{-1})$
Cl^-	1.5×10^2	9
Br^-	67	–
I^-	34	–
AcO^-	2.6×10^2	23
$H_2PO_4^-$	1.1×10^3	26

these conditions, iodoimidazolium $\mathbf{12a}^+$ displayed modest affinity for the halides, and relatively strong binding to $H_2PO_4^-$. This constitutes a rare example of a halogen bonding-based receptor showing a preference for oxoanions over halides. A single crystal X-ray structure of the $\mathbf{12a}^+ \cdot H_2PO_4^-$ was determined, which revealed a short $I \cdots O^-$ bond distance of 2.60 Å and a 177.8° C–$I \cdots O^-$ angle, both consistent with formation of a strong halogen bond. The parent imidazolium $\mathbf{12c}^+ \cdot I^-$ showed only weak anion binding in d_6-DMSO.

The group of Huber has conducted a systematic investigation of the anion binding behavior of bis(haloimidazolium)-type bidentate halogen bond donors [54]. Compounds explored in their study are depicted in Fig. 8. Bidentate donors of this type had previously been identified as halide-abstracting promoters of Ritter reactions of benzhydryl bromide [55]. Detailed descriptions of this reactivity, and of the thermodynamics of anion binding by these receptors, are provided in another chapter of this volume. Data for interactions of halides with the haloimidazolium receptors in acetonitrile solvent, as determined by isothermal titration calorimetry (ITC), are assembled in Table 11. Whereas the bis(iodoimidazoliums) $\mathbf{13a}^{2+}$ and $\mathbf{13a}^{2+}$ displayed high halide affinities under these conditions, the control imidazoliums $\mathbf{13c}^{2+}$ and $\mathbf{14b}^{2+}$ did not give rise to a measurable ITC signal upon addition of $Bu_4N^+Br^-$. Consistent with the general trend in halogen bond donor ability, the halide binding constants of bis(bromoimidazolium) $\mathbf{13b}^{2+}$ were significantly lower than those of $\mathbf{13a}^{2+}$. The use of ITC enabled determination of the enthalpic and entropic contributions to binding, which were found to vary significantly according the identity of the receptor, anion and solvent.

Halogen bonding between bromide anion and bromoimidazolium moieties was used to template the formation of catenane $\mathbf{17}^{2+} \cdot Br^- PF_6^-$ through ring-closing metathesis (Scheme 1) [56]. The combination of precursors $\mathbf{16}^+ \cdot PF_6^-$ and $\mathbf{16}^+ \cdot Br^-$ in the presence of the Grubbs second-generation ruthenium benzylidene complex led to the formation of the catenated structure in 24% yield. In the absence of the

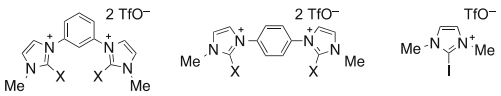

X = I: **13a**$^{2+}$•2TfO$^-$
X = Br: **13b**$^{2+}$•2TfO$^-$
X = H: **13c**$^{2+}$•2TfO$^-$

X = I: **14a**$^{2+}$•2TfO$^-$
X = H: **14b**$^{2+}$•2TfO$^-$

15$^+$•TfO$^-$

Fig. 8 (Halo)imidazolium-based anion receptors studied by Huber and co-workers

Table 11 Association constants K_a for interactions between receptors **13a**$^{2+} \cdot 2\text{TfO}^-$–**15**$^+ \cdot \text{TfO}^-$ and tetrabutylammonium salts $Bu_4N^+X^-$ (acetonitrile, 303 K)

Receptor	K_a ($X^- = Cl^-$; M^{-1})	K_a ($X^- = Br^-$; M^{-1})	K_a ($X^- = I^-$; M^{-1})
13a$^{2+} \cdot 2\text{TfO}^-$	5.2×10^5	4.5×10^5	2.5×10^5
13b$^{2+} \cdot 2\text{TfO}^-$	1.3×10^3	1.0×10^3	4.9×10^2
14a$^{2+} \cdot 2\text{TfO}^-$	3.3×10^4	3.7×10^4	2.2×10^4
15$^+ \cdot \text{TfO}^-$	ND	3.5×10^3	ND

Scheme 1 Bromide-templated formation of catenane **17**$^{2+} \cdot \text{Br}^-\text{PF}_6^-$

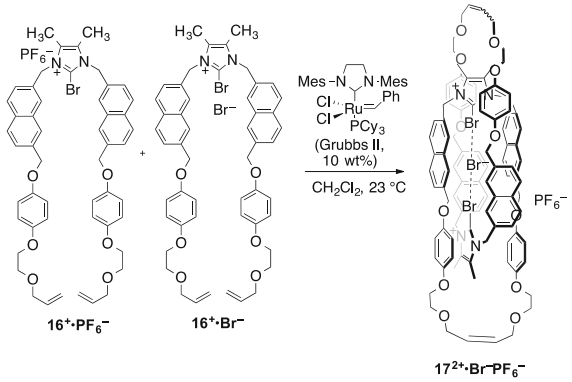

16$^+$•**PF**$_6^-$ **16**$^+$•**Br**$^-$ **17**$^{2+}$•**Br**$^-$**PF**$_6^-$

Br^- template, the catenane was not obtained. The templating anion was removed by anion metathesis with $NH_4^+PF_6^-$, and the anion recognition properties of the obtained **17**$^{2+} \cdot 2\text{PF}_6^-$ investigated by fluorescence spectroscopy. Upon addition of $Bu_4N^+Cl^-$ and $Bu_4N^+Br^-$, a roughly 30-fold increase in emission at 445 nm (corresponding to a naphthyl-based excimer) was observed. Based on the concentration dependence of the fluorescence response, 1:1 binding constants of 3.7×10^6 and 1.5×10^5 M–1 were determined for binding of Cl^- and Br^-, respectively, in acetonitrile at 293 K. Tetrabutylammonium salts of other anions (F^-, I^-, AcO^-, $H_2PO_4^-$, NO_3^-, and HCO_3^-) showed no evidence of binding, pointing to the need for complementarity between the anionic guest and the binding site of **17**$^{2+}$.

5 Anion Recognition Through Combinations of Halogen and Hydrogen Bonding

The prospect of distinctions between halogen and hydrogen bonding in terms of such features as anion selectivity, solvent effects, and directionality hints at interesting opportunities for anion receptors making use of both types of interactions. Rotaxane **20a**$^+ \cdot PF_6^-$, synthesized by Beer and co-workers, constitutes an example of such a system. Based on the group's earlier observations of anion-templated pseudorotaxane formation from bromoimidazolium and isophthalamide components [49], the transformation depicted in Scheme 2 was devised [50]. The assembly of **18**, iodotriazolium **19a**$^+$, and Br^- was trapped by ring-closing metathesis, generating **20a**$^+ \cdot Br^-$ in 15% yield. An analogous chloride-templated protocol was used to access the unsubstituted triazolium-based rotaxane **20b**$^+ \cdot Cl^-$ [57]. After the templating ions were exchanged for non-coordinating PF_6^-, the halide affinities of the rotaxanes were studied. In a 45:45:10 $CDCl_3/CD_3OD/D_2O$ ternary solvent mixture, iodotriazolium **20b**$^+ \cdot PF_6^-$ displayed selective binding of the heavier halides: association constants of 4.6×10^2, 1.3×10^3, and 2.2×10^3 M^{-1} were determined for Cl^-, Br^-, and I^-, respectively. The iodo group of **20a**$^+$ had a significant influence on its behavior as an anion receptor: in 1:1 $CDCl_3/CD_3OD$, the association constant of **20a**$^+$ for Br^- was at least an order of magnitude higher than that of **20b**$^+$ ($>10^4$ and 9.7×10^2 M^{-1}, respectively). An X-ray crystal structure of **20a**$^+ \cdot Br^-$ confirmed the presence of halogen and hydrogen bonding interactions with the guest anion. The I···Br^- halogen bond was elongated (3.13 vs 3.09 Å) and distorted from linearity (165 vs 177°) relative to the one in **19a** $\cdot Br^-$, perhaps because of limitations of the ability of the rotaxane to accommodate the ideal geometry for both hydrogen and halogen bonding interactions.

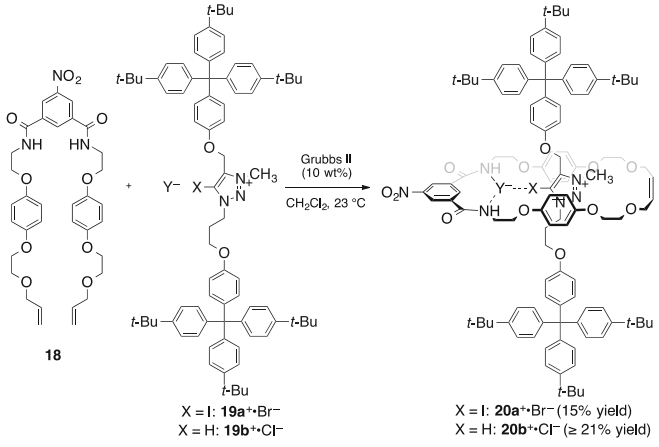

Scheme 2 Anion-templated preparation of rotaxanes **20a**$^+ \cdot Br^-$ and **20b**$^+ \cdot Cl^-$

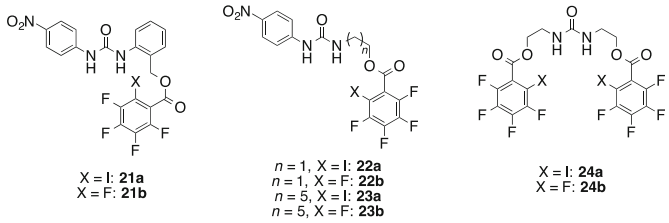

Fig. 9 Iodoperfluorobenzoate-functionalized ureas **21a**–**24a**, and perfluorinated controls **21b**–**24b**

Receptors **21a**–**24a** (Fig. 9) present a combination of hydrogen-bond donor urea and halogen-bond donor iodoperfluorobenzoate groups for anion binding [58]. Indeed, addition of salts $Bu_4N^+X^-$ to solutions of these receptors in d_3-acetonitrile resulted in NMR spectral changes consistent with both types of interactions: namely, downfield changes in ^{1}H NMR chemical shift of the N–H signals and upfield changes in ^{19}F NMR chemical shift of the Ar–F signals. Nitroaniline-derived arylureas **21a** and **22a** underwent red-shifts in the wavelength of maximal UV–vis absorbance which enabled determinations of association constants by spectrophotometry in addition to ^{1}H and ^{19}F NMR spectroscopy. To provide a quantitative estimate of the role of halogen bonding, the association constants for interactions of anions with perfluorinated receptors **21b**–**24b** were also determined. For example, the quantity $\Delta\Delta G_{XB} = \Delta G_{binding(\mathbf{22a})} - \Delta G_{binding(\mathbf{22b})}$ was used to gauge the contribution of halogen bonding to the free energy of binding of **21a** to a given anion.

A comparison of the values of $\Delta\Delta G_{XB}$ for **21a**–**23a** revealed an effect of the linker group on the apparent strength of the halogen bonding interaction: for Cl^- binding, values of $\Delta\Delta G_{XB}$ were −0.7, −3.8, and −1.1 kJ/mol for **21a**, **22a**, and **23a**, respectively. Computational modeling pointed towards a rationale for this dependence on linker group: the ethylene linker of **22a** is better able to accommodate the linear geometry required for optimal halogen bonding than is the benzyl-based linker of **21a** (C–I···Cl^- angles of 170° and 155°, respectively, were calculated for models of the **22a**–Cl^- and **21a**–Cl^- complexes). While several lines of investigation (e.g., gas-phase spectroscopy, X-ray crystallography, and computation) suggest that halogen bonding shows particularly stringent directionality, evidence for this effect in solution has been relatively rare. Receptor **23a** was also predicted to allow for a near-linear halogen bond (179.6°), but presumably its conformationally flexible linker incurs an entropic penalty which largely negates the enthalpic benefit of the halogen bond.

Table 12 summarizes the anion binding properties of receptor **24a**, which bears two halogen- and two hydrogen-bond donor sites and incorporates the ethylene linker group identified from the studies described above. The quantity $\Delta\Delta G_{XB}$ (defined in the previous paragraph) was determined based on the association constants of **24a** and perfluorinated control **24b**. Significant contributions from halogen bonding were evident for the halides, consistent with the data described in Sect. 2.2 for interactions of anions with mono- or multidentate iodoperfluoroaryl-

Table 12 Association constants K_a for interactions between receptors **24a** or **24b** and tetrabutylammonium salts $Bu_4N^+X^-$ (acetonitrile, 295 K)

Anion	K_a (**24a**, M^{-1})	K_a (**24b**, M^{-1})	$\Delta\Delta G_{XB}$ (kJ/mol)
BzO^-	3.3×10^3	1.0×10^3	−2.9
Cl^-	2.4×10^3	86	−8.2
$H_2PO_4^-$	8.3×10^2	2.0×10^2	−3.5
Br^-	7.0×10^2	24	−8.3
I^-	1.4×10^2	8.5	−6.9
TsO^-	54	38	−0.9
HSO_4^-	30	19	−1.1
NO_3^-	21	14	−1.0

Values of $\Delta\Delta G_{XB}$ were calculated from the association constants of the two receptors with a given anion, as described above

type receptors. Although halogen bonding with the oxoanions TsO^-, HSO_4^-, and NO_3^- was negligible, the values of $\Delta\Delta G_{XB}$ for the more basic BzO^- and $H_2PO_4^-$ suggested an attractive interaction, albeit weaker than with the halides. On the whole, the data for **24a** and **24b** indicate that incorporation of halogen bond donor groups markedly alters the anion recognition behavior of the urea functional group, conferring halide affinity to a receptor which otherwise interacts selectively with Y-shaped or tetrahedral oxoanions.

6 Summary, Conclusions, and Outlook

Given that the formation of trihalides from halogens and halides has been acknowledged for well over a century [59], and that evidence for halogen bonding of organic donors has been available for decades [60, 61], it is arguably surprising that the interaction has largely been ignored until recently by the supramolecular chemistry community in general, and the anion recognition field in particular. The rapid progress made over the past 5 years in developing halogen bonding-based anion receptors, and the diversity of donor types and architectures employed, suggest that there is much room for continued exploration. It is also noteworthy that applications in anion transport and anion-binding catalysis have already been demonstrated. Receptors containing multiple electron-deficient halo substituents often present a significant synthetic challenge, and the development of methods for late-stage halogenation would probably accelerate further progress in this field. Several of the studies described above point towards distinctions between halogen bond-donor receptors and those based on hydrogen bonding: halogen bonds are longer than hydrogen bonds and yet are highly directional, and anion selectivity appears to vary between the two types of interactions. It is anticipated that future work can deepen our understanding of these distinctions and reveal new ways to exploit them.

References

1. Shriver DF, Biallas MJ (1967) Observation of the chelate effect with a bidentate Lewis acid, $F_2BCH_2CH_2BF_2$. J Am Chem Soc 89:1078
2. Park CH, Simmons HE (1968) Macrobicyclic amines. III. Encapsulation of halide ions by in, in-1,(k + 2)-diazabicyclo[k.l.m]alkane-ammonium ions. J Am Chem Soc 90:2431
3. Graf E, Lehn JM (1976) Anion cryptates: highly stable and selective macrotricyclic anion inclusion complexes. J Am Chem Soc 98:6403
4. Gale PA, Busschaert N, Haynes CJE, Karagiannidis LE, Kirby IL (2014) Anion receptor chemistry: highlights from 2011 and 2012. Chem Soc Rev 43:205
5. Haynes CJE, Gale PA (2011) Transmembrane anion transport by synthetic systems. Chem Commun 47:8203
6. Brak K, Jacobsen EN (2013) Asymmetric ion-pairing catalysis. Angew Chem Int Ed 52:534
7. Pimentel GC (1951) The bonding of trihalide and bifluoride ions by the molecular orbital method. J Chem Phys 19:446
8. Hach RJ, Rundle RE (1951) The structure of tetramethylammonium pentaiodide. J Am Chem Soc 73:4321
9. Novoa J, Mota F, Alvarez S (1988) Structure and stability of the X_3^- systems (X=F, Cl, Br, I) and their interaction with cations. J Phys Chem 92:6561
10. Landrum GA, Goldberg N, Hoffmann R (1997) Bonding in the trihalides (X_3^-), mixed trihalides (X_2Y^-) and hydrogen bihalides (X_2H^-). The connection between hypervalent, electron-rich three-center, donor–acceptor and strong hydrogen bonding. J Chem Soc Dalton Trans 3605
11. Reed AE, Schleyer PR (1990) Chemical bonding in hypervalent molecules. The dominance of ionic bonding and negative hyperconjugation over d-orbital participation. J Am Chem Soc 112:1434
12. Braïda B, Hiberty PC (2004) What makes the trifluoride anion F_3^- so special: a breathing-orbital valence bond ab initio study. J Am Chem Soc 126:14890
13. Migchelsen T, Vos A (1967) The crystal structure of two modifications of tetraethylammonium triiodide, $(C_2H_5)_4NI_3$. Acta Crystallogr 23:796
14. Nizzi KE, Pommerening CA, Sunderlin LS (1998) Gas-phase thermochemistry of polyhalide anions. J Phys Chem A 102:7674
15. Arta A, Nizzi KE, Hill BT, Sunderlin LS, Wenthold PG (2000) Bond dissociation energy in trifluoride ion. J Am Chem Soc 122:10667
16. Metrangolo P, Murray JS, Pilati T, Politzer P, Resnati G, Terraneo G (2011) The fluorine atom as a halogen bond donor, *viz*. a positive site. CrystEngComm 13:6593
17. Nelson IV, Iwamoto RT (1964) Voltammetric evaluation of the stability of trichloride, tribromide, and triiodide ions in nitromethane, acetone, and acetonitrile. J Electroanal Chem 7:218
18. Crawford E, McIndoe JS, Tuck DG (2006) The energetics of the $X_2 + X^- \rightarrow X_3^-$ equilibrium (X = Cl, Br, I) in aqueous and nonaqueous solution. Can J Chem 84:1607
19. Schmidtchen FP (2010) Hosting anions. The energic perspective. Chem Soc Rev 39:3916
20. Metrangolo P, Pilati T, Terraneo G, Biella S, Resnati G (2009) Anion coordination and anion-templated assembly under halogen bonding control. CrystEngComm 11:1187
21. Cavallo G, Metrangolo P, Pilati T, Resnati G, Sansotera M, Terraneo G (2010) Halogen bonding: a general route in anion recognition and coordination. Chem Soc Rev 39:3772
22. Metrangolo P, Carcenac Y, Lahtinen M, Pilati T, Rissanen K, Vij A, Resnati G (2009) Nonporous organic solids capable of dynamically resolving mixtures of diiodoperfluoroalkanes. Science 323:1461
23. Bogdanov B, McMahon TB (2006) Gas phase S_N2 reactions of halide ions with trifluoromethyl halides: front- and back-side attack vs complex formation. J Phys Chem A 110:1350

24. Gillis EAL, Demireva M, Sarwar MG, Chudzinski MG, Taylor MS, Williams ER, Fridgen TD (2013) Structure and energetics of gas phase halogen-bonding in mono-, bi- and tri-dentate anion receptors as studied by BIRD. Phys Chem Chem Phys 15:7638
25. Sarwar MG, Dragisic B, Dimitrijevic E, Taylor MS (2013) Halogen bonding between anions and iodoperfluoroorganics: solution-phase thermodynamics and multidentate-receptor design. Chem Eur J 19:2050
26. Lindeman SV, Hecht J, Kochi JK (2003) The charge-transfer motif in crystal engineering. Self-assembly of acentric (diamondoid) networds from halide salts and carbon tetrabromide as electron-donor/acceptor synthons. J Am Chem Soc 125:11597
27. Rosokha SV, Neretin IS, Rosokha TY, Hecht J, Kochi JK (2006) Charge-transfer character of halogen bonding: molecular structures and electronic spectroscopy of carbon tetrabromide and bromoform complexes with organic σ- and π-donors. Heteroat Chem 17:449
28. Rosokha SV, Stern CL, Ritzert JT (2013) Experimental and computational probes of the nature of halogen bonding: complexes of bromine-containing molecules with bromide anions. Chem Eur J 19:8774
29. Shen QJ, Jin WJ (2011) Strong halogen bonding of 1,2-diiodoperfluoroethane and 1,6-diiodoperfluorohexane with halide anions revealed by UV-vis, FT-IR, NMR spectroscopies and crystallography. Phys Chem Chem Phys 13:13721
30. Wang H, Zhao XR, Jin WJ (2013) The C–I···X^- halogen bonding of tetraiodoethylene with halide anions in solution and cocrystals investigated by experiment and calculation. Phys Chem Chem Phys 15:4320
31. Sarwar MG, Dragisic B, Sagoo S, Taylor MS (2010) A tridentate halogen-bonding receptor for tight binding of halide anions. Angew Chem Int Ed 49:1674
32. Mulliken RS, Person WB (1969) Molecular complexes. A lecture and reprint volume. Wiley, New York
33. Sarwar MG, Dragisic B, Salsberg LJ, Gouliaras C, Taylor MS (2010) Thermodynamics of halogen bonding in solution: substituent, structural, and solvent effects. J Am Chem Soc 132:1646
34. Huber SM, Jimenez-Izal E, Ugalde JM, Infante I (2012) Unexpected trends in halogen-bond based noncovalent adducts. Chem Commun 48:7708
35. Jentzsch AV, Emery D, Mareda J, Nayak SK, Metrangolo P, Resnati G, Sakai N, Matile S (2012) Transmembrane anion transport mediated by halogen-bond donors. Nat Commun 3:905
36. Jentzsch AV, Emery D, Mareda J, Metrangolo P, Resnati G, Matile S (2011) Ditopic ion transport systems: anion-p interactions and halogen bonds at work. Angew Chem Int Ed 50:11675
37. Jentzsch AV, Matile S (2013) Transmembrane halogen-bonding cascades. J Am Chem Soc 135:5302
38. Beer PD, Gale PA (2001) Anion recognition and sensing: the state of the art and future perspectives. Angew Chem Int Ed 40:486
39. Mele A, Metrangolo P, Neukirch H, Pilati T, Resnati G (2005) A halogen-bonding-based heteroditopic receptor for alkali metal halides. J Am Chem Soc 127:14972
40. Walter SM, Sarwar MG, Chudzinski MG, Herdtweck E, Lough AJ, Huber SM, Taylor MS (2013) Halogen bonding and π–π interactions in the solid-state structure of a butadiynylene-linked bis(iodoperfluoroarene). CrystEngComm 15:3097
41. Wang X, Hof F (2012) (How) does 1,3,5-triethylbenzene scaffolding work? Analyzing the abilities of 1,3,5-triethylbenzene and 1,3,5-trimethylbenzene-based scaffolds to preorganize the binding elements of supramolecular hosts and to improve binding of targets. Beil J Org Chem 8:1
42. Dimitrijevic E, Kvak O, Taylor MS (2010) Measurements of weak halogen bond donor abilities with tridentate anion receptors. Chem Commun 46:9025
43. Frontera A, Gamez P, Mascal M, Mooibroek TJ, Reedijk J (2011) Putting anion-π interactions into perspective. Angew Chem Int Ed 50:9564

44. Politzer P, Murray JS, Clark T (2013) Halogen bonding and other σ-hole interactions: a perspective. Phys Chem Chem Phys 15:11178
45. Riley KE, Murray JS, Politzer P, Concha MC, Hobza P (2009) Br···O complexes as probes of factors affecting halogen bonding: interactions of bromobenzenes and bromopyridines with acetone. J Chem Theory Comput 5:155
46. Kniep F, Jungbauer SH, Zhang Q, Walter SM, Schindler S, Schnapparelle I, Herdtweck E, Huber SM (2013) Organocatalysis by neutral multidentate halogen-bond donors. Angew Chem Int Ed 52:7028
47. Gilday LC, White NG, Beer PD (2013) Halogen- and hydrogen-bonding triazole-functionalised porphyrin-based receptors for anion recognition. Dalton Trans 42:15766
48. Kubik S (2010) Anion recognition in water. Chem Soc Rev 39:3648
49. Serpell CJ, Kilah NL, Costa PJ, Félix V, Beer PD (2010) Halogen bond anion templated assembly of an imidazolium pseudorotaxane. Angew Chem Int Ed 49:5322
50. Kilah NL, Wise MD, Serpell CJ, Thompson AL, White NG, Christensen KE, Beer PD (2010) Enhancement of anion recognition exhibited by a halogen-bonding rotaxane host system. J Am Chem Soc 132:11893
51. Caballero A, White NG, Beer PD (2011) A bidentate halogen-bonding bromoimidazoliophane receptor for bromide ion recognition in aqueous media. Angew Chem Int Ed 50:1845
52. Zapata F, Caballero A, White NG, Claridge TDW, Costa PJ, Félix V, Beer PD (2012) Fluorescent charge-assisted halogen-bonding macrocyclic haloimidazolium receptors for anion recognition and sensing in aqueous media. J Am Chem Soc 134:11533
53. Cametti M, Raatikainen K, Metrangolo P, Pilati T, Terraneo G, Resnati G (2012) 2-Iodo-imidazolium receptor binds oxoanions via charge-assisted halogen bonding. Org Biomol Chem 10:1329
54. Walter SM, Kniep F, Rout L, Schmidtchen FP, Herdtweck E, Huber SM (2012) Isothermal titration calorimetric titrations on charge-assisted halogen bonds: role of entropy, counterions, solvent, and temperature. J Am Chem Soc 134:8507
55. Walter SM, Kniep F, Herdtweck E, Huber SM (2011) Halogen-bond-induced activation of a carbon–heteroatom bond. Angew Chem Int Ed 50:6932
56. Caballero A, Zapata F, White NG, Costa PJ, Félix V, Beer PD (2012) A halogen-bonding catenane for anion recognition and sensing. Angew Chem Int Ed 51:1876
57. Mullen KM, Mercurio J, Serpell CJ, Beer PD (2009) Exploiting the 1,2,3-triazolium motif in anion-templated formation of a bromide-selective rotaxane host assembly. Angew Chem Int Ed 48:4781
58. Chudzinski MG, McClary CA, Taylor MS (2011) Anion receptors composed of hydrogen- and halogen-bond donor groups: modulating selectivity with combinations of distinct noncovalent interactions. J Am Chem Soc 133:10559
59. Johnson GS (1877) On potassium triiodide. J Chem Soc 31:249
60. Hassel O (1970) Structural aspects of interatomic charge-transfer bonding. Science 170:497
61. Laurence C, Queignec-Cabanetos M, Dziembowska T, Queignec R, Wojtkowiak B (1981) 1-Iodoacetylenes. 1. Spectroscopic evidence of their complexes with Lewis bases. A spectroscopic scale of soft basicity. J Am Chem Soc 103:2567

Top Curr Chem (2015) 359: 49–76
DOI: 10.1007/128_2014_607

Published online: 25 March 2015

Halogen Bonding in Solution

Anna-Carin C. Carlsson, Alberte X. Veiga, and Máté Erdélyi

Abstract Because of its expected applicability for modulation of molecular recognition phenomena in chemistry and biology, halogen bonding has lately attracted rapidly increasing interest. As most of these processes proceed in solution, the understanding of the influence of solvents on the interaction is of utmost importance. In addition, solution studies provide fundamental insights into the nature of halogen bonding, including, for example, the relative importance of charge transfer, dispersion, and electrostatics forces. Herein, a selection of halogen bonding literature is reviewed with the discussion focusing on the solvent effect and the electronic characteristics of halogen bonded complexes. Hence, charged and neutral systems together with two- and three-center bonds are presented in separate sub-sections. Solvent polarity is shown to have a slight stabilizing effect on neutral, two-center halogen bonds while strongly destabilizes charged, two-center complexes. It does not greatly influence the geometry of three-center halogen bonds, even though polar solvents facilitate dissociation of the counter-ion of charged three-center bonds. The charged three-center bonds are strengthened by increased environment polarity. Solvents possessing hydrogen bond donor functionalities efficiently destabilize all types of halogen bonds, primarily because of halogen vs hydrogen bond competition. A purely electrostatic model is insufficient for the description of halogen bonds in polar systems whereas it may give reasonable correlation to experimental data obtained in noninteracting, apolar solvents. Whereas dispersion plays a significant role for neutral, two-center halogen bonds, charged halogen bond complexes possess a significant charge transfer characteristic.

Keywords Halogen bond, Solution, Solvation, Solvent effect

A.-C.C. Carlsson, A.X. Veiga, and M. Erdélyi (✉)
Department of Chemistry and Molecular Biology, Gothenburg University, Gothenburg, Sweden
e-mail: mate@chem.gu.se

Contents

1 Introduction

By determining the structure, properties, and interactions of molecules, secondary chemical forces are of immense importance for chemical and biological processes. The fact that these almost always take place in solution reflects the importance of a thorough understanding of the influence of solvation on weak chemical forces. Consequently, solvent effects are of vast practical importance for numerous scientific fields, e.g., materials sciences, organocatalysis, structural chemistry, structural biology, and supramolecular and pharmaceutical chemistry. The four basic types of weak chemical forces, i.e., the hydrogen bond, the London dispersion, the dipole–dipole, and the cation–π interactions have received close attention over the past century, generating a considerable body of literature. Although the halogen bonding phenomenon was detected 150 years ago [1], was repeatedly assessed in the early twentieth century [2–6], and received the attention of the Nobel laureate Odd Hassel [7, 8], it has long remained neglected in the chemical toolbox of academic and industrial research. "Halogen bond" as a specific term for the description of the attractive interaction of halogens with Lewis bases has been in use for over 30 years [9, 10], yet received wider recognition upon the identification of the similarities between the concepts of halogen and hydrogen bonds by Legon [11] and subsequently by Metrangolo and Resnati [12]. The past 15 years of the history of the halogen bond has been dominated by studies focusing on its accurate description in vacuum and in crystals, largely neglecting environmental effects, whilst the behavior of halogen bonds in solution has received far less attention [13, 14]. The rapidly increasing utilization of halogen bonds in structural and organic chemistry, structural biology, and pharmaceutical research accentuates the need for a thorough understanding of solvent effects.

Because of their inherent electronic differences, charged and neutral as well as two- and three-center halogen bonds respond differently to changes in the environment, motivating their separate discussion. Conventional two-center halogen bonds are formed by the attractive interaction of the antibonding orbital, commonly termed sigma hole, of a covalently bound halogen and a Lewis base. A stronger interaction is reflected by shorter halogen bond donor–acceptor, and longer carbon–halogen distances. Three-center halogen bonds arise through excessive progress of these distance changes, thereby, by true equalization of the two bonds, yielding the

shortest and strongest known halogen bonds. Here, extensive weakening of the covalent bond of the halogen simultaneously with excessive strengthening of its halogen bond results in two secondary (halogen) bonds with substantial orbital (covalent) contributions. Such systems can be seen as the simultaneous interaction of a formally positively charged halogen with two halogen bond acceptors of comparable Lewis base strength in a linear fashion. This linear geometry is enforced by the antiparallel lobes of the empty p-orbital of the halogen, forming two "p-holes" framed by the negative belt of electron density of its filled p-orbitals ($p_x^2 p_y^2 p_z^0$) [127]. Thus, the halogen bond donor of three-center bonds possesses analogous anisotropic electron distribution to that of two-center bonds. Two-center bonds are dominated by electrostatic and dispersion forces; three-center bonds, in contrast, are predominantly of mixed charge transfer (orbital, covalent) and electrostatic character.

2 Neutral, Two-Center Halogen Bond Complexes

The initial solution phase studies of halogen bonding were generally carried out by mixing a simple, strong halogen bond donor with a variety of halogen bond acceptor solvents, and detecting spectral changes as compared to a non-interacting reference solvent, such as alkanes [9, 15–17]. These studies were of immense importance, providing impactful evidence for the existence of halogen bonds in the solution phase; however, they did not give specific information on solvent effects.

Based on UV spectroscopic data, both stabilization [18] and destabilization [19] of the N···I halogen bond of the pyridine-I_2 complex have been suggested upon increasing solvent polarity. These early studies discussed the interaction in terms of a charge transfer bond. The contradicting outcome of the two analyses probably originates from differences in solvent selection (Fig. 1). The dipole moments of the pyridine–I_2 complex, I_2, and pyridine, are 4.90, 2.20, and 0 D and, consequently, more polar media is expected to stabilize the N···I halogen bond, which hypothesis is supported by the investigation of McKinney [18]. The outcome of this study remains better interpretable in terms of a "trend" with limited generality because of the rather narrow range of dielectric constants (1.92–10.36) having been addressed.

By following the alkynic ^{13}C NMR shift alteration upon coordination of 1-cyano-2-iodoacetylene with pyridine, Laurence et al. observed that the halogen bond is modulated by solvent polarity, with the N···I interaction getting strengthened when changing the solvent from benzene (epsilon 2.27) to the less polar carbon tetrachloride (epsilon 2.24) [20]. Making use of this observation, a novel, halogen bond-based spectroscopic scale of soft basicity was developed utilizing the spectroscopic changes detectable upon interaction of the halogen bond donor 1-iodoacetylenes with various Lewis bases [21, 22]. Subsequently, Kochi et al. studied the association of carbon tetrahalides with nitrogenous electron donors in a small series of

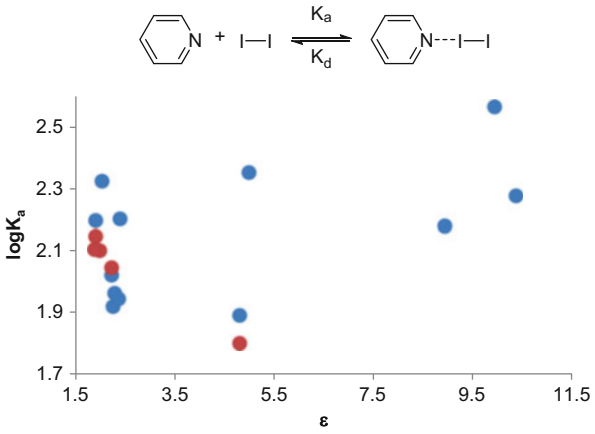

Fig. 1 UV-spectroscopically derived association constant (K_a) of pyridine-I_2 complex as a function of the solvent dielectric constant (ε). The *red data points* were reported by Bashkar and Singh [19] and the *blue* ones by McKinney et al. [18]. Data points: *n*-heptane (ε 1.92), *n*-hexadecane (ε 2.05), carbon tetrachloride (ε 2.24), benzene (ε 2.27), *p*-xylene (ε 2.30), toluene (ε 2.38), 1,1,2,-trifluoro-trichloroethane (ε 2.41), chloroform (ε 4.81), *m*-dichlorobenzene (ε 5.00), dichloromethane (ε 8.93), *o*-dichlorobenzene (ε 9.93), and 1,2-dichloroethane (ε 10.36)

solvents using NMR, IR, and UV–vis spectroscopies [10]. The interaction of carbon tetrabromide and diazabicyclo[2.2.2]octane (DABCO) was reported to be weakly solvent dependent with a stronger association observed in the more polar, aprotic acetonitrile (ε 37.5, K_a 4.8 M^{-1}) than in the apolar, weakly acidic chloroform (ε 1.7, K_a 4.2 M^{-1}), whilst the polar, strong hydrogen bond donor methanol efficiently weakened the interaction (ε 33.1, K_a 0.06 M^{-1}). The strongest carbon tetrabromide–DABCO interaction was observed for isooctane solution (ε 1.9), as revealed by the frequency of the UV charge transfer band of the complex. The data acquired by Kochi et al. suggests that the hydrogen bond donor ability of the solvent has a detrimental effect on halogen bonding, whereas environmental polarity possesses a considerably weaker and ambiguous influence. This conclusion is further supported by the observations of Goroff et al. [23], who studied the interaction of 1-iodoalkynes with pyridine, quinolone, THF, acetone, benzophenone, and chloroform in a mixture with hexanes. Based on correlations of the ^{13}C NMR shifts to a variety of empirical models of solvent basicity, Goroff suggested that basicity plays an important role for the interaction strength, but not polarity.

Cabot and Hunter investigated the influence of solvent polarity on halogen bonding by studying the interaction of 1-iodoperfluorohexane with eight Lewis bases in three solvents [24]. Of the three apolar solvents used in this study, benzene was the most polarizable, whilst chloroform was the only one capable of weak hydrogen bond donation. For each and every halogen bond complex, the strongest interactions were detected for benzene solutions. Somewhat lower association constants were seen for carbon tetrachloride, whereas halogen bonds were hardly detectable for chloroform solutions (Table 1). A purely electrostatic interaction

Table 1 The association constants ($\log K_a$) of the halogen bond complexes of 1-iodoperfluoro-*n*-hexane and eight Lewis bases in chloroform, carbon tetrachloride, and benzene, as reported by Cabot and Hunter [24]

Lewis base	C_6H_6	Carbon tetrachloride	$CHCl_3$
$(n\text{-Bu})_3P{=}O$	0.7 ± 0.2	0.6 ± 0.2	<-0.3
Quinuclidine	1.6 ± 0.2	1.2 ± 0.2	0.6 ± 0.2
DABCO	1.5 ± 0.2	1.0 ± 0.3	0.5 ± 0.2
Piperidine	0.9 ± 0.2	0.7 ± 0.2	0.2 ± 0.2
Hexylamine	0.3 ± 0.2	-0.2 ± 0.6	<-0.3
Et_2NH	0.6 ± 0.2	0.1 ± 0.2	<-0.3
Et_3N	0.3 ± 0.2	0.3 ± 0.2	<-0.3
Pyridine	0.0 ± 0.2	-0.1 ± 0.2	<-0.3

model is able to give a reasonable prediction of this trend; however, it underestimates halogen bond strength by an order of magnitude. Furthermore, the strength of the interaction of 1-iodoperfluorohexane with cyclic amines suggests a significant role of charge transfer effects or possibly an exceptional electrostatic complementarity. The charge transfer hypothesis, presuming an orbital interaction of the lone-pair of the amines and the antibonding (σ*) orbital of the C–I covalent bond, is supported by a weak, but still detectable, correlation of the association constants to the HOMO energy and to the nucleophilicity of the Lewis bases.

By a systematic study of ^{19}F NMR chemical shift changes upon interaction of iodoperfluorooctane with trimethylamine, the Taylor group compared the effect of ten solvents on the I···N halogen bond [25]. In line with previous observations, the interaction was found strongest in nonpolar, aprotic solvents, such as cyclohexane and benzene, of intermediate strength in polar, aprotic ones, and barely stable or immeasurable weak in polar, protic solvents, such as isopropanol and methanol (Fig. 2). Importantly, the association constants do not correlate well to a purely electrostatic interaction model [26]. The evaluation of the data in comparison to solvent polarity descriptors, such as $E_T(30)$ [27], the π* [28] and the Py [29] scales (Fig. 3) suggests that the halogen bond is affected by the polarity change of its environment to a lesser extent, yet is disrupted by solvents capable of hydrogen bond donation (Fig. 2). The acquisition of association constants in dimethylsulfoxide solution was unsuccessful.

An instructive conclusion of this study is that polar, aprotic solvents, commonly used in synthetic organic chemistry, for instance, do not necessarily weaken the halogen bond by competition. The comparable $\log K_a$ observed for the $C_8F_{17}I$–trimethylamine interaction in acetonitrile and dichloromethane solutions, only slightly weaker than in benzene and cyclohexane, is in line with the independent computational prediction of a halogen bond stabilizing effect of increased solvent polarity [30–32]. In Taylor's study, this may be partly compensated by competition for the halogen bond donor site of the nonbonding orbital of the polar, aprotic solvents, such as acetonitrile, present in large excess.

Binding constants for the pyridine–perfluoropropyliodide halogen bond interaction were obtained in cyclohexane, hexane, chloroform, acetone, and acetonitrile solutions using ^{19}F NMR by Hawthorne et al. [33]. A weakening of the halogen bond was observed for this complex upon increasing the solvent polarity (Fig. 4) In

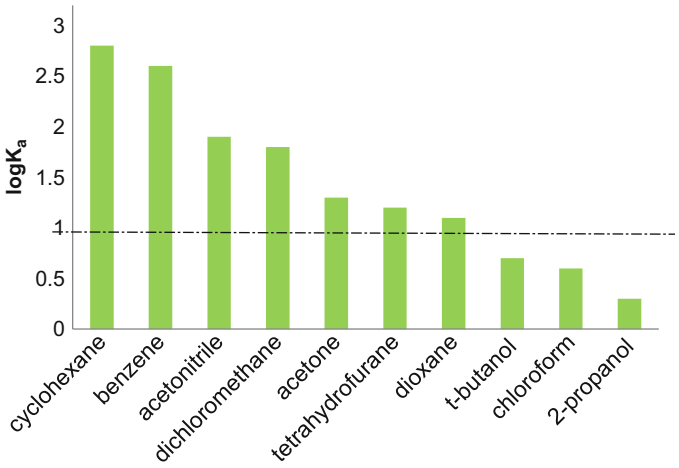

Fig. 2 Association constants (K_a) for the iodoperfluorooctane-triethylamine complex obtained in ten solvents. The *dotted line* highlights the limit ($K_a > 1$) until formation of the halogen bond complex is favorable [25]

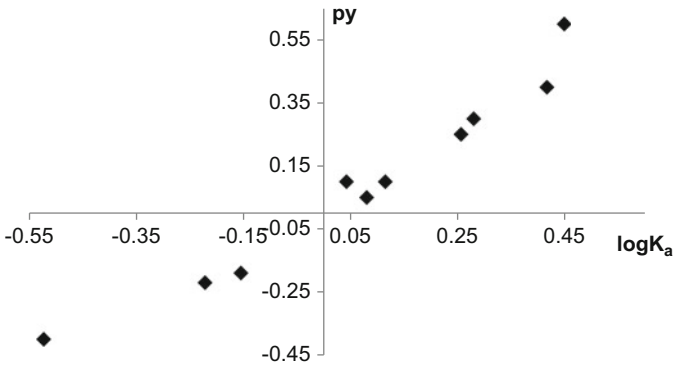

Fig. 3 The experimental association constants ($\log K_a$) of the iodoperfluorooctane–triethylamine interaction in ten solvents, plotted against the py-index of each solvent [25]. In contrast to numerous other solvent polarity scales, the py-scale provides a hydrogen bonding independent measure of polarity which largely correlates to the dielectric constant

contrast, the largest blue shift of pyridine ring breathing vibration (FT-IR) was seen for the complexes dissolved in the polar acetonitrile and acetone solutions. The latter data were interpreted by a more negative enthalpy change for halogen bond formation in polar solvents as compared to apolar ones with an overcompensating entropy change accountable for the overall Gibbs free energy change which is manifested in the association constants. Hence, in cyclohexane and hexane, the perfluoropropyliodides were proposed to exist as aggregates and consequently halogen bond formation to pyridine was proposed to be associated with a large increase of entropy. In chloroform, acetone, and acetonitrile solutions, free pyridine

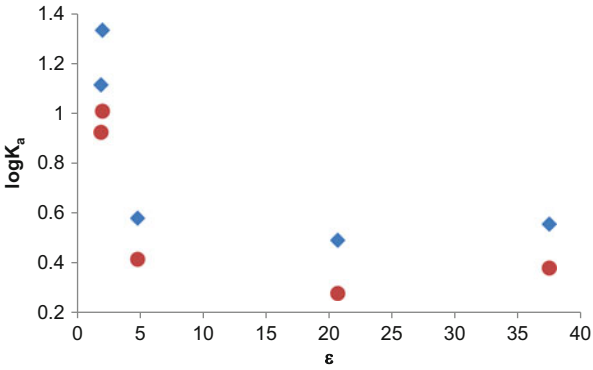

Fig. 4 The association constants ($\log K_a$) of pyridine – 1-iodoheptafluoropropane (*red circles*) and 2-iodoheptafluoropropane (*blue squares*) [33]

and perfluoropropyliodides were presumed to exist as monomeric hydrogen or halogen bonded complexes with the solvent. Consequently, the establishment of pyridine–perfluoropropyliodide halogen bonds was expected to have a much lower effect on entropy. The ^{19}F NMR observation of an overall larger association constant for the formation of C–I···N halogen bonds in apolar solvents as compared to polar ones is in good agreement with the previous reports discussed above.

Brammer et al. studied the interaction of iodopentafluorobenzene with the fluorous electron donor *trans*-(tetrafluoropyrid-2-yl)bis(triethylphosphine)fluoronickel(II) having observed considerably stronger C–I···F interaction in heptane than in toluene (K_a 21.8 vs. 3.41 M^{-1}, respectively) by ^{19}F NMR [34]. This fact has been rationalized by a likely competing π-stacking interaction of toluene with iodopentafluorobenzene, weakening the apparent bond strength.

The experimental dependence of halogen bond strength on solvent polarity was reproduced by computation. Sironi et al. predicted interaction energies for C–I···O halogen bonds on the MP2 and DFT levels, applying a variety of common exchange correlation functions (PBE, PBE0, B3LYP, NH&HLYP, M06-2X, and M06-HF) and a conductor-like polarizable continuum solvent model (CPCM) for diethyl ether and water [35]. Upon changing the solvent from ether to water, decreased interaction energies, shortening of the I···O distance, and a greater tendency for linearity of the C–I···O bond angle were predicted. Thus, increasing solvent polarity has an overall destabilizing effect on the interaction which is neither reflected by the halogen bond donor–acceptor distance nor by the bond angle. This is self-contradictory. The applicability of these parameters to the description of halogen bond strength is therefore questionable. Although the reliability of the conclusions drawn for aqueous solutions may be debatable because of the neglected disruptive competition of hydrogen and halogen bonds and the low aqueous solubility of some of the substances, the outcome of the computation is in agreement with the polarity dependence of halogen bonding which was reported by others for apolar, aprotic solutions.

By a combined NMR spectroscopic and computational study, Wang and coworkers have demonstrated that the lone pair of the heteroatom of common solvents, e.g., acetonitrile, acetone, DMSO, and methanol, may donate electron

density to the π system of perfluorohaloarenes, which, because of their favorable halogen bond donor strength, are often utilized as model substrates in theoretical and spectroscopic investigation of the halogen bonding phenomenon [36]. Importantly, the solvent lone pair–halogen bond donor π interaction was shown to be energetically favorable over the corresponding halogen bond for C_6F_5Cl and C_6F_5Br. The halogen bond of perfluoroiodoarenes was somewhat stronger than the corresponding lone pair–π interaction, yet the competition of the two interactions is still expected to have significant influence on the experimental parameters commonly used to describe halogen bond strength, such as the NMR chemical shift. Thus, this competition ought to be taken into account in the evaluation of data collected for the halogen bonds of perfluorinated systems. Further important aspects of solvent effects were evaluated by additional computational studies. The work of Li et al. provided insight into the competition of hydrogen and halogen bonds [37] and that of Zhang et al. into the competition of π–π interactions and halogen bonds [38]. Jin and coworkers have reported the concentration dependence of the C–Br···O interaction of carbon tetrabromide and oxygen-containing organic solvents [39]. Systematic DFT/MP2 calculations focusing on the evaluation of the influence of the solvent environment on weak, neutral, two-center halogen bonds of halobenzenes with water, formaldehyde, and ammonia using implicit solvent models for cyclohexane, chloroform, and water were carried out by Lu and coworkers [32]. Here, slightly stronger halogen bonds were predicted to shorten, i.e., to become stabilized because of polarization, whereas weaker bonds were predicted to lengthen or remain unchanged. In general, solvation was anticipated to have a slight destabilizing effect on halogen bonding with weak attenuation of the differences in relative strength between the bonds of various halogen bond donors ($I > Br > Cl$).

3 Charged, Two-Center Halogen Bond Complexes

Solution studies of negatively charged halogen bonded complexes of the C–X···X^- type were primarily reported as part of the effort towards the development of selective anion receptors. Whereas cooperative effects clearly play an important role in the high affinity of anion receptors, the conclusions drawn from these studies are of general relevance for halogen bonding. Taylor has found the affinity order $Cl^- > Br^- > I^-$, which corresponds to the order of the anion charge densities, for the C–I···X^- interactions in acetone solution [40]. Beer and coworkers, however, have reported the opposite affinity order for the same C–I···X^- interaction using a pseudorotaxane-type anion receptor dissolved in a solution mixture of 45:45:10 $CDCl_3/CD_3OD/D_2O$, with K_a values of 457, 1,251, and 2,228 M^{-1} for Cl^-, Br^-, and I^-, respectively [41]. Upon removing water from the solvent mixture ($CDCl_3$/CD_3OD), the K_a of Br^- to the C–I of the receptor increased above 10^4 M^{-1}. This observation is in good agreement with the previous reports on the halogen bond disrupting ability of protic solvents. Systematic evaluation of the solvent effects on

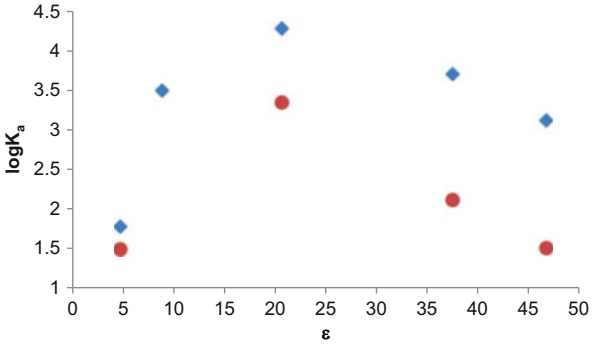

Fig. 5 Solvent polarity dependence of the C–I···Cl^- halogen bond association constants (log K_a), for the interaction of $C_8F_{17}I$ (*red circles*) and a tridentate anion receptor (*blue squares*). Solvents from *left* to *right*: chloroform (ε 4.81), dichloromethane (ε 8.93), acetone (ε 20.70), acetonitrile (ε 37.5), and dimethylsulfoxide (ε 46.70) [42]

the C–I···Cl^- interaction using 1-iodoperfluorooctane and an anion receptor displaying three iodoperfluorobenzene halogen bond donor sites [42] indicated a considerable solvent dependence of the affinity constants (Fig. 5). Nevertheless, the interpretation of this data is ambiguous as the affinity constants do not correlate to typical descriptors of solvent polarity, polarizability, or hydrogen bonding ability, such as the ε, $E_T(30)$, py, π^*, or Z-scales. Another difficulty in the interpretation of this data is the different hygroscopicities of the applied solvents, which may affect the apparent affinity constants. The comparable trend of solvent influence observed for the K_a of $C_8F_{17}I$ and of the tridentate receptor confirms similar mechanism of their Cl^- binding. Simultaneously, this indicates that the data obtained on halogen bonding of polydentate receptors are comparable to those derived from simple 1:1 complexes. When studying the acetone, tetrahydrofuran, and dichloromethane solutions of a bidentate bis(haloimidazolium) anion receptor model by ITC, a very low and difficult to interpret solvent dependence was observed for the C–I···X^- interaction by Huber et al. [43]. It should be stressed that the solvent polarity dependence of the strengths of charged (Fig. 5) and neutral (Fig. 4) halogen bonds are different. This experimental finding was to a large degree confirmed and rationalized by the computational work (DFT/B3LYP, PCM) of Lu et al. [31]. Thus, quantum chemical calculations predicted significant weakening of charged halogen bonds (Fig. 6) with a concomitant elongation of the intermolecular distances upon increased solvent polarity, in contrast to a slight strengthening and bond shortening predicted for neutral bonds.

Solvent polarity was reported to have a far larger influence on charged complexes than on neutral ones. The influence of solvent polarity is greatest when going from apolar to weakly polar environments, but on changing the solvent from acetone (ε 20.7) to water (ε 78.4) the stability of the bond is affected to a much lesser degree. Charged halogen bonds are considerably stronger than neutral ones, with the C–I···X^- bond strength following the order of charge density and

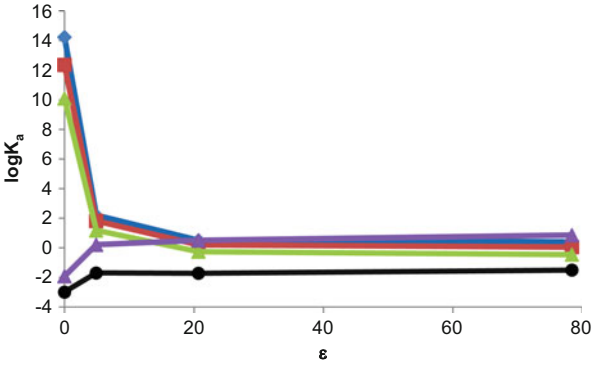

Fig. 6 Predicted association constants of $C_2F_3I\cdots X^-$ interaction with Cl^- (*blue*), Br^- (*red*), I^- (*green*), NH_3 (*violet*), and H_2O (*black*) as a function of solvent polarity for vacuum, chloroform, acetone, and water solutions, from *left* to *right* [31]

inversely correlates to anion size, i.e., $Cl^- > Br^- > I^-$. The dissimilarity between various types of halogen bonds is greatest in vacuum and rapidly diminishes with increasing solvent polarity (Fig. 6). The entropy contribution to the interaction energies is predicted to be substantial and disfavors the formation of halogen bonds in solution. The solvation energies for both the neutral and charged systems become more negative as the solvent polarity increases. For charged systems, the difference between the solvation energies of the halogen bonded complexes and the sum of the solvation energies of their subunits is large and positive (50–85 kJ/mol), revealing an overall destabilization upon solvation. This, to a large extent, may be attributed to the large solvation energies of the charged interaction partners, in this case X^-. The opposite trend is seen for neutral halogen bonded complexes, with a slight stabilizing effect of solvation on their formation. Overall, the halogen bonds of charged systems are stronger than those of neutral ones. Solvation has a large, destabilizing effect on charged halogen bonds, in contrast to its slight stabilizing effect on neutral complexes. The destabilization of protic solvents is expected to be even stronger through formation of hydrogen bonds, which could not be taken into account in the above study as it employed an implicit solvent model.

4 Neutral, Three-Center Halogen Bond Complexes

Neutral three-center halogen bonds may be formed by the interaction of a neutral halogen bond acceptor and a neutral halogen bond donor. Here, the halogen is attached to a functionality of comparable electronic properties to the halogen bond acceptor. Three-center N–X–N bonds were computationally assessed by Parra on the MP2 level using the model system of cyclic dimers and trimers of lithium formamidinate and monohalogenated formamidines (Fig. 7) [44]. Asymmetric N–X$\cdots$N bonds (X–I, Br, Cl) were predicted to possess ~30 kJ/mol stabilization energies in vacuo. Upon formation of a symmetric N$\cdots$I$\cdots$N bond, the interaction energy increases by a factor of 3.36, suggesting a great degree of stabilization by

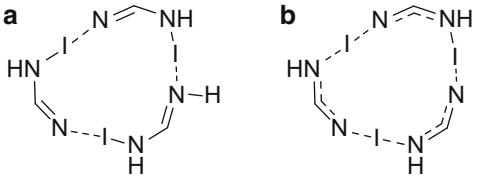

Fig. 7 The cyclic trimer of monoiodinated formamidine: (**a**) conventional Lewis structure; (**b**) depiction emphasizing its C_3 symmetric geometry

establishment of a three-center-four-electron system. Experimental confirmation of this conclusion remains the subject of future work, along with the investigation of the stability of these systems to elucidate whether the difference observed between neutral and charged two-center halogen bonds is valid for three-center bonds as well. The effect of solvent on the geometry and strength of neutral tree-center halogen bonds has so far not been investigated.

5 Charged, Three-Center Halogen Bond Complexes

Charged, three-center halogen bond complexes may encompass a partially or fully positively charged halogen which simultaneously acts as a halogen bond donor towards two nucleophiles of comparable Lewis basicity. Alternatively, it may be formed by the interaction of a neutral halogen bond donor with an anionic Lewis base. Here, the functionality covalently holding the halogen bond donor atom has to be of comparable electronic properties as the halogen bond acceptor, with the trihalide ions being illustrative examples. It should be stressed that the halogen bond donor of such systems interacts with two Lewis basic functions of comparable basicity.

The existence of pyridine-I_2 complexes ($Py \cdot I_2$) in nonpolar solvents, such as *n*-heptane, cyclohexane, benzene, carbon tetrachloride, and carbon disulfide, has been known for decades [45–49]. In more polar solvents, however, and in the presence of a large excess of pyridine, this complex easily dissociates to generate ionic species [3, 46, 48–53], as revealed by the rapid increase of electrical conductivity in such solutions [54]. The nature of these ions and the equilibrium processes involved in their formation were studied with UV–vis spectroscopy [50, 51, 55] and by conductivity measurements [56]. Upon addition of I_2, ICl, or IBr to pyridine, significant spectral changes, and appearance of a new absorption maximum were noted, indicating the formation of an iodine–pyridine cation complex and of IX_2^- anions. In 1957, Popov and Pflaum defined the cationic species as bis(pyridine) iodine(I) (Py_2I^+), in which two molecules of pyridine are coordinated to I^+ [52]. The ionization occurs via the equilibrium [53, 57, 58] $Py + IX \leftrightarrows Py \cdot IX$, typically taking place in nonpolar solutions with pyridine in excess. In polar solutions, the neutral $Py \cdot IX$ complex undergoes ionic dissociation following the $2Py \cdot IX \leftrightarrows Py_2I^+ + IX_2^-$ equilibrium. Analogous reactions were also observed by UV–vis [46] and infrared [47, 59] spectroscopic studies for the methyl-substituted pyridines

2-picoline, 4-picoline, and 2,6-lutidine in nonpolar (benzene, chloroform, cyclohexane, and carbon tetrachloride) and polar (dichloromethane, acetonitrile, and neat Lewis base) solvents. Dissociation was also observed for nonpolar carbon disulfide (ε 2.6) solution, indicating the probable ability of sulfur to assist iodine ionization via secondary interaction [47, 59]. Tassing and Bernard confirmed the previously proposed reversible ionization of pyridine · I_2 by studying it in binary, ternary, and quaternary solvent mixtures with conductivity, far-infrared, and Raman spectroscopic measurements [48, 49]. Upon increasing the acetonitrile concentration in a mixture of I_2/pyridine/carbon tetrachloride/acetonitrile, the bands characteristic of I_3^- (Raman, 112 cm^{-1}) and of [bis(pyridine)iodine]$^+$ (IR, 636 and 436 cm^{-1}; Raman, 180 cm^{-1}) increased. Ionization was also shown to be favored by decreasing the temperature, because of the consequently increased solvent polarity (dipolar ordering). The electrical conductivity of a binary I_2/pyridine mixture increased over time with the characteristic infrared bands of I_3^- (123 cm^{-1}) increasing despite the lack of simultaneous change of the bands corresponding to [bis(pyridine)iodine]$^+$ (636 and 436 cm^{-1}). A similar observation indicating the irreversible formation of I_3^- was made upon increasing the temperature. A possible explanation for these observations might be the absorption of moisture and concomitant formation of hypoiodous acid which can further react with I_2 to form I_3^- [60]. Temperature-dependent reversible ionization was confirmed by Larsen and Allred by ^{1}H NMR studies of 2,4,6-collidine and I_2 in carbon tetrachloride/nitrobenzene solution [61].

Schuster and Roberts have provided a detailed NMR spectroscopic description of the equilibria present in polar solutions of I_2 or ICl and pyridine, 2,6-lutidine, or 2,4,6-collidine dissolved in mixtures of nitrobenzene (ε 34.8) and chloroform (ε 4.8) [62]. In 1:1 mixtures of I_2 and any of the three pyridine bases, pyridine · I_2 and [bis(pyridine)iodine]$^+$ and the corresponding complexes and cations of the other bases were detected as major and minor species, respectively. The ease of cation generation was proposed to be controlled by both electronic and steric factors, leading to cation formation of 17.6%, 8.3%, and 8.0% for 2,4,6-collidine, pyridine, and bis(2,6-lutidine)iodine, respectively (Fig. 8). Increased I_2 concentration relative to the free base 2,4,6-collidine (1:1 to 3:1) yielded less of the 1:1 charge transfer complex and more of [bis(2,4,6-collidine)iodine]$^+$. When the stronger electrophile ICl was used instead of I_2, a faster interconversion of the 2,4,6-collidine · I_2 complex and the [bis(2,4,6-collidine)iodine]$^+$ was observed, and, in addition, peaks corresponding to the monocoordinated (2,4,6-collidine)-iodine$^+$ cation were found. Substantial deshielding of the ^{13}C NMR signals of the β- and γ-carbons (5–9 ppm) of the [bis(pyridine)iodine]$^+$-type complexes were noted as compared to the shifts of the free base, reflecting a decrease in electron density of these positions. The ^{13}C chemical shift changes of the α-carbons, and α-methyl-carbons when applicable, were found to be helpful indicators for the nature of the N–I bond formed. The α- and α-methyl carbons of the dicoordinated iodine(I) complexes are deshielded compared to the free bases ($\Delta\delta_{C\alpha}$ 1–3 ppm; $\Delta\delta_{C\alpha M\varepsilon}$ 7.5 ppm), whereas they are shielded for the monocoordinated iodine(I) cations ($\Delta\delta_{C\alpha}$ (−)2–4 ppm;

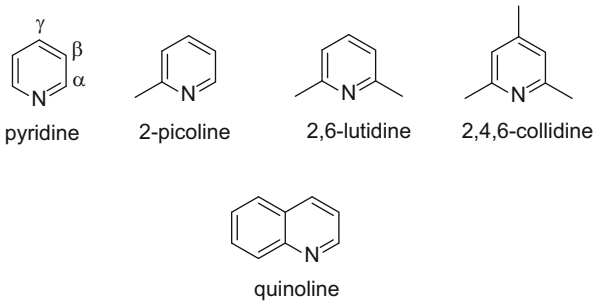

Fig. 8 Pyridine and some of its derivatives used by Schuster and Roberts to study the influence of steric and electronic factors on the geometry of $[N–X–N]^+$ complexes [62]

$\Delta\delta_{C\alpha M\varepsilon}$ (−)4 ppm). For the charge transfer complexes, however, the α-carbons were shielded but the α-methyl carbons deshielded ($\Delta\delta_{13C\alpha}$ (−)1–2 ppm; $\Delta\delta_{C\alpha M\varepsilon}$ 2 ppm). Hence, the interaction type at the nitrogen of the complexes is controlled by two mechanisms with opposite effects on the ^{13}C shifts: the reduction of electron densities has a deshielding effect, whilst the change in bond order results in increased shielding.

Solid salts of $[bis(pyridine)iodine]^+$ and $[bis(pyridine)bromine]^+$ complexes were first investigated in the 1930s by Carlsohn [63, 64] and Uschakow and Tchistow [65]. The mono- and dicoordinated picoline and quinoline analogues were addressed along with the influence of counter-ions on complex formation [66–70], revealing that benzoate and acetate promote the crystallization of monocoordinated salts, whilst the NO_3^- provides a mixture of mono- and dicoordinated complexes. Most other counter-ions, such as PF_6^-, SbF_6^-, and ClO_4^- stimulate formation of dicoordinated salts. The linear, centrosymmetric structure of $[bis(pyridine)iodine]^+$ complexes was proven by Hassel and Hope using X-ray diffraction [71]. Infrared and Raman spectroscopic investigation of the dichloromethane and acetonitrile solutions of the iodine and bromine centered bis(pyridine) and bis(4-picoline)complexes has shown that the symmetric, linear geometry observed in the solid state is retained in solution, although no spectroscopic evidence was found for retained coplanarity [72]. Upon changing the solvent environment (dichloromethane, ε 8.9; acetonitrile, ε 37.5) the vibrational frequencies remained unaltered, proving that solvent polarity does not affect the geometry of such three-center halogen bonded complexes. The proposed N–X stretching and interaction force constants are comparably large to that of the isoelectric trihalide ions. The motion of the central halogen in the $[N–X–N]^+$ complex was suggested to follow a flat, single-well energy potential. Sabin's contemporary computational calculations supported this hypothesis [73]. It should be noted that in the solution studies of Haque and Wood the halogen(I) complexes were all rather unstable in solution, with the $[bis(picoline)bromine]^+$ complex decomposing most rapidly [72]. Carter's electronic absorption spectroscopic study of dichloromethane and ethanol solutions of $[bis(pyridine)iodine]^+$-type complexes with BF_4^- and PF_6^- counter-ions [74] confirmed the conclusions of Haque and Wood that the environment does not substantially affect the geometry of such charged, three-centered

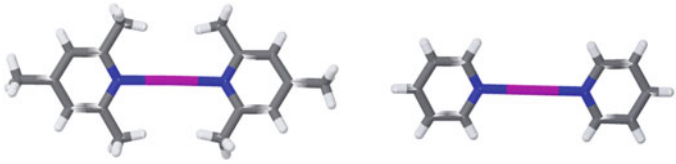

Fig. 9 The X-ray structures of [bis(collidine)iodine]$^+$ (*left*) and [bis(pyridine)iodine]$^+$ (*right*), determined by Wada et al. [76]. The aromatic rings of the collidine complex have a dihedral angle of 18.5° and of the pyridine complex 1.2°. The [N–I–N]$^+$ bond of the sterically hindered, twisted complex is asymmetric while that of the pyridine complex is centrosymmetric

complexes [74]. The infrared spectroscopic study of dicoordinated 2- and 3-picoline complexes of iodine(I) and bromine(I) in dichloromethane indicated splitting of the bands in the sensitive mode, within the frequency range of 1.030–990 cm^{-1}, interpretable as a symmetry breakage resulting from steric hindrance close to the halogen bond acceptor [75]. The spectral changes were most pronounced for the sterically maximally hindered 2-picoline complexes.

In good agreement, the crystallographic analysis of [bis(pyridine)iodine]$^+$ and [bis(collidine)iodine]$^+$ (Fig. 9) by Wada et al. suggested loss of the planar centrosymmetric arrangement upon introduction of α-methyl functionalities, which in turn also leads to increased reactivity of the iodine(I) complex [76].

The ^{1}H NMR spectroscopic study of dicoordinated iodine(I) and bromine (I) complexes comprising pyridine, picoline, and lutidine halogen bond acceptors and the BF_4^- or ClO_4^- counter-ion indicated uniformly larger deshielding of the pyridine β- and γ-protons than of the α-protons upon complex formation [77]. This shift change is the result of the redistribution of π-electron density upon coordination to a positively charged species, and was reported to be greater for the bromine (I) than for the iodine(I) complexes. A particularly large deshielding of the α-protons of the iodine(I) complexes with 2-picoline was noticed (BF_4^- 0.49 ppm; ClO_4^- 0.59 ppm).

Short secondary bonds are usually believed to be especially strong. Three-center-four-electron halogen bonded complexes were repeatedly reported to have unusually short donor–acceptor distances and to possess remarkably high bond energies. This unusual bond strength is likely to be the result of either resonance stabilization or the formation of a symmetric three-center bond possessing a significant covalent character. Importantly, the first arrangement is a combination of two asymmetric structures which have a classical covalent N–X, and a classical secondary halogen bond, which differ greatly in bond strength and length. In contrast, a symmetric structure presupposes two equally long and strong N···X halogen bonds, none of them being fully primary or secondary yet both possessing some covalent character while also retaining features typical for secondary interactions. Analogous three-center hydrogen bonds were frequently claimed to prefer the symmetric arrangement in solution and to be unusually strong; however, decades of investigations were unable to provide evidence for this hypothesis [78, 79]. Recent solution NMR studies addressed the nature of the [N–I–N]$^+$ and [N–Br–

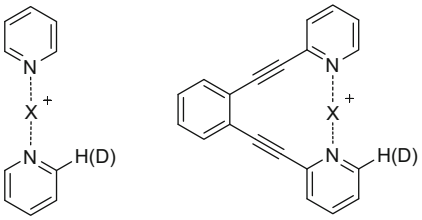

Fig. 10 The structure of [bis(pyridine)iodine]$^+$ complexes utilized in the investigation of the symmetry of three-center halogen bonds in solutions [80–82]. Whereas the [bis(pyridine)halogen]$^+$ complex allows free adjustment of N···X bond distances and angles, the [bis(pyridinylethynyl)benzene)halogen]$^+$ backbone introduces a slight geometric restraint

N]$^+$ halogen bonds by investigation of flexible and structurally restrained [bis(pyridine)halogen]$^+$ complexes (Fig. 10) [80, 81].

As standard spectroscopic methods are unable to distinguish between a static symmetric and a rapidly equilibrating mixture of asymmetric structures, the latter providing time averaged signals, Saunder's isotopic perturbation of equilibrium technique [83, 84] was utilized with ^{13}C NMR detection and the possible minimal perturbation introduced by deuterium substitution, close to the [N–X–N]$^+$ interaction site. Spectroscopic data obtained for dichloromethane and acetonitrile solutions indicated static symmetric structures and a slight strengthening of the iodine and bromine-centered bonds upon increasing solvent polarity (^{15}N NMR coordination shifts for [N–Br–N]$^+$ −76 to −81 ppm; for [N–I–N]$^+$ −108 to −110 ppm). The experimental data was supported by DFT estimation of the binding energies; the stability of the complexes increases when going from the less polar dichloromethane to the more polar acetonitrile solvent ([N–Br–N]$^+$ −126.6 to −149.5 kJ/mol; [N–I–N]$^+$ −105.1 to −134.3 kJ/mol) [82]. Importantly, the charge distribution of the complexes remains unaffected by polarity change of the environment, suggesting high stabilization by formation of a truly symmetric three-center-four-electron complex. Energy decomposition analysis indicates that the bromine and iodine-centered interactions have comparable electrostatic and covalent contributions (N···Br: 54% vs 46%; N···I: 50% vs 50%) [85]. The positive charge is, to a large extent, transferred to the pyridine rings in these systems: in the [N–Br–N]$^+$ complex barely 28% of the positive charge remains on the bromine, whereas in the corresponding iodine-centered complex 41% of the charge is located on the iodine [82] Thus, the solvent polarity dependence of charged three-center halogen bonds better resembles that of neutral than of charged two-center halogen bonds. This may best be interpreted by the overall solvent effect on charged two-center halogen bonds being primarily determined by the solvation of their charged constituent. The more polar solvents tend to solvate better the charged halogen bond acceptor than the asymmetric, two-center halogen bonded complex. This induces dissociation of the complex and hence weakens the halogen bond. In contrast, the formation of the symmetric inter- and intramolecular, three-center charged halogen bonds addressed above (Fig. 10) results in a large energetic gain which is not disrupted by solvation. In addition, the charge is delocalized to a larger

degree in these systems as compared to the charge of the two-center halogen bonds. Diffusion NMR indicated that solvation affects primarily the counter-ion of the charged three-center systems, making the partially positively charged halogen more accessible for nucleophilic attack [86]. Accordingly, the $[N–I–N]^+$ and $[N–Br–N]^+$ complexes were found to be significantly less stable in acetonitrile than in dichloromethane solution. The hygroscopicity of acetonitrile was suggested to play an important role in the observed faster degradation of the complexes as compared to that observed for dichloromethane solutions. Based on electronic absorption spectroscopy, Tytko and Schmeisser reported the formation of pyridinium ions in the acetonitrile solution of [bis(pyridine)bromine]$^+$ ClO_4^-, NO_3^-, and $SbCl_6^-$ complexes in 1973 [87]. They gave the bromination of the acetonitrile solvent as an explanation, but, in light of later studies, the generation of pyridinium ions is more likely to be the consequence of a chemical reaction of [bis(pyridine)bromine]$^+$ with the contaminant water, originating from the hygroscopicity of acetonitrile. Worth mentioning is that some studies of [bis(pyridine)iodine]$^+$ and [bis(pyridine)bromine]$^+$ complexes applied recrystallization from polar, protic methanol for purification [70]. This presupposes both the electrophilicity and the acidity of methanol to be too weak to break the highly stabilized three-center $[N–X–N]^+$ bond. It should be noted here that the 13C NMR data reported for this complex corresponds to that of the corresponding protonated pyridine complex, its degradation product.

Competition of acetonitrile with pyridine for halogen binding was shown unlikely by computation, in agreement with the NMR spectroscopic data which does not indicate existence of mixed complexes [82]. In the absence of a strong Lewis base, however, acetonitrile is capable of forming centrosymmetric [bis(acetonitrile)iodine]$^+$ complexes [86, 88]. In the acetonitrile solution of [bis(acetonitrile)iodine]$^+$ salts, the iodine-bound acetonitrile is readily displaced by the stronger electron donor pyridine to give the corresponding [bis(pyridine)iodine]$^+$ complex. Analogous ligand exchange has also been observed by other investigators [85, 89]. Brown et al. reported a tenfold increase of exchange rate for the ligand replacement upon changing the solvent from dichloromethane to the more polar acetonitrile [89].

[Bis(pyridine)iodine]$^+$ and [bis(pyridine)bromine]$^+$ salts are useful reagents for organic synthesis [90]. As sources of electrophilic halogens, they are applicable for I^+ or Br^+ transfer reactions, in, for example, the halogenation of alkenes, alkynes, and aromatics, in oxidations, and in halocyclizations [76, 90, 91]. The earliest [bis(pyridine)iodine]$^+$ and [bis(pyridine)bromine]$^+$ complexes were generated in situ from chloroform solutions of pyridine and $AgNO_3$ upon addition of Br_2 [92] or INO_3 [93]. To date, stable dicoordinated iodine(I) and bromine(I) salts of low hygroscopicity comprising either pyridine or collidine (2,4,6-trimethylpyridine) as the Lewis base, and BF_4^- [94], ClO_4^- [95], or PF_6^- [96] as the counter-ion are used as synthetic reagents. Of these, [bis(pyridine)iodine]BF_4 has been marketed as Barluenga's reagent [90, 94, 97, 98]. The [bis(pyridine)halogen]$^+$ reagents show a solvent-dependent reactivity, with occasionally higher yields obtained upon carrying out a transformation in acetonitrile as compared to dichloromethane solution [76, 98], a difference emphasizing the high importance of solvation [82].

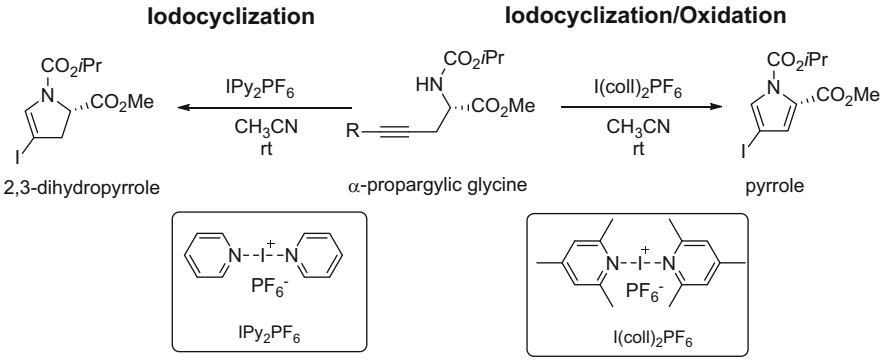

Fig. 11 The choice of the iodonium complex of pyridines provides control over the iodocyclization/oxidation of α-propargylic glycine

The correlation of structure and reactivity of $[N–I–N]^+$ complexes was powerfully demonstrated by the recent study of Wada et al. [76], in which [bis(pyridine)iodine]PF_6 yielded iodocyclization whilst [bis(collidine)iodine]PF_6 yielded oxidation of the same substrate (Fig. 11). The higher reactivity of [bis(collidine)iodine]PF_6 was suggested to be caused by its slightly twisted, asymmetric structure (N–I, 2.272 Å and 2.304 Å), as consequence of the 2,6-dimethyl substitution. The less reactive [bis(pyridine)iodine]PF_6 was, in contrast, reported to be coplanar and symmetric, with N–I distances of 2.259 Å. The observed reactivity difference may also be satisfactorily explained from a mechanistic point of view, as was done by Brown et al. for the corresponding [bis(collidine)bromine]OTf and [bis(pyridine)bromine]OTf reagents [89, 99]. Thus, the lower reactivity by [bis(pyridine)iodine]PF_6 might also be caused by the higher overall activation energy required for dissociation of the [bis(pyridine)iodine]$^+$ complex to generate the key pyridine–iodine$^+$ intermediate. Obviously, the reactivity of $[N–X–N]^+$-type reagents is tunable by solvation as well as by small structural modifications. Attempts to develop a stereoselective halogenation reagent based on the [bis(pyridine)iodine]$^+$ ion has been attempted, but so far without success [100, 101].

The structure of the F- and Cl-centered $[N–X–N]^+$ bonds was first addressed by semi-empirical CNDO/2 calculations by Sabin [102], predicting isolable stable [bis(pyridine)fluorine]$^+$ and [bis(pyridine)chlorine]$^+$ complexes with 1.365 and 1.795 Å N···F and N···Cl bonds, respectively. A large extent of charge transfer resulting in 70–80% of the positive charge being located in the pyridine rings was foreseen, comparing well to that predicted for their iodine and bromine-centered analogues [82]. The fluorine-centered complex was later predicted to be asymmetric (M06-2X level) with one covalent N^+–F and another dispersion-driven F···N bond [85]. In the same study by Dutton et al., the chlorine-centered bond was predicted to be symmetric. Additional analysis of the dissociation thermochemistry and the Wiberg bond index emphasized the dative character of the $[N–X–N]^+$ bonds. Although

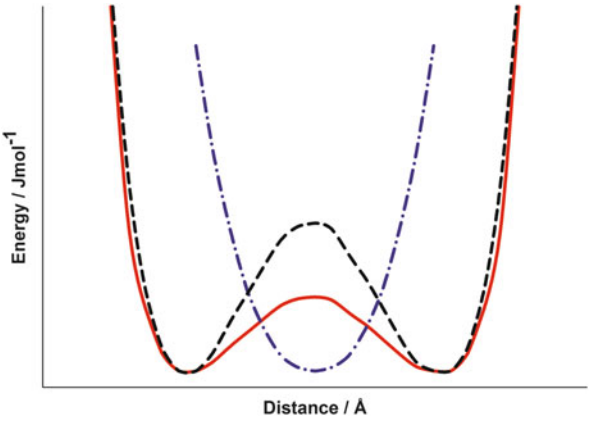

Fig. 12 The possible potential energy curves for halogen motion in trihalide ions. (**a**) In a symmetric $[X\cdots X\cdots X]^-$ arrangement, the halogen motion follows a single-well potential (*blue*). (**b**) Upon a shallow energy barrier, two equal asymmetric geometries interconvert, $[X-X\cdots X]^+ \leftrightarrows [X\cdots X-X]^+$, providing a dynamic mixture best described by an isoenergetic double well (*red*). (**c**) A high energy barrier, in contrast, results in a static, asymmetric arrangement, $[X–X\cdots X]^+$, with a distinct covalent and a distinct secondary bond (*black*)

predicted to possess high enough stability for isolation, no experimental studies of the chlorine- and fluorine-centered complexes have so far been presented.

Trihalide ions (X_3^-) are isoelectronic to the three-center-four-electron $[N–X–N]^+$ complexes discussed above. An extensive computational analysis of their structure and bonding mechanism was presented by Wolters and Bickelhaupt [103]. Among them, I_3^- is the most extensively studied and it was reported to possess the strongest known halogen bond so far (180 kJ/mol) [12]. It is centrosymmetric in the gas-phase, whereas it was both reported symmetric and asymmetric in the solid state [104, 105]. The motion of the central halogen follows a single-well energy potential for the symmetric, and a double-well potential with a shallow barrier for the asymmetric geometry (Fig. 12). Other trihalide ions capable of forming a symmetric arrangement (e.g., Br_3^-, Cl_3^-, ICl_2^-, and IBr_2^-, etc.) were also found either symmetric or asymmetric in the solid state [104, 105]. This reflects comparable energies for the symmetric and asymmetric arrangements, and a high importance of the chemical environment and of crystal packing forces.

Large cations, such as the tetraalkylammonium ion, promote symmetric whereas small cations promote asymmetric trihalide geometry [106]. To study the symmetry of trihalide ions in solution experimentally, i.e., whether their preferred geometry is static, symmetric ($^{\delta-}X\cdots X^{+}\cdots X^{\delta-}$), or is comprised of rapidly flipping, asymmetric structures with unequal bond lengths ($X-X\cdots X^- \leftrightarrows X^-\cdots X-X$), is a challenge. Apart from fluorine, they do not give NMR signals useful for symmetry studies and thus vibrational optical spectroscopies remain the crucial tool for such investigations. In the 1960s, a comparative infrared and Raman spectroscopic study of the trihalide salts ICl_2^-, $BrCl_2^-$, Br_3^-, IBr_2^-, and I_3^- in both solid and solution

phases (e.g., water, dichloroethane, chloroform, nitrobenzene, and methanol) was performed. Slightly asymmetric trihalide geometry [107] corresponding to a flat, single-well energy potential easily affected by weak forces [108] was suggested to exist in solution. Based on the vibrational spectroscopic data, force constants were estimated, and their unusual strengths were explained by a major contribution from the halogen p-orbitals to the interaction, following Pimentel's proposal [109]. The infrared and Raman spectroscopic study of the Et_4N^+ and Bu_4N^+ salts of trihalides, carried out by Gabes and Gerding, indicated comparable vibrational frequencies in the solid state and in dichloromethane solutions [110]. However, there was an obvious breakdown of the selection rules for a symmetric $D_{\infty h}$. Bands with asymmetric stretching modes were observed in the Raman spectra, especially for the ions IBr_2^-, I_3^-, and Br_3^-, but weak and broad bands with asymmetric stretching modes were also found for the ions ICl_2^- and $BrCl_2^-$. The same trend was also seen for nitrobenzene, ethanol, methanol, chloroform, and nitromethane solutions, leading to the conclusion that trihalide ions are slightly asymmetric in solutions, but are linear and symmetric in the solid-state. KBr_3 was regarded to contain Br_2 molecules in interaction with Br^- ions. The independent infrared and Raman spectroscopic study by Kuwano et al. of ICl_2^- and IBr_2^- with pyridinium or 4-aminopyridinium counter-ions in methanol solution indicated the coexistence of the symmetric and the asymmetric geometries for the ICl_2^- ion [111]. In contrast, for IBr_2^- only the asymmetric geometry was observed.

The I_3^- ion was studied by resonance Raman spectroscopy excited with a UV-laser in the polar, protic solvents water, methanol, and ethanol [112, 113]. For aqueous solution the band characterized as the symmetric vibration mode (116 cm^{-1}) was observed, whereas both a strong symmetric (111–112 cm^{-1}) and a weaker asymmetric (143 cm^{-1}) stretching mode were observed for methanol and ethanol solutions. Johnson and Myers studied I_3^- in the polar, protic solvent ethanol [114, 115] and in the polar, aprotic solvents ethylacetate and acetonitrile [116] by Raman spectroscopy. The ethanol solution of I_3^- showed antisymmetric stretching modes, indicating symmetry breaking by the local protic environment. For ethyl acetate these "forbidden" broken symmetry bands were much weaker, whereas for acetonitrile they were, in principle, undetectable. From these observations it was postulated that the I_3^- ion is symmetric in acetonitrile, less symmetric in ethyl acetate, and least symmetric in the hydrogen bonding solvent ethanol. Based on infrared spectroscopic investigation of I_3^- in a mixture of 2,3-diaminopyridine and I_2 in dichloromethane solution, Al-Hashimi proposed an asymmetric, bent geometry for I_3^- [117].

By thorough computational investigations applying a variety of solvent models, a general trend for the solvent effect on the symmetry of I_3^- was postulated [118–123]. Because of hydrogen bond-induced polarization, protic solvents, such as water, methanol, and ethanol, induce an asymmetric geometry with unequal bond lengths and an asymmetric charge distribution. The energy barrier for the interconversion between the equivalent, asymmetric geometries $[I-I\cdots I]^- \leftrightarrows [I\cdots I-I]^-$ was predicted to be best described by a double-well energy potential (Fig. 12), with a very high barrier for the aqueous but a low barrier for the ethanol solutions. In

polar, aprotic solvents the motion of the central iodine of I_3^- may either follow a broad, flat single-well or a very low-barrier double well potential. At room temperature, the former was predicted for tetrahydrofuran and the latter for acetonitrile. Symmetry breaking was also predicted to be inducible by lowering the temperature, as a consequence of the temperature dependence of the dielectric constant of common solvents [120, 121]. Johnson and Myers, and Lynden-Bell et al., have raised concern that for rate constants equivalent to or larger than 10 cm^{-1} the antisymmetric mode would be undetectable. Accordingly, a very low-barrier interconversion and a no-barrier state would provide virtually identical vibrational spectra [116, 118]. All in all, both experimental evidence and computational arguments indicate that the symmetry of the linear, centrosymmetric ground-state of X_3^- ions is sensitive to the chemical environment. Symmetry breaking may be induced by electrostatic interaction with the solvent and/or the counter-ion. Hydrogen bond donor solvents efficiently desymmetrize the trihalide ions.

6 Conclusions and Outlook

Halogen bonds have a dominant electrostatic component, manifested by their computationally predicted increasing linearity upon solvation. In apolar, non-interacting solvents, halogen bonding is arguably well described by a simple electrostatic model. For more polar solutions, the correlation between experimental stabilities and stability predicted by a purely electrostatic model is weaker. The charge transfer component of the interaction is larger for the stronger three-center bonds. Neutral halogen bonds exhibit a larger dispersion contribution and are thus more dependent on appropriate correction of the basis set superposition error than charged halogen bonds. Solvation has a significant influence on halogen bonding, with its impact being largely dependent on the electronic character of the interaction partners and of the resulting bond:

The most conventional neutral, two-centered halogen bonds experience a slight stabilization upon increasing environment polarity. Solvation has a slight stabilizing effect on them. However, the heteroatom of the most common polar, aprotic solvents may themselves interact with the halogen bond donor and acceptor functionalities, yielding an overall slight destabilizing effect. Two-center halogen bonds have in general only marginal stability in solutions. Accordingly, their experimental studies have to a large extent been carried out on substances in which halogen bond donor ability is enhanced by perfluorination. Charged, two-center halogen bonds are considerably stronger than their neutral analogues, and accordingly they are fairly stable in solution. Their bond strength rapidly decreases with increasing solvent polarity. Their solvation energies are smaller than the sum of the solvation energies of their subunits, yielding their overall destabilization by polar solvents.

Formation of a three-center halogen bond through extensive shortening of the halogen bond donor–acceptor distance and concomitant elongation of the covalent bond of the halogen yields a very significant stabilization. Three-center halogen

bonds appear much stronger than conventional two-center bonds. Their symmetry and stability is virtually unaffected by alteration of solvent polarity, even if some small stabilization is expected for charged three-center bonds upon better solvation. In analogy to two-center bonds, they are disrupted by protic solvent.

The overall energy difference of halogen bonds decreases with increasing environment polarity. In contrast to the opposite effect of polarity on neutral and charged complexes, protic solvents efficiently disrupt any types of halogen bonds. Consequently, even a small percentage of water in hygroscopic solvents, such as DMSO, is expected to have a strong, detrimental effect on the observed overall stability of a halogen bond. Whereas neutral halogen bonds are practically non-existent in methanol or water, the most stable charged halogen bonded complexes remain even in these solvents, with some well-known examples being the halogen bonds of multidentate anion receptors and those of trihalide anions.

The seemingly inconsistent effect of solvent polarity on halogen bonds can be rationalized by the opposing influence of solvation on the electronically different halogen bonds. The formation of neutral bonds yields polar complexes which are better solubilized in a polar environment. Consequently, they are stabilized by higher solvent polarity. Charged halogen bond acceptors are well solubilized in polar solvents. As a consequence, the dissociation of charged two-center halogen bonded complexes, which have a lower charge separation compared to the corresponding subunits, is promoted by solvation of more polar solvents, whilst they are stabilized by apolar solvents which facilitate charge delocalization. The charged three-center halogen bond is barely affected by alteration of solvent polarity. Its counter-ion is prone to dissociate in more polar solvents, but the dissociation or asymmetrization of the three-center bond itself is disfavored because of the exceptionally large stabilization associated with its formation. This is true, despite the substantial entropic gain accompanying the dissociation of secondary bonds in general which further contributes to the destabilization of weaker two-center bonds upon solvation.

Rational application of the halogen bonding phenomenon in chemistry and biology necessitates a thorough understanding of the influence of solvents on its properties. Instructive spectroscopic and computational studies of small model systems provided the fundaments of the required knowledge. Further progress in the field is greatly supported by computations using explicit solvation models taking into consideration the competition of halogen and hydrogen bonds of the solvent and the solutes. Detailed studies of more complex than oligoatomic systems are certainly both helpful and influential for real-life applications.

7 Addendum

Since the submission of this manuscript several publications of importance to its topic have appeared. The $[N\cdots Cl\cdots N]^+$ and $[N\cdots F{-}N]^+$ halogen bonds of [bis (pyridine)chlorine]$^+$ and bis(pyridine)fluorine]$^+$ that were previously only studied

computationally, [85, 102] were demonstrated to be symmetric and asymmetric, respectively, in solution [124]. Suzaki et al. reported the asymmetric $[N\cdots Cl\text{-}N]^+$ arrangement for a related, sterically highly constrained [bis(pyridine)chlorine]$^+$ complex possessing two 1,2-dialkyl benzene units, and a corresponding symmetric $[N\cdots Br\cdots N]^+$ complex [125]. In contrast to the study of Karim et al. [124] that was performed at −80°C and under dry conditions, the latter investigation was done at room temperature in an open system. Accordingly, the mass (HRMS) of the chlorine-centered complex corresponded to that of the hydrochloric acid adduct of the ligand. Koskinen et al. has recently described analogous $[S\text{-}I\text{-}S]^+$ complexes in the solid state [126]. Three-center halogen bonds were reviewed [127]. Beer et al. reported the covalency of halogen bonds in a catenane-based receptor system in various solvents [128]. The solvent dependency of the association of a multipoint halogen bond donor motif with orthoamide was described by Huber et al. [129], whereas anion recognition in aqueous media, utilizing halogen bonding, by Beer [130]. Hunter et al. reported the solvent independent strength of the halogen bond of iodine and tetramethylthiourea [131]. Rissanen et al. disclosed the solution NMR study of multivalent halogen bonded deep cavity cavitands [132], whereas Diedrich et al. reported the thermodynamics of halogen bonding of substituted (iodoethynyl) benezene derivatives in solution.[133] The solvent and temperature effects on an intramolecular halogen bonding was studied by Bowling et al. [134]. The applications of halogen bonding in solution were recently reviewed by Vargas Jetzsch [135].

Acknowledgments The research leading to these results has received funding from the European Union Seventh Framework Programme (FP7/2007–2013) under grant agreement no. 259638, and from the Swedish Research Council (VR 2012–3819). Jenny Mattsson (University of Gothenburg) is gratefully acknowledged for linguistic improvement of the text.

References

1. Guthrie F (1863) On the iodide of iodammonium. J Chem Soc 16:239–244
2. Lachman A (1903) A probable cause of the different colors of iodine solutions. J Am Chem Soc 25:50–55
3. Kleinberg J, Davidson AW (1948) The nature of iodine solutions. Chem Rev 42:601–609
4. Walker OJ (1935) Absorption spectra of iodine solutions and the influence of the solvent. Trans Faraday Soc 31:1432–1438
5. Benesi HA, Hildebrand JH (1949) A spectrophotometric investigation of the interaction of iodine with aromatic hydrocarbons. J Am Chem Soc 71:2703–2707
6. Mulliken RS (1950) Structures of complexes formed by halogen molecules with aromatic and with oxygenated solvents. J Am Chem Soc 72:600–608
7. Hassel O, Hvoslef J (1954) The structure of bromine 1,4-dioxanate. Acta Chem Scand 8:873
8. Hassel O (1970) Structural aspects of interatomic charge transfer bonding. Science 170:497–502
9. Bertran JF, Rodriguez M (1979) Detection of halogen bond formation by correlation of proton solvent shifts. 1. Haloforms in normal-electron donor solvents. Org Magn Resonance 12:92–94

10. Blackstock SC, Lorand JP, Kochi JK (1987) Charge transfer interactions of amines with tetrahalomethanes - X-ray crystal-structures of the donor-acceptor complexes of quinuclidine and diazabicyclo[2.2.2]octane with carbon tetrabromide. J Org Chem 52:1451–1460
11. Legon AC (1999) Prereactive complexes of dihalogens XY with Lewis bases B in the gas phase: a systematic case for the halogen analogue B–XY of the hydrogen bond B–HX. Angew Chem Int Ed 38:2687–2714
12. Metrangolo P, Neukirch H, Pilati T et al (2005) Halogen bonding based recognition processes: a world parallel to hydrogen bonding. Acc Chem Res 38:386–395
13. Erdelyi M (2012) Halogen bonding in solution. Chem Soc Rev 41:3547–3557
14. Beale TM, Chudzinski MG, Sarwar MG et al (2013) Halogen bonding in solution: thermodynamics and applications. Chem Soc Rev 42:1667–1680
15. Bertran JF, Rodriguez M (1981) On the nature of haloform-aromatic complexes. Org Magn Resonance 16:79–81
16. Bertran JF, Rodriguez M (1980) Detection of halogen bond formation by correlation of proton solvent shifts. 2. Methylene halides in *N*-electron donor solvents. Org Magn Resonance 14:244–246
17. Metrangolo P, Panzeri W, Recupero F et al (2002) Perfluorocarbon-hydrocarbon self-assembly – Part 16. ^{19}F NMR study of the halogen bonding between halo-perfluorocarbons and heteroatom containing hydrocarbons. J Fluor Chem 114:27–33
18. McKinney WJ, Popov AI (1969) Studies on chemistry of halogens and of polyhalides. 30. Influence of solvent properties on formation of pyridine-iodine charge transfer complexes. J Am Chem Soc 91:5215–5218
19. Bhaskar KR, Singh S (1967) Spectroscopic studies of N-donor-sigma-acceptor systems – pyridines. Spectrochim Acta A 23:1155–1159
20. Laurence C, Queigneccabanetos M, Wojtkowiak B (1983) 1-Iodoacetylenes. 4. Structure-reactivity relationships for the complexation of substituted 1-iodoacetylenes with Lewis-bases. Can J Chem 61:135–138
21. Laurence C, Queigneccabanetos M, Dziembowska T et al (1981) 1-Iodoacetylenes. 1. Spectroscopic evidence of their complexes with Lewis-bases - a spectroscopic scale of soft basicity. J Am Chem Soc 103:2567–2573
22. Laurence C, Queigneccabanetos M, Wojtkowiak B (1982) 1-Iodoacetylenes. 2. Formation-constants of their complexes with Lewis-bases. J Chem Soc Perkin Trans 2:1605–1610
23. Webb JA, Klijn JE, Hill PA et al (2004) Experimental studies of the ^{13}C NMR of iodoalkynes in Lewis-basic solvents. J Org Chem 69:660–664
24. Cabot R, Hunter CA (2009) Non-covalent interactions between iodo-perfluorocarbons and hydrogen bond acceptors. Chem Commun 2005–2007
25. Sarwar MG, Dragisic B, Salsberg LJ et al (2010) Thermodynamics of halogen bonding in solution: substituent, structural, and solvent effects. J Am Chem Soc 132:1646–1653
26. Hunter CA (2004) Quantifying intermolecular interactions: guidelines for the molecular recognition toolbox. Angew Chem Int Ed 43:5310–5324
27. Dimroth K, Bohlmann F, Reichard C et al (1963) Über Pyridinium-*N*-phenol-betaine und ihre Verwendung zur Charakterisierung der polarität von Losungsmitteln. Liebigs Ann Chem 661:1–37
28. Kamlet MJ, Abboud JL, Taft RW (1977) Solvatochromic comparison method. 6. π* scale of solvent polarities. J Am Chem Soc 99:6027–6038
29. Dong DC, Winnik MA (1982) The Py scale of solvent polarities - solvent effects on the vibronic fine-structure of pyrene fluorescence and empirical correlations with E_T-value and *Y*-value. Photochem Photobiol 35:17–21
30. Li QZ, Li R, Zhou ZJ et al (2012) S···X halogen bonds and H···X hydrogen bonds in H_2CS-XY (XY=FF, ClF, ClCl, BrF, BrCl, and BrBr) complexes: cooperativity and solvent effect. J Chem Phys 136:014302
31. Lu YX, Li HY, Zhu X et al (2011) How does halogen bonding behave in solution? A theoretical study using implicit solvation model. J Phys Chem A 115:4467–4475

32. Lu YX, Li HY, Zhu X et al (2012) Effects of solvent on weak halogen bonds: density functional theory calculations. Int J Quantum Chem 112:1421–1430
33. Hawthorne B, Fan-Hagenstein H, Wood ER et al (2013) Study of the halogen bonding between pyridine and perfluoroalkyl iodide in solution phase using the combination of FTIR and ^{19}F NMR. Int J Spectrosc 2013:216518
34. Libri S, Jasim NA, Perutz RN et al (2008) Metal fluorides form strong hydrogen bonds and halogen bonds: measuring interaction enthalpies and entropies in solution. J Am Chem Soc 130:7842–7844
35. Forni A, Rendine S, Pieraccini S et al (2012) Solvent effect on halogen bonding: the case of the I···O interaction. J Mol Graph Model 38:31–39
36. Ma N, Zhang Y, Ji B et al (2012) Structural competition between halogen bonds and lone-pair···pi interactions in solution. Chemphyschem 13:1411–1414
37. Li QZ, Xu XS, Liu T et al (2010) Competition between hydrogen bond and halogen bond in complexes of formaldehyde with hypohalous acids. Phys Chem Chem Phys 12:6837–6843
38. Zhang Y, Ji BM, Tian AM et al (2012) Communication: competition between π···π interaction and halogen bond in solution: a combined ^{13}C NMR and density functional theory study. J Chem Phys 136:141101
39. Zou WS, Han J, Jin WJ (2009) Concentration-dependent Br···O halogen bonding between carbon tetrabromide and oxygen-containing organic solvents. J Phys Chem A 113:10125–10132
40. Sarwar MG, Dragisic B, Sagoo S et al (2010) A tridentate halogen-bonding receptor for tight binding of halide anions. Angew Chem Int Ed 49:1674–1677
41. Kilah NL, Wise MD, Serpell CJ et al (2010) Enhancement of anion recognition exhibited by a halogen-bonding rotaxane host system. J Am Chem Soc 132:11893–11895
42. Sarwar MG, Dragisic B, Dimitrijevic E et al (2013) Halogen bonding between anions and iodoperfluoroorganics: solution-phase thermodynamics and multidentate-receptor design. Chem Eur J 19:2050–2058
43. Walter SM, Kniep F, Rout L et al (2012) Isothermal calorimetric titrations on charge-assisted halogen bonds: role of entropy, counterions, solvent, and temperature. J Am Chem Soc 134:8507–8512
44. Parra RD (2012) Dimers and trimers of formamidine and its mono-halogenated analogues HN=CHNHX, (X=H, Cl, Br, or I): a comparative study of resonance-assisted hydrogen and halogen bonds. Comput Theor Chem 998:183–192
45. Waentig P (1910) On the state of dissolved iodine. Z Phys Chem 68:513–571
46. Popov AI, Rygg RH (1957) Studies on the chemistry of halogens and of polyhalides. XI. Molecular complexes of pyridine, 2-picoline and 2,6-lutidine with iodine and iodine halides. J Am Chem Soc 79:4622–4625
47. Haque I, Wood JL (1967) The infra-red spectra of pyridine-halogen complexes. Spectrochim Acta A 23:959–967
48. Tassaing T, Besnard M (1997) Ionization reaction in iodine/pyridine solutions: what can we learn from conductivity measurements, far-infrared spectroscopy, and Raman scattering? J Phys Chem A 101:2803–2808
49. Tassaing T, Besnard M (1997) Vibrational spectroscopic studies of the chemical dynamics in charge transfer complexeses of the type iodine-pyridine 1. Experimental results. Mol Phys 92:271–280
50. Zingaro RA, VanderWerf CA, Kleinberg J (1951) Evidence for the existence of unipositive iodine ion in solutions of iodine in pyridine. J Am Chem Soc 73:88–90
51. Reid C, Mulliken RS (1954) Molecular compounds and their spectra. IV. The pyridine-iodine system. J Am Chem Soc 76:3869–3874
52. Popov AI, Pflaum RT (1957) Studies on the chemistry of halogens and of polyhalides. X. The reactions of iodine monochloride with pyridine and with 2,2′-bipyridine. J Am Chem Soc 79:570–572
53. Creighton JA, Haque I, Wood JL (1966) The iododipyridinium ion. Chem Commun 229

54. Audrieth LF, Birr EJ (1933) Anomalous electrolytes. I. The electrical conductivity of solutions of iodine and cyanogen iodide in pyridine. J Am Chem Soc 55:668–673
55. Kleinberg J, Colton E, Sattizahn J et al (1953) The behavior of iodine species in pyridine and quinoline. J Am Chem Soc 75:442–445
56. Kortüm G, Wilski H (1953) Über die elektrische Leitfähigkeit von Jod-Pyridin-Lösungen. Z Phys Chem 202:35–55
57. Ginn SGW, Wood JL (1965) The structure of the triiodide ion. Chem Commun 262–263
58. Ginn SGW, Wood JL (1966) Intermolecular vibrations of charge transfer complexes. Trans Faraday Soc 62:777–787
59. Haque I, Wood JL (1967) The infra-red spectra of γ-picoline-halogen complexes. Spectrochim Acta A 23:2523–2533
60. Bell RP, Gelles E (1951) The halogen cations in aqueous solution. J Chem Soc 2734–2740
61. Larsen DW, Allred AL (1965) Halogen complexes. II. The types and mean lifetimes of complexes formed by iodine and 2,4,6-trimethylpyridine. J Am Chem Soc 87:1219–1226
62. Schuster II, Roberts JD (1979) Halogen complexes of pyridines: a proton and carbon-13 nuclear magnetic resonance study. J Org Chem 44:2658–2662
63. Carlsohn H (1932) Habilitationsschrift: Über eine neue Klasse von Verbindungen des positive Einwertigen Jod. Verlag von S. Hirzel, Liepzig
64. Carlsohn H (1935) Beiträge zur Chemie des Broms, I. Mitteil.: Darstellung von Brom (I)-dipyridin-perchlorat und Brom (I)-dipyridin-nitrat. Chem Ber 68B:2209–2211
65. Uschakow MI, Tchistow WO (1935) Über salzartige Eigenschaften der Halogene. Einwerkungsprodukte von Brom auf Silbersalze. Chem Ber 68B:824–830
66. Kleinberg J (1946) The positive character of the halogens. J Chem Educ 23:559–562
67. Zingaro RA, Goodrich JE, Keinberg J et al (1949) Reactions of the silver salts of carboxylic acids with iodine in the presence of some tertiary amines. J Am Chem Soc 71:575–576
68. Zingaro RA, Van der Werf CA, Kleinberg J (1950) Further observation on the preparation and reactions of positive iodine salts. J Am Chem Soc 72:5341–5342
69. Schmidt H, Meinert H (1959) Zur Darstellung von Salzen mit positiv einwertigen Halogen-Kationen. Angew Chem 71:126–127
70. Kleinberg J (1963) Unipositive halogen complexes. Inorg Synth 7:169–176
71. Hassel O, Hope H (1961) Structure of the solid compound formed by addition of two molecules of iodine to one molecule of pyridine. Acta Chem Scand 15:407–416
72. Haque I, Wood JL (1968) The vibrational spectra and structure of the bis(pyridine)iodine(I), bis(pyridine)bromine(I), bis(γ-picoline)iodine(I) and bis(γ-picoline)bromine(I) cations. J Mol Struct 2:217–238
73. Sabin JR (1971) A theoretical study of the bis(pyridine)iodine(I) cation. J Mol Struct 7:407–419
74. Carter S, Gray NAB, Wood JL (1971) The electronic spectra of the bis(pyridine)iodine(I) and related cations. J Mol Struct 7:481–485
75. Baruah SK (2004) Infrared studies of some sensitive vibrational modes of pyridines on complex formation with halogens and interhalogens. Asian J Chem 16:706–710
76. Okitsu T, Yumitate S, Sato K et al (2013) Substituent effect of bis(pyridines)iodonium complexes as iodinating reagents: control of the iodocyclization/oxidation process. Chem Eur J 19:4992–4996
77. Baruah SK, Baruah PK (2004) Studies of nuclear magnetic resonance spectra of positive halogen salts of pyridine and substituted pyridines. Asian J Chem 16:688–694
78. Perrin CL (2009) Symmetry of hydrogen bonds in solution. Pure Appl Chem 81:571–583
79. Perrin CL (2010) Are short, low-barrier hydrogen bonds unusually strong? Acc Chem Res 43:1550–1557
80. Carlsson A-CC, Gräfenstein J, Laurila JL et al (2012) Symmetry of $[N\text{-}X\text{-}N]^+$ halogen bonds in solution. Chem Commun 48:1458–1460
81. Carlsson A-CC, Gräfenstein J, Budnjo A et al (2012) Symmetric halogen bonding is preferred in solution. J Am Chem Soc 134:5706–5715

82. Carlsson A-CC, Uhrbom M, Karim A et al (2013) Solvent effects on halogen bond symmetry. CrystEngComm 15:3087–3092
83. Saunders M, Jaffe MH, Vogel P (1971) A new method for measuring equilibrium deuterium isotope effects. Isomerization of 3-deuterio-2,3-dimethylbutyl-2-ium ion. J Am Chem Soc 93:2558–2559
84. Siehl H-U (1987) Isotope effects on NMR spectra of equilibrating systems. Adv Phys Org Chem 23:63–163
85. Georgiuo DC, Butler P, Browne EC et al (2013) On the bonding in bis-pyridine iodonium cations. Aust J Chem 66:1179–1188
86. Anderson GM, Winfield JM (1986) Preparation and properties of bis(acetonitrile)iodine (I) hexafluoromolybdate(V) and hexafluorouranate(V). J Chem Soc Dalton Trans 337–340
87. Tytko K-H, Schmeisser M (1973) Chemische Charakterisierung des $[py_2X]^+$-Ions (X=Br, J). Z Naturforsch B Chem Sci 28:731–735
88. Tornieporth-Oetting I, Klapötke T (1990) Die Reaktivität des I_3^+-Kations gegenüber Ammoniak, Nitrilen und Pyridin. Z Anorg Allg Chem 586:93–98
89. Neverov AA, Xiaomei Feng H, Hamilton K et al (2003) Bis(pyridine)-based bromonium ions. Molecular structures of bis(2,4,6-collidine)bromonium perchlorate and bis(pyridine) bromonium triflate and the mechanism of the reactions of 1,2-bis(2′-pyridylethynyl) benzenebrominum triflate and bis(pyridine)bromonium triflate with acceptor olefins. J Org Chem 68:3802–3810
90. Barluenga J (1999) Transferring iodine: more than a simple functional group exchange in organic synthesis. Pure Appl Chem 71:431–436
91. Snyder SA, Treitler DS, Brucks AP (2011) Halonium-induced cyclization reactions. Aldrichim Acta 44:27–40
92. Uschakow MJ, Tschistow WO (1935) Über salzartige Eigenschaften der Halogene. Einwirkungsprodukte von Brom auf Silbersalze. Ber Deutsch Chem Ges A (68):824–830
93. Diner UE, Lown JW (1971) Addition of iodonium nitrate to unsaturated hydrocarbons. Can J Chem 49:403–415
94. Barluenga J, Gonzalez JM, Campos PJ et al (1985) $I(Py)_2BF_4$, a new reagent in organic-synthesis – general-method for the 1,2-iodofunctionalization of olefins. Angew Chem Int Ed 24:319–320
95. Lemieux RU, Morgan AR (1965) Synthesis of beta-*D*-glucopyranosyl 2-deoxy-alpha-*D*-arabino-hexopyranoside. Can J Chem 43:2190–2197
96. Simonot B, Rousseau G (1993) Preparation of 7-membered and medium-ring lactones by iodo lactonization. J Org Chem 58:4–5
97. Chalker JM, Thompson AL, Davis BG (2010) Safe and scalable preparation of Barluenga's reagent. Org Synth 87:288
98. Barluenga J, González-Bobes F, Murguía MC et al (2004) Bis(pyridine)iodonium tetrafluoroborate (IPy_2BF_4): a versatile oxidizing reagent. Chem Eur J 10:4206–4213
99. Neverov AA, Brown RS (1998) Mechanistic evaluation of the transfer of Br^+ from bis(*sym*-collidine)bromonium triflate to acceptor alkenes. J Org Chem 63:5977–5982
100. Cui X-L, Brown RS (2000) Mechanistic evaluation of the halocyclization of 4-penten-1-ol by some bis(2-substituted pyridine) and bis(2,6-disubstituted pyridine)bromonium triflates. J Org Chem 65:5653–5658
101. Grossman RB, Trupp RJ (1998) The first reagent-controlled asymmetric halolactonizations. Dihydroquinidine-halogen complexes as chiral sources of positive halogen ion. Can J Chem 76:1233–1237
102. Sabin JR (1972) Some calculations on lighter bis(pyridine)halogen(I) cations. J Mol Struct 11:33–55
103. Wolters LP, Bickelhaupt FM (2012) Halogen bonding versus hydrogen bonding: a molecular orbital perspective. ChemstryOpen 1:96–105
104. Bakshi PK, James MA, Cameron TS et al (1996) Polyhalide anions in crystals. 1. Triiodides of the Me_4N^+, Me_4P^+, quinuclidinium, 1-azoniapropellane, and 1,4-diazoniabicyclo[2.2.2]

octane ($DabcoH_2^{2+}$) cations, and 1,10-phenanthrolinium$^+$ tribromide. Can J Chem 74:559–573
105. Robertson KN, Cameron TS, Knop O (1996) Polyhalide anions in crystals. 2. I3− asymmetry and N-H. . .I bonding: triiodides of the Me2NH2+, Ph2I+, tropanium, N, N, N′, N′-Me(4)-1,2-ethanediammonium, N, N, N′, N′-Me(4)-1,3-propanediammo-nium, N-Me-piperazinium2+, and N, N′-Me2-piperazinium2+ cations, and Me2NH2I. Can J Chem 74:1572–1591
106. Hayward GC, Hendra PJ (1967) Far infra-red and Raman spectra of trihalide ions IBr_2^- and I_3^-. Spectrochim Acta A 23:2309–2314
107. Person WB, Anderson GR, Fordemwalt JN et al (1961) Infrared and Raman spectra, force constants, and structures of some polyhalide ions - ICl_2^-, ICl_4^-, $BrCl_2^-$, and Br_3^-. J Chem Phys 35:908–914
108. Maki AG, Forneris R (1967) Infrared and Raman spectra of some trihalide ions - ICl_2^-, IBr_2^-, I_3^-, I_2Br^- and $BrICl^-$. Spectrochim Acta A 23:867–880
109. Pimentel GC (1951) The bonding of trihalide and bifluoride ions by the molecular orbital method. J Chem Phys 19:446–448
110. Gabes W, Gerding H (1972) Vibrational-spectra and structures of trihalide ions. J Mol Struct 14:267–279
111. Sasaki K, Aida K (1980) IR-spectra of charge transfer complexes between ICl, IBr and aminopyridines. J Inorg Nucl Chem 42:13–15
112. Kiefer W, Bernstei HJ (1972) UV-laser excited resonance Raman spectrum of I_3^- ion. Chem Phys Lett 16:5–9
113. Kaya K, Mikami N, Ito M et al (1972) Resonance Raman effect of I_3^- ion by ultraviolet laser excitation. Chem Phys Lett 16:151–153
114. Johnson AE, Myers AB (1995) Emission cross-sections and line-shapes for photodissociating triiodide in ethanol - experimental and computational studies. J Chem Phys 102:3519–3533
115. Johnson AE, Myers AB (1996) A comparison of time- and frequency-domain resonance Raman spectroscopy in triiodide. J Chem Phys 104:2497–2507
116. Johnson AE, Myers AB (1996) Solvent effects in the Raman spectra of the triiodide ion: observation of dynamic symmetry breaking and solvent degrees of freedom. J Phys Chem 100:7778–7788
117. Al-Hashimi NA (2004) Spectroscopic studies of the reaction of iodine with 2,3-diaminopyridine. Spectrochim Acta A 60:2181–2184
118. Margulis CJ, Coker DF, Lynden-Bell RM (2001) Symmetry breaking of the triiodide ion in acetonitrile solution. Chem Phys Lett 341:557–560
119. Sato H, Hirata F, Myers AB (1998) Theoretical study of the solvent effect on triiodide ion in solutions. J Phys Chem A 102:2065–2071
120. Zhang FS, Lynden-Bell RM (2003) Solvent-induced symmetry breaking. Phys Rev Lett 90:185505
121. Zhang FS, Lynden-Bell RM (2003) Temperature and solvent dependence of vibrational relaxation of triiodide: a simulation study. J Chem Phys 119:6119–6131
122. Zhang FS, Lynden-Bell RM (2005) Solvent-induced symmetry breaking: varying solvent strength. Phys Rev E 71:021502
123. Zhang FS, Lynden-Bell RM (2005) Interactions of triiodide cluster ion with solvents. Eur Phys J D 34:129–132
124. Karm A, Reitti M, Carlsson A-CC et al (2014) The nature of the [N-Cl-N]+ and [N-F-N]+ halogen bonds in solution. Chem Sci 5:3226–3233
125. Suzaki Y, Saito T, Ide T et al (2014) A rhomboid-shaped organic host molecule with small binding space. Unsymmetrical and symmetrical inclusion of halonium ions. Dalton Trans 43:6643–6649
126. Koskinen L, Hirva P, Kalenius E et al (2015) Halogen bonds with coordinative nature: halogen bonding in a S-I$^+$-S iodonium complex. CrystEngComm 17:1231–1236
127. Hakkert SB, Erdelyi M (2015) Halogen bond symmetry: the N-X-N bond. J Phys Org Chem 28:226–233

128. Robinson SW, Mustoe CL, White NG et al (2015) Evidence for halogen bond covalency in acyclic and interlocked halogen-bonding receptor anion recognition. J Am Chem Soc 137:499–507
129. Jungbauer SH, Bulfield D, Kniep F et al (2014) Toward molecular recognition: three-point halogen bonding in the solid state and in solution. J Am Chem Soc 136:16740–16743
130. Lim JY, Beer PB (2015) Superior perrhenate anion recognition in water by a halogen bonding acyclic receptor. Chem Commun 51:3686–3688
131. Robertson CC, Perutz RN, Brammer L et al (2014) A solvent-resistant halogen bond. Chem Sci 5:4179–4183
132. Kodiah BN, Arto V, Sandip B, Fangfang P, Rissanen K (2015) Org Chem Frontiers doi:10.1039/C4QO00326H
133. Dumele O, Wu D, Trapp N, Goroff N, Diedrich F (2014) Halogen bonding of (iodoethynyl) benzene derivatives in solution. 16:4722–4725
134. Thorson RA, Woller GR, Driscoll ZL, Geiger BE, Moss CA, Schlapper AL, Speetzen ED, Bosch E, Erdelyi M, Bowling NP (2015) Intramolecular halogen bonding in solution: 15N, 13C and 19F NMR studies of temperature and solvent effects. doi:10.1002/ejoc.201403671
135. Vargas Jetzsch A (2015) Applications of halogen bonding in solution. Pure Appl Chem 87:15–41

Top Curr Chem (2015) 359: 77–90
DOI: 10.1007/128_2014_587

Published online: 12 April 2015

Halonium Ions as Halogen Bond Donors in the Solid State $[XL_2]Y$ Complexes

Kari Rissanen and Matti Haukka

Abstract The utilization of halogen bonding interactions is one of the most rapidly developing areas of supramolecular chemistry. While the other weak non-covalent interactions and their influence on the structure and chemistry of various molecules, complexes, and materials have been investigated extensively, the understanding, utilizations, and true nature of halogen bonding are still relatively unexplored. Thus its final impact in chemistry in general and in materials science has not yet been fully established. Because of the polarized nature of a Z–X bond (Z=electron-withdrawing atom or moiety and X=halogen atom), such a moiety can act as halogen bond donor when the halogen is polarized enough by the atom/moiety Z. The most studied and utilized halogen bond donor molecules are the perfluorohalocarbons, where Z is a perfluorinated aryl or alkyl moiety and X is either iodine or bromine. Complementing the contemporary halogen bonding research, this chapter reviews the solid state structural chemistry of the most extremely polarized halogen atoms, viz. halonium ions, X^+, and discussed them as halogen bond donors in the solid state $[XL_2]Y$ complexes (X=halonium ion, Y=any anion).

Keywords Halonium ions · Halogen bonding · Solid state · X-ray structure

Contents

K. Rissanen (✉)
Department of Chemistry, Laboratory of Organic Chemistry, University of Jyväskylä, P.O. Box 35, 40014 Jyväskylä, Finland
e-mail: kari.t.rissanen@jyu.fi

M. Haukka
Department of Chemistry, Laboratory of Inorganic Chemistry, University of Jyväskylä, P.O. Box 35, 40014 Jyväskylä, Finland

1 Introduction

Despite the pioneering work by Odd Hassel in the 1950s and 1960s [1–8], halogen bonding [9], nowadays the acronym XB being accepted into general use, did not play an important role in Supramolecular Chemistry until the beginning of the current millennium. Halogen bonding was virtually forgotten for 25 years (1970–1995) during which the focus in supramolecular chemistry was on the investigation of other non-covalent intermolecular interactions, most notably hydrogen bonding. One of the major reason for this was the fact that, until very recently, halogen bonding was mostly observed in the solid state and for a long time was only seldom unambiguously observed in solution [10–15], despite the fact that the halogen bonding in solution had already been reported by Benesi and Hildebrand in 1949 [16]. As such, the available analytical methods which could be used to investigate halogen bonding, especially in solution, were rather limited, which could explain the relatively mild interest in halogen bonding for several years [17]. However, after being a kind of a 'chemical curiosity' for many years, halogen bonding was, besides others, revived primarily by the works of Legon [18–29] (Exeter and Bristol, UK) and Resnati and Metrangolo [30–32] (Milan, Italy) in the mid-1990s. As fluorine and materials chemists, Resnati and Metrangolo used perfluorohalocarbons (PFHC) as the XB donors and examined their interaction with various Lewis bases as XB acceptors, and nowadays PFHCs are considered to be 'iconic' halogen bond donors [30–52]. Inspired by the outstanding experimental work of the Milan group, halogen bonding regained its importance in chemical research and is nowadays a rapidly developing research topic [9, 53–60].

1.1 Halogen Bond: The Long Lost Brother of the Hydrogen Bond...

Not so surprisingly, halogen bonding (XB) has several similar properties to hydrogen bonding [61, 62]. In both cases attractive interactions between a positively polarized, i.e., electrophilic atom (hydrogen or halogen) and a nucleophilic atom (O, N, S, any anion, etc.) are formed, wherein the latter ones act as Lewis bases [63, 64]. At the beginning, purely electrostatic interactions were used to describe

halogen bonds, but recently it has become evident that they do not fully characterize these interactions [65–68]. The work over the last 15 years has now led to the definition of halogen bonds (Z–X···A) such that the halogen bond is donated by the positively polarized halogen atom (X) to an acceptor atom or molecule (A) [61, 69, 70]. Halogen bonds are strongly directional [61, 71], another similarity to hydrogen bonds and one of the characteristics of a halogen bond. The directionality directly reflects the polarization along the Z–X bond. Based on this, linear halogen bonds (angle Z–X···A being larger than 175°) are stronger than nonlinear ones (angle Z–X···A being smaller than 160°) and the strength of the interaction decreases with decreasing Z–X···A bond angle [53–71].

The special features of halogen bonds, and especially their directionality, has made them an interesting alternative for hydrogen bonding. In contemporary crystal engineering [53–60], halogen bonding plays an increasing role in the design of new materials or as an active structural motif in bioactivity [72] or biomolecules [73–75]. Although halogen bonding occurs mainly in the solid state, it is now unambiguously demonstrable in solution too [12–14]. Clearly the research interest in halogen bonding is nowadays shifting from the pure solid state structural aspects to the understanding of the nature of the halogen bond itself and the use of halogen bonds in solution.

1.2 . . .. or Simply a Charge Transfer Interaction?

According to the definition of the halogen bond, dihalogens, X_2, can act as halogen bonding donors. However, halogen bonded systems involving X_2 can also be rationalized in terms of charge transfer complexes. From this point of view, the halogen bond has never really been completely lost or forgotten. The terminology concerning charge transfer complexes is more closely related to photochemistry than hydrogen bonds. In a charge transfer system a good electron donor (D_e), such as nitrogen or sulfur with free electron pair(s), interacts with X_2, which in turn, acts as an electron acceptor. The interaction can be interpreted as mixing of the HOMO orbital of the electron donor with the antibonding σ* LUMO orbital of X_2 [76]. Formally, the charge transfer results in a system which can be described as a hybrid of $D_e \cdots X_2 \Leftrightarrow D_e^+ \cdots X_2^-$. In this view, the charge transfer generates an attractive interaction between the donor and acceptor. If the charge transfer effect is strong, it eventually changes the charge distribution on X_2 molecule in such a way that the negative charge is accumulated on the non-coordinated X, leaving a positive charge on the coordinated halogen. In the extreme case, the charge transfer is completed and the X–X bond is cleaved heterolytically, leading, at least formally, to a coordinatively bound D_e–X^+ system and release of X^-. Even if simple D_e–X^+ systems are not usually stable, a limited number of systems with a bridging X^+ are known [77–79] (see the examples below). One of the classic examples is $[I(Py)_2]^+$ (Fig. 1) published for the first time in the early 1960s [77].

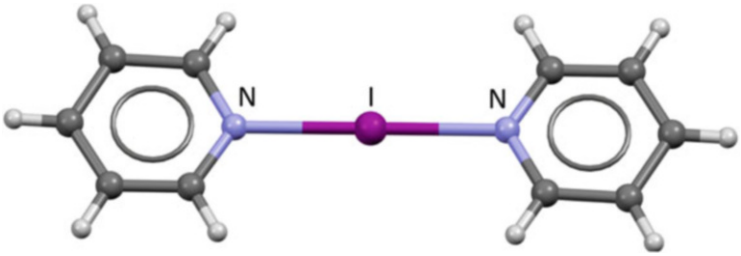

Fig. 1 The crystal structure of $[I(Py)_2]^+$. The counteranion BF_4^- has been omitted for clarity [77]

The heterolytic breakage of the X–X bond through the charge transfer process has been observed with sulfur donors such as thiourea [80] and 2-imidazolidinethione (imit) [81]. In the latter case, the gradual fission of the X–X bond is nicely demonstrated by the intermediate structure of $(imit)_2I^+\cdots I_3^-$[81]. Another example of a similar process with complete charge transfer is the reaction of I_2 with thioazolidine-2-thione (tzdtH) and formation of $[(tzdtH)_2I]^+$ [82]. It should be remembered that in those cases where the charge transfer is complete, the formed $D_e\cdots X^+\cdots D_e$ is no longer strictly speaking charge transfer complexes but more like molecular ionic compounds with dative or 3 center-4-electron bond [13, 14, 83, 84]. It has been shown that in this type of system, X^+ actually behaves very similar to Ag^+, Au^+, or Cu^+ cations in the corresponding coordination complexes [80].

In late 2013, a definition of halogen bond was published [61]. The definition also included systems with X^+ cations. The fundamental difference between the charge transfer complex and halogen bonded adduct arises from the nature of the D_e–X interaction. As long as the interaction is mainly electrostatic it can be seen as pure halogen bond. When the interaction has considerable covalent nature, the term halogen bond does not completely describe the contact. The dative covalent nature of the bond should be recognized and it would be more accurate to define such a system as a *coordinative halogen bond* or a *halogen bond with coordinative nature*. This would apply especially to systems with bridging X^+ which could also be seen as an extreme case of halogen bonding. The positively charged X^+ can thus be taken as the ultimately polarized halogen bond donor.

At present the halogen bonding studies of halonium ions, X^+, are often overlooked. In general, systems with X^+ ions are rather well understood in terms of charge transfer complexes, but there are only limited number of publications where these systems are analyzed from the halogen bond point of view [13, 14, 83–85]. In this chapter we give a brief overview of the solid state complexes of halonium ion complexes, $[XL_2]Y$, where the X is the halonium ion (Cl^+, Br^+, or I^+) halogen bond donor, L is the halogen bond acceptor (a Lewis base), and Y is any anion. We base our chapter mainly on crystal structures of halonium ion complexes, $[XL_2]Y$, found in the CSD (Cambridge Structural Database), and CSD refcodes are given for all the structures discussed [86]. To exclude the hyperpolarized halonium complexes and "organic halonium cations" [87, 88], only structures of those $[XL_2]$

Y which satisfy the definition of the halogen bond [61] are discussed. In many cases the halogen bond interactions can be identified simply by calculating the ratio [89–91] R_{XB} ($R_{XB} = \frac{d_{XB}}{X_{vdw}+B_{vdw}}$, where the distance d_{XB} [Å] between the XB donor (X) and XB acceptor (B) is divided by the sum of VDW radii [Å] of X and B). The R_{XB} values are calculated using the atoms radii defined by Bondi [92, 93]. However, it should be kept in mind that the R_{XB} values do not unambiguously correlate with the actual strength of the interaction. The Hirschfeld surfaces (Crystal Explorer [94]) depicted in the figures are given to help the reader distinguish the atoms involved in the examples shown for halogen bonding.

2 Halonium-Nitrogen Complexes

2.1 *Aromatic* sp^2 *Nitrogen*

As a highly nucleophilic atom, nitrogen is an excellent halogen bond acceptor. Among the vast number of XB systems, the number of those involving the linear $N\cdots X^+\cdots N$ complexes is surprising small. One of the very first reported systems with positively charged halogen ion, i.e., $[I(Py)_2]^+$ with $BF4^-$ as the counter anion, is an archetypical member of this category (Fig. 1). There are no reported X-ray structures of linear $N\cdots Cl^+\cdots N$ complexes but both I^+ and Br^+ are able to form this type of structures.

Pyride, its derivatives and quinoline (CSD refcodes HUMMAD, PYRIDI, BAZNAR, DEFXIW, GANXEZ, AKOXON, AKOXUT, and QUBRPB) form a group where the halonium ion, either iodonium, I^+, or bromonium, Br^+, are halogen bonded to the aromatic sp^2 nitrogen of the heteroaromatic ring system. Figure 2 displays the chemical structures of the complexes discussed.

In most cases the complexes are symmetrical with two equal $X^+\cdots N$ (X=Br or I) distances and 180° $N\cdots X^+\cdots N$ angles. Some small variations in the bond distances and angles occur. The only marked deviation from the average $I^+\cdots N$ distance of 2.25 Å and $Br^+\cdots N$ distance of 2.12 Å is for the iconic $[I(Py)_2]^+$ complex (refcode PYRIDI) by O. Hassel ($I^+\cdots N$ distance of 2.16 Å), which may be because of the quality of the structure published in 1961 and can be considered as an artefact. In four complexes (BAZNAR, AKOXON, AKOXUT, and QUBRPB) the $N\cdots X^+\cdots N$ angle is between 176.3° and 178.4°. The $R_{XB} = 0.65$ for the $N\cdots I^+\cdots N$ and $R_{XB} = 0.63$ for the $N\cdots Br^+\cdots N$ complexes, indicating very strong halogen bonding, now defined as *coordinative halogen bonds* (Fig. 3).

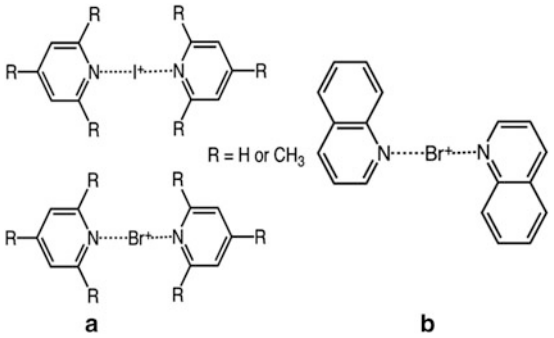

Fig. 2 The chemical structures of the pyridine (**a**) and quinolone (**b**) halonium complexes

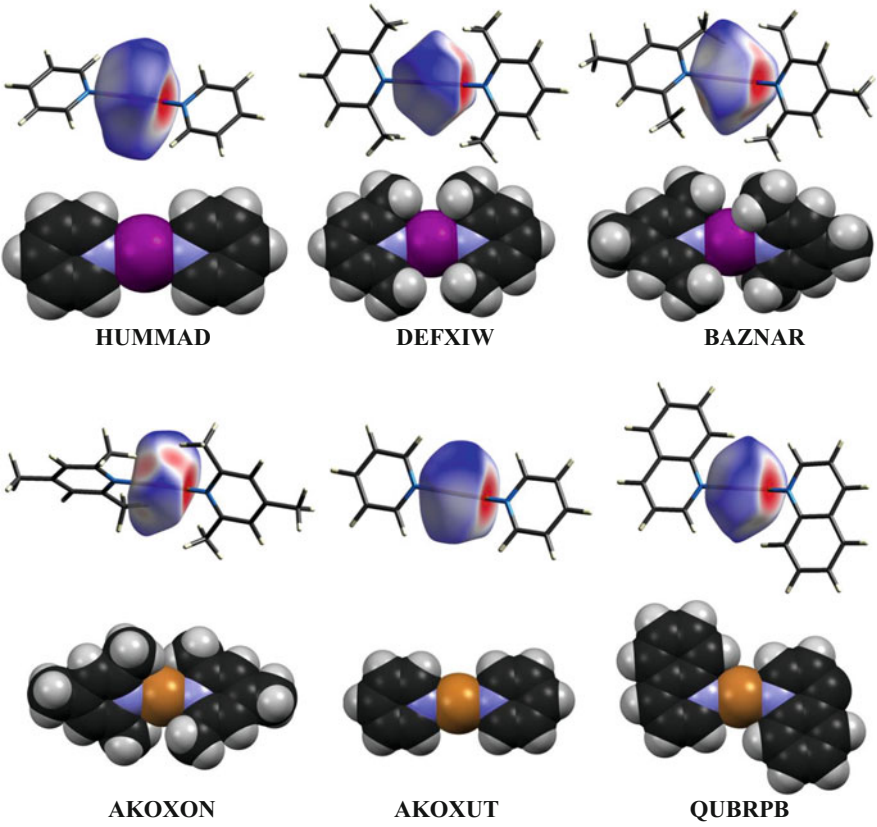

Fig. 3 The Hirshfeld surfaces and VDW representations of three iodonium and three bromonium complexes

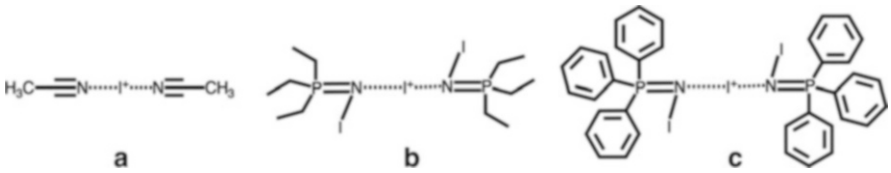

Fig. 4 The chemical structures of the acetonitrile (**a**) and phosphazene (**b**, **c**) iodonium complexes

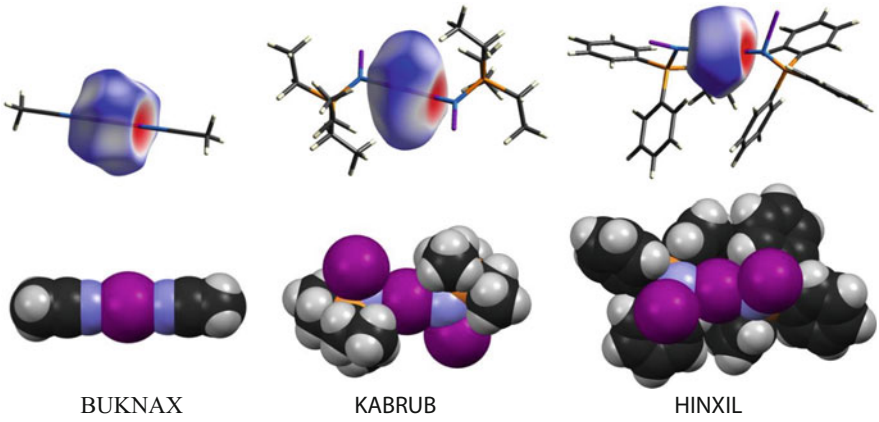

Fig. 5 The Hirshfeld surfaces and VDW representations of three iodonium complexes

2.2 Halonium to sp *and Other* sp^2 *Nitrogens*

There exist only a few examples (Fig. 4) of N···X^+···N complexes where a non-aromatic *sp* or sp^2 nitrogen acts as the halogen bond acceptor for the halonium ions. The *sp* nitrogen in acetonitrile (BUKNAX) and the sp^2 nitrogen in a P=N–I phosphazene moiety (KABRUB and HINXIL) act as the acceptor atoms towards iodonium ions. There are no solid state structures for similar bromonium ion complexes.

The *sp* nitrogen in the acetonitrile is quite nucleophilic, resulting in a highly symmetric structure with an I^+...N distance of 2.20 Å (x2) and a 180° N...I^+...N angle with $R_{XP} = 0.62$. One of the phosphazene complexes (KARRUB) is symmetrical with both I^+...N distances 2.29 Å and a 180° N...I^+...N angle with the other (HINXIL) slightly asymmetric with I^+...N distances 2.25 and 2.30 Å with a 176.1° N...I^+...N angle. The *sp* nitrogen induces stronger XB, $R_{XB} = 0.62$, while the sp^2 nitrogen complexes, in both of them $R_{XB} = 0.65$, are very close to the values observed for aromatic sp^2 nitrogen. Figure 5 depicts the Hirshfeld surfaces and VDW representations of these complexes, revealing similar environments around the iodonium cation.

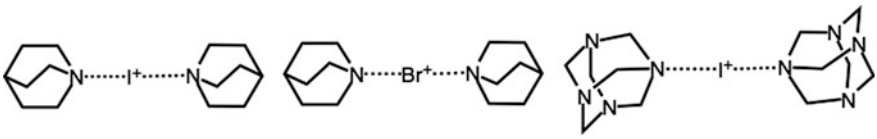

Fig. 6 The chemical structures of the iodonium and bromonium quinuclidine (**a**, **b**) and iodonium hexamethylenetetraamine (**c**) complexes

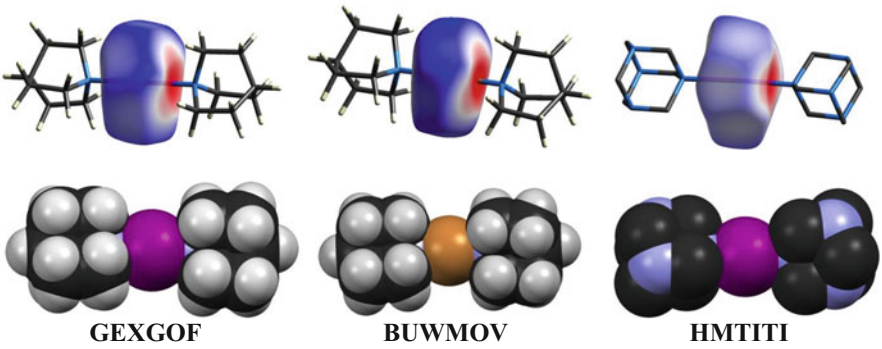

Fig. 7 The Hirshfeld surfaces and VDW representations of three iodonium complexes

2.3 *Halonium to* sp^3 *Nitrogens*

As with non-aromatic *sp* or sp^2 nitrogens, there are not many examples (Fig. 6) of N. . .X^+. . .N complexes where an sp^3 nitrogen acts as the halogen bond acceptor for the halonium ions. Representative examples are the iodonium and bromonium complexes of quinuclidine (GEXGOF and BUWMOV, respectively) and the iodonium complex of hexamethylenetetramine (HTMA, refcode HMTITI).

The sp^3 nitrogen behaves very similar to the *sp* and sp^2 nitrogen as a halogen bond acceptor. The nitrogen atom is the most nucleophilic in quinuclidine and HMTA, and, probably because of electronic effects (no possibility to donate π-electrons to the iodonium cation), produces very similar structures. The iodonium and bromonium quinuclidine complexes are highly symmetrical with X^+. . .N distances of 2.27 and 2.32 Å for the iodonium, 2.12 and 2.16 Å for the bromonium, respectively, with 180° N. . .I^+. . .N angles in both complexes. The $R_{XB} = 0.65$ (I^+) and 0.63 (Br^+). The HMTA iodonium complex is slightly asymmetric with I^+. . .N distances of 2.30 and 2.31 Å with an N. . .I^+. . .N angle of 176.5° and $R_{XB} = 0.65$. Figure 7 depicts the Hirshfeld surfaces and VDW representations of these complexes, revealing a similar environment around the halonium cations.

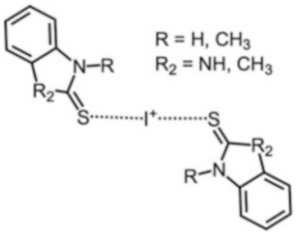

Fig. 8 The chemical structure of a typical S···I^+···S system

3 Halonium–Sulfur Complexes

To date, only linear S···I^+···S halonium systems have been reported in the CSD database. No linear S···Br^+···S or S···Cl^+···S can be found. This is, of course, because of the high polarizability of iodine compared to the other halogens. Altogether, 11 structures with an average I^+···S distance of 2.64 Å and S···I^+···S angle of 175.8° are listed in the database. The short I^+···S distances indicate considerable shortening of the interatomic contact compared to the sum of van der Waals radii. The average R_{XB} value is around 0.70, indicating a slightly less nucleophilic nature of the sulfur atoms when compared to nitrogen atoms. Also, the variation of the I^+···S distance is larger than those of nitrogen atoms. The I^+···S distances in the S···I^+···S system range from 2.59 to 2.70 Å, in most cases being symmetrical around the iodonium cation. The differences between the S^-···I^+ distances in the same molecule range from 0 to 0.064 Å. A typical S···I^+···S complex contains fused heteroatom molecules where the sulfur atoms act as halogen bond acceptors (Fig. 8). Representative examples from CSDD have refcodes DAXXIK, DAXXUW, and HAKJAE.

Other acceptor variants include thiourea (ISUERA01, LOPQAI), thioaminocyclohexyl (IBOCUX), aminothiolato ethylene (IOENCO), thiazolidine thione (XOVRAB), or diathiazole thiones (WURHEX, WURHEX01) as the ligand molecules.

The polarization of I^+ has an impact on the Hirshfeld surface of the iodonium ion (Fig. 9). Iodonium cation is polarized in such a way that the electron-deficient areas are located on both sides of the I^+ along the S···I^+···S and the electron-rich areas around the S···I^+···S direction. The electron density is expected to be polarized around the halonium ion in such a way that two positive σ-holes are formed on the opposite sides of the I^+. The remaining electron density forms a "disk" around the halonium center perpendicular to the bonds. The Hirshfeld surface plot is very indicative for the interaction as the red areas depict the interatomic distances shorter than the sum of van der Waals radii (Fig. 9). The complex is slightly more asymmetrical than observed for the asymmetric N···I^+···N complexes, the X^+···S distances are 2.60 and 2.70 Å, and the S···X^+···S angles are 171.3° with $R_{XB} = 0.69$ and 0.71, respectively.

The electron-rich area of the polarized I^+ can act as electron donor for other intermolecular yet interatomic contacts such as hydrogen bonds or even for I^+-metal contacts, as in the structure of $[\{Ni(C_{14}H_{28}N_2S_2)\}_2NiI_2]^+$ (IBOCUX) where the

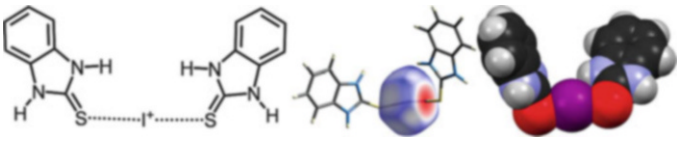

Fig. 9 The chemical structure, Hirshfeld surface around I^+ and VDW representations of the bis (benzimidazole-2-thione) iodonium complex

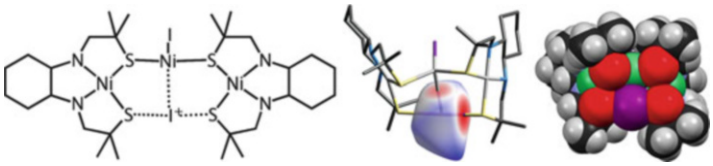

Fig. 10 The additional I^+-Ni^+-contact between the polarized I^+ and sulfur in $[\{Ni(C_{14}H_{28}N_2S_2)\}_2NiI_2]^+$ (IBOCUX). Formally, $[\{Ni(C_{14}H_{28}N_2S_2)\}_2NiI_2]^+$ is constructed by two neutral $Ni(II)N_2S_2$ units bridged by bridged by positively charged $Ni(II)I_2^+$ unit

acceptor is a Ni atom (Fig. 10). This additional interaction does not, however, influence the I$^+\cdots$S bonds, so they are very similar, as in other S$\cdots$I$^+\cdots$S systems (2.64 and 2.69 Å, 171.9° for IBOCUX).

4 Halonium–Selenium and Halonium–Tellurium Complexes

Just as in S$\cdots$I$^+\cdots$S systems, the iodonium is the most common halonium in linear Se$\cdots$X$^+\cdots$Se systems. All in all, only nine entries can be found in the CSD database. The average I$^+\cdots$Se distance in these structures is 2.78 Å and the average Se$\cdots$I$^+\cdots$Se angle 178°. Again, the shortening of the interatomic distances with respect to the sum of van der Waals radii is considerable. The average R_{XB} is 0.72, indicating nearly the same 30% shortening of the contacts found in S$\cdots$I$^+\cdots$S systems. The I$^+\cdots$S distances range from 2.72 to 2.80 Å and differences of the distances in the same molecule are small, ranging from 0 to 0.081 Å. Again, the Se$\cdots$I$^+\cdots$Se systems are highly symmetrical. With selenium, the ligands include fused heterocyclic N- or N,S-rings (GEWRIL, GEWROR, GEWRUX, HAKHUW) just as with sulfur, but with Se as the XB acceptor (Fig. 11).

As with nitrogen and sulfur atoms, the shortening of the interatomic distances with respect to the sum of van der Waals radii is considerable. The average R_{XB} is 0.72, indicating a slightly weaker XB interaction than with N ($R_{XB} = 0.65$) and S ($R_{XB} = 0.70$) atoms, again because of the diminishing nucleophilic character of the XB acceptor atom. Other known Se$\cdots$I$^+\cdots$Se structures contain phosphine selenides (DIJYUG, EZOXUM, POHZIW, POHZOC, POHZUI) (Fig. 11) and *N*-morpholinoselenocarbonyl (BUZCOO) as halogen bond acceptors.

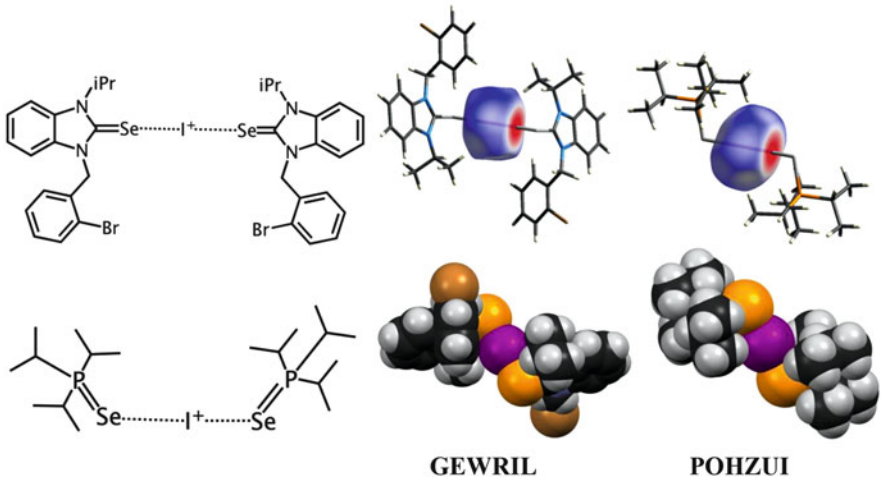

Fig. 11 The chemical structure, Hirshfeld surface around I^+ and VDW representations of the $[C_{34}H_{34}Br_2IN_4Se_2]^+$ (GEWRIL) and phosphine selenide complex (POHZUI)

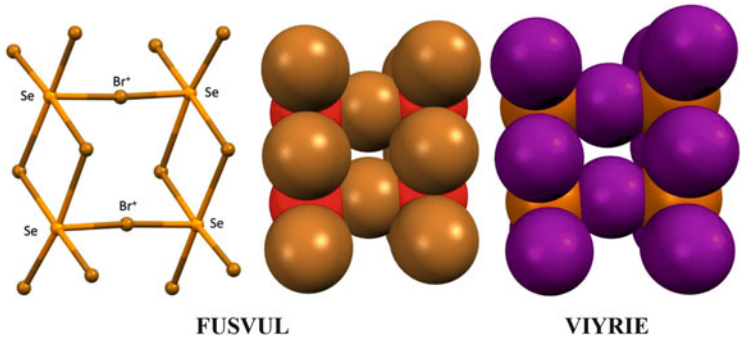

Fig. 12 The ball-and-stick (*left*) and VDW representations of the $[Se_2Br_6]^{2-}$ and $[Te_2I_6]^{2-}$ complex dianions

Unlike with sulfur, complex dianions, $[Se_4Br_{14}]^{2-}$ and $[Te_4I_{14}]^{2-}$, both containing two Se···Br^+···Se or Te···I^+···Te moieties, have been reported (VIYRIE and FUSVUL). In these complex dianions formally two anionic $[Se_2Br_6]^{2-}$/$[Te_2I_6]^{2-}$ units are linked together through two linear Br^+ or I^+ bridges with Br^+···Se distances of 2.57 and 2.62 Å and I^+···Te distances of 3.01 and 3.04 Å. The Se···Br^+···Se angle is 176.1° and the Te^-···I^+···Te^- angle 175.7° (Fig. 12).

These complex dianions represent a special case with R_{XB} values of 0.69 ($[Se_4Br_{14}]^{2-}$) and 0.75 ($[Te_4I_{14}]^{2-}$), as they do not follow the formulation of the $[XL_2]^+$ halonium complex. Yet formally, and by their overall structural and bonding characteristics, they can be considered as halonium complexes.

References

1. Hassel O, Hvoslef J (1954) Acta Chem Scand 8:873
2. Strømme KO (1959) Acta Chem Scand 13:268–274
3. Hassel O, Strømme KO (1959) Acta Chem Scand 13:275–280
4. Hassel O, Strømme KO (1959) Acta Chem Scand 13:1775–1780
5. Hassel O, Hope H (1960) Acta Chem Scand 14:391–397
6. Hassel O, Rømming C, Tufte T (1961) Acta Chem Scand 15:967–974
7. Groth P, Hassel O (1964) Acta Chem Scand 18:402–408
8. Hassel O (1970) Science 170:497–502
9. Metrangolo P, Resnati G (eds) (2008) Halogen bonding: fundamentals and applications. Springer, Berlin
10. Priimagi A, Cavallo G, Forni A, Gorynsztejn-Leben M, Kaivola M, Metrangolo P, Milani R, Shishido A, Pilati T, Resnati G, Terraneo G (2013) Acc Chem Res 46:2686–2695
11. Troff RW, Mäkelä T, Topić F, Valkonen A, Raatikainen K, Rissanen K (2013) Eur J Org Chem 1617–1637
12. Beale TM, Chudzinski MG, Sarwar MG, Taylor MS (2013) Chem Soc Rev 42:1667–1680
13. Carlsson A-CC, Gräfenstein J, Budnjo A, Laurila JL, Bergquist J, Karim A, Kleinmaier R, Brath U, Erdélyi M (2012) J Am Chem Soc 134:5706–5715
14. Erdélyi M (2012) Chem Soc Rev 41:3547–3557
15. Bertani R, Sgarbossa P, Venzo A, Lelj F, Amati M, Resnati G, Pilati T, Metrangolo P, Terraneo G (2010) Coord Chem Rev 254:677–695
16. Benesi HA, Hildebrand JH (1949) J Am Chem Soc 71:2703–2707
17. Schalley CA (ed) (2012) Analytical methods in supramolecular chemistry, 2nd edn. Wiley-VCH, Weinheim
18. Legon AC, Thorn JC (1993) J Chem Soc Faraday Trans 89:4157–4162
19. Legon AC, Lister DG, Thorn JC (1994) J Chem Soc Chem Commun 757–758
20. Bloemink HI, Hinds K, Legon AC, Thorn JC (1994) Angew Chem Int Ed Engl 33:1512–1513
21. Ding FJ, Lister DG, Legon AC (1995) J Chem Soc Chem Commun 113–114
22. Bloemink HI, Hinds K, Legon AC, Thorn JC (1995) Chem Eur J 1:17–25
23. Cooke SA, Cotti G, Evans CM, Holloway JH, Legon AC (1996) Chem Commun 2327–2328
24. Cooke SA, Cotti G, Holloway JH, Legon AC (1997) Angew Chem Int Ed Engl 36:129–130
25. Bloemink HI, Cooke SA, Holloway JH, Legon AC (1997) Angew Chem Int Ed Engl 36:1340–1342
26. Legon AC (1998) Chem Eur J 4:1890–1897
27. Legon AC (1998) Chem Commun 2737–2738
28. Legon AC (1999) Angew Chem Int Ed 38:2687–2714
29. Legon AC (2008) In: Metrangolo P, Resnati G (eds) Halogen bonding: fundamentals and applications. Springer, Berlin
30. Amico V, Meille SV, Corradi E, Messina MT, Resnati G (1998) J Am Chem Soc 120:8261–8262
31. Farina A, Meille SV, Messina MT, Metrangolo P, Resnati G, Vecchio G (1999) Angew Chem Int Ed 38:2433–2436
32. Corradi E, Meille SV, Messina MT, Metrangolo P, Resnati G (2000) Angew Chem Int Ed 39:1782–1786
33. Hauchecorne D, van der Veken BJ, Herrebout WA, Hansen PE (2011) Chem Phys 381:5–10
34. Clarke SM, Friščić T, Jones W, Mandal A, Sun C, Parker JE (2011) Chem Commun 47:2526–2528
35. Abate A, Marti-Rujas J, Metrangolo P, Pilati T, Resnati G, Terraneo G (2011) Cryst Growth Des 11:4220–4226
36. Metrangolo P, Murray JS, Pilati T, Politzer P, Resnati G, Terraneo G (2011) Cryst Growth Des 9:4238–4246
37. Viger-Gravel J, Korobkov I, Bryce DL (2011) Cryst Growth Des 11:4984–4995

38. Davy KJP, McMurtrie J, Rintoul L, Bernhardt PV, Micallef AS (2011) CrystEngComm 13:5062–5070
39. Dordonne S, Crousse B, Bonnet-Delpon D, Legros J (2011) Chem Commun 47:5855–5857
40. Metrangolo P, Murray JS, Pilati T, Politzer P, Resnati G, Terraneo G (2011) CrystEngComm 13:6593–6596
41. Hauchecorne D, Moiana A, van der Veken BJ, Herrebout WA (2011) Phys Chem Chem Phys 13:10204–10213
42. Vargas Jentzsch A, Emery D, Mareda J, Metrangolo P, Resnati G, Matile S (2011) Angew Chem Int Ed 50:11675–11678
43. Shen QJ, Jin WJ (2011) Phys Chem Chem Phys 13:13721–13729
44. Vargas Jentzsch A, Emery D, Mareda J, Nayak SK, Metrangolo P, Resnati G, Sakai N, Matile S (2012) Nat Commun 3:905
45. Priimagi A, Cavallo G, Forni A, Gorynsztejn-Leben M, Kaivola M, Metrangolo P, Milani R, Shishido A, Pilati T, Resnati G, Terraneo G (2012) Adv Funct Mater 22:2572–2579
46. Eccles KS, Morrison RE, Stokes SP, O'Mahony GE, Hayes JA, Kelly DM, O'Boyle NM, Fábián L, Moynihan HA, Maguire AR, Lawrence SE (2012) Cryst Growth Des 12:2969–2977
47. Nayak SK, Terraneo G, Forni A, Metrangolo P, Resnati G (2012) CrystEngComm 14:4259–4261
48. Arman HD, Rafferty ER, Bayse CA, Pennington WT (2012) Cryst Growth Des 12:4315–4323
49. Gao HY, Zhao XR, Wang H, Pang X, Jin WJ (2012) Cryst Growth Des 12:4377–4387
50. Shen QJ, Pang X, Zhao XR, Gao HY, Sun H-L, Jin WJ (2012) CrystEngComm 14:5027–5034
51. Gao HY, Shen QJ, Zhao XR, Yan XQ, Pang X, Jin WJ (2012) J Mater Chem 22:5336–5343
52. Mínguez Espallargas G, Recuenco A, Romero FM, Brammer L, Libri S (2012) CrystEngComm 14:6381–6383
53. Metrangolo P, Resnati G (2001) Chem Eur J 7:2511–2519
54. Fourmigué M, Batail P (2004) Chem Rev 104:5379–5418
55. Metrangolo P, Resnati G, Pilati T, Liantonio R, Meyer F (2007) J Polym Sci A Polym Chem 45:1–15
56. Metrangolo P, Meyer F, Pilati T, Resnati G, Terraneo G (2008) Angew Chem Int Ed 47:6114–6127
57. Rissanen K (2008) CrystEngComm 10:1107–1113
58. Metrangolo P, Pilati T, Terraneo G, Biella S, Resnati G (2009) CrystEngComm 11:1187–1196
59. Fourmigué M (2009) Curr Opin Solid State Mater Sci 13:36–45
60. Cavallo G, Metrangolo P, Pilati T, Resnati G, Sansotera M, Terraneo G (2010) Chem Soc Rev 39:3772–3783
61. Desiraju GR, Ho PS, Kloo L, Legon AC, Marquardt R, Metrangolo P, Politzer P, Resnati G, Rissanen K (2013) Pure Appl Chem 85:1711–1713
62. Arunan E, Desiraju GR, Klein RA, Sadlej J, Scheiner S, Alkorta I, Clary DC, Crabtree RH, Dannenberg JJ, Hobza P, Kjaergaard HG, Legon AC, Mennucci B, Nesbitt DJ (2011) Pure Appl Chem 83:1637–1641
63. Metrangolo P, Neukirch H, Pilati T, Resnati G (2005) Acc Chem Res 38:386–395
64. Metrangolo P, Resnati G (2008) Science 321:918–919
65. Politzer P, Lane P, Concha MC, Ma Y, Murray JS (2007) J Mol Model 13:305–311
66. Karpfen A (2008) Struct Bond 126:1–15
67. Politzer P, Murray JS, Clark T (2010) Phys Chem Chem Phys 12:7748–7757
68. Murray JS, Riley KE, Politzer P, Clark T (2010) Austr J Chem 63:1598–1607
69. Sarwar MG, Dragisic B, Salsberg LJ, Gouliaras C, Taylor MS (2010) J Am Chem Soc 132:1646–1653
70. Huber SM, Jimenez-Izal E, Ugalde JM, Infante I (2012) Chem Commun 48:7708–7710
71. Shields ZP, Murray JS, Politzer P (2010) Int J Quant Chem 110:2823–2832
72. Valkonen A, Chukhlieb M, Moilanen J, Tuononen H, Rissanen K (2013) Cryst Growth Des 13:4769–4775
73. Scholfield MR, Zanden CM, Carter M, Ho PS, Shing P (2013) Protein Sci 22:139–152

74. Voth AR, Ho PS (2007) Curr Top Med Chem 7:1336–1348
75. Parisini E, Metrangolo P, Pilati T, Resnati G, Terraneo G (2011) Chem Soc Rev 40:2267–2278
76. Aragoni MC, Acra M, Devillanova FA, Garau A, Isaia F, Lippolis V, Verani G (1999) Coord Chem Rev 184:271–290
77. Hassel O, Hope H (1961) Acta Chem Scand 15:407–416
78. Alvarez-Rua C, Garcia-Granda S, Ballesteros A, Gonzalez-Bobes F (2002) Acta Cryst E58: o1381–o1383
79. Chalker JM, Thompson AL, Davis BG (2010) Org Synth 87:288–298
80. Herbstein FH, Schwotzer W (1984) J Am Chem Soc 106:2367–2373
81. Hung-Yin G, Hope H (1972) Acta Cryst B28:643–646
82. Daga V, Hadjikakou SK, Hadjiliadis N, Kubicki M, dos Santos JHZ, Butler IS (2002) Eur J Inorg Chem 1718–1728
83. Carlsson A-CC, Uhrbom M, Karim A, Brath U, Gräfenstein J, Erdélyi M (2012) CrystEngComm 15:3087–3092
84. Hakkert SB, Erdélyi M (2015) J Phys Org Chem 28:226–233
85. Koskinen L, Hirva P, Kalenius E, Jääskeläinen S, Rissanen K, Haukka M (2015) CrystEngComm 17:1231–1236
86. Cambridge Structural Database (V5.35 2013) (2013) The Cambridge Crystallographic Data Centre, Cambridge, UK
87. Denmark SE, Kuester WE, Burk MT (2012) Angew Chem Int Ed 51:10938–10953
88. Brown RS, Nagorski RW, Benuet AJ, McClung RED, Aarts GHM, Klobukowski M, McDonald R, Santaniero BD (1994) J Am Chem Soc 116:2448–2456
89. Lommerse PM, Stone AJ, Taylor R, Allen FH (1996) J Am Chem Soc 118:3108–3116
90. Brammer L, Bruton EA, Sherwood P (2001) Cryst Growth Des 1:277–290
91. Zordan F, Brammer L, Sherwood P (2005) J Am Chem Soc 127:5979–5989
92. Bondi A (1964) J Phys Chem 68:441–451
93. Shannon RD (1976) Acta Cryst Sect A 32:751–767
94. Wolff SK, Grimwood DJ, McKinnon JJ, Turner MJ, Jayatilaka D, Spackman MA (2012) Crystal explorer (Version 3.1). University of Western Australia, Crawley

Top Curr Chem (2015) 359: 91–114
DOI: 10.1007/128_2014_604

Published online: 10 April 2015

Organizing Radical Species in the Solid State with Halogen Bonding

Marc Fourmigué and Julien Lieffrig

Abstract The electronic properties (conductivity, magnetism) of radical systems in the solid state essentially depend on (1) the extent of delocalization of the spin density in the molecule and (2) the intermolecular interactions between radicals. The halogen bond has proven very efficient in engineering such magnetic or conducting structures and recent advances along these lines are reviewed here. Three situations are considered: (1) halogenated radical species acting as halogen bond donors, as found in iodotetrathiafulvalene-based chiral conductors or bilayer systems, and in spin crossover (SCO) complexes with halogenated ligands, (2) radical species acting as halogen bond acceptors, such as neutral nitronyl species or anionic, mixed-valence dithiolene complexes, interacting with closed-shell halogen bond donors (iodoperfluoro alkanes and arenes, iodo- or bromo-pyridinium cations), and, finally, (3) charge transfer salts where both halogen bond donor and acceptor are radical species.

Keywords Charge transfer · Chirality · Dithiolene · Halogen bond · Magnetism · Nitronyl · Organic conductors · Radical · Spin crossover · Tetrathiafulvalene

Contents

M. Fourmigué (✉) and J. Lieffrig
Institut des Sciences Chimiques de Rennes, Université Rennes 1 and CNRS, Campus de Beaulieu, 35042 Rennes, France
e-mail: marc.fourmigue@univ-rennes1.fr

1 Introduction

Radical species are investigated particularly in the solid state for their magnetic (and eventually conductive) properties, which closely depend on the interaction pathways established between them [1, 2]. In this respect, intermolecular interactions are expected to play two strikingly different roles. They can introduce some control elements into the solid state organization of the radical species and, accordingly contribute to the specific magnetic and/or conductive properties of the material induced by its crystal structure. However, this structural role can be further complemented by an added functionality, i.e., the introduction of a new electronic interaction path for radical interactions or delocalization (electronic control) *through* the non-bonding interaction, provided some spin density or orbital overlap takes place. Such effects have been reported for hydrogen bonding interactions [3–5] and the question arises as to whether they could also be investigated with halogen bonding interactions, as they have proven to be very good and predictable crystal engineering tools [6, 7]. The halogen bond "structural" approach to control the solid state associations of radical species has been investigated in the last 20 years and several reviews are available up to 2008 which describe the use of halogen bonding in molecular conductors [8] in conducting or magnetic systems [9, 10]. In this chapter we want to complement these reviews by more recent results on this topic, but with special emphasis on those situations where radical interactions or delocalization (electronic control) through the halogen bond are investigated and eventually identified. This contribution is organized into three main sections, the first dedicated to radical molecules or complexes acting as halogen bond donors, the second describing radical molecules or complexes acting as halogen bond acceptors, and the third reporting on charge transfer salts where both halogen bond donors and acceptors are also radical species, a rare situation which provides an opportunity to evaluate the electronic interactions between radical species. It should be noted that, in the following, intermolecular distances are compared with the sum of the van der Waals radii, as defined by Bondi [11], with H: 1.20; N: 1.55; O: 1.52; F: 1.47; S: 1.80; Cl: 1.75; Br: 1.85, and I: 1.98 Å.

2 Radicals as Halogen Bond Donors

To act as halogen bond donors, molecules not only need to be in their radical form but also need to bear halogen atoms as substituents. Furthermore, as for any halogen bond interactions (see other chapters in this book), the strongest effects are anticipated with the most polarizable bromine and iodine atoms. Such molecules are actually extremely rare among neutral radicals, being either C-centered or N–O centered. In the latter, halogen bonding interactions within halogenated neutral nitroxides have been identified [9], the main information being that the oxygen atom in N–O-based radical species is able to act as an efficient halogen bond acceptor. Such a situation is detailed in Sect. 3.1.

Many neutral organic radicals are based on heavily chlorinated aryl derivatives (Fig. 1), such as the perchlorophenalenyl or the polychlorotriphenyl radicals [12, 13]. When described, the X-ray crystal structures of such compounds inevitably show intermolecular Cl···Cl contacts, without identifying particularly short ones. In perchlorophenalenyl, for example, steric interactions between the Cl atoms in *peri* position in the molecules lead to a strong distortion from planarity, which induces a ruffled molecular structure [13]. As a consequence, the shortest intermolecular Cl···Cl distances within the stacks amount to 3.78 Å, above the sum of the van der Waals radii (3.50 Å). The bromo or iodo analogs of such complexes were not described, probably for stability reasons.

In that respect, the brominated trioxytriangulene (Fig. 2a), described in Sect. 2.1, is an exception which deserves special mention. Besides, the other efficient source of stable radical species acting as halogen bond donors remains the cation radical of iodinated tetrathiafulvalene derivatives (Fig. 2b). It has been shown that these radical species are not only stable but also able to act as efficient halogen bond donors, thanks to the iodine activation by the cationic state of the TTF core. In the last few years, the halogen bonding interaction with iodinated TTFs has been purposely used to favor very specific solid state structures, such as chiral, non-centrosymmetric, or hexagonal organizations, as detailed in Sect. 2.2. A third possibility is associated with cationic and paramagnetic coordination complexes, with halogenated organic ligands (Fig. 2c). The solid state organization of such complexes was shown to be controlled to some extent by the halogen bonding

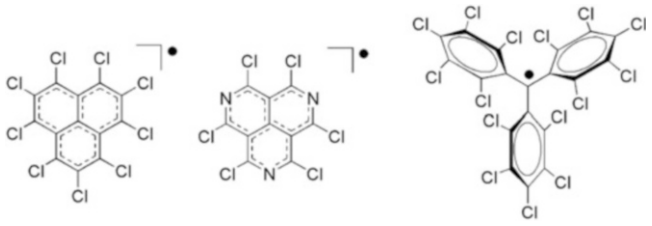

Fig. 1 Examples of heavily chlorinated carbon-based radicals. The crystal structure of the triazahexachlorophenalenyl

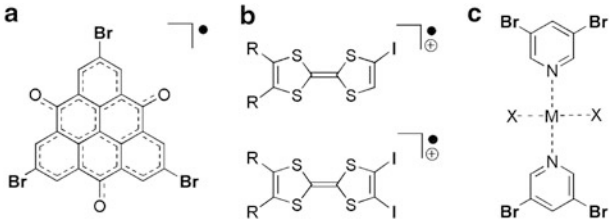

Fig. 2 Structures of radical, halogen bond donors described in Sect. 2

interactions, an important issue for the engineering of magnetic properties, particularly when associated with spin crossover (SCO) systems.

2.1 Halogenated Trioxytriangulene Radical

Following earlier work on the 6-oxophenalenoxyl neutral radical for its use as cathode-active materials for battery applications [14], Morita et al. recently introduced the trioxytriangulene motif (denoted as TOT in the following), characterized by a SOMO and two degenerate LUMOs, arising from the topological symmetry of the π-system [15]. Among these series, the tribromo derivative, denoted as Br_3TOT, forms a one-dimensional columnar structure stabilized by strong π–π stacking. The outside of these columns is covered by bromine and hydrogen atoms susceptible to act as halogen (respect. hydrogen) bond donors, and bromine atoms. The molecule is located on a mirror plane incorporating one bromine, Br(1) and one oxygen O (2) atoms, while Br(2) and O(1) are in general positions. As shown in Fig. 3, Br (2) atoms from two coplanar molecules are halogen bonded to the oxygen O (2) atom located on a mirror plane, while the other bromine atom is essentially non-bonded. The Br(2)···O(2) distance is not very short, that is 95% of the sum of the van des Waals radii. The other oxygen atom O(1) is engaged in a cyclic $R_2^2(10)$ hydrogen bonded motif with a C–H group. Magnetic properties of this compound were not described, but their comparison with the known tris(*tert*-butyl) analog would be particularly interesting to investigate the role of the intermolecular interactions taking place between the columns. Another attractive perspective would be the preparation of the triiodo analog.

2.2 TTF Radical Cations Salts: Toward Chiral Conductors

Halogen-bonded TTF salts were first described by Kato in 1998 [16], from the electrocrystallization of EDT-TTF-I in the presence of counter ions acting as halogen bond acceptors, as detailed in Fig. 4. This topic was reviewed in 2004 [8], and more recent results can be found in more general reviews [9, 10]. Many

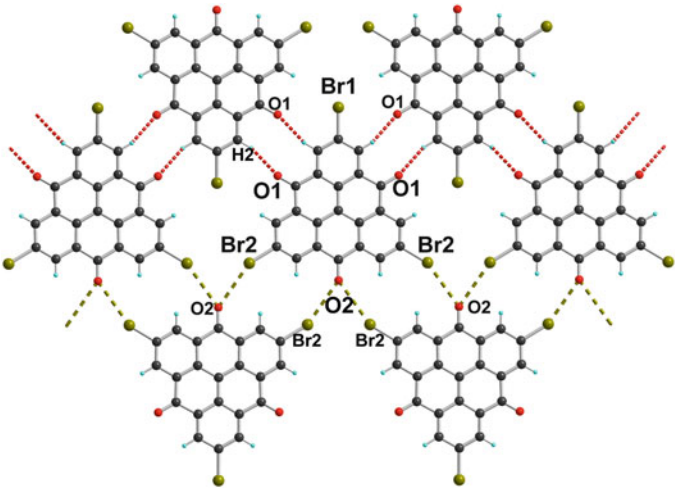

Fig. 3 Projection view of the crystal structure of Br_3TOT, perpendicular to the molecular plane, showing the C–Br(2)···O(2) halogen bond [Br(2)···O(2): 3.21 Å; C–Br(2)···O(2): 156.4°; Br(2)···O(2)=C: 144.6°] and C–H(2)···O(1) [H(2)···O(1): 2.44 Å; C–H(2)···O(1): 150.7°: H(2)···O(1)=C: 153.4°] hydrogen bonds

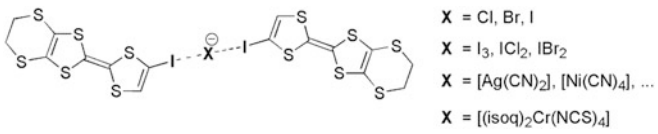

Fig. 4 Examples of halogen bonded TTF salts

different anions were used as halogen bond acceptors, from the simple halides [16, 17] and polyhalides (I_3^-, IBr_2^-, ...) [18], polyhalometallates, polycyanometallates, polythiocyanatometallates [19] to cluster anions such as $[Re_6Se_6(CN)_6]^{4-}$ [20, 21] or $[Mo_3S_7Cl_6]^{2-}$ [22], polymeric anionic networks such as $[PbI_3]_\infty^-$ [23], the layered $[Pb_{5/6}\square_{1/6}I_2]^-$ system with a PbI_2 structure [24], or complex cadmium thiocyanate lacunar networks such as $[Cd_3(NCS)_8]^{2-}$ and $[Cd_5(SCN)_{14}]^{4-}$ [25].

In essentially all cases, the halogen bonding interactions were shown to co-exist with the stacking of partially oxidized TTF derivatives, affording highly conducting salts. It was also demonstrated that the halogen atoms (Br, I) directly linked to the TTF core, as in EDT-TTFI or EDT-$TTFI_2$, also contribute to the band dispersion, as the HOMO of such TTFs exhibits no-zero coefficients on the halogen atoms. It should also be noted that, in most cases, the counter ion acting as Lewis base is centrosymmetric, affording halogen bonded systems with high symmetry. An illustrative counter example is obtained with the tetrahedral ClO_4^- anion, as detailed in Sect. 2.2.1.

More recently, the XB interaction has also been used to favor tentatively the formation of *chiral conductors*. Indeed, as described by Rikken et al. [26],

such conductors are expected to exhibit a weak magneto-chiral effect on conductivity, which can be tentatively described as an added contribution to the magnetoresistance of a compound, only present in chiral compounds. This effect, first observed in chiral nanotubes [27] or in bismuth twisted wires [28], has been a strong incentive in the domain of molecular conductors where the large chiral pool of organic molecules should allow for an easy functionalization with chiral substituents, either of the TTF core itself [29, 30], or within chiral counter ions [31]. This ambitious objective was recently reached by Avarvari et al. [32], in a cation radical salt of a chiral BEDT-TTF derivative. To enhance further the structuring effect of a localized chiral center on the whole crystalline structures, intermolecular interactions such as hydrogen bonding [30] or halogen bonding can also be considered, as detailed in Sects. 2.2.2 and 2.2.3.

2.2.1 IodoTTFs with Non-centrosymmetric ClO_4^- Anion

Both EDT-$TTFI_2$ [33] and tTTF-I [34] were reported to form halogen bonded salts with the ClO_4^- anion (Fig. 5). In the 1:1 (EDT-$TTFI_2$)(ClO_4) salt, the EDT-$TTFI_2$·$^+$ radical cations are associated two-by-two into face-to-face dyads, allowing for a strong σ overlap of the frontier orbitals [1]. The shortest I···O halogen bond is found at 84% of the sum of the van des Waals radii. A similar 1:1 salt was also reported with tTTF-I, formulated as (tTTF-I)(ClO_4), with one I···O distance at 2.997 Å, i.e., 86% of the sum of the van des Waals radii.

A particularly interesting 2:1 salt was also isolated with tTTF-I, formulated as (tTTF-I)$_2ClO_4$, where two oxygen atoms of the ClO_4^- anion are engaged in I···O interactions, each of them however with a crystallographically independent tTTF-I molecule (Fig. 6) [34]. This asymmetry induced by the differential halogen bonding interaction is transferred to the whole salt, as each crystallographically independent molecule segregates into two crystallographically independent slabs. Band structure calculations for each of them gives a different Fermi level for a hypothetical common +0.5 charge for both tTTF-I molecules. Since there is only one Fermi level associated with the chemical potential of the salt, a charge transfer has necessarily to occur between both stacks, implying a deviation from a common +0.5 charge for each donor molecule.

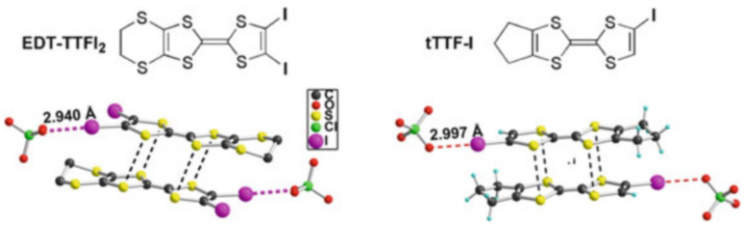

Fig. 5 Detail of the 1:1 ClO_4^- salts with EDT-$TTFI_2$ (*left*) and tTTF-I (*right*) showing the I···O halogen bonds and the face-to-face interaction between radical species

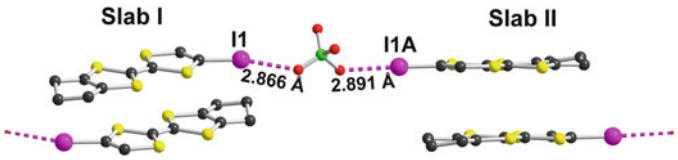

Fig. 6 Detail of the two crystallographically independent conducting slabs in $(tTTF\text{-}I)_2ClO_4$

2.2.2 IodoTTFs with Halogen Bonding to Chiral Anions

The electrocrystallization of iodoTTF derivatives such as EDT-TTF-I in the presence of chiral counter ions is a powerful way to introduce chiral center into halogen-bonded organic conductors, provided one has at hand chiral anionic species able to act as XB acceptors. We have shown that sulfonate anions are efficient XB acceptors and various $EDT\text{-}TTFI_2$ salts were reported with 1,5-naphthalene-bis(sulfonate), 2,6-naphthalene-bis(sulfonate), or 2,6-anthracene-bis(sulfonate) [33]. Camphorsulfonate is a chiral anion, available both as enantiopure compound and racemic mixture. The electro-crystallization of $EDT\text{-}TTFI_2$ in the presence of the D-isomer afforded a 2:1 salt with metallic conductivity and two-dimensional Fermi surface [35]. Interestingly, the two crystallographically independent $EDT\text{-}TTFI_2$ molecules exhibit a different XB pattern. Molecule A is halogen bonded both to the sulfonate and the carbonyl moieties of D-camphorsulfonate anions while molecule B is only interacting with the oxygen atom of a water molecule (see Fig. 7 for structural XB characteristics). This differentiation is associated with a departure from the averaged +0.5 charge on the two $EDT\text{-}TTFI_2$ molecules. Indeed, based on the comparison of intramolecular bond lengths, the compound is tentatively formulated as $[A^{+0.75}B^{+0.25}]$[D-camphorsulfonate], i.e., with the most oxidized molecule A involved in the strongest intermolecular halogen-bond interactions, an observation to be correlated with the electrostatic contribution to the halogen bond.

It should also be stressed that the racemic salt obtained with DL-camphorsulfonate is not isostructural with its enantiopure counterpart [33]. Albeit a mixed-valence 2:1 salt was also obtained, crystallizing with solvent inclusion, giving rise to a one-dimensional electronic structure and semi-conducting character. Halogen bonding interactions with the $EDT\text{-}TTFI_2^{+0.5}$ molecules are still present with the shortest O···I distances above 2.81 Å, which is 80% of the sum of the van der Waals radii.

2.2.3 Chiral IodoTTF Salts

Another approach to chiral conductors exhibiting halogen bonding in the solid state relies on the preparation of halogenated *and* chiral tetrathiafulvalene derivatives. Only one example has been reported to date, where the ethylene group of $EDT\text{-}TTFI_2$ is replaced by a 1,3-dimethyl-1,3-propylene substituent in $Me_2PDT\text{-}TTFI_2$ [36]. Its

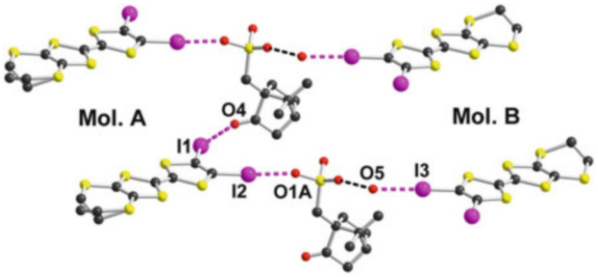

Fig. 7 Detail of the asymmetric unit in (EDT-TTFI$_2$)$_2$(D-camphorsulfonate). Halogen bonds with *red dotted lines*: I(1)···O(4) 3.02 Å, I(2)···O(1A) 2.68 Å, I(3)···O(5) 2.84 Å. Hydrogen bond between water molecule and sulfonate moiety as *black dotted line*

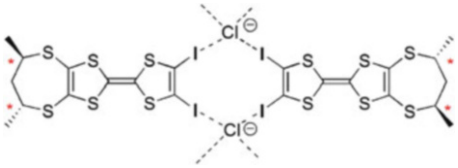

Fig. 8 The chiral Me$_2$PDT-TTFI$_2$ and the structural motif observed in its chloride salt

electrocrystallization with halide anions afforded a 2:1 mixed valence salt, whose conductivity is limited by the steric constraints imposed by the bulky dimethylpropylene moiety (Fig. 8).

To conclude this section on chiral conductors, it appears that the introduction of low symmetry counter ions systematically favor the presence of multiple crystallographically independent molecules, with then the possibility of different degrees of charge transfer, and competition with charge localization [37].

2.3 *Paramagnetic Metal Complexes with Halogenated Ligands*

2.3.1 Halopyridine Complexes of Metal Halides

The ability of halometallates [38–40] (as well as cyano [41, 42] and thiocyanato [19] analogs) to act as halogen bond acceptors has been extensively explored [43], particularly by Brammer et al., and several series of salts with halo-pyridinium cations as halogen bond donors were reported.

Neutral halopyridines (Fig. 9) were also used with a twin role, as they act as Lewis bases for metal coordination through the nitrogen atom and, simultaneously, as halogen bond donors [44]. It is found, for example, in *trans*-[MCl$_2$(4-X′-py)$_2$] (M=Pd, Pt; X′=Cl, Br) and *trans*-[PdI$_2$(4-I-py)$_2$]. While no specific magnetic interactions can be

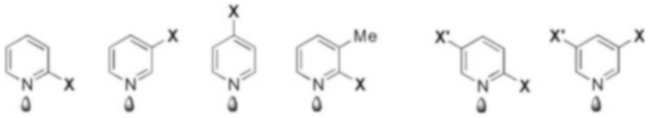

Fig. 9 Mono- and dihalopyridines used in the coordination of metal halides (X, X′=Cl, Br, I)

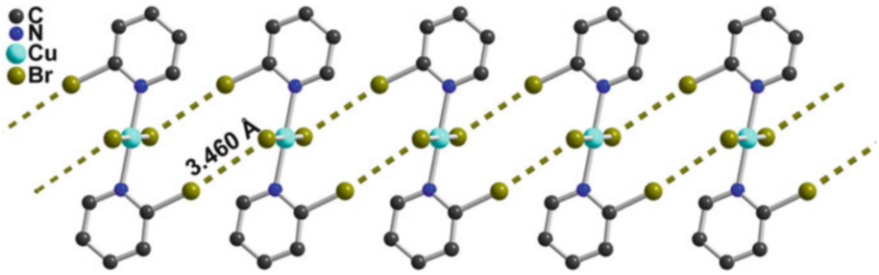

Fig. 10 View of the halogen bonded chains in $[CuBr_2(2\text{-Br-py})_2]$. The Br···Br distance, 3.46 Å, is to be compared with the sum of the van der Waals radii, namely 3.70 Å

expected from these low spin d^8 complexes, other examples have been reported, incorporating $S = ½$ ions, in d^7 Co^{2+} or d^9 Cu^{2+} species.

Several CuX_2 complexes with halogenated pyridine ligands were reported, as in *trans*-$[CuCl_2(3\text{-Cl-py})_2]$ [45], or $[CuX_2(2\text{-Br-py})_2]$ and $[CuX_2(3\text{-Br-py})_2]$ [46]. The data indicate that the halogen bond interaction taking place between the coordinated chloro- or bromopyridine are much weaker than those observed in the cationic bromo- or chloropyridinium salts, a clear indication of electrostatic activation in the salts. Furthermore, the bromine–halide distances are almost equal to the sum of their van der Waals radii (r_{vdW}) in the *meta*-substituted $[CuX_2(3\text{-Br-py})_2]$ but less than the sum of the r_{vdW} by ~0.24 Å in the *ortho*-substituted analog $[CuX_2(2\text{-Br-py})_2]$ (Fig. 10). Magnetic data for $[CuBr_2(2\text{-Br-py})_2]$ show an absence of any interactions, with perfect Curie-type behavior [46].

On the other hand, the analogous 2,5-dibromopyridine derivatives, formulated as $[CuCl_2(2,5\text{-Br}_2\text{-py})_2]$ and $[CuBr_2(2,5\text{-Br}_2\text{-py})_2]$, are not isostructural and exhibit antiferro- or ferromagnetic interactions, respectively [46, 47]. The antiferromagnetic interactions in the copper chloride salt have been attributed, in spite of a relative long Cl···Cl distance (4.16 Å), to this two-halide exchange pathway, in accordance with a non-negligible spin density on the chloride ions (0.109). The copper bromide salt $[CuCl_2(2,5\text{-Br}_2\text{-py})_2]$ adopts a structure comparable with that of $[CuBr_2(2\text{-Br-py})_2]$ (Fig. 10). Since the bromides are too far apart from each other, the proposed rationale for the observed ferromagnetic interaction is based on the orthogonal interaction between the very small spin density on the organic bromine (0.005), located along the C–Br bond, and the spin density of the bromide along the Cu–Br bond. Similar ferromagnetic interactions mediated by the halogen bonds were already reported in similar copper chloride and bromide with 2-chloro-3-methylpyridine and 2-bromo-3-methylpyridine [48].

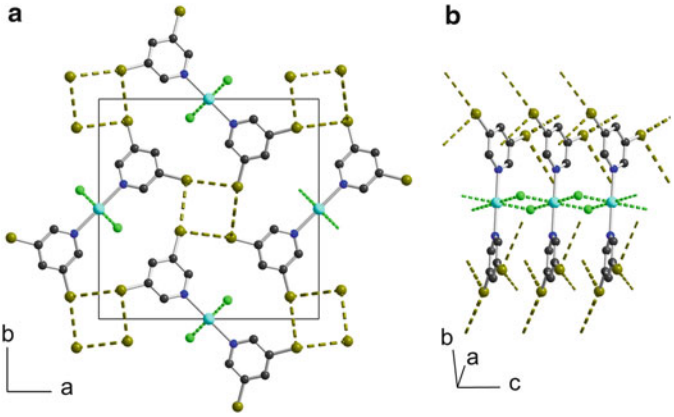

Fig. 11 Views of *trans*-[$CoCl_2$(3,5-Br_2py)$_2$] with (**a**) projection along the *c* axis showing the tetrameric halogen bonded motif and (**b**) the $CoCl_2$ chain running along *c*

The structures of *trans*-[$CoCl_2$(3,5-X_2py)$_2$], X=Cl, Br, are characterized (Fig. 11) by short XB interactions which develop in the ab plane, giving rise to original tetrameric motifs [49]. Magnetic interactions between cobalt ions are characteristic of linear cobalt chloride chain compounds, albeit the XB interactions limit here the magnetic interactions between the chains.

Concluding this section, it appears that spin density on the halogen atoms of coordinated halogenated pyridines is extremely weak and, as a consequence, magnetic interactions through the halogen bond cannot be expected to play an important role.

2.3.2 Spin Crossover Cooperativity and Halogen Bonding

As illustrated above, the XB interactions introduce structural constraints which can play an important role in the solid state organization of magnetic systems. This can be particularly important in spin crossover systems (SCO) where the high spin/low spin (HS/LS) *conversion* can be turned into an abrupt structural *transition* in the presence of *cooperative* intermolecular interactions [50]. Only a few examples of complexes showing the involvement of halogen bonding in SCO have been described to date, and involve either Fe^{II} or Fe^{III} complexes (Fig. 12).

The Fe^{II} [Fe(phen)$_2$(NCS)$_2$] complex is regarded as the prototypical mononuclear SCO system, between a high temperature HS state ($S = 2$) and a low temperature LS state ($S = 0$) [51]. The observed abrupt transition has been extensively investigated and can be tentatively attributed to the presence of intermolecular π–π interactions. Among the various modifications of the phenanthroline ligand explored to date, the 3-bromophenanthroline (Fig. 12a) afforded a series of solvated iron thiocyanate complexes, formulated as [Fe(3-Br-phen)$_2$(NCS)$_2$]·S ($S = 0.5$ MeOH, 2 CH_2Cl_2, 0.5 Me_2CO) [52], which exhibit magnetic features atypical of the classic

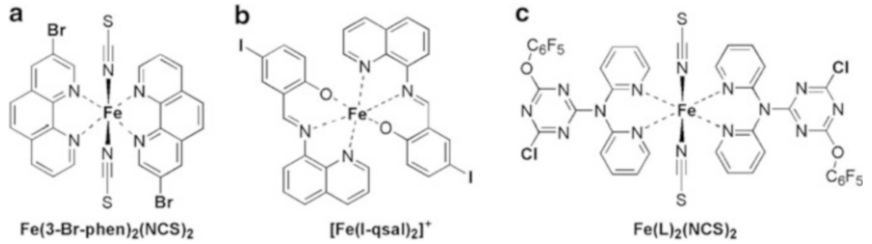

Fig. 12 Metal complexes with halogenated ligands exhibiting spin crossover conversion

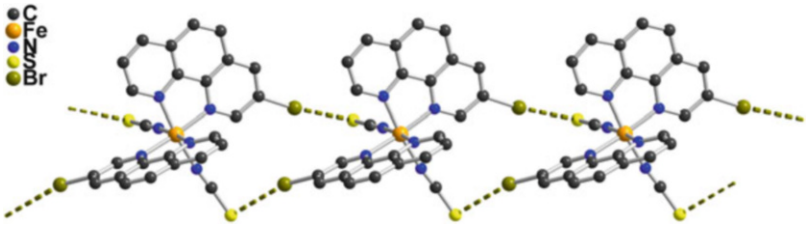

Fig. 13 Br···S interactions in $[Fe(3\text{-Br-phen})_2(NCS)_2]\cdot 2\ CH_2Cl_2$

$[Fe(phen)_2(NCS)_2]$ [51]. In the solid state (Fig. 13), a characteristic halogen bond interaction takes places between the bromine atom and the sulfur atom of the thiocyanate ligand. As already observed with non-coordinated NCS^- anion [53], the halogen bond donor points toward the sulfur atom, perpendicular to the C–S bond, with a Br···S distance 91% of the sum of the r_{vdW}.

Another example of an SCO system involves the Fe^{III} $[Fe(Iqsal)_2]^+$ species, as $[Ni(dmit)_2]^-$ salt (dmit = 1,3-dithiole-3-thione-4,5-dimercapto) (Fig. 12b). This salt could have been described in Sect. 4 dedicated to halogen bonded systems between two radical species, as the $[Ni(dmit)_2]^-$ is also paramagnetic, but is shown here in this section on SCO compounds for completeness. As shown in Fig. 14, a directional I···S interaction takes place between cationic and anionic moieties [54]. The $[Ni(dmit)_2]^-$ radical anions are organized into face-to-face dyads, paralleling the one already observed with radical *cations*. A cooperative spin crossover occurs at $T_{½}\downarrow = 150$ K, characterized with an abrupt decrease of the $\chi_M T$ product. One remarkable feature is that the I···S distance found as 3.690(2) at 293 K and 3.634(3) Å at 175 K, above $T_{½}\downarrow$, actually increases abruptly up to 3.796 (3) Å at 130 K, indicating that the halogen-bond interactions disappeared when crossing the SCO process. These observations, along with the spin-singlet formation in the $[Ni(dmit)_2]$ dimer, suggest that the halogen-bond interactions between the cation and the anion compete with the π-stacking interactions between the face-to-face $[Ni(dmit)_2]$ anions.

The last example with the complex ligand L shown in Fig. 12c [55] exhibits a short Cl···F interaction between the strongly activated chlorine atom of the triazine ring and one fluorine atom of the pentafluorophenyloxy moiety. The Cl···F

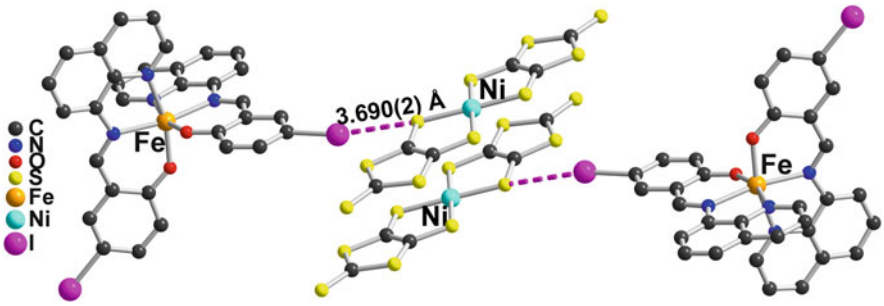

Fig. 14 I···S interactions in the RT structure of $[Fe(Iqsal)_2][Ni(dmit)_2]\cdot CH_3CN\cdot H_2O$

distance varies between, 2.969(4) Å and 3.013(4) Å in the LS and HS phase, respectively, both notably shorter than the sum of the van der Waals radii (3.22 Å). Together with other intermolecular interactions, this Cl···F contact is believed to contribute to the strongly cooperative SCO, characterized by an abrupt transition with hysteresis loop. These three rare examples demonstrate that halogen bonding interactions can provide an efficient and powerful tool to modify and eventually control cooperativity in SCO systems. The extreme sensitivity of such complexes to minute modifications of their structural environment, however, makes it difficult to rationalize fully the observed effects.

3 Radicals as Halogen Bond Acceptors

The association of radical molecules acting as halogen bond acceptors is based on two conditions: (1) the presence of halogen bond donor moieties in the radical molecules and (2) the availability of strong halogen bond donor molecules. This second point is essentially fulfilled with perfluorinated iodoalkanes and iodo-arenes which have been used extensively in crystal engineering [6, 7, 10], and specifically here also with radical molecules. The first point gives us a way to classify the radical halogen bond acceptors. The interest in the solid state structure of radical molecules in the solid state is associated with their magnetic properties, which are closely related to the spatial arrangement of the spin carriers in the crystal lattice. The introduction of XB interactions involving radical species might modify the way they interact with each other and, accordingly, their magnetic and/or transport properties. Three main classes of radical species acting as halogen bond acceptors are identified, and developed in the three following sections – nitronyl radicals, paramagnetic metallic complexes, and metal complexes with non-innocent ligands.

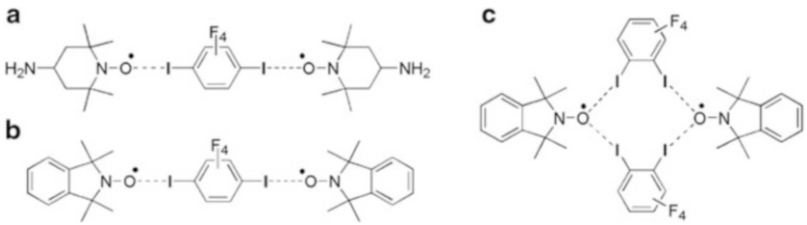

Fig. 15 Trimeric or tetrameric motifs observed in halogen bonded nitronyl radicals

3.1 Nitronyl Radicals

As shown from theoretical [56, 57] and temperature-dependent EPR studies [58], nitronyl radicals act as very good halogen bond donors and their co-crystallization with 1,4-diiodotetrafluorobenzene provided the very first example of a halogen bonded TEMPO radical, namely, a trimeric entity obtained with 4-amino-TEMPO (Fig. 15a) [59]. This work was extended by Micallef to isoindoline nitroxide [60, 61]: a similar trimeric entity was crystallized (Fig. 15b) while EPR spectroscopy performed in solution with pentafluoroiodobenzene indicated that halogen bonding induces an increase in electron density at the nitroxide nitrogen nucleus and an increase in the nitroxide rotational correlation time. With 1,2-diiodotetrafluorobenzene [61, 62], tetrameric motifs were isolated (Fig. 15c), with the NO group acting as a simple or bifurcated halogen bond acceptor, allowing for modulation of the magnetic properties, when compared with the radicals alone.

Nitronyl nitroxide radicals can also act as good halogen bonds acceptors and as bidendate donors, with a spin density delocalized on both NO groups [63]. Their co-crystallization with 1,4-diiodotetrafluorobenzene or the extended 4,4′-diiodo-octafluoro-biphenyl (Fig. 16a, b) afforded magnetic chains with very short I···O distances, below 80% of the sum of the van der Waals radii [64]. The lack of magnetic exchange through halogen bonds has been confirmed by EPR spectroscopy, and the magnetic interactions rely only on direct weak overlap between the radical species.

3.2 Metal Complexes with Essentially Metallic Spin Density

Paramagnetic metal complexes can act efficiently as halogen bond acceptors, and attractive interactions dominated by electrostatics were described by Brammer et al. in a series of systematic studies on C–X···X′–M [65–67]. This work was also recently extended to cyanometallates (C−X···N≡C−M) as halogen bond donors, in a series of halopyridinium salts of hexacyanometallates $[M(CN)_6]^{3-}$ (M=Cr, Fe, Co) [68]. The geometry of interaction of the halogen bond donor (C−X) with the cyanide ligand is either a shorter interaction, predominantly with the *exo* lone pair of the nitrogen atom (C≡N···X > 145°), or a longer interaction

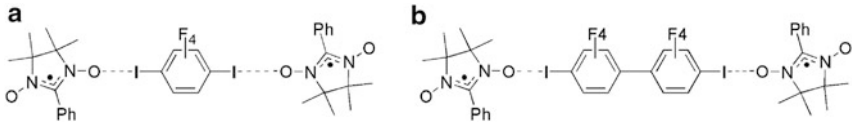

Fig. 16 Tetrameric motifs observed in halogen bonded nitronyl nitroxide radicals

with the C≡N π-bond (C≡N···X < 105°). These studies provide important structural information which can be further used when associating such paramagnetic complexes with radical species, particularly cation radical derived from tetrathiafulvalenes [8]. One can cite in this context halometallates such the $S = 5/2$ Fe^{III} $FeCl_4^-$ [69, 70], cyanometallates such as $[Cr(CN)_6]^{3-}$ [71], or isothiocyanatometallates such as the $S = 3/2$ Cr^{III} $[Cr(isoq)_2(NCS)_4]^-$ complexes [19], all acting as halogen bond acceptors vs iodinated tetrathiafulvalenium cations. In all reported examples, however, the halogen bond was found to provide a very poor channel for super-exchange magnetic interactions between the paramagnetic complex and the $S = ½$ iodotetrathiafulvalenium cation.

3.3 Metal Complexes with Non-innocent Ligands

Dithiolene complexes such as $[M(mnt)_2]^{-\bullet}$ and $[M(dmit)_2]^{-\bullet}$ (M=Ni, Pd, Pt) are paramagnetic species ($S = ½$) with a spin density strongly delocalized on the two dithiolene moieties. They have been acting as halogen bond acceptors, either through the CN group in $[Ni(mnt)_2]^{-\bullet}$ [72, 73] or through the sulfur atoms in $[Pd(dmit)_2]^{-\bullet}$ [74], particularly when engaged in salt with iodinated tetrathiafulvalenium cations [9]. More recently, Kato et al. investigated mixed valence salts of $[Ni(dmit)_2]^{-\bullet}$ with non-magnetic halogenated cations such as *N*-Me-3,5-dihalopyridinium, *N*-Me-2,5-dihalopyridinium, or *N*-ethyl-4-halothiazolium [75].

In all of them, strong I···S interactions were identified together with C–H···S hydrogen bonds, involving the outer thioketone S=C group of the dmit ligand, with I···S distances of 3.27 and 3.49 Å [76]. The important point about these salts is their mixed valence character inferred from their stoichiometry, which is two $[Ni(dmit)_2]$ complexes for one pyridinium cation. Such salts are obtained by electrocrystallization of the anionic $[Ni(dmit)_2]^{-\bullet}$ in the presence of the pyridinium cation. The latter is found in the solid state associated with two crystallographically independent $[Ni(dmit)_2]$ complexes, each of them forming two crystallographically independent conducting layers. The consequences are essentially twofold: (1) the two layers might exhibit different solid state arrangement of the partially oxidized $[Ni(dmit)_2]$ complexes and, accordingly, different band structures and (2) the two independent complexes might have a formal charge deviating from the averaged −0.5 charge. Raman spectra in $(3,5\text{-}I_2py)[Ni(dmit)_2]_2$ indicated that the formal charge is the same in the two slabs, which exhibit different structures and transport properties (Fig. 17), with a localized state in layer I and a two-dimensional closed Fermi surface in layer II. ^{13}C NMR showed evidence for the coexistence of

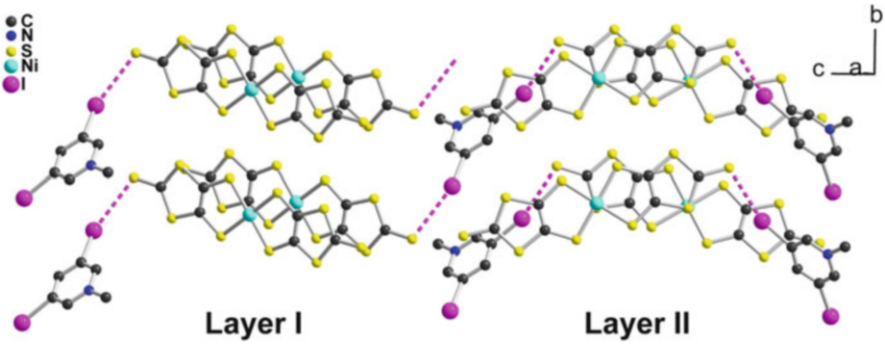

Fig. 17 Anionic dithiolene complexes and their halogenated cations

localized spins (layer I) and conduction π electrons (layer II) [77], while Shubnikov–de Haas and angular-dependent magnetoresistance oscillations clearly show that there exists a two-dimensional Fermi surface in layer II, whose spins are strongly coupled with the localized spins in layer I [78]. It is believed that the asymmetric environment mediated by the halogen (and weak hydrogen) bond interactions favors here the formation of such *bilayer systems*, as already mentioned in Sect. 2.2.2 for $(tTTF\text{-}I)_2ClO_4$ [34].

Varying the electrocrystallization conditions or the nature of the halogens in the analogous 3,5-dibromo- and 3,5-bromoiodopyridinium salts afforded a series of salts formulated as $(3,5\text{-}Br_2Py)[Ni(dmit)_2]_2$, $(3,5\text{-}I_2py)[Ni(dmit)_2]_3$, α-$(3,5\text{-}I_2py)[Ni(dmit)_2]_2$, β-$(3,5\text{-}I_2py)[Ni(dmit)_2]_2$, and $(3,5\text{-}BrIpy)[Ni(dmit)_2]_2$ [79]. Another series was developed with the 2,5-dihalopyridium cations [80], as well as with N-ethyl-4-halothiazolium cations (see Fig. 18) [81].

4 Halogen-Bonded Charge Transfer Salts

This last section is dedicated to systems where both the halogen bond donor and the halogen bond acceptor are radical species. Such a rare situation is actually found in a few charge-transfer salts between *electron* donor and acceptor molecules. We have detailed in Sect. 3 the possibility of radical species acting as halogen bond acceptors. In this respect, it is surprising that radical anion species such as $TCNQ^{-}\cdot$ were only recently reported to form salts with halogenated cations where XB could be observed. Actually, neither its neutral complex with para-diiodobenzene [82], nor various pyridinium salts [83, 84], exhibit any halogen bond interaction with the nitrile substituents of TCNQ. Perhaps the first mentioned is to be found in a charge-transfer complex with an iodinated TTF (Fig. 19), formulated as $(EDO\text{-}TTF\text{-}I)_2(TCNQ)$ [85].

In this compound, a short and directional I···N interaction is found at 3.07 Å, between the centrosymmetric TCNQ molecule and the EDO-TTF-I electron donor (Fig. 20). Close inspection of the *intramolecular* bond lengths within both the TTF

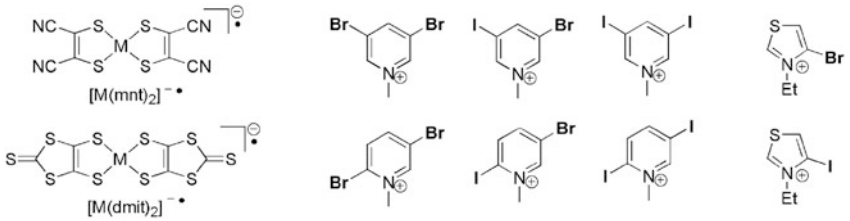

Fig. 18 Detail of the crystal structure of (3,5-I_2py)[Ni(dmit)$_2$]$_2$

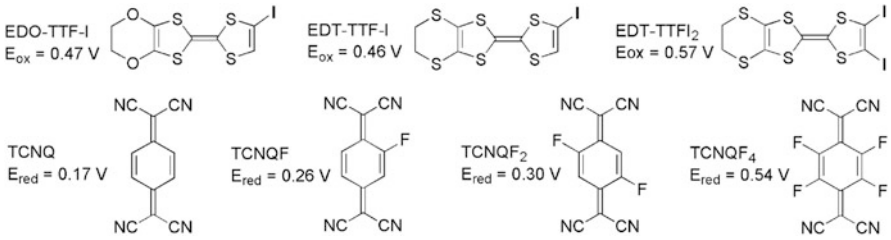

Fig. 19 Structures of halogenated TTFs and different TCNQs involved in charge transfer complexes and salts

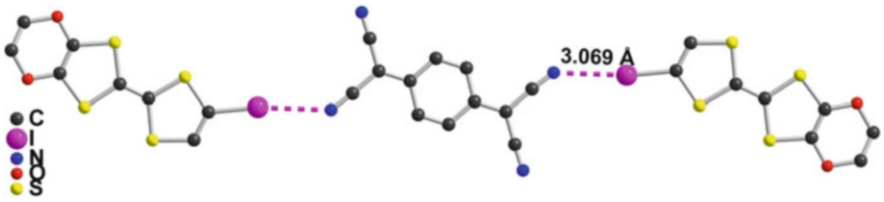

Fig. 20 Halogen-bonded trimers in neutral (EDO-TTF-I)$_2$(TCNQ) [85]

and TCNQ cores shows, however, that an electron transfer does not take place upon complex formation. In other words, we are in the presence of a neutral, so-called charge-transfer complex (and not salt). This behavior finds its origin in the relative redox potentials of both molecules. EDO-TTF-I oxidizes at $E_{ox} = +0.47$ V vs SCE, a potential too high when compared with the reduction potential of TCNQ ($E_{red} = +0.17$ V). A very similar complex is obtained with EDT-TTF-I ($E_{ox} = +0.46$ V) [86], with a comparable I···N contact at 3.08 Å. These two examples demonstrate that the electron transfer, and ionic species, is not a necessary condition to observe the halogen bonding interaction between the iodine of the TTF derivative and the nitrile of TCNQ. The question then arises as to whether this interaction is actually strengthened in the salts. For this purpose, TCNQ was replaced by the more oxidizing $TCNQF_2$ ($E_{red} = +0.36$ V), affording an ionic salt formulated as (EDT-TTF-$I^{+0.5}$)$_2$($TCNQF_2^{-}$) with a slightly shorter N···I interaction at 3.04 Å [86].

Table 1 Evolutions of the $TCNQF_n$ charge (ρ) and the I···N distance, within the series $(EDT\text{-}TTFI_2)_2(TCNQF_n)$

	TCNQ [87]	TCNQF [87]	$TCNQF_2$ [87]	$TCNQF_4$ [88]
ΔE (V)	−0.40	−0.31	−0.27	−0.03
$T = 293$ K	$\rho \approx -0.2$ I···N = 3.08 Å	$\rho \approx -0.1$ I···N = 3.08 Å	$\rho \approx -1$ I···N = 2.99 Å	$\rho \approx -1$ I···N = 2.94 Å
$T = 150$ K	$\rho \approx -0.1$ I···N = 3.05 Å	$\rho \approx -0.1$ I···N = 3.01 Å	$\rho \approx -1.1$ I···N = 2.96 Å	
$T = 100$ K		$\rho \approx -0.2$ I···N = 2.99 Å		
$T = 15$ K	$\rho \approx -0.1$ I···N = 3.00 Å	$\rho \approx -0.5$ I···N = 2.94 Å	$\rho \approx -0.9$ I···N = 2.93 Å	

ΔE stands for $E_{red}(TCNQF_n) - E_{ox}(EDT\text{-}TTFI_2)$

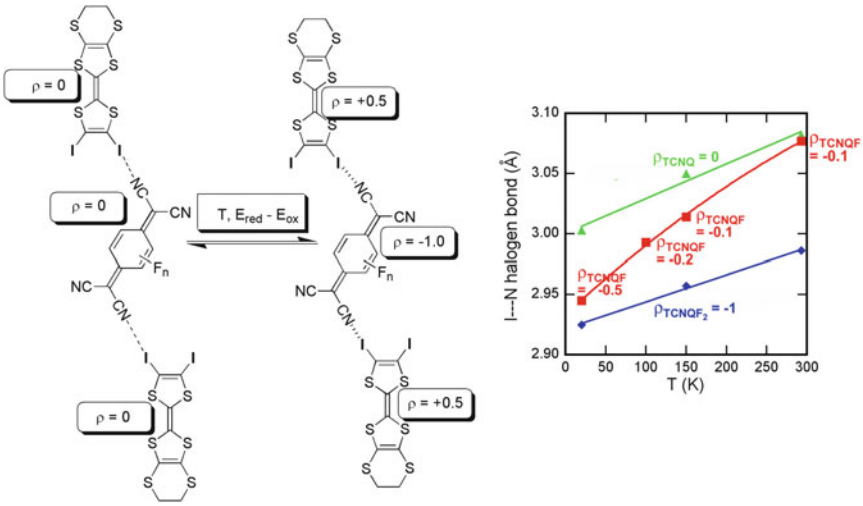

Fig. 21 Evolutions of the I···N distance with charge and temperature within the $(EDT\text{-}TTFI_2)_2(TCNQF_n)$ trimers, $n = 0 - 2$

The situation is, however, not so simple, since moving from $TCNQF_2$ to the even more oxidizing $TCNQF_4$ afforded a 1:1 ionic salt, formulated as $(EDT\text{-}TTF\text{-}I^{+\bullet})(TCNQF_4^{-\bullet})$, where cations and anions are actually linked by a strong C–H···N hydrogen bond rather than the expected C–I···N halogen bond [86].

A similar series of compounds was obtained with the diiodo TTF derivative, $EDT\text{-}TTFI_2$ [87, 88], where the competition with the C–H···N hydrogen bond cannot take place. To establish a correlation between the halogen bond length and the degree of charge transfer, a complete series was crystallized from the less oxidizing TCNQ to the most oxidizing $TCNQF_4$. All four compounds exhibit the very same halogen bonded trimeric motif $(EDT\text{-}TTFI_2)(TCNQF_n)(EDT\text{-}TTFI_2)$, $n = 0, 1, 2, 4$, similar to the one shown in Fig. 20. Three important conclusions were

drawn from the structural, electronic, and spectroscopic investigations of these series (Table 1 and Fig. 21):

1. The degree of electron transfer is directly correlated to the redox difference $\Delta E = E_{red}(TCNQF_n) - E_{ox}(EDT\text{-}TTFI_2)$ with ionic salts even when ΔE is slightly negative, an indication of the Coulombic stabilization of ionic forms in the solid state.
2. The degree of electron transfer can be modified with the temperature, with a neutral-to-ionic conversion observed upon cooling in the intermediate $(EDT\text{-}TTFI_2)_2(TCNQF)$.
3. The degree of electron transfer is correlated to the length of the I···N halogen bond. In other words, shorter halogen bonds are found with the most ionic compounds, indicated unambiguously an added electrostatic contribution to the halogen bond interaction.

5 Summary, Conclusions, and Outlook

A first very active research period, started at the end of the 1990s and aimed at investigating halogen bonding interactions essentially in organic conductors and radical nitronyl systems, has provided numerous examples of radical systems with solid state structures controlled to a large extent by halogen···Lewis base interactions. While the contribution of halogen atoms to the band dispersion of organic metals was demonstrated, the preliminary assumptions that this intermolecular interaction could also work as a channel for magnetic interactions were not really fulfilled, essentially because the halogen atoms in radical halogen bond donors most often bear a very small part of the spin density. On the other hand, the predictability of halogen bonding associated with its strong linearity allowed for an efficient structural control of the solid state associations of radical species. We believe that this structural control can still play an important role in the tuning of intermolecular interactions, particularly in systems where cooperativity and delocalization play a crucial role. This is particularly true in molecular conductors and recent examples, based on mixed valence salts, halogen bonded to non-centrosymmetric counter ions, provide novel bilayer conducting systems. Similarly, cooperativity effects are particularly involved in the nature of the spin crossover (SCO) between high spin and low spin states. Halogen bonding in the crystal structure of such SCO complexes opens the way to new structural organizations and new behaviors.

References

1. Fourmigué M (2012) The importance of π-interactions in crystal engineering, chap 6. Wiley, New York, pp 143–162
2. Hicks RG (ed) (2010) Stable radicals. Wiley, New York

3. Otsuka T, Okuno T, Awaga K, Inabe T (1998) Crystal structures and magnetic properties of acid–base molecular complexes, (p-pyridyl nitronylnitroxide)$_2$X (X = hydroquinone, fumaric acid and squaric acid). J Mater Chem 8:1157–1163
4. Romero FM, Ziessel R, Bonnet M, Pontillon Y, Ressouche E, Schweitzer J, Delley B, Grand A, Paulsen C (2000) Evidence for transmission of ferromagnetic interactions through hydrogen bonds in alkyne-substituted nitroxide radicals: magnetostructural correlations and polarized neutron diffraction studies. J Am Chem Soc 122:1298–1309
5. Maspoch D, Catala L, Gerbier P, Ruiz-Molina D, Vidal-Gancedo J, Wurst K, Rovira C, Veciana J (2002) Radical para-benzoic acid derivatives: transmission of ferromagnetic interactions through hydrogen bonds at long distances. Chem Eur J 8:3635–3645
6. Metrangolo P, Neukirch H, Pilati T, Resnati G (2005) Halogen bonding based recognition processes: a world parallel to hydrogen bonding. Acc Chem Res 38:386–395
7. Meyer F, Dubois P (2013) Halogen bonding at work: recent applications in synthetic chemistry and materials science. CrystEngComm 15:3058–3071
8. Fourmigué M, Batail P (2004) Activation of hydrogen- and halogen-bonding interactions in tetrathiafulvalene-based crystalline molecular conductors. Chem Rev 104:5379–5418
9. Fourmigué M (2008) Halogen bonding in conducting or magnetic molecular materials. Struct Bond 126:181
10. Metrangolo P, Meyer F, Pilati T, Resnati G, Terraneo G (2008) Halogen bonding in supramolecular chemistry. Angew Chem Int Ed 47:6114–6127
11. Bondi A (1964) van der Waals volumes and radii. J Phys Chem 68:441–451
12. Veciana J, Ratera I (2010) In: Hicks RG (ed) Stable radicals, chap 2. Wiley, New York, pp 33–80
13. Koutentis PA, Chen Y, Cao Y, Best TP, Itkis ME, Beer L, Oakley RT, Cordes AW, Brock CP, Haddon RC (2001) Perchlorophenalenyl radical. J Am Chem Soc 123:3864–3871
14. Morita Y, Nishida S (2010) In: Hicks RG (ed) Stable radicals, chap 3. Wiley, New York, pp 81–145
15. Morita Y, Nishida S, Murata T, Moriguchi M, Ueda A, Satoh M, Arifuku K, Sato K, Takui T (2011) Organic tailored batteries materials using stable open-shell molecules with degenerate frontier orbitals. Nat Mater 10:947–951
16. Imakubo T, Sawa H, Kato R (1995) Novel radical cation salts of organic π-donors containing iodine atom(s): the first application of strong intermolecular-I···X-(X=CN, halogen atom) interaction to molecular conductors. Synth Metals 73:117–122
17. Imakubo T, Shirahata T, Hervé K, Ouahab L (2006) Supramolecular organic conductors based on diiodo-TTFs and spherical halide ion X−(X=Cl, Br). J Mater Chem 16:162–173
18. Domercq B, Devic T, Fourmigué M, Auban-Senzier P, Canadell E (2001) Hal···Hal interactions in a series of three isostructural salts of halogenated tetrathiafulvalenes. Contribution of the halogen atoms to the HOMO–HOMO overlap interactions. J Mater Chem 11:1570–1575
19. Hervé K, Cador O, Golhen S, Costuas K, Halet JF, Shirahata T, Muto T, Imakubo T, Miyazaki A, Ouahab L (2006) Iodine substituted tetrathiafulvalene radical cation salts with $[M(isoq)_2(NCS)_4]^-$ anions where $M=Cr^{III}$, Ga^{III}: role of I···S and S···S contacts on structural and magnetic properties. Chem Mater 18:790–797
20. Ranganathan A, El-Ghayoury A, Mézière C, Harté E, Clérac R, Batail P (2006) Balancing framework densification with charged, halogen-bonded-π-conjugated linkages: $[PPh_4]_2$\{[*E*-TTF–I_2][$Re_6Se_8(CN)_6$]\} vs $[PPh_4]_2$[EDT-TTF–I]$_2$\{[EDT-TTF–I][$Re_6Se_8(CN)_6$]\}. Chem Commun 2878–2880
21. Barrès AL, El-Ghayoury A, Zorina LV, Canadell E, Auban-Senzier P, Batail P (2008) The 8:1:1 ternary hybrid framework in the system [EDT-$TTF^{\cdot+}$] [1,4-bis(iodoethynyl)benzene] $[Re_6Se_8(CN)_6]^{4-}$: dual noncovalent expression of the octahedral halogen-bond hexa-acceptor nanonode. Chem Commun 2194–2196
22. Alberola A, Fourmigué M, Gómez-García CJ, Llusar R, Triguero S (2008) Halogen bonding interactions with the $[Mo_3S_7Cl_6]^{2-}$ cluster anion in the mixed valence salt [EDT-$TTFI_2$]$_4$[$Mo_3S_7Cl_6$]·CH_3CN. New J Chem 32:1103–1109

23. Devic T, Canadell E, Auban-Senzier P, Batail P (2004) (EDT-TTF-I_2)$_2$$PbI_3$·$H_2O$: an ambient pressure metal with a β′ donor slab topology. J Mater Chem 14:135–137
24. Devic T, Evain M, Moëlo Y, Canadell E, Senzier P, Fourmigué M, Batail P (2003) Single crystalline commensurate metallic assemblages of π-slabs and CdI_2-type layers: synthesis and properties of β-(EDT-TTF-I_2)$_2$[$Pb_{5/6}\square_{1/6}I_2$]$_3$ and β-(EDT-TTF-I_2)$_2$[$Pb_{2/3+x}Ag_{1/3-2x}\square_xI_2$]$_3$, x = 0.05. J Am Chem Soc 125:3295–3301
25. Fourmigué M, Auban-Senzier P (2008) Anionic layered networks reconstructed from [Cd(SCN)$_3$]$_\infty^-$ chains in pseudo one-dimensional conducting salts of halogenated tetrathiafulvalenes. Inorg Chem 47:9979–9986
26. Rikken GLJA, Fölling J, Wyder P (2001) Electrical magnetochiral anisotropy. Phys Rev Lett 87:236602
27. De Martino A, Egger R, Tsvelik AM (2006) Nonlinear magnetotransport in interacting chiral nanotubes. Phys Rev Lett 97:076402
28. Krstic V, Rikken GLJA (2002) Magneto-chiral anisotropy of the free electron on a helix. Chem Phys Lett 364:51–56
29. Avarvari N, Wallis JD (2009) Strategies towards chiral molecular conductors. J Mater Chem 19:4061–4076
30. Griffiths JP, Nie H, Brown RJ, Day P, Wallis JD (2005) Synthetic strategies to chiral organosulfur donors related to bis(ethylenedithio)tetrathiafulvalene. Org Biomol Chem 3: 2155–2166
31. Galan-Mascaros J, Coronado E, Goddard PA, Singleton J, Coldea AI, Wallis JD, Coles SJ, Alberola A (2010) A chiral ferromagnetic molecular metal. J Am Chem Soc 132:9271–9273
32. Pop F, Auban-Senzier P, Canadell E, Rikken GLJA, Avarvari N (2014) Electrical magnetochiral anisotropy in a bulk chiral molecular conductor. Nat Commun 5(3757):1–6
33. Shin KS, Brezgunova M, Jeannin O, Roisnel T, Camerel F, Auban-Senzier P, Fourmigué M (2011) Strong iodine···oxygen interactions in molecular conductors incorporating sulfonate anions. Cryst Growth Des 11:5337–5345
34. Shin KS, Jeannin O, Brezgunova M, Dahaoui S, Aubert E, Espinosa E, Auban-Senzier P, Swietlik R, Frackowiak A, Fourmigué M (2014) Inter-layer charge disproportionation in the dual-layer organic metal (tTTF-I)$_2$$ClO_4$ with unsymmetrical I···O halogen bond interactions. Dalton Trans 43:5280–5291
35. Brezgunova M, Shin KS, Auban-Senzier P, Jeannin O, Fourmigué M (2010) Combining halogen bonding and chirality in a two-dimensional organic metal (EDT-TTF-I_2)$_2$(D-camphorsulfonate)·H_2O. Chem Commun 3926–3928
36. Lieffrig J, Le Pennec R, Jeannin O, Auban-Senzier P, Fourmigué M (2013) Toward chiral conductors: combining halogen bonding ability and chirality within a single tetrathiafulvalene molecule. CrystEngComm 15:4408–4412
37. Lieffrig J, Jeannin O, Auban-Senzier P, Fourmigué M (2012) Chiral conducting salts of nickel dithiolene complexes. Inorg Chem 51:7144–7152
38. Libri S, Jasim NA, Perutz RN, Brammer L (2008) Metal fluorides form strong hydrogen bonds and halogen bonds: measuring interaction enthalpies and entropies in solution. J Am Chem Soc 130:7842–7844
39. Mínguez Espallargas G, Brammer L, Allan DR, Pulham CR, Robertson N, Warren JE (2008) Noncovalent interactions under extreme conditions: high-pressure and low-temperature diffraction studies of the isostructural metal−organic networks (4-chloropyridinium)$_2$[CoX_4] (X=Cl, Br). J Am Chem Soc 130:9058–9071
40. Awwadi F, Haddad SF, Willett RD, Twamley B (2010) The analogy of C−Br···Br−C, C−Br···Br−Fe, and Fe−Br···Br−Fe contacts: crystal structures of (26DAPH)$FeBr_4$ and (26DA35DBPH)$_2$$FeBr_4$·Br. Cryst Growth Des 10:158–164
41. Derossi S, Brammer L, Hunter CA, Ward MD (2009) Halogen bonded supramolecular assemblies of [Ru(bipy)(CN)$_4$]$^{2-}$ anions and *N*-methyl-halopyridinium cations in the solid state and in solution. Inorg Chem 48:1666–1677

42. Ormond-Prout JE, Smart P, Brammer L (2012) Halogen bonded supramolecular assemblies of $[Ru(bipy)(CN)_4]^{2-}$ anions and *N*-methyl-halopyridinium cations in the solid state and in solution. Cryst Growth Des 12:205–216
43. Bertani R, Sgarbossa P, Venzo A, Lelj F, Amati M, Resnati G, Pilati T, Metrangolo P, Terraneo G (2010) Halogen bonding in metal–organic–supramolecular networks. Coord Chem Rev 254:677–695
44. Zordan F, Brammer L (2006) M−X···X′−C halogen-bonded network formation in MX_2(4-halopyridine)$_2$ complexes (M=Pd, Pt; X=Cl, I; X′=Cl, Br, I). Cryst Growth Des 6: 1374–1379
45. Mínguez Espallargas G, Hippler M, Florence AJ, Fernandes P, van de Streek J, Brunelli M, David WIF, Shamkland K, Brammer L (2007) Reversible gas uptake by a nonporous crystalline solid involving multiple changes in covalent bonding. J Am Chem Soc 129:15606–15614
46. Awwadi FF, Willett DD, Haddad SF, Twamley B (2006) The electrostatic nature of aryl−bromine−halide synthons: the role of aryl−bromine−halide synthons in the crystal structures of the *trans*-bis(2-bromopyridine)dihalocopper(II) and *trans*-bis(3-bromopyridine)dihalocopper (II) complexes. Cryst Growth Des 6:1833–1836
47. Awwadi FF, Haddad SF, Turnbull MM, Landee CP, Willett RD (2013) Copper–halide bonds as magnetic tunnels; structural, magnetic and theoretical studies of *trans*-bis (2,5-dibromopyridine)dihalo copper(II) and *trans*-bis(2-bromopyridine)dibromo copper(II). CrystEngComm 15:3111–3118
48. Herringer SN, Turnbull MM, Landee CP, Wikaira JL (2011) Copper(II) complexes of 2-halo-3-methylpyridine: synthesis, structure, and magnetic behaviour of Cu(2-X-3-CH_3py)$_2$X′$_2$ [X, X′=chlorine or bromine; py=pyridine]. Dalton Trans 40:4242–4252
49. Clemente-Juan JM, Coronado E, Minguez Espallargas G, Adams H, Brammer L (2010) Effects of halogen bonding in ferromagnetic chains based on Co(II) coordination polymers. CrystEngComm 12:2339–2342
50. Halcrow MA (2011) Structure:function relationships in molecular spin-crossover complexes. Chem Soc Rev 40:4119–4142
51. Gütlich P (1981) Spin-crossover materials: properties and applications. Struct Bond 44:83–195
52. Naik AD, Tinant B, Muffler K, Ja W, Schünemann V, Garcia Y (2009) Relevance of supramolecular interactions, texture and lattice occupancy in the designer iron(II) spin crossover complexes. J Solid State Chem 182:1365–1376
53. Cauliez P, Polo V, Roisnel T, Llusar R, Fourmigué M (2010) The thiocyanate anion as a polydentate halogen bond acceptor. CrystEngComm 12:558–566
54. Fukuroi K, Takahashi K, Mochida T, Sakurai T, Ohta H, Yamamoto T, Einaga Y, Mori H (2014) Synergistic spin transition between spin crossover and spin-Peierls-like singlet formation in the halogen-bonded molecular hybrid system: $[Fe(Iqsal)_2][Ni(dmit)_2]\cdot CH_3CN\cdot H_2O$. Angew Chem Int Ed 53:1983–1986
55. Nassirinia N, Amani S, Teat SJ, Roubeau O, Gamez P (2014) Enhancement of spin-crossover cooperativity mediated by lone pair–π interactions and halogen bonding. Chem Commun 50: 1003–1005
56. Cimino P, Pavone M, Barone V (2007) Halogen bonds between 2,2,6,6-tetramethylpiperidine-N-oxyl radical and C=HyFzI species: DFT calculations of physicochemical properties and comparison with hydrogen bonded adducts. J Phys Chem A 111:8482–8490
57. Zhao XR, Pang X, Yan XQ, Jin WJ (2013) Halogen bonding or hydrogen bonding between 2,2,6,6-tetramethylpiperidine-noxyl radical and trihalomethanes CHX_3(X=CI, Br, I). Chin J Chem Phys 26:172–180
58. Mugnaini V, Punta C, Liantonio R, Metrangolo P, Recupero F, Resnati G, Pedulli GF, Lucarini M (2006) Noncovalent paramagnetic complexes: detection of halogen bonding in solution by ESR spectroscopy. Tetrahedron Lett 47:3265–3269
59. Boubekeur K, Syssa-Magalé JL, Palvadeau P, Schöllhorn B (2006) Self-assembly of nitroxide radicals via halogen bonding directional NO· · ·I interactions. Tetrahedron Lett 47:1249–1252

60. Hanson GR, Jensen P, McMurtrie J, Rintoul L, Micallef AS (2009) Halogen bonding between an isoindoline nitroxide and 1,4-diiodotetrafluorobenzene: new tools and tectons for self-assembling organic spin systems. Chem Eur J 15:4156–4164
61. Davy KJP, McMurtrie J, Rintoul L, Bernhardt PV, Micallef AS (2011) Vapour phase assembly of a halogen bonded complex of an isoindoline nitroxide and 1,2-diiodotetrafluorobenzene. CrystEngComm 13:5062–5070
62. Pang X, Zhao XR, Wang H, Sun HL, Jin WJ (2013) Modulating crystal packing and magnetic properties of nitroxide free radicals by halogen bonding. Cryst Growth Des 13:3739–3745
63. Hosokoshi Y, Tamura M, Nozawa K, Suzuki S, Kinoshita M, Sawa H, Kato R (1995) Magnetic properties and crystal structures of 2-hydro and 2-halo nitronyl nitroxide radical crystals. Synth Met 71:1795–1796
64. Mínguez Espallargas G, Recuenco A, Romero FM, Brammer L, Libri S (2012) One-dimensional organization of free radicals via halogen bonding. CrystEngComm 14:6381–6383
65. Zordan F, Brammer L (2005) Supramolecular chemistry of halogens: complementary features of inorganic (M−X) and organic (C−X′) halogens applied to M−X···X′−C halogen bond formation. J Am Chem Soc 127:5979–5989
66. Mínguez Espallargas G, Brammer L, Sherwood P (2006) Designing intermolecular interactions between halogenated peripheries of inorganic and organic molecules: electrostatically directed M–X···X′–C halogen bonds. Angew Chem Int Ed 45:435–440
67. Brammer L, Minguez Espallargas G, Libri S (2008) Combining metals with halogen bonds. CrystEngComm 10:1712–1727
68. Ormond-Prout JE, Smart P, Brammer L (2012) Cyanometallates as halogen bond acceptors. Cryst Growth Des 12:205–216
69. Nishijo J, Miyazaki A, Enoki T, Watanabe R, Kuwatani Y, Iyoda M (2005) *d*-Electron-induced negative magnetoresistance of a π−d interaction system based on a brominated-TTF donor. Inorg Chem 44:2493–2506
70. Shirahata T, Kibune M, Maesato M, Kawashima T, Saito G, Imakubo T (2006) New organic conductors based on dibromo- and diiodo-TSeFs with magnetic and non-magnetic MX_4 counter anions (M=Fe, Ga; X=Cl, Br). J Mater Chem 16:3381–3390
71. Thoyon D, Okabe K, Imakubo T, Golhen S, Miyazaki A, Enoki T, Ouahab L (2002) Conducting materials containing paramagnetic hexacyanometallate $[Cr(CN)_6]^{3-}$ and iodine substituted organic donor [DIETS]. Mol Cryst Liq Cryst 376:25–32
72. Nishijo J, Ogura E, Yamaura J, Miyazaki A, Enoki T, Takano T, Kuwatani Y, Iyoda M (2000) Molecular metals with ferromagnetic interaction between localized magnetic moments. Solid State Commun 116:661–664
73. Devic T, Domercq B, Auban-Senzier P, Molinié P, Fourmigué M (2002) Cyano-halogen interactions in $[EDT\text{-}TTF\text{-}I]_2[Ni(mnt)_2]$ and $[EDT\text{-}TTF\text{-}I_2]_2[Ni(mnt)_2]$ and geometrical evolutions within mixed-valence or fully oxidized TTF dyads. Eur J Inorg Chem 2002:2844–2849
74. Imakubo T, Sawa H, Kato R (1995) Synthesis and crystal structure of the molecular metal based on iodine-bonded π-donor, $(IEDT)[Pd(dmit)_2]$. Chem Commun 1097–1098
75. Kato R (2014) Development of π-electron systems based on $[M(dmit)_2]$ (M=Ni and Pd); dmit: 1,3-dithiole-2-thione-4,5-dithiolate) anion radicals. Bull Chem Soc Jpn 87:355–374
76. Kosaka Y, Yamamoto HM, Nakao A, Tamura M, Kato R (2007) Coexistence of conducting and magnetic electrons based on molecular π-electrons in the supramolecular conductor $(Me\text{-}3,5\text{-}DIP)[Ni(dmit)_2]_2$. J Am Chem Soc 129:3054–3055
77. Fujiyama S, Shitade A, Kanoda K, Kosaka Y, Yamamoto HM, Kato R (2008) Suppression of electronic susceptibility in metal–Mott-insulator alternating material $(Me\text{-}3,5\text{-}DIP)[Ni(dmit)_2]_2$ observed using C^{13} NMR. Phys Rev B 77:060403(R)
78. Hazama K, Uji S, Takahide Y, Kimata M, Satsukawa H, Harada A, Terashima T, Kosaka Y, Yamamoto HM, Kato R (2011) Fermi surface and interlayer transport in the two-dimensional magnetic organic conductor $(Me\text{-}3,5\text{-}DIP)[Ni(dmit)_2]_2$. Phys Rev B 83:165129

79. Kosaka Y, Yamamoto HM, Tajima A, Nakao A, Cui H, Kato R (2013) Supramolecular Ni $(dmit)_2$ salts with halopyridinium cations-development of multifunctional molecular conductors with the use of competing supramolecular interactions. CrystEngComm 15:3200–3211
80. Kusamoto T, Yamamoto HM, Tajima N, Oshima Y, Yamashita S, Kato R (2012) Bilayer Mott system based on $Ni(dmit)_2$ (dmit =1,3-dithiole-2-thione-4,5-dithiolate) anion radicals: two isostructural salts exhibit contrasting magnetic behavior. Inorg Chem 51:11645–11654
81. Kusamoto T, Yamamoto HM, Kato R (2013) Utilization of σ-holes on sulfur and halogen atoms for supramolecular cation···anion interactions in bilayer $Ni(dmit)_2$ anion radical salts. Cryst Growth Des 13:4533–4541
82. Allen FH, Goud BS, Hoy VJ, Howard JAK, Desiraju GR (1994) Molecular recognition via iodo···nitro and iodo···cyano interactions: crystal structures of the 1:1 complexes of 1,4-diiodobenzene with 1,4-dinitrobenzene and 7,7,8,8-tetracyanoquinodimethane (TCNQ). Chem Commun 2729–2730
83. Chen Y-C, Wang P-F, Liu G-X, Xu H, Ren X-M, Song Y, Ni Z-P (2008) Organic radical molecular solids based on $[(TCNQ)_n]^-$ (n = 1 or 2): syntheses, crystal structures, magnetic properties and DFT analyses. J Phys Chem Solids 69:2445–2452
84. Liu G-X, Huang R-Y, Ren X-M (2008) Four novel ion-pair compounds consisting of 7,7,8,8-tetracyanoquinodimethane (TCNQ) radical: syntheses, crystal structures and properties. J Mol Struct 891:11–18
85. Iyoda M, Kuwatani Y, Ogura E, Hara K, Suzuki H, Takano T, Takeda K, Takano J, Ugawa K, Yoshida M, Matsuyama H, Nishikawa H, Ikemoto I, Kato T, Yoneyama N, Nishijo J, Miyazaki A, Enoki T (2001) Syntheses, structure and conducting properties of halogenated ethylene-dioxytetrathiafulvalenes. Heterocycles 54:833–848
86. Lieffrig J, Jeannin O, Guizouarn T, Pascale Auban-Senzier P, Fourmigué M (2012) Competition between the C−H···N hydrogen bond and C−I···N halogen bond in $TCNQF_n$ (n = 0, 2, 4) salts with variable charge transfer. Cryst Growth Des 12:4248–4257
87. Lieffrig J, Jeannin O, Frackowiak A, Olejniczak I, Swietlik R, Dahaoui S, Aubert E, Espinosa E, Auban-Senzier P, Fourmigué M (2013) Charge-assisted halogen bonding: donor–acceptor complexes with variable ionicity. Chem Eur J 19:14804–14813
88. Lieffrig J, Jeannin O, Vacher A, Lorcy D, Auban-Senzier P, Fourmigué M (2014) C–I···NC halogen bonding in two polymorphs of the mixed-valence 2:1 charge-transfer salt $(EDT\text{-}TTF\text{-}I_2)_2(TCNQF_4)$, with segregated versus alternated stacks. Acta Cryst B70:141–148

Top Curr Chem (2015) 359: 115–146
DOI: 10.1007/128_2014_614

Published online: 28 April 2015

Halogen Bonding in the Design of Organic Phosphors

Xue Pang and Wei Jun Jin

Abstract Halogen bonding as a new strategy for introducing heavy atom perturbers in defined stoichiometry in the design of organic phosphors is reviewed. Considering ten novel cocrystals assembled by polyaromatic hydrocarbons (PAHs) and their heterocyclic analogues and haloperfluorobenzenes using the new strategy, apart from biphenyl cocrystals they all phosphoresce strongly, showing that the new methodology can induce phosphorescence by a heavy atom effect. More interesting, the phosphorescence properties, including excitation/emission wavelengths and decay dynamics, show dependence on the structure of the PAHs and interaction patterns, which is very important and valuable in modulation of the expected colors of luminescent materials.

Keywords Cocrystallization • Halogen bonding • Haloperfluorobenzenes • Phosphorescence • Polycyclic aromatic hydrocarbons

Contents

X. Pang and W.J. Jin (✉)
College of Chemistry, Beijing Normal University, Beijing 100875, P. R. China
e-mail: wjjin@bnu.edu.cn

Abbreviations

1,2-DITFB	1,2-Diiodotetrafluorobenzene
1,4-DBrTFB	1,4-Dibromotetrafluorobenzene
1,4-DITFB	1,4-Diiodotetrafluorobenzene
Bp	Biphenyl
Cz	Carbazole
Dbf	Dibenzofuran
Dbt	Dibenzothiophene
Flu	Fluorene
Nap	Naphthalene
PAHs	Polycyclic aromatic hydrocarbons
Phe	Phenanthrene
Pyr	Pyrene

1 Introduction

Phosphorescence of organic molecules can be defined as the radiative transition originating from the lowest excited triplet state, T_1, to the singlet ground state, S_0. Different from fluorescence, which is the radiative transition from the first excited singlet S_1 to singlet ground state S_0, phosphorescence is a spin-forbidden process and usually the S_1 and T_1 states are widely separated and more easily quenched, especially by dioxygen molecules with triplet ground states, which makes phosphorescence more difficult to obtain than fluorescence. However, phosphorescent materials have attracted more and more attention, especially in the field of organic electronics because of higher internal quantum efficiency by recombination of both singlet and triplet excitons [1, 2]. Until now, the most widely used method to induce phosphorescence is taking advantage of the heavy atom effect which works by enhancing spin-orbit coupling to promote the S_1–T_1 intersystem crossing rate and finally inducing a phosphorescent emission. In the field of organic phosphors, the heavy atom effect can be divided into three kinds of patterns: intrinsic heavy atom effect, extrinsic heavy atom effect, and complexation or coordination heavy atom effect. Halogen atoms, as substituent groups in organic compounds, can directly affect intersystem crossing rate, which is the intrinsic heavy atom effect. The extrinsic heavy atom effect is a pure physically spin-orbital coupling occurring in a simple mixture of metal cations or iodide anions and organic molecules with uncertain stoichiometry in solution/vitreous media, on solid supports, or in cyclodextrin inclusion complexes of halogenated alkanes with organic molecule [3]. When metal ions coordinate luminescent organic ligands, the extrinsic heavy atom effect may become more efficient, e.g., when Ag(I) interacts with polyaromatic hydrocarbons by Ag-π complexation or Hg(II) with *N*-heterocyclic aromatic hydrocarbons by Hg–N bonding [4, 5]. Metal ions can sometimes act as intrinsic or a special heavy atom effect between extrinsic and intrinsic by

complexation or coordination with phosphor as chelator with exact stoichiometry, corresponding to directly or indirectly acting on a luminescent central group of organic molecules [6–8].

In this chapter, a new design strategy – halogen bonding – for introducing metal-free heavy atom perturbers in organic phosphors in defined stoichiometry is reviewed.

2 New Strategy of Introducing Metal-Free Heavy Atom Perturber by Halogen Bonding in Defined Stoichiometry

2.1 Halogen Bonding Acceptors as Phosphors

Polycyclic aromatic hydrocarbons (PAHs) are divided into biphenyls and acenes, phenes, starphenes, pyrenes, etc., depending on the arrangement mode of their benzene rings. Usually, the phenyls in biphenyls are connected by rotatable C–C single bond/s which can result in non-radiative loss of excitation energy, so they are rarely used as luminophors. Thanks to the rigid planar structure and large π-conjugated chromophores, PAHs and their derivatives, as well as heterocyclic compounds, provide a unique luminescent character and have been widely used in bio/chemoanalysis [9, 10] and organic light-emitting diodes (OLEDs) [11]. However, most applications of PAHs were based on fluorescence rather than phosphorescence. Besides the difficulty in obtaining phosphorescence, the quenching of luminescence of the emitters caused by the formation of excimers or ground state aggregates is another great obstacle limiting the application of PAHs luminescence, including both fluorescence and phosphorescence, in solid/film state or crystal materials. It is important to develop a method by which the phosphorescence of PAHs/heterocyclic compounds in the solid state can be not only effectively induced but also partly modulated, at the same time avoiding all kinds of quenching effects. The halogen bond [12] between different donors and PAHs/heterocyclic compounds possessing the planar large π-electron conjugation system as typical π-type acceptors can take on these tasks. Up to now, some excellent exploratory work has been reported [13, 14].

2.2 Donors as Heavy Atom Perturbing Sources

The halogen substituent in perfluorinated haloalkanes can more easily form halogen bond because of the strong electron-withdrawing character of fluorine resulting in more positive σ-hole [15] and π-hole [16], as shown in Fig. 1. It is amazing that the halogen bonding donor can act as a heavy atom perturbation agent for inducing phosphorescence of organic phosphors by enhanced spin-orbital coupling. Halogen

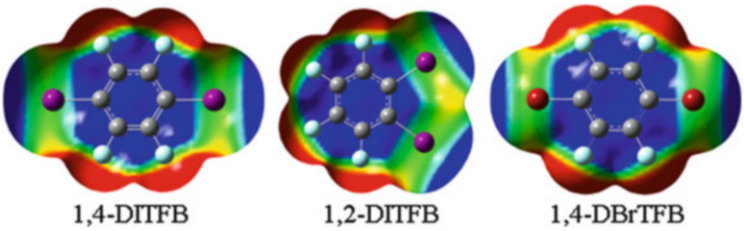

Fig. 1 Electrostatic potential surface of some donor molecules cited in the chapter: 1,4-DITFB: $V_{s,\,max} = 67.0$ kJ/mol (π-hole); $V_{s,\,max} = 146.4$ kJ/mol (σ-hole); 1,2-DITFB: $V_{s,\,max} = 46.5$ kJ/mol (π-hole); $V_{s,\,max} = 130.0$ kJ/mol (σ-hole); 1,4-DBrTFB: $V_{s,\,max} = 73.2$ kJ/mol (π-hole); $V_{s,\,max} = 113.6$ kJ/mol (σ-hole)

bonding, as a new strategy for introducing heavy atom perturbers can therefore be used to assemble phosphorescence-functionalized cocrystals [17].

2.3 Advantages of Halogen Bonding

Halogen bonding, as a new strategy for introducing heavy atom perturbers, really has some advantages. Two important components considered in assembling phosphorescent materials are phosphors with rigid planar π-conjugated systems (XB acceptors) and those with efficient solid emission-inducing agents (XB donors). Usually they are held together primarily by halogen bonding, with additional assisting intermolecular interactions on some occasions. The solid emission-inducing agent plays a key role in the process of turning on the phosphorescence of chromophores and might have multiple functions: acting as a cement to link the emitters together in certain arranged modes, acting as "solid dilution agent" to protect the emitter from self-quenching, serving as a heavy atom perturber in defined stoichiometry to induce strong phosphorescence by enhanced spin-orbital coupling, and acting as possible dopant source to activate the photo- or photoelectronic behavior of the materials.

3 Phosphorescent Cocrystals Assembled by the New Strategy

3.1 Structural Features of Cocrystals

By using co-crystallization via halogen bonding and other assisting interactions, ten cocrystals between PAHs and their heterocyclic analogues and haloperfluorobenzenes were successfully assembled. The structures and cocrystal components are shown in Scheme 1 and Table 1.

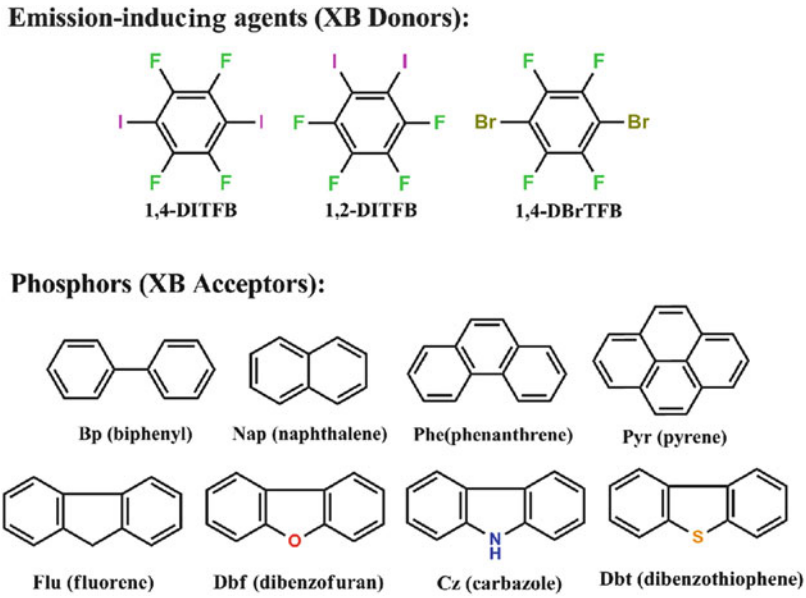

Scheme 1 Structures of emission-inducing agents (XB donors) and phosphors (XB acceptors)

Table 1 Components of cocrystals **1**–**10**

Components	Cocryst. **1** [18]	Cocryst. **2** [18]	Cocryst. **3** [18]
	Bp · $(1,4\text{-DITFB})_2$	Nap · $(1,4\text{-DITFB})_2$	Phe · $(1,4\text{-DITFB})_2$
Components	Cocryst. **4** [19]	Cocryst. **5** [19]	Cocryst. **6** [16]
	Pyr · 1,4-DITFB	Pyr · $(1,2\text{-DITFB})_2$	$(Phe)_3 \cdot (1,4\text{-DBrTFB})_2$
Components	Cocryst. **7** [20]	Cocryst. **8** [20]	Cocryst. **9** [21]
	Flu · 1,4-DITFB	Dbf · 1,4-DITFB	Cz · $(1,4\text{-DITFB})_2$
Components	Cocryst. **10** [20]		
	Dbt · $(1,4\text{-DITFB})_2$		

3.1.1 Cocrystals by PAHs and Haloperfluorobenzenes

In cocrystals **1**, **2**, and **3**, the main driving forces were all C–I···π halogen bonds assisted by other weak interactions, as shown in Fig. 2. The stoichiometry of PAH to 1,4-DITFB in all three cocrystals is 1:2. Each iodine atom in the donor 1,4-DITFB molecule connects with PAH by C–I···π contacts and each side of the PAH molecular plane connects to two 1,4-DITFB molecules. In **2** and **3**, both Nap and Phe are bridged by 1,4-DITFB to form a 1D infinite chain structure. Unlike **2** and **3**, a rhombic structure was formed in **1**, caused by the rotation of the C–C single bond in the Bp molecule. Additionally, other weak interactions, such as the C–F···F–C contact, π–π stacking and C–H···I hydrogen bonding, exist between the layers and chains in these cocrystals to maintain the stability of the supramolecular structures.

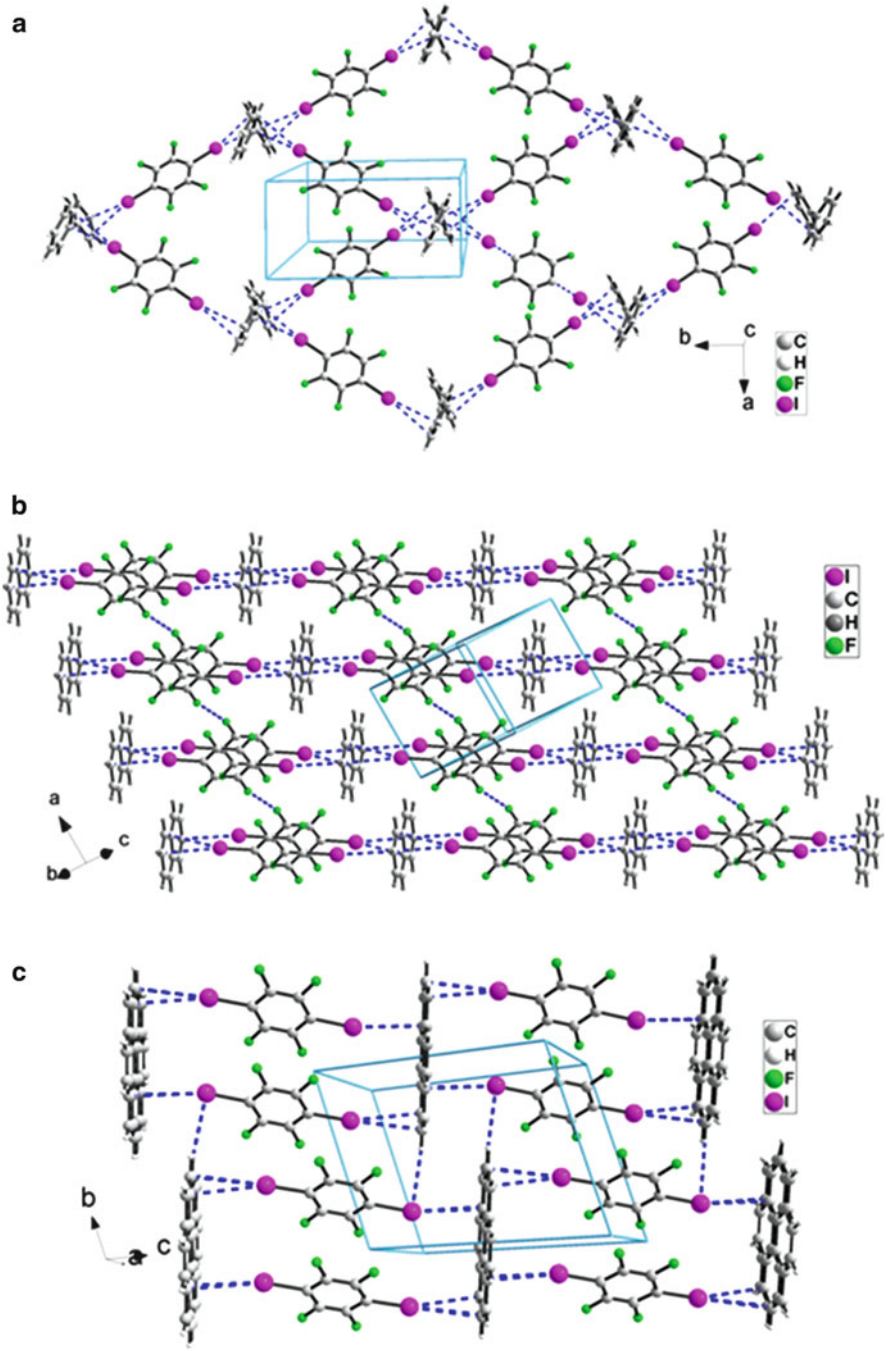

Fig. 2 Structures of cocrystals **1** (**a**), **2** (**b**), and **3** (**c**)

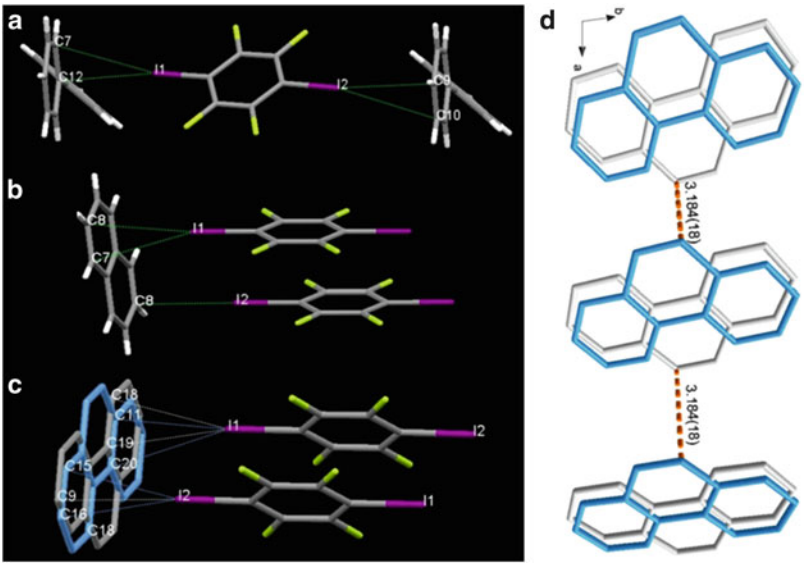

Fig. 3 C–I···π interactions in cocrystals **1** (**a**), **2** (**b**), and **3** (**c**) and edge-to-edge π–π interaction between Phe rings in cocrystal **3** (**d**)

The C–I···π halogen bonds extracted from the three cocrystals are shown in Fig. 3 and the bonding angles and contact distances are listed in Table 2. It can be seen that all iodine atoms in the three cocrystals interact with PAHs along the C–I bond axis extension and preferentially select the vertical direction to the PAH plane to interact with the conjugated π-electrons distributed on the two sides of the PAHs planar molecules. The angle ∠C–I···π ranges from 73° to 80°, and the bonding angle ∠C–I···C′ changes in the range 160–175° close to 180°. These are typical geometrical features of π-type halogen bonding. In terms of contact distances, the length between the iodine atom and multi C atoms in PAH molecule changes from 3.434 Å to 3.566 Å, being less than the sum of their van der Waals (vdW) radii (3.68 Å) [22]. The difference in contact distances can be attributed to different structure of PAHs. Unlike **1** and **2**, **3** possesses a disordered structure because two orientation of Phe ring along its short axis are unresolved at each site of crystal cell (Fig. 3c). Compared with Nap and Bp, Phe lacks a symmetry center and its highly delocalized distribution of π-electrons makes each carbon atom a possible interacting site for the I atom. So both orientations of Phe in **3** are equally probable. An edge-to-edge type π–π stacking was also observed in cocrystal **3** between different Phe rings, as shown in Fig. 3d. The edge-to-edge π–π stacking between 1,4-DITFBs may solely contribute to the maintenance of a tenuous balance of 3D structure, but the edge-to-edge π–π stacking between Phe rings should contribute to another important aspect, *i.e.*, the possible modulation of Phe luminescing behavior.

Table 2 Geometrical parameters of C–I···π interactions in **1**, **2**, and **3**

Cocrystal	Interactions	$d_{C–I···C'}$/Å	∠C–I···C/°	∠C–I···π
1	C1I1···C7	3.649 (6)	163.4 (2)	73.1 (2)
	C1I1···C12	3.618 (5)	172.0 (2)	
	C4I2···C9	3.566 (8)	172.5 (2)	73.8 (2)
	C4I2···C10	3.635 (8)	162.0 (2)	
2	C1I1···C7	3.553 (7)	159.4 (2)	75.1 (2)
	C1I1···C8	3.506 (6)	169.7 (2)	
	C4I2···C8	3.474 (6)	163.7 (2)	74.9 (2)
3 (a)[a]	C1I1···C11	3.434 (11)	167.1 (2)	79.0 (3)
	C1I1···C20	3.630 (13)	159.7 (2)	
	C4I2···C15	3.530 (12)	163.0 (3)	80.6 (3)
	C4I2···C16	3.515 (15)	166.9 (3)	
3 (b)[a]	C1I1···C18	3.547 (12)	164.1 (2)	79.0 (3)
	C1I1···C19	3.538 (9)	169.5 (2)	
	C4I2···C9	3.501 (14)	174.9 (3)	80.6 (3)

[a](a) and (b) indicate C–I···π interactions originated from two Phe molecules with different orientation in the disordered cocrystal **3**

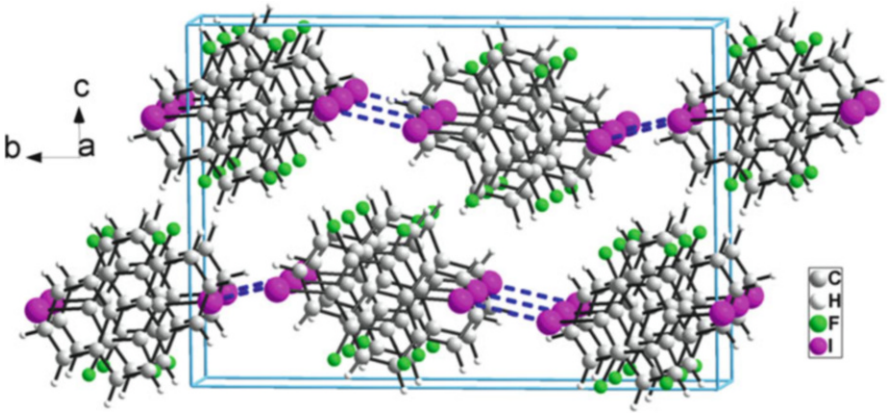

Fig. 4 Structure of cocrystal **4**

Unlike cocrystals **1**, **2**, and **3**, column-like structures are formed via the π-hole···π bond between 1,4-DITFB and pyrene in cocrystal **4** instead of C–I···π interactions observed in **1**, **2**, and **3**, as shown in Fig. 4. One pyrene and one 1,4-DITFB molecule are alternately stacked (A···B···A···B···) together in a face-to-face style with interplanar distances of 3.395 Å and a tilted angle of 4.5°. The parallel columns in the cocrystal are further linked together by C–I···π, C–I···I–C, and C–H···F interactions to form the 3D architecture, the geometrical parameters of which are summarized in Table 3.

Table 3 Interaction patterns and geometrical parameters in cocrystals **4**, **5**, and **6**

	Interactions	*d*/Å	*θ*/°
Cocrystal **4**	π-hole···π (1,4-DITFB···pyrene)	3.395 (6)	4.5 (2)[a]
	C–I···I	3.807 (1)	167.1 (1), 115.2 (1)
	C–I···π	3.469 (1)	165.8 (1)
	C–H···F	2.567 (2)	144.6 (1)
Cocrystal **5**	π-hole···π (1,2-DITFB···pyrene)	3.492 (7)	5.6 (6)[a]
	π–π (1,2-DITFB···1,2-DITFB)	3.654 (7)	0.0 (5)[a]
	C–I···I	4.059 (2)	150.6 (1), 116.0 (1)
	C–H···F	2.602 (2)	153.2 (1)
Cocrystal **6**	π-hole···π (1,4-DBrTFB-Phe)	3.303 (3)	1.7 (1)[a]
	π–π (Phe–Phe)	3.345 (9)	0.7 (3)[a]
	C–Br···π (To Phe-C/Phe plane)	3.314 (1)	156.4 (1)/61.6 (2)
	C–H···π	2.805 (1), 2.740 (1)	149.5 (3), 146.5 (3)
	C–H···F	2.661 (2), 2.629 (2)	131.1 (2), 173.2 (2)
	C–H···Br	2.988 (1)	145.9 (2)

[a]Tilted angle for π-hole···π or π–π interaction

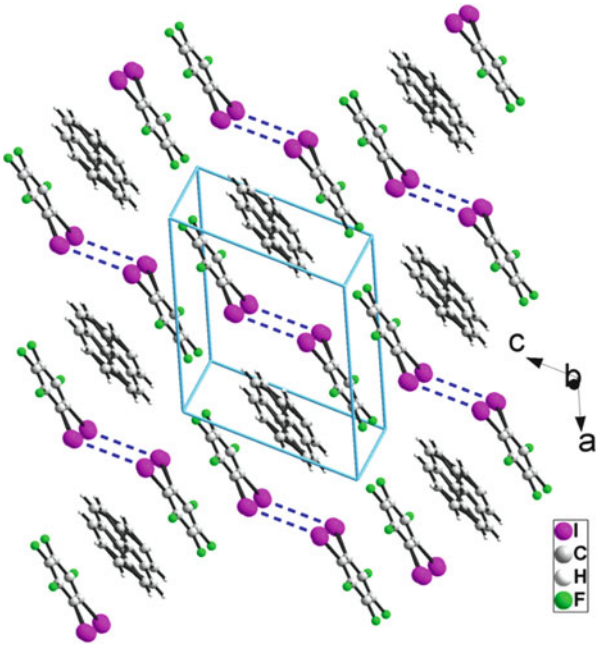

Fig. 5 Structure of cocrystal **5**

Besides 1,4-DITFB, other similar XB donors such as 1,2-DITFB and 1,4-DBrTFB can also act as efficient emission-inducing agents. Unfortunately, only two cocrystals, **5** and **6**, were obtained here. For **5**, a column-like architecture similar to **4** was observed, as shown in Fig. 5, although the mode of π-hole···π bonding was

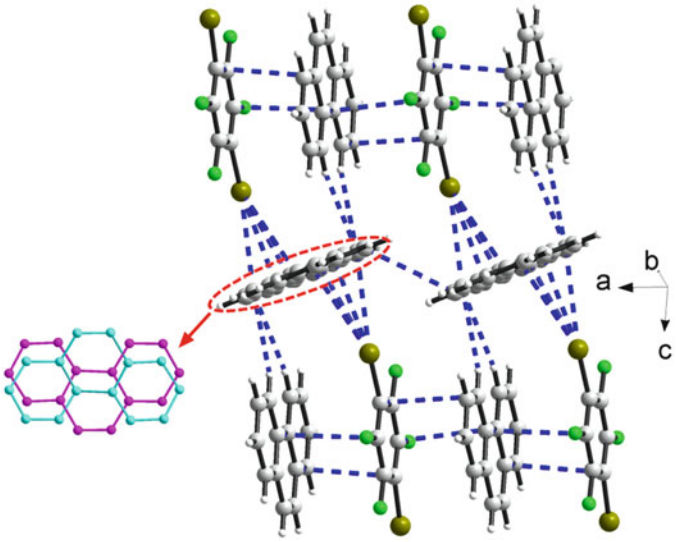

Fig. 6 Structure of cocrystal **6**

different from **4**. Each packing unit comprised two 1,2-DITFB molecules in a "head-to-tail" fashion and one pyrene molecule, resulting in an A···B···B···A···B···B··· array with interplanar distances of 3.492 Å and a tilted dihedral angle of 5.6° between pyrene molecule and 1,2-DITFB, and interplanar distances of 3.654 Å between two parallel 1,2-DITFB molecules. In **5**, both the interplanar distance and tilted angle between pyrene and 1,2-DITFB were greater than that of pyrene and 1,4-DITFB, because the two iodine atoms were *ortho*-positioned in 1,2-DITFB instead of being *para*-positioned as in 1,4-DITFB. Weak C–I···I and C–H···F interactions also existed to maintain the 3D structure (Table 3).

In cocrystal **6**, an infinite column-like structure is also formed via a π-hole···π bond between 1,4-DBrTFB and Phe, similar to the structure of Pyr with 1,4-DITFB, as shown in Fig. 6. In one column, one Phe and one 1,4-DBrTFB molecule are alternately stacked together in a face-to-face style (A···B···A···B···), with an inter-planar vertical distance of 3.303(3) Å and a tilted angle of 1.7°. However, the interaction mode between the parallel placed columns differ sharply from the cocrystal of Pyr with 1,4-DITFB, which are linked together by C–Br···π halogen bonding and C–H···π hydrogen bonding between one column and a Phe molecule located in inter-column (Fig. 6). It is also interesting to note that the structure of inter-columnar Phe molecules is disordered and are connected to each other by an edge-to-edge π–π interaction with almost parallel planes (tilted angle only 0.7°). This should be regarded as a transmolecular π–π conjugation[1] [23–26] which can

[1] The similar terms in molecular spectroscopy are transannular conjugation or transannular charge transfer. See [23–26].

reduce the triplet energy of Phe. Thus, Phe exists in the cocrystal as two states: an isolated state with π-hole···π bonding between the 1,4-DBrTFB and Phe molecules in the columns and a delocalized state for Phe molecules located at inter-column positions, which may be significant in the modulation of luminescent behavior. In addition, the C–H···Br and C–H···F contacts of intercolumn molecules should be assigned to the weak hydrogen bonding by which the 2D network was linked together, giving rise to the 3D supramolecular architecture.

It can be seen that the interaction modes in the PAHs/haloperfluorobenzenes cocrystals show a striking difference, which can be ascribed to two major factors. The preliminary discussion is summarized as follows, based on the limited experiments herein.

On one hand, the structures of both XB donors and acceptors/PAHs have a remarkable effect on the interaction pattern of haloperfluorobenzenes with PAHs. PAHs with smaller conjugation systems (such as torsional Bp, linear Nap, and bent Phe) easily form cocrystals with 1,4-DITFB by C–I···π halogen bonding. These PAHs have relatively higher localized π-density in their smaller delocalization systems. Larger PAHs with larger 2D planes, such as pyrenes, are apt to be arranged by π–π stacking between themselves or by π-hole···π bonding between Pyr and haloperfluorobenzenes. However, for linear anthracene, π-electrons are easily mobile through the benzene rings and the attempt to obtain the cocrystals was not successful. In contrast, a single crystal of anthracene is easily obtained, in which C–H···π interaction is found to lead to a herringboned assignment along the short axis of anthracene, while the π–π stacking between anthracenes or C–I···π interaction between anthracene and DITFB does not occur. In other words, linear acenes do not easily form cocrystals by C–I···π interaction between DITFB and acenes, except for smaller Nap. Additionally, based on molecular orbital theory, anthracenes or pyrenes with larger delocalization π-conjugation systems have low energy levels which are separated by a large gap to/from the σ* orbital of the C–I bond. This may be another important factor affecting C–I···π interaction between DITFB and PAHs.

On the other hand, the competition between C–I···π halogen bonding and π-hole···π bonds also has a strong impact on the structural properties of the cocrystals reported herein. Apparently, the structure of the cocrystal assembled by 1,4-DBrTFB and Phe is distinctly different from that formed by 1,4-DITFB and Phe, in which there is no π–π stacking or π-hole···π bonding between 1,4-DITFB and Phe. The structural difference can be ascribed to the competition between π-hole···π bonding and halogen or hydrogen bonds, which is proved by the calculated results based on the interaction units extracted from single cocrystal structure data, as shown in Fig. 7. In the Phe/1,4-DBrTFB cocrystal, the BSSE-corrected energies of π-hole···π (DBrTFB-Phe) and C–Br···π interactions are −12.1 and −4.26 kcal mol^{-1}, respectively. It is probable that the π-hole···π bonding (DBrTFB-Phe) is more competitive here than the C–Br···π halogen bonding, or even than two C–Br···π halogen bonding types in combination. However, in the Phe/1,4-DITFB cocrystal, the C–I···π energy (−5.73 kcal mol^{-1})

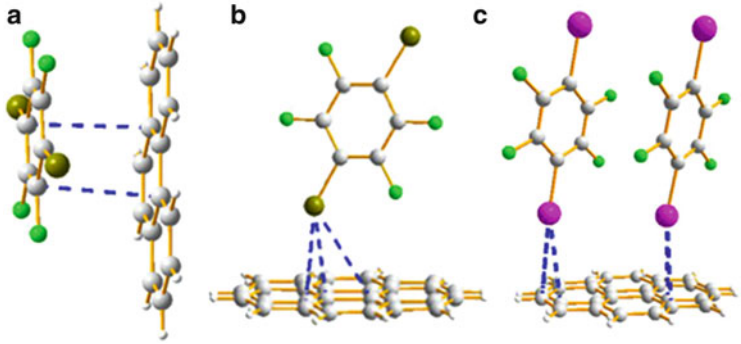

Fig. 7 Interaction units extracted from single cocrystal structure data: (**a**) π-hole···π bonding in Phe/1,4-DBrTFB cocrystal; (**b**) C–Br···π halogen bonding in Phe/1,4-DBrTFB cocrystal; (**c**) C–I···π halogen bonding in Phe/1,4-DITFB cocrystal

is stronger than C–Br···π. Thus, in consideration of the synergistic effect from two C–I···π halogen bonds, the C–I···π halogen bonding may be more competitive and possess a dominant position in the Phe-1,4-DITFB cocrystal.

3.1.2 Cocrystals by Fluorene and Its Heterocyclic Analogues and Haloperfluorobenzenes

Fluorene and its heterocyclic analogues, such as carbazole, dibenzofuran, and dibenzothiophene, *etc*., have peculiar extensive π-conjugation electronic structures and highly emissive electron-conducting properties, which make them also promising candidates for the investigated systems. In this section, fluorene (Flu), dibenzofuran (Dbf), carbazole (Cz), and dibenzothiophene (Dbt) were selected to assemble cocrystals with 1,4-DITFB. XRD analysis revealed a 1:1 stoichiometry for both **7** (fluorene/1,4-DITFB) and **8** (dibenzofuran/1,4-DITFB) and a 1:2 stoichiometry for **9** (carbazole/1,4-DITFB) and **10** (dibenzothiophene/1,4-DITFB). Multiple interesting intermolecular interactions, including C–I···π halogen bonding, C–H···π, C–H···I, C–H···F hydrogen bonding, and F···F, S···S interactions, are observed in these cocrystals, and the main bonding parameters are summarized in Table 4.

For cocrystals **7** and **8**, the infinite zigzag chain is constructed by C–I···π halogen bonding in an over-the-bond pattern of the I atom to the π-system (expressed in red and blue in Figs. 8 and 9, respectively). In **7** the resulting I···C distances are 3.409 and 3.534 Å with ∠C–I···C bonding angles of 171.3° and 164.3°, respectively. No obvious differences in distances and angles were observed in **8**, the resulting I···C distances are 3.434 and 3.517 Å, or 3.546 and 3.390 Å with ∠C–I···C bonding angles of 176.9° and 156.8°, or 166.8° and 167.8°, respectively.

Table 4 Bonding properties and geometrical parameters of cocrystals **7**, **8**, **9**, and **10**

	Interactions	d/Å	θ/°
Cocrystal **7**	C–I···5C	3.409 (10)	171.3 (0)
	C–I···6C	3.534 (0)	164.3 (0)
	C–H···6C	2.707 (1)	142.4 (0)
	C–H···7C	2.837 (0)	135.1 (1)
Cocrystal **8**	C–I···6C	3.434 (1)	176.9 (0)
	C–I···7C	3.517 (1)	156.8 (1)
	C–I···12C	3.546 (1)	166.8 (1)
	C–I···13C	3.390 (1)	167.8 (1)
	C–H···I	3.080 (0)	170.4 (1)
	C–H···F	2.506 (1)	160.5 (0)
Cocrystal **9**	C–I···12C	3.460 (1)	175.2 (1)
	C–I···5C	3.561 (1)	159.1 (1)
	C–I···2C	3.449 (0)	165.2 (0)
	C–I···3C	3.479 (1)	165.9 (0)
	C–H···I	3.132 (1)	170.1 (0)
	C···C ($\pi\cdots\pi$)	3.389 (5)	93.9 (0)
	F···F	2.586 (0)	168.3 (0)
	C–H···F	2.657 (1)	150.2 (1)
Cocrystal **10**	C–I···9C	3.502 (1)	168.8 (0)
	C–I···10C	3.596 (1)	162.3 (1)
	C–I···13C	3.556 (1)	172.6 (0)
	C–I···14C	3.607 (1)	160.4 (0)
	C–I···7C	3.411 (1)	170.6 (1)
	C–I···8C	3.655 (2)	148.3 (1)
	C–I···12C	3.613 (1)	159.5 (2)
	C–I···16C	3.487 (1)	170.4 (0)
	C–I···17C	3.536 (37)	158.8 (5)
	C–F···F–C	2.669 (1)	167.0 (1)
	S···S-plane	3.465 (1)	

However, in **7**, the unsolvable orientation of dibenzofuran molecules along their short axis in the cocrystal results in a disorder structure, which is not observed in **8**. The adjacent zigzag chains were further united by C–H···π interaction in **7** and C–H···I, C–H···F contacts in **8**, which should contribute to maintain the stability of the 3D structure of the cocrystals.

Unlike cocrystals **7** and **8**, the column-like infinite chains in **9** and **10** are constructed by C–I···π halogen bonding (Figs. 10 and 11). In the chain of cocrystal **9**, an A···2D···A···2D··· arrangement was formed, where A and D stand for halogen bonding acceptor (carbazole) and donor (1,4-DITFB), respectively. The geometrical parameters of the cocrystal are listed in Table 4. The distance $d_{\mathrm{I}\cdots\pi}$ is 3.460, 3.561, 3.449, or 3.479 Å, iodine to 12C, 5C, 2C, or 3C atom on carbazole,

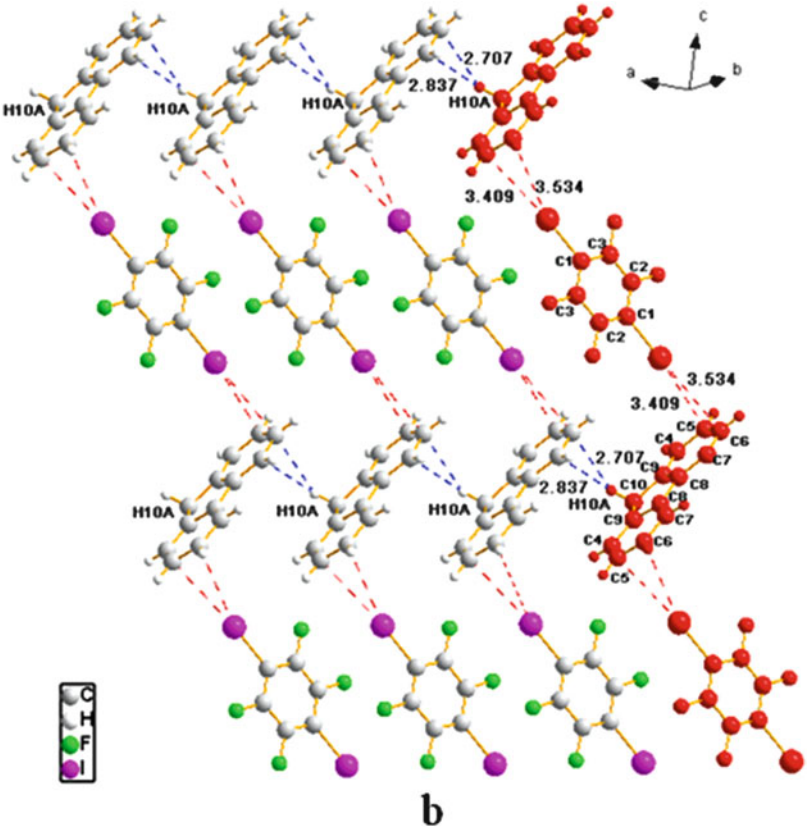

Fig. 8 Infinite zigzag chain stacking structures of cocrystal **7** (halogen bonded infinite chains are shown in *red*)

respectively. The angles C–I···π are in the range 159–175°. The bonding direction and bonding angle are in agreement with halogen···π interaction [27, 28] and that predicted by σ-hole [15]. Between two different 1,4-DITFB molecules, an edge-to-edge π–π stacking analogous to J-aggregation was observed, which stabilized the 1D infinite chain. The π–π distance from the edge of one 1,4-DITFB to the edge of another is 3.389 Å (while the centroid–centroid distance between 1,4-DITFB ring is 4.49 Å, the angle is 77°). These distances are less than the sum of their van der Waals radii (Bondi radii, I = 1.98 Å; Pauling radii, I = 2.15 Å; half of the aromatic ring thickness 1.85 Å) [22, 29]. It can also be seen that the parallel placed columns in cocrystal **9** are further linked together by C–H···I, C–H···F hydrogen bonding, and finally formed the 3D architecture. Thus the iodine atom acts simultaneously as an XB donor (in C–I···π) and a hydrogen bond acceptor (in C–H···I). Such cooperative character of the iodine atom is well studied [30–32]. So it might be

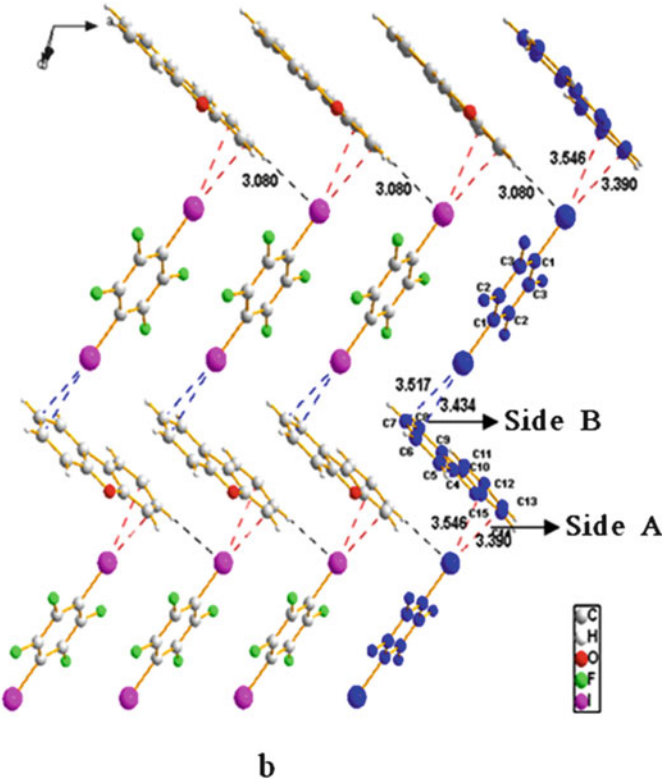

Fig. 9 Infinite main chain stacking structure of cocrystal **8** (halogen bonded infinite chains are colored in *blue*)

reasonable to describe the above system as a $\pi_{XA\cdots XD}I_{HA}\cdots H_{HD}$ mode, where XD and XA represent the halogen bond donor and acceptor, and HD and HA represent the hydrogen bond donor and acceptor, respectively.

Similar to cocrystal **9**, a column-like infinite chain (expressed in yellow) is also formed via C–I$\cdots\pi$ halogen bonding in cocrystal **10**, as shown in Fig. 11. The C–I$\cdots\pi$ interaction in cocrystal **10** can be divided into two groups. In group one, the resulting I$\cdots$C distances are 3.502, 3.596, 3.556, and 3.607 Å, with bonding angles of 168.8, 162.3, 172.6, and 160.4°, respectively. In group two, the bonding distances are 3.411, 3.655, 3.613, 3.487, and 3.536 Å, with bonding angles of 170.6°, 148.3°, 159.5°, 170.4°, and 158.8°, respectively. If a dibenzothiophene molecule is given a reversed orientation, the bonding distances and bonding angles in the sequentially resulting cocrystal structure are the same as the original ones. For the 3D structure, the adjacent and parallel chains are connected mainly through S$\cdots$S interactions and F$\cdots$F contacts, as well as alternative bonding of groups two and one.

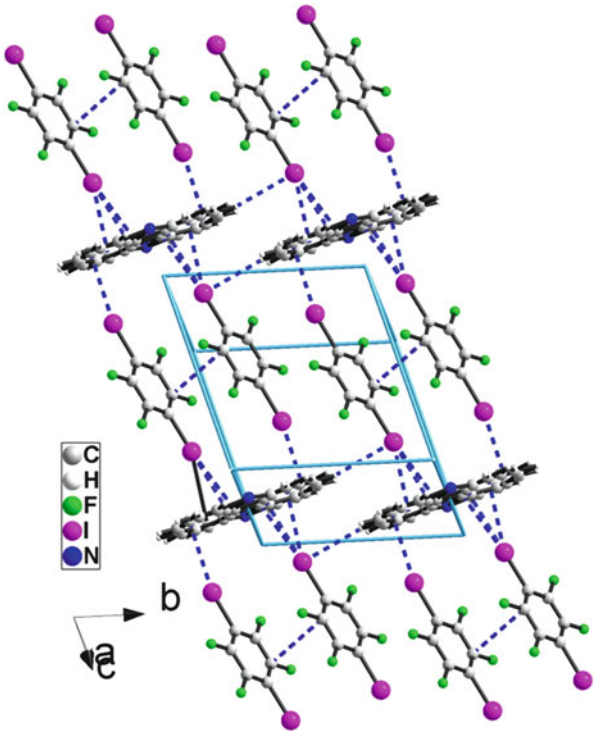

Fig. 10 Infinite chain structures of cocrystal **9** formed by C–I···π and π···π stacking of edge to edge between two 1,4-DITFB, and interchains C–H···I bond

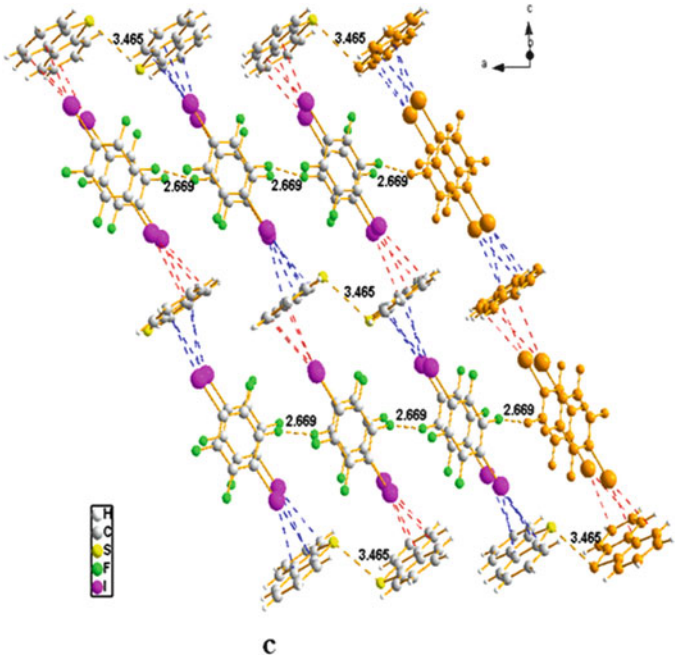

Fig. 11 Packing diagram for cocrystal **10**

3.2 *Phosphorescent Properties of Cocrystals*

PAHs with large π-conjugation systems and rigid planar structures are excellent luminescence molecules and structural units for preparing organic luminescent materials. However, it is difficult to observe their phosphorescence because the transition from singlet to triplet is spin-forbidden. So it is expected that the introduction of haloperfluorobenzene as a halogen bonding donor and heavy atom perturber into PAHs crystals could change the situation and induce strong phosphorescence.

3.2.1 Emission from PAHs in Cocrystals

Free Bp is fluorescent in solution although its quantum yield is low. However, cocrystal **1** does not fluoresce or phosphoresce because the two phenyls in Bp are not co-planar. Compared to **1**, cocrystals **2–6** emit strong phosphorescence, and their phosphorescence excitation and emission characteristics are listed in Table 5. On one hand, the introduction of haloperfluorobenzenes into the crystal dilutes the concentration of phosphors (Nap, Phe, and Pyr), thus preventing luminescence from concentration- or aggregation-quenching. On the other hand, the strong spin-orbital coupling of heavy atom iodine/bromine makes the forbidden S_1–T_1 and T_1–S_0 transitions possible.

It can be seen that the maximum excitation wavelength of **2** is 323 nm (Fig. 12a), which is longer than the 280–290 nm reported in the literature [3, 33]. The emission spectra are characterized by well-resolved vibrational fine-structures. The vibrational bands in the emission spectra are located at 481 (0–0 band), 514, 552, and 585 nm. The maximum peak at 514 nm is a little higher than the 0–0 band. These bands are slightly red-shifted compared with those reported at 472 and 500 nm [3, 33, 34]. The phosphorescence decay of cocrystal **2** has also been investigated, as

Table 5 Phosphorescent properties of cocrystals **2–6**

	Phosphorescent spectra		Decay		
	λ_{ex}/nm	λ_{em}/nm	τ_1/ms (f1/%)	τ_2/ms (f1/%)	$\tau_{average}$/ms
1	–	–	–	–	–
2	323	481 (0–0), **514** (λ_{max}), 552, 585	–	–	0.067[a]
3	360	**568** (λ_{max}), 615, 675, 737	–	–	1.449[a]
4	308, **378**	595, 618, 668, 692, **720**, 801	1.774 (17.9)	0.312 (82.1)	0.574
5	300, **375**	**595**, 653, 720, 787	5.756 (75.4)	0.809 (24.6)	4.539
6	334	**565**, 612, 672, 741	5.312 (77.0)	2.312 (23.0)	4.695
	334	565, 612, **672**, 741	6.583 (39.6)	3.221 (60.4)	4.552
	355	565, 612, **672**, 741	6.760 (32.1)	3.478 (67.9)	4.532
	378	565, 612, **672**, 741	3.943 (92.3)	0.671 (7.7)	3.691

[a]The decay curve obeys the monoexponential model. Bold black means maximum excitation and emission wavelength λ_{max}

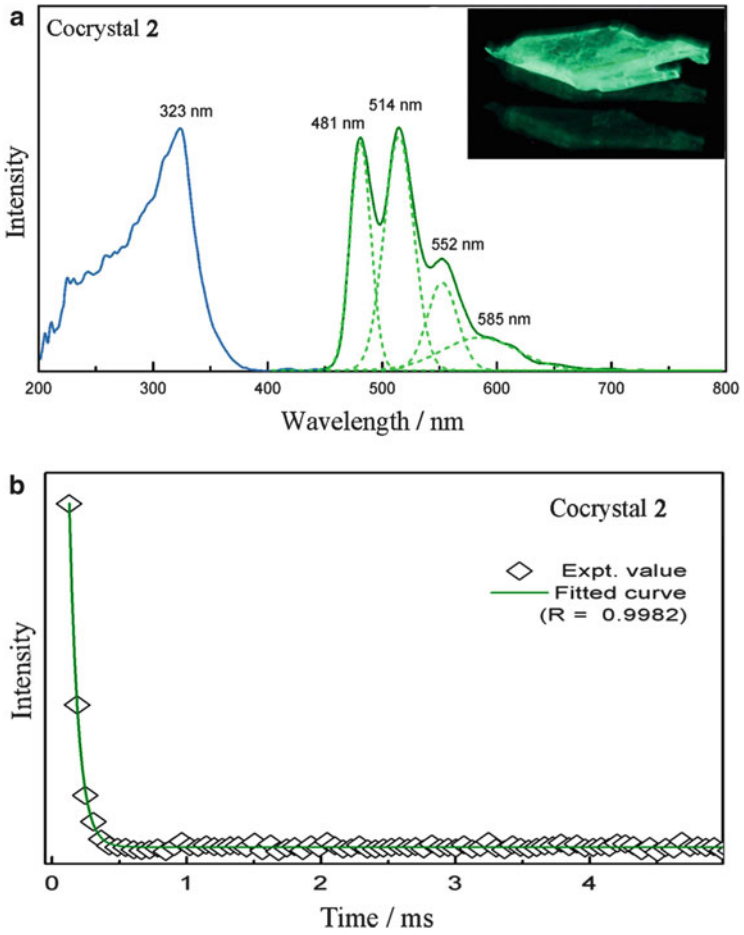

Fig. 12 Phosphorescent spectra (**a**) and decay (**b**) of cocrystal **2**. The vibration bands were separated by assuming a Gaussian distribution of each band. *Insets*: the photos of **2** excited by UV 365 nm lamp which refer to the real phosphorescent color of the cocrystals

shown in Fig. 12b. The decay curve obeys the monoexponential model and the phosphorescent lifetime is 0.067 ms. It can be seen that the phosphorescence could be induced by introducing haloperfluorobenzenes into the crystal structures.

In cocrystals **3** and **6**, both phosphors are Phe. It is well known that fluorescence can be easily observed in a pure crystal of Phe, which emits blue fluorescence under 365-nm light (Fig. 13). The heavy atom effect can promote the singlet–triplet conversion by enhancing spin-orbit coupling between the excited-state electrons of a compound and the massive nucleus of the heavy atom [3, 35]. Thus, in cocrystals **3** and **6**, 1,4-DITFB and 1,4-DBrTFB functional tectons are introduced into the Phe crystal, respectively. After co-crystallization, Phe in cocrystal **3** emits a strong orange phosphorescence under 365-nm light (Fig. 14a). The vibrational

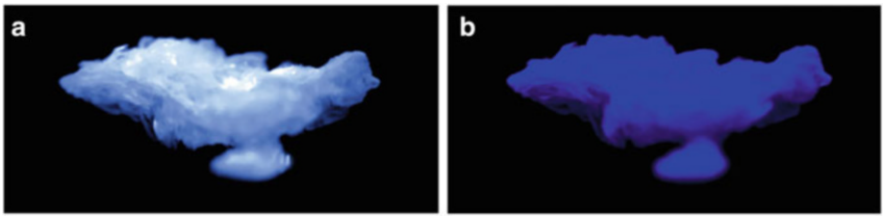

Fig. 13 Pictures of Phe crystal under (**a**) ambient light and (**b**) 365-nm light

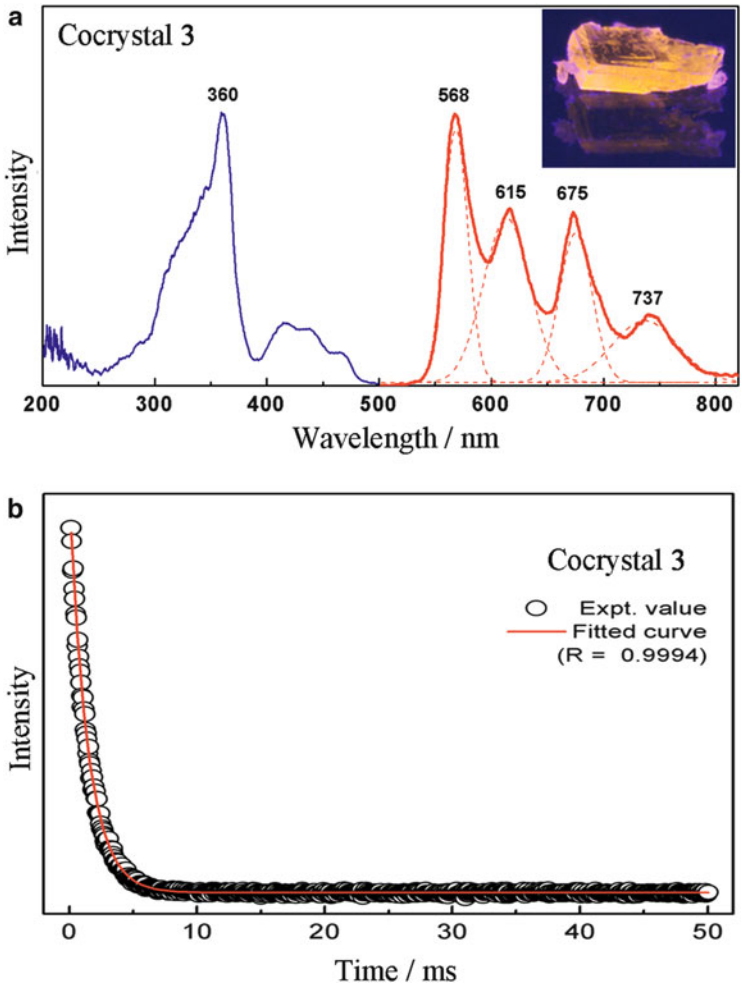

Fig. 14 Phosphorescent spectra (**a**) and decay (**b**) of cocrystal **3**. The vibration bands were separated by assuming a Gaussian distribution of each band. *Insets*: the photos of **3** excited by UV 365 nm lamp which refer to the real phosphorescent color of the cocrystals

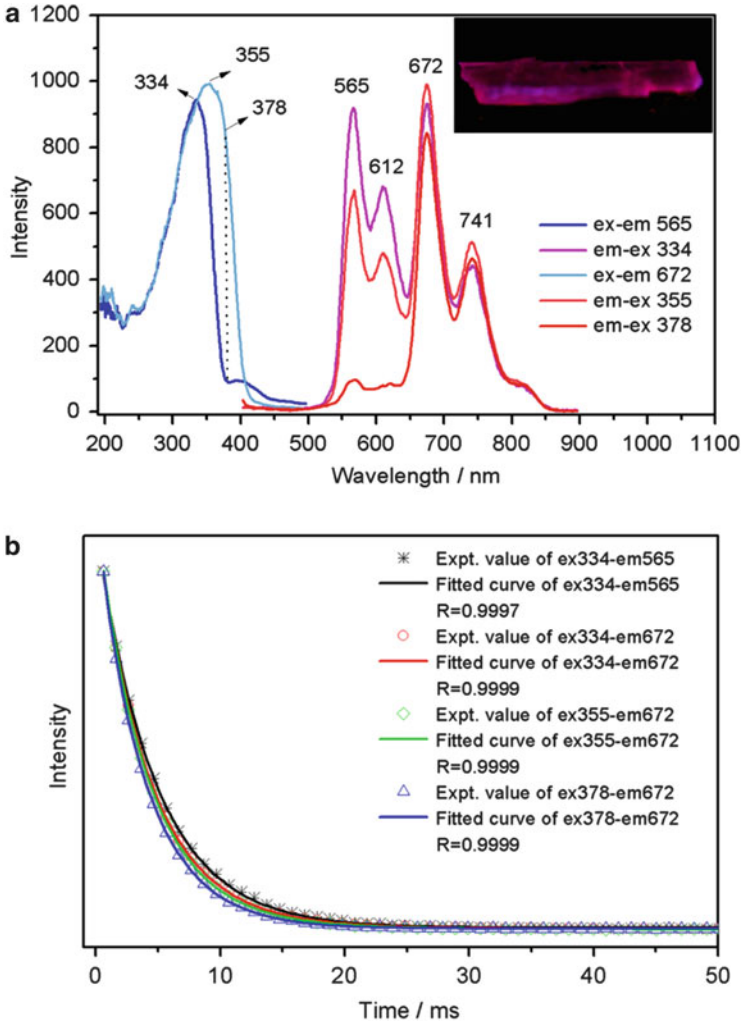

Fig. 15 Phosphorescent spectra (**a**) and decay (**b**) of cocrystal **6**. *Insets*: the photos of **6** excited by UV 365 nm lamp which refer to the real phosphorescent color of the cocrystals

bands in the emission spectra of cocrystal **3** are located at 568, 615, 675, and 737 nm. The maximum peak at 568 nm belongs to the 0–0 transition band. Unlike **3**, Phe in cocrystal **6** emits a strong magenta phosphorescence under 365-nm light (Fig. 15a). The phosphorescence spectra also possess defined vibrational structure bands at room temperature, as shown in Fig. 15a. It can be seen that the maximum excitation wavelength lay at 334 nm with a wide extension toward red-edge. The emission spectra were located at 565 (0–0 band), 612, 672, and 741 nm with a vibrational interval of *ca*. 1,430 cm^{-1}. It can be seen that all bands observed here in both **3** and **6** are largely red-shifted compared with two maximum emission bands of Phe, 473 nm (0–0) and 505 nm [3, 33, 34]. This is probably caused by the

co-action of various interactions, such as C–I···π/ C–Br···π interactions between Phe and 1,4-DITFB/1,4-DBrTFB and additional edge-to-edge type π–π stacking between Phe rings in the cocrystal as described above rather than the change of environment around Phe. The last interaction can also be regarded as a transmolecular π–π conjugation between Phe molecules, which should reduce the triplet energy of Phe in the cocrystal and result in the large red shift of phosphorescence emission.

Additionally, the phosphorescent spectra of cocrystal **6** showed an interesting difference, compared to **3**. Unlike the phosphorescent emission of **3**, which is settled and cannot be modulated, in cocrystal **6** distinctly different emission spectra were obtained, when different excitation wavelengths were used. Under 334 nm excitation, all the vibrational fine-structural peaks (565, 612, 672, and 741 nm) appeared. Under 378 nm or slightly longer excitation, the phosphorescent emissions still have a similar intensity at 672 and 741 nm, the intensity at 565 and 612 nm being weak. This interesting phenomenon must be attributed to the two different states of Phe in the cocrystal. The transmolecular π–π conjugation between Phe molecules reduces the triplet energy of Phe in the cocrystal and results in the large red-shift of phosphorescence emission. So the emission spanning 565–741 nm should be originated from the isolated Phe in the columns and 672–741 nm from the disordered, *i.e.*, delocalized Phe. It makes the modulation of phosphorescence in one cocrystal come true. It should be mentioned that the modulation of phosphorescence by weak interactions should be significant in the design of luminescent materials.

The phosphorescence decays of both cocrystals **3** and **6** were also investigated and the results are shown in Figs. 14b and 15b and Table 5. The decay curve of cocrystal **3** obeys the monoexponential model and the phosphorescent lifetime is 1.45 ms. The lifetime of **6** displays a large difference from that of **3**. The lifetime of the monitoring wavelength at 565 nm and excitation at 334 nm is di-componential and the percentage of the long-lived component is up to 77%. However, it reduced to 40% as the monitoring wavelength was red-shifted from 565 to 672 nm. Also, with a red-shift of the excitation wavelength from 334 to 355 nm, the percentage of long-lived component is reduced to 32%. Moreover, when the excitation is set at 378 nm or slightly longer and the monitor is still at 672 nm, the decay is actually monoexponential with a lifetime of 3.94 ms. All these phenomena suggest that the longer lifetime is originated from the isolated Phe with the emission spanning from 565 to 741 nm and the shorter lifetime belongs to the delocalized ones with emission from 672 to 741 nm. It can also imply that only the delocalized Phe can be excited at the control conditions, while both Phe molecules can be excited at 334 nm.

Compared with cocrystals **2** and **3** which consist of Nap/Phe and 1,4-DITFB, the phosphorescent intensities of **4** and **5** are slightly weaker because Pyr has a smaller triplet-singlet gap [34]. Cocrystals **4** and **5** also emit strong phosphorescence with defined vibrational structure bands even at room temperature, as shown in Fig. 16 and Table 5. Being distinct from the common maximum excitation wavelength (335 nm, S_0–S_2 absorption), the maximum excitation wavelength lies at 375 or 378 nm in this case; this is assigned to the S_0–S_1 absorption of the pyrene [36]. The same emission band (595 nm) of the highest energy is assigned to a 0–0 transition

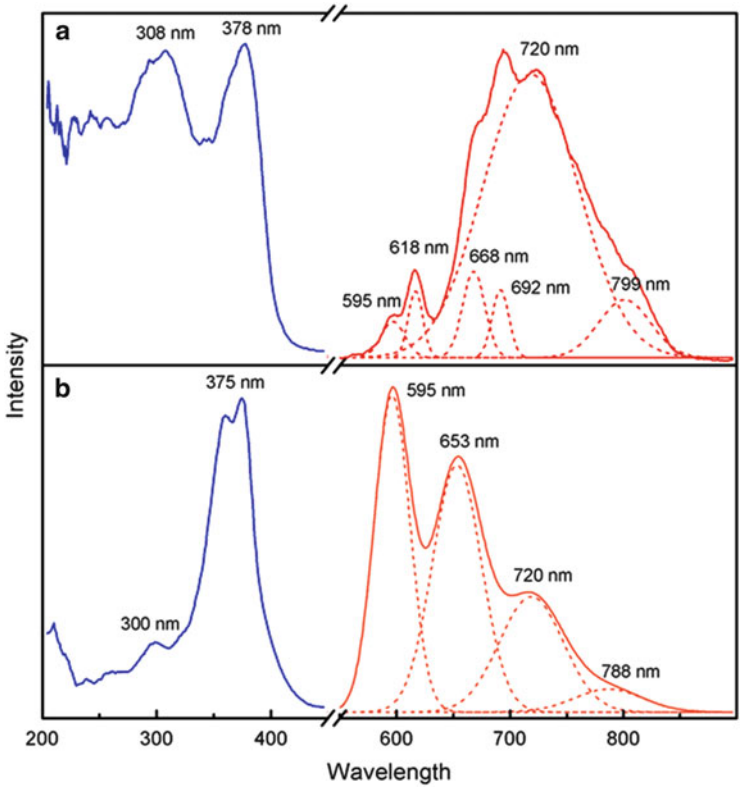

Fig. 16 Normalized phosphorescent excitation and emission spectra of cocrystal **4** (**a**) and **5** (**b**). The vibration bands were separated by assuming a Gaussian distribution of each band

from T_1 to S_0 of the pyrene molecule [37–39]. However, there is a remarkable difference in the maximum vibrational band between **4** and **5**. In **4**, the band at 720 nm is the strongest, while the 0–0 band (595 nm) is the dominant emission in **5**. The energy gap between the 595 and 720 nm bands is almost 3,000 cm^{-1}, consistent with a C–H stretching vibration of the pyrene molecule. Moreover, because the lowest vibration energy level (0 vibration energy level) of the pyrene molecule is very sensitive to the polarity of its environment, the emission intensity of the 0–0 band probably increases with the increases in the local molecular polarity [40]. The difference in the maximum emission bands should arise from the diverse local environments surrounding the pyrene molecule in these two cocrystals. The calculated dipole moment of 1,2-DITFB is 2.2 Debye, while 1,4-DITFB has no dipole moment. This means that 1,2-DITFB creates a local polar molecular environment in **5**, while 1,4-DITFB creates a local apolar molecular environment, indicating that the 0–0 band emission in **4** is significantly restrained.

The 0–0 band phosphorescence decays of **4** and **5** were also studied and the results are shown in Fig. 17 and Table 5. The phosphorescence of both cocrystals has a bi-exponential decay property with an average lifetime of 0.574 ms for **4** and

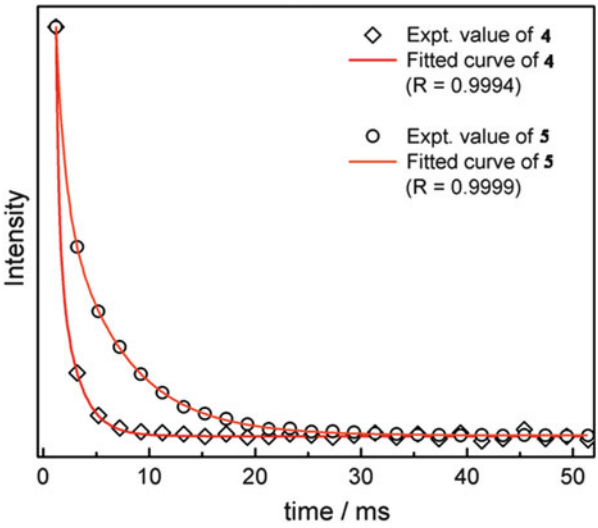

Fig. 17 Phosphorescence decay curves for **4** and **5**

4.539 ms for **5**. As with the vibrational bands, the difference in lifetimes is also associated with the local molecular environment in the cocrystals. Additionally, C–I···π interactions might be important irradiative channels which decrease phosphorescence lifetime. In **4**, besides the π···π interactions, there are C–I···π interactions between 1,4-DITFB and the pyrene molecules. The distance of the I···pyrene ring in **4** is shorter than in **5**, suggesting a stronger heavy atom effect in **4** compared to **5**. An over-disturbance effect from the iodine atom makes the phosphorescence lifetime of **4** far shorter than that of **5**.

Another factor affecting phosphorescent emission of **4** and **5** may be the different "dilution degrees" in **4** and **5** as stated in the cocrystal structures section. The A···B···B···A···B···B arrangement in **5** implies a lower "concentration" than the A···B···A···B arrangement in **4**, resulting in a more efficient prevention of the pyrene–pyrene interactions in **5**, as can be seen from Figs. 4 and 5, and thus stronger phosphorescent emission is observed for **5**.

3.2.2 Emission from Fluorene or Its Heterocyclic Analogues in Cocrystals

The cocrystals of fluorene and its heterocyclic analogues, assembled using the new methodology, also emit strong phosphorescence. From the structure sections, it can be seen that **7** and **8** are very similar in structural features; **9** and **10** also possess similar structures, although different from **7** and **8**. An analogous trend was also observed in their phosphorescence behavior: emission spectra of **7** and **8** are very similar; **9** and **10** also show a similarity, which proves that phosphorescent properties can be modulated by the design of cocrystal structures. The phosphorescent characteristics are summarized in Table 6.

Table 6 Phosphorescent properties of cocrystals **7**–**10**

	Phosphorescent spectra		Decay
	λ_{ex}/nm	λ_{em}/nm	τ/ms
7	280	496 (0–0), **531** (max), 569, 610	0.34
8	330	496 (0–0), **529** (max), ~572, ~597	0.51
9	360	**571** (0–0, max), 615, 675, 742	2.75
10	380	520 (0–0), **564** (max), 618, 669, 748	2.50

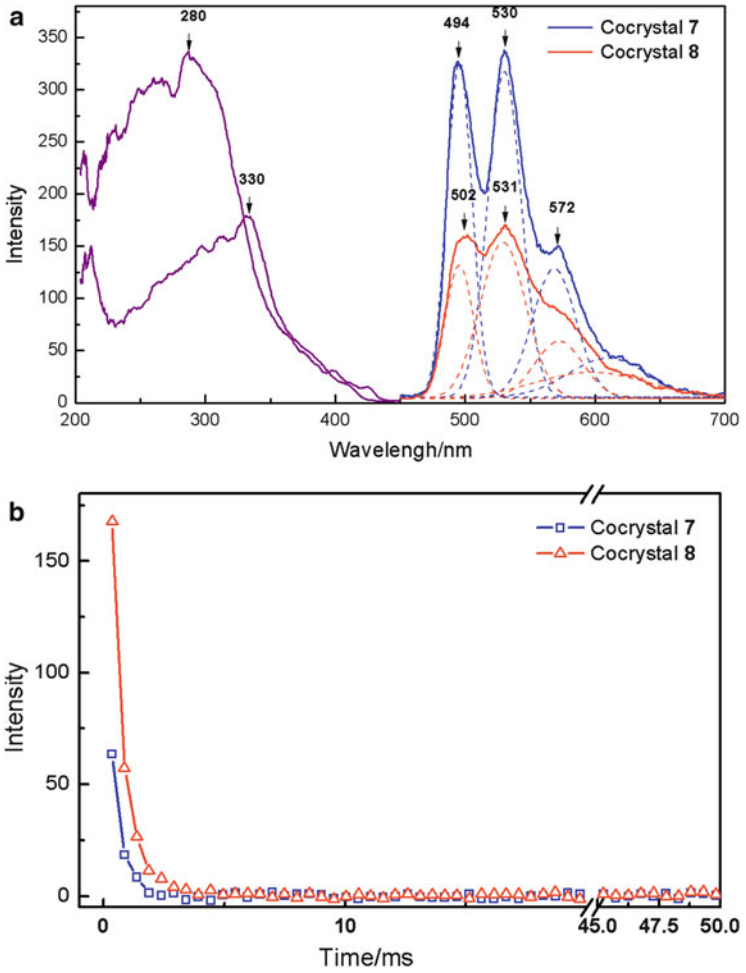

Fig. 18 Phosphorescent spectra (**a**) and decays (**b**) of cocrystal **7** and **8**

In cocrystal **7**, the phosphorescence emission spectrum goes from 490 to near 580 nm with well-defined vibrational bands at 496 (0–0), 531 (max), 569, and 610 nm at the excitation wavelength of 280 nm as shown in Fig. 18a.

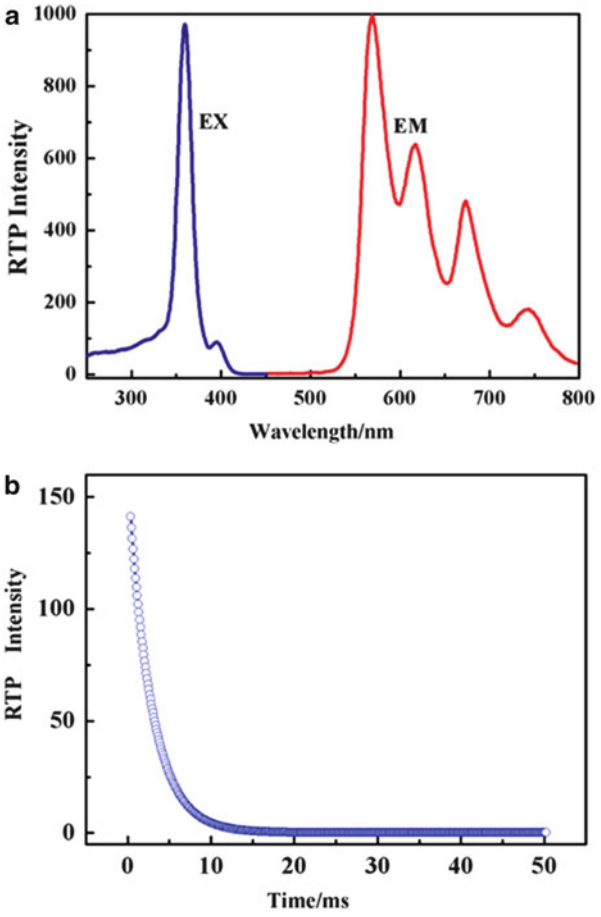

Fig. 19 Phosphorescent spectra (**a**) and decays (**b**) of cocrystal **9**

The phosphorescent emission of cocrystal **8** is similar to **7**, but obviously weaker, with well defined vibrational bands at 496 (0–0), 529 (max), 572, and ~597 nm at the excitation wavelength of 330 nm (Fig. 18a). The phosphorescence decays of both cocrystals **7** and **8** obey a monoexponential law with the lifetime of 0.34 ms for cocrystal **7** and 0.51 ms for cocrystal **8**, respectively (Fig. 18b).

The cocrystals **9** and **10** also emit strong phosphorescence. The phosphorescence emission spectrum of **9** (Fig. 19a) goes from 520 to near 800 nm with fine vibrational bands at 571, 615, 675, and 742 nm at the excitation wavelength of 360 nm. Compared with the previous reports on phosphorescence of carbazole [41–43] or 3-iodocarbazole [44], the phosphorescence of **9** displays larger red-shifts. Comparatively, the phosphorescence of cocrystal **10** is weaker, with resolvable bands at 520 (0–0), 564 (max), 618, 669, and 748 nm at the excitation wavelength of 380 nm (Fig. 20a). The S···S interaction (assigned to π–π

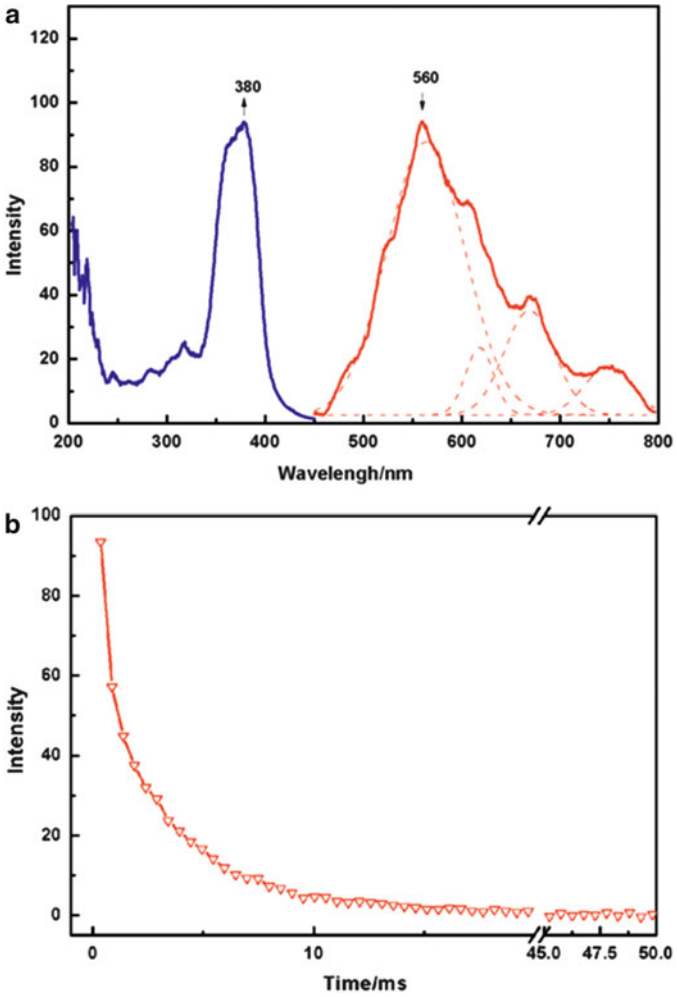

Fig. 20 Phosphorescent spectra (**a**) and decays (**b**) of cocrystal **10**

conjugation by σ-type overlap of π-orbitals of two different S atoms) [26] may make the gap between triplet and singlet ground states narrower and sequentially phosphorescence weaker compared with the case of cocrystal **9**. It may also provide the cocrystal with additional functions, such as electron transport [45, 46]. The phosphorescent decays of both **9** and **10** obey a monoexponential law with a lifetime of 2.75 ms for cocrystal **9** and 2.50 ms for **10**, respectively (Figs. 19b and 20b).

4 Concluding Remarks

Halogen bonding is a really novel tool in assembling organic phosphorescent materials. The main issue, among various possible functions of halogen atom as halogen bond donor, should be the development of a new strategy to introduce metal-free heavy atom perturbers in defined stoichiometry into organic phosphors. Different donors, leading to different halogen bonding strength or pattern, induce changes in phosphorescence color or decay. Modulation of phosphorescence can also be realized by the structure, shape, and position of a heteroatom in polyaromatic hydrocarbons. For example, recent work shows that phosphorescent cocrystals, assembled by a same donor and different bent 3-ring-*N*-heterocyclic hydrocarbons, are modified via halogen bonds from green, orange to light orange emission, because of the *N*-position [47]. In future, the synthesis of various new donors and acceptors aimed at specific color or application of phosphorescence should be pursued. Furthermore, a theoretical analysis of halogen bonding effect on the triplet state energy level of organic phosphors and their most possible vibrational transition, as well as the effect of molecular structures on phosphorescence behavior in XB-based cocrystals, is necessary.

	Cocryst. **1**	Cocryst. **2**	Cocryst. **3**	Cocryst. **4**	Cocryst. **5**	Cocryst. **6**	Cocryst. **7**	Cocryst. **8**	Cocryst. **9**	Cocryst. **10**
Formula	$C_{24}H_{10}F_8I_4$	$C_{22}H_8F_8I_4$	$C_{26}H_{10}F_8I_4$	$C_{22}H_{10}F_4I_2$	$C_{28}H_{10}F_8I_4$	$C_{27}H_{15}Br_2F_4$	$C_{19}H_{10}F4I2$	$C_{18}H_8F_4I_2O$	$C_{24}H_9F_8I_4N$	$C_{24}H_8F_8I_4S$
Formula weight	957.92	931.88	981.94	604.10	1,005.96	575.21	568.07	570. 04	969.91	987.96
Crystal system	Monoclinic	Triclinic	Triclinic	Monoclinic	Monoclinic	Triclinic	Monoclinic	Triclinic	Triclinic	Triclinic
Space group	$P\ 2_1/c$	$P\bar{1}$	$P\bar{1}$	$P\ 2_1/c$	$P\ 2_1/c$	$P\bar{1}$	C2	$P\bar{1}$	$P\bar{1}$	$P\bar{1}$
a/Å	6.156 (1)	6.136 (1)	6.190 (2)	8.3885 (2)	10.277 (3)	6.9513 (10)	8.587 (1)	5.425 (2)	5.9625 (11)	6.146 (2)
b/Å	12.183 (1)	9.599 (2)	9.381 (3)	18.3017 (4)	15.593 (5)	8.9349 (13)	7.114 (1)	5.769 (1)	9.3712 (18)	9.385 (2)
c/Å	18.149 (1)	11.437 (2)	12.462 (3)	13.1838 (4)	9.715 (3)	17.922 (2)	14.78 (1)	13.91 (1)	12.051 (2)	12.21 (1)
α/°	90	70.149 (2)	104.290 (4)	90.00	90.00	83.047 (2)	90	90.58 (0)	75.207 (3)	74.32 (1)
β/°	99.044 (10)	86.359 (3)	90.952 (4)	105.2680 (10)	114.844 (6)	84.916 (2)	99.20 (1)	101.0 (0)	88.706 (3)	89.80 (0)
γ/°	90	82.980 (3)	97.561 (4)	90.00	90.00	79.039 (2)	90	101.5 (1)	80.057 (3)	82.23 (1)
Unit cell volume, $Å^3$	1,344.2 (2)	628.7 (2)	694.2 (3)	1,952.59 (9)	1,412.7 (8)	1,082.3 (3)	891.6 (1)	418.3 (2)	641.1 (2)	671.8 (3)
T/K	297 (2)	296 (2)	300 (2)	296 (2)	293 (2)	110 (2)	296 (2)	150 (2)	150 (2)	296 (2)
Z	2	1	1	4	2	2	2	1	1	1
Density, $g{\cdot}m^{-3}$	2.367	2.461	2.349	2.055	2.356	1.765	2.116	2.263	2.512	2.442
F (000)	876	424	450	1,136	924	566	532	266	443	452
Absorption coefficient, μ/mm^{-1}	4.704	5.024	4.557	3.262	4.482	3.793	3.564	3.803	4.934	4.785
No. of reflections measured	6,541	2,874	3,180	9,480	5,729	5,369	2,026	2,157	3,264	3,215

No. of independent reflections	2,439	2,111	2,420	4,472	2,491	3,798	1,379	1,487	2,296	2,399
R_{int}	0.0238	0.0244	0.0141	0.0167	0.0193	0.0205	0.0115	0.0247	0.0200	0.0302
Final R_1 values ($I > 2\sigma\ (I)$)	0.0404	0.0380	0.0364	0.0373	0.0459	0.0307	0.0208	0.0535	0.0325	0.0503
Final wR (F^2) values ($I > 2\sigma\ (I)$)	0.0930	0.0925	0.0872	0.0889	0.1029	0.0667	0.0488	0.1328	0.0746	0.1361
Final R_1 values (all data)	0.0524	0.0444	0.0456	0.0560	0.0545	0.0428	0.0227	0.0575	0.0410	0.0577
Final wR (F^2) values (all data)	0.1000	0.0981	0.0934	0.0991	0.1074	0.0710	0.0510	0.1367	0.0789	0.1437
Goodness of fit on F^2	1.035	1.060	1.058	1.016	1.087	1.028	1.111	1.058	1.018	1.042

Acknowledgments The authors thank the Natural Science Foundation of China (No.90922023), the Doctoral Program Fund of Higher Education of China (No. 20110003110011) for support.

References

1. Adachi C, Baldo MA, Forrest SR, Thompson ME (2000) High-efficiency organic electrophosphorescent devices with tris(2-phenylpyridine)iridium doped into electron-transporting materials. Appl Phys Lett 77:904–906
2. Baldo MA, O'Brien DF, You Y, Shoustikov A, Sibley S, Thompson ME, Forrest SR (1998) Highly efficient phosphorescent emission from organic electroluminescent devices. Nature 395:151–154
3. Zhu RH, Jin WJ (2006) Room temperature phosphorimetry: principle and applications (in Chinese). Science Press, Beijing
4. Bower EL-Y, Winefordner JD (1978) The effect of sample environment on the room-temperature phosphorescence of several polynuclear aromatic hydrocarbons. Anal Chim Acta 102:1–13
5. Abbott DW, Vo-Dinh T (1985) Detection of specific nitrogen-containing compounds by room-temperature phosphorescence. Anal Chem 57:41–45
6. Burress CN, Bodine MI, Elbjeirami O, Reibenspies JH, Omary MA, Gabbaï FP (2007) Enhancement of external spin−orbit coupling effects caused by metal−metal cooperativity. Inorg Chem 46(4):1388–1395
7. Ballardini R, Varani G, Indelli MT, Scandola F (1986) Phosphorescent 8-quinolinol metal chelates. Excited-state properties and redox behavior. Inorg Chem 25:3858–3865
8. Hsu C-C, Lin C-C, Chou P-T, Lai C-H, Hsu C-W, Lin C-H, Chi Y (2012) Harvesting highly electronically excited energy to triplet manifolds: state-dependent intersystem crossing rate in Os(II) and Ag(I) complexes. J Am Chem Soc 134:7715–7724
9. Focsaneanu K-S, Scaiano JC (2005) Potential analytical applications of differential fluorescence quenching: pyrene monomer and excimer emissions as sensors for electron deficient molecules. Photochem Photobiol Sci 4:817–821
10. Østergaard M, Hrdlicka PJ (2011) Pyrene-functionalized oligonucleotides and locked nucleic acids (LNAs): tools for fundamental research, diagnostics, and nanotechnology. Chem Soc Rev 40:5771–5788
11. Figueira-Duarte TM, Müllen K (2011) Pyrene-based materials for organic electronics. Chem Rev 111:7260–7314
12. Desiraju GR, Ho PS, Kloo L, Legon AC, Marquardt R, Metrangolo P, Politzer P, Resnati G, Rissanen K (2013) Definition of the halogen bond. Pure Appl Chem 85:1711–1713
13. Bolton O, Lee K, Kim HJ, Lin KY, Kim J (2011) Activating efficient phosphorescence from purely organic materials by crystal design. Nat Chem 3:205–210
14. Lee D, Bolton O, Kim BC, Youk JH, Takayama S, Kim J (2013) Room temperature phosphorescence of metal-free organic materials in amorphous polymer matrices. J Am Chem Soc 135:6325–6329
15. Clark T, Hennemann M, Murray JS, Politzer P (2007) Halogen bonding: the σ-hole. J Mol Model 13:291–296
16. Pang X, Wang H, Zhao XR, Jin WJ (2013) Co-crystallization turned on the phosphorescence of phenanthrene by C-Br···π halogen bonding, π-hole···π bonding and other assisting interactions. CrystEngComm 15:2722–2730
17. Gao HY, Zhao XR, Wang H, Pang X, Jin WJ (2013) Cocrystal assembled by 1,2-diiodotetrafluorobenzene and acridine via C-I···N halogen bond and π-hole···F bonds. Chin J Chem 31:1279–1284

18. Shen QJ, Pang X, Zhao XR, Gao HY, Sun HL, Jin WJ (2012) Phosphorescent cocrystals constructed by 1,4-diiodotetrafluorobenzene and polyaromatic hydrocarbons based on C-I···π halogen bonding and other assisting weak interactions. CrystEngComm 14:5027–5034
19. Shen QJ, Wei HQ, Zou WS, Sun HL, Jin WJ (2012) Cocrystals assembled by pyrene and 1,2- or 1,4-diiodotetrafluorobenzenes and their phosphorescent behaviors modulated by local molecular environment. CrystEngComm 14:1010–1015
20. Gao HY, Zhao XR, Wang H, Pang X, Jin WJ (2012) Phosphorescent cocrystals assembled by 1,4-diiodotetrafluorobenzene and fluorene and its heterocyclic analogues based on C-I···π halogen bonding. Cryst Growth Des 12:4377–4387
21. Gao HY, Shen QJ, Zhao XR, Yan XQ, Pang X, Jin WJ (2012) Phosphorescent co-crystal assembled by 1,4-diiodotetrafluorobenzene with carbazole based on C-I···π halogen bonding. J Mater Chem 22:5336–5343
22. Bondi A (1964) van der Waals volumes and radii. J Phys Chem 68:441–451
23. Smith RC (2009) Covalently scaffolded inter-π-system orientations in π-conjugated polymers and small molecule models. Macromol Rapid Commun 30:2067–2078
24. Wang WL, Xu JW, Lai Y-H (2003) Alternating conjugated and transannular chromophores: tunable property of fluorene-paracyclophane copolymers via transannular pi-pi interaction. Org Lett 5:2765–2768
25. Kalsi PS (2004) Spectroscopy of organic compounds, 6th edn. New Age International (P) Ltd, New Delhi
26. Huang L, Yu DQ (2000) Application of UV spectroscopy in organic chemistry (I) (in Chinese). Science Press, Beijing
27. Rosokha SV, Neretin IS, Rosokha TY, Hecht J, Kochi JK (2006) Charge-transfer character of halogen bonding: molecular structures and electronic spectroscopy of carbon tetrabromide and bromoform complexes with organic σ- and π-donors. Heteroatom Chem 17:449–459
28. Strieter FJ, Templeton DH (1962) Crystal structure of the carbon tetrabromide-p-xylene complex. J Chem Phys 37:161–164
29. Pauling L (1945) The nature of the chemical bond. Cornell University Press, Ithaca/New York
30. Dey A, Desiraju GR (2004) Supramolecular equivalence of ethynyl, chloro, bromo and iodo groups. A comparison of the crystal structures of some 4-phenoxyanilines. CrystEngComm 6:642–646
31. Bosch E, Barnes CL (2002) Triangular halogen-halogen-halogen interactions as a cohesive force in the structures of trihalomesitylenes. Cryst Growth Des 2:299–302
32. Weiss HC, Boese R, Smith HL, Haley MM (1997) ≡CH· · ·π versus≡CH···Halogen interactions-the crystal structures of the 4-halogenoethynylbenzenes. Chem Commun (24):2403–2404
33. Vo-Dinh T (1984) Room temperature phosphorimetry for chemical analysis. Wiley, New York
34. Jin WJ, Liu CS (1993) Luminescence rule of polycyclic aromatic hydrocarbons in micelle-stabilized room-temperature phosphorescence. Anal Chem 65:863–865
35. Turro NJ (1991) Modern molecular photochemistry. University Science, Sausalito, California
36. Crawford AG, Dwyer AD, Liu Z, Steffen A, Beeby A, Palsson L-O, Tozer DJ, Marder TB (2011) Experimental and theoretical studies of the photophysical properties of 2- and 2,7-functionalized pyrene derivatives. J Am Chem Soc 133:13349–13362
37. Azumi T, McGlynn SP (1963) Delayed fluorescence of solid solutions of polyacenes. IV. The origin of excimer fluorescence. J Chem Phys 39:3533–3534
38. Hochstrasser RM, Lower SK (1964) Polarized emission and triplet-triplet absorption spectra of aromatic hydrocarbons in benzophenone crystals. J Chem Phys 40:1041–1046
39. Talapatra GB, Misra TN (1982) Homofusion and heterofusion of triplet excitons in a “real” organic mixed crystal: biphenyl host-naphthalene and pyrene guests system. J Chem Phys 77:2290–2301
40. Kalyanasundaran K, Thomas JK (1977) Environmental effects on vibronic band intensities in pyrene monomer fluorescence and their application in studies of micellar systems. J Am Chem Soc 99:2039–2044

41. Gereltu B, Odengaowa (1994) Preparation of water soluble copolymer of N-vinyl-carbazole and acrylic acid and its fluorescence. Chin J Appl Chem 11:110–112
42. Skrilec M, Love LJC (1981) Micelle-stabilized room-temperature phosphorescence characteristics of carbazole and related derivatives. J Phys Chem 85:2047–2050
43. Vo-Dinh T, Hooyman JR (1979) Selective heavy-atom perturbation for analysis of complex mixtures by room-temperature phosphorimetry. Anal Chem 51:1915–1921
44. Liang WJ, Wang Y, Feng F, Jin WJ (2006) Novel self-protective phosphorescence from crystalline nanoparticles assembled by 3-bromo- and 3-iodo-carbazoles based on halogen-halogen interaction in suspension solutions. Anal Chim Acta 572:295–302
45. Huang TH, Whang WT, Shen JY, Wen YS, Lin JT, Ke TH, Chen LY, Wu CC (2006) Dibenzothiophene/oxide and quinoxaline/pyrazine derivatives serving as electron-transport materials. Adv Funct Mater 16:1449–1456
46. Wang L, Wu ZY, Wong WY, Cheah KW, Huang H, Chen CH (2011) New blue host materials based on anthracene-containing dibenzothiophene. Org Electron 12:595–601
47. Wang H, Hu RX, Pang X, Gao HY, Jin WJ (2014) The phosphorescent co-crystals of 1,4-diiodotetrafluorobenzene and bent 3-ring-N-heterocyclic hydrocarbons by C–I…N and C–I…π halogen bonds. CrystEngComm 16:7942–7948

Top Curr Chem (2015) 359: 147–166
DOI: 10.1007/128_2014_615

Published online: 27 March 2015

Halogen-Bonded Photoresponsive Materials

Marco Saccone, Gabriella Cavallo, Pierangelo Metrangolo, Giuseppe Resnati, and Arri Priimagi

Abstract The aim of the present review is to illustrate to the reader the state of the art on the construction of supramolecular azobenzene-containing materials formed by halogen bonding. These materials include several examples of polymeric, liquid crystalline or crystalline species whose performances are either superior to the corresponding performances of their hydrogen-bonded analogues or simply distinctive of the halogen-bonded species.

Keywords Azobenzene · Halogen bonding · Liquid crystals · Photoresponsive materials · Polymers

M. Saccone (✉)
Department of Applied Physics, Aalto University, P.O. Box 13500, 00076 Aalto, Finland
e-mail: marco.saccone@aalto.fi

G. Cavallo and G. Resnati
Laboratory of Nanostructured Fluorinated Materials (NFMLab), Department of Chemistry, Materials, and Chemical Engineering "Giulio Natta", Politecnico di Milano, Via Mancinelli 7, 20131 Milan, Italy
e-mail: gabriella.cavallo@polimi.it; giuseppe.resnati@polimi.it

P. Metrangolo
Laboratory of Nanostructured Fluorinated Materials (NFMLab), Department of Chemistry, Materials, and Chemical Engineering "Giulio Natta", Politecnico di Milano, Via Mancinelli 7, 20131 Milan, Italy

VTT, Technical Research Centre of Finland, Tietotie 2, 02044 VTT, Finland
e-mail: pierangelo.metrangolo@polimi.it

A. Priimagi
Laboratory of Nanostructured Fluorinated Materials (NFMLab), Department of Chemistry, Materials, and Chemical Engineering "Giulio Natta", Politecnico di Milano, Via Mancinelli 7, 20131 Milan, Italy

Department of Chemistry and Bioengineering, Tampere University of Technology, P.O. Box 541, 33101 Tampere, Finland
e-mail: arri.priimagi@tut.fi

Contents

1 Preface

Halogen bonding [1–4] is among the most recent and least exploited noncovalent interactions in the toolbox of supramolecular chemistry. However, it has recently emerged as a first-class tool in fields as diverse as self-assembly [5], medicinal chemistry [6], crystal engineering [7], biochemistry [8], and materials science [9, 10]. The present chapter focuses on a specific subset of the latter field where halogen bonding seems to be particularly effective, namely photoresponsive azobenzene-containing materials, the first reports on the topic appearing as recently as 2012 [11, 12]. This field is therefore still in its infancy but has already shown huge potential, as highlighted by the examples given herein. The outline of this chapter comprises first a general introduction to azobenzene derivatives, the key photoactive unit of the studies presented here, followed by a survey of recent advances in halogen-bonded photoactive polymers, liquid crystals, and crystals, respectively. Finally, some discussion on possible future perspectives of the field is given.

2 Introduction to Azobenzene

Azobenzene derivatives contain two aromatic rings held together by a nitrogen–nitrogen double bond. Thanks to the N=N link, they exist in two stereoisomeric forms, *trans* and *cis* (Fig. 1a). The rod-like *trans* form is thermodynamically more stable than the bent *cis* form, and at ambient conditions azobenzene derivatives, whether in solution or in the solid state, exist usually in the *trans* form. Most azobenzenes can be optically isomerized from *trans* to *cis* using any wavelength within their broad absorption band, which can be tuned by the substituents R_1 and R_2 [14]. The substitution pattern, together with the local environment, also dictates the timescale of the *cis–trans* thermal relaxation. The "photofunction" of azobenzene-containing materials can be based on either efficient *trans–cis* conversion or rapid cycling between the *trans* and *cis* forms. The latter is obtained when the molecule is substituted with strong electron-donating and electron-withdrawing groups, in which case a single blue–green wavelength of light activates both forward and reverse reactions. Concerning functional materials, the power of

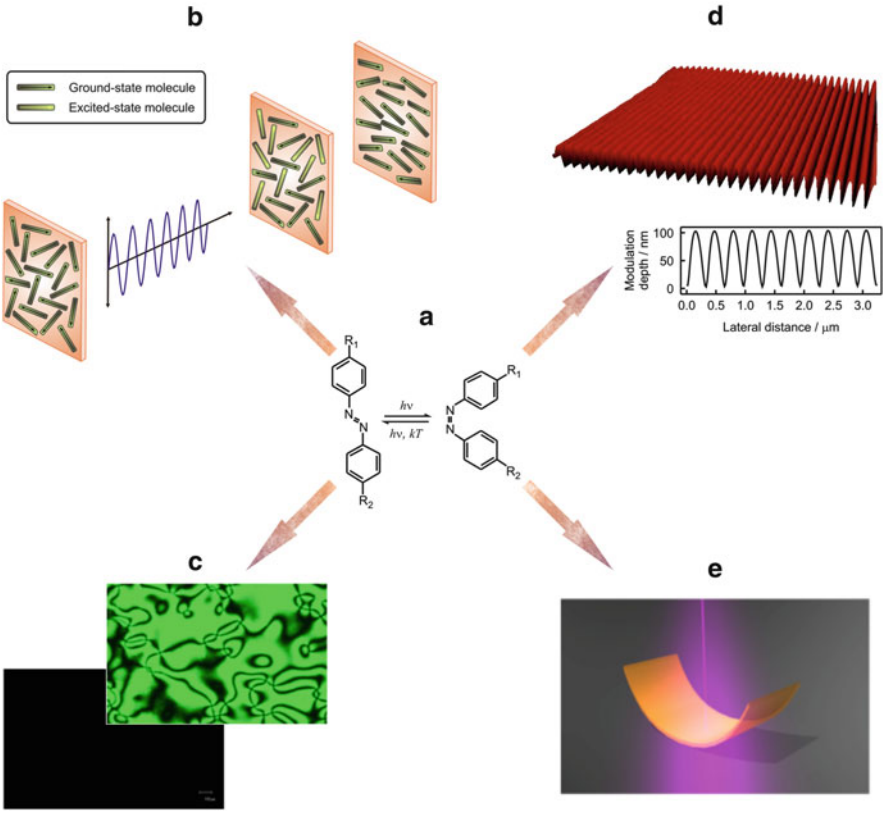

Fig. 1 Photoisomerization of azobenzene derivatives (**a**) can give rise to a cascade of molecular motions into the material system it is incorporated into. The substituents R_1 and R_2 dictate the physical and photochemical properties of the molecules, and can also be used to attach noncovalently/covalently the azobenzenes to different host matrices. The light-induced motions relevant for this review are (**b**) photoalignment, (**c**) photoinduced phase transition in liquid-crystalline materials, (**d**) photoinduced surface patterning of initially flat polymer surfaces (reproduced with permission from Kravchenko et al. [13]. Copyright 2014, Wiley), and (**e**) photoinduced bending of azobenzene-containing crosslinked liquid-crystalline polymers

azobenzene lies in the chemical stability of the moiety even after prolonged switching and in the possibility for the molecular-scale photoisomerization to give rise to a cascade of motions beyond the size scale of an individual molecule, eventually emerging as macroscopic motions. Therefore, azobenzene photoswitching is equally useful in both molecular machinery/electronics [15, 16] and macroscopic actuation [17, 18]. Herein, four types of photoinduced motions deserve special attention, namely photoalignment (Fig. 1b) [19], photoinduced phase transition (Fig. 1c) [20], photoinduced surface patterning (Fig. 1d) [21], and photoinduced bending (Fig. 1e) [22]. By photoalignment we refer to a process where an initially isotropic azobenzene-containing sample is made anisotropic

(exhibiting birefringence and dichroism) upon irradiation with linearly polarized light. This process can be interpreted through statistical reorientation of the azobenzene molecules and their accumulation in the direction(s) perpendicular to the polarization plane, where the interaction of the incident light beam is minimized (Fig. 1b) [23]. The anisotropic molecular alignment can be randomized by irradiating the sample with circularly polarized or unpolarized light [19].

The photoalignment process is particularly useful at the mesoscopic level in the context of liquid crystals, the alignment of which can be controlled with azobenzene "command surfaces" [24, 25]. Alternatively, a small portion of "master" azobenzene molecules can be doped into a liquid crystal material where they control the orientation of passive "slave" molecules through collaborative movements. In an extreme case, the azobenzene dopants can induce order–disorder transitions of the liquid crystal material, as illustrated in Fig. 1c [20].

In amorphous azopolymers the predominant macroscopic photomechanical effect triggered by photoisomerization is photoinduced surface patterning (Fig. 1d). In 1995 it was observed that, upon irradiating an azopolymer thin film with an optical interference pattern (Fig. 2a), the polymer starts to migrate and forms a replica of the incident irradiation pattern on the polymer surface in the form of a surface-relief grating (SRG) [28, 29]. As a result, high-quality temporally stable diffraction gratings can easily be inscribed via a one-step fabrication process, well below the glass-transition temperature of the polymer. The kinetics of the SRG formation can be followed in situ by monitoring the first-order diffraction efficiency

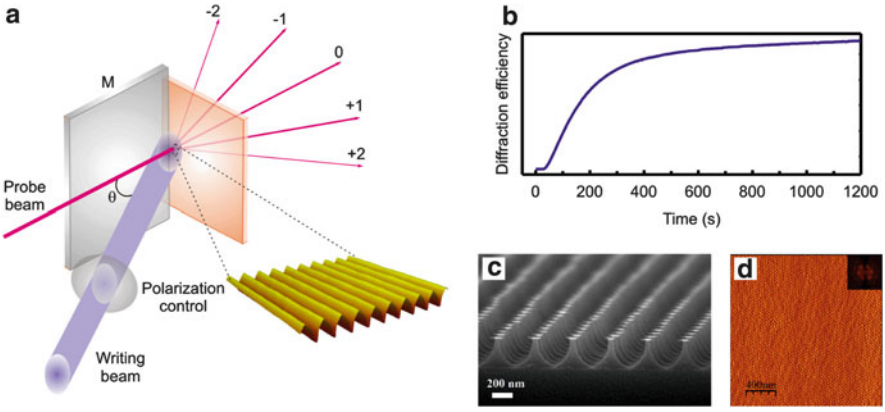

Fig. 2 (**a**) Experimental setup for the inscription of surface-relief gratings. M refers to a mirror which reflects half of the incident beam onto the sample to form the interference pattern. Reproduced with permission from Priimagi et al. [26]. Copyright 2010, World Scientific. (**b**) During the grating inscription, the diffraction efficiency can be monitored in real time using a non-resonant probe beam. (**c**) The SRGs can be used as masks to pattern other materials, e.g., to prepare silicon nanostructures. Reproduced with permission from Kravchenko et al. [13]. Copyright 2014, Wiley. (**d**) As another example, SRGs can be used as substrates to obtain long-range-ordered block copolymer nanostructures. Reproduced with permission from Aissou et al. [27]. Copyright 2014, Wiley

of the gratings (Fig. 2b) [30]. Once inscribed, the gratings can be used as, for example, diffractive optical elements and nanostructuring tools [31, 32], examples of which are illustrated in Fig. 2c, d. Importantly, the gratings only form efficiently when the azobenzene units are bound to the polymer matrix, either covalently or non-covalently [30, 33]. As shown in the rest of this chapter, halogen bonding appears as a particularly suitable noncovalent interaction for this purpose.

In crosslinked liquid-crystalline polymers and elastomers, and more recently also in azobenzene crystals, photoisomerization can lead to reversible macroscopic shape changes and complex 3D movements [34] as illustrated in Fig. 1e. The key for achieving large-scale photomechanical response is an efficient control over molecular alignment and, as mentioned earlier, liquid-crystalline materials are particularly useful in this respect. The optical-to-mechanical energy conversion provides a pathway to the use of light to fuel photomechanical oscillators [35], plastic micromotors [36], robotic-arm movements [37], etc.

In the past 2 years or so, halogen-bond-based supramolecular materials have emerged in the context of all the aforementioned phenomena. No matter whether dealing with photoactive polymers, liquid crystals, or crystals, the directionality of the halogen bond is the key to its success. Its tunability, on the other hand, provides unprecedented possibilities to carry out fundamental studies on light-induced motions unrelated to other types of material systems. The road is wide open, and the first steps taken are presented in the following sections.

3 Photoinduced Surface Patterning in Azopolymers: What Does Halogen Bonding Have to Offer?

Halogen bonding is a noncovalent interaction distinctively characterized by a quite high directionality [5]. In the case of hydrogen bonding, the electropositive area responsible for the attractive interaction formation is hemispherically distributed over the hydrogen atom. In contrast, in halogen bonding this positive area is narrowly confined in a well-defined area along the extension of the covalent bond involving the halogen atom, i.e., the σ-hole [2]. This difference typically renders halogen bonds more directional than hydrogen bonds [38, 39]. Many papers have been published recently on the coexistence or competition between halogen and hydrogen bonding in fields such as crystal engineering [40], anion recognition/sensing [41], and biochemistry [42]. In addition to the fundamental interest in halogen vs hydrogen bonding, a better understanding of the conditions when these intermolecular forces coexist or compete is highly pertinent from the viewpoint of potential technological applications of specialty supramolecular materials, fine-tuned to perform a desired function. Extensive studies have recently been carried out on the potential use of halogen-bonded supramolecular polymers for photoinduced surface patterning [11, 43]. These studies utilized an extensive molecular library of azobenzenes substituted with dimethylamino groups to

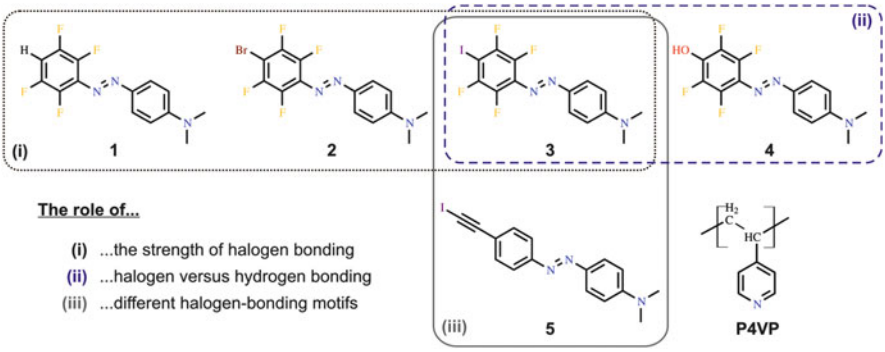

Fig. 3 Chemical structures of selected compounds studied in Priimagi et al. [11] and Saccone et al. [43]

promote SRG formation [44], and several halogen- and hydrogen-bond donor groups. Because of their structural similarities, molecules **1–5** shown in Fig. 3 provided excellent structures for investigating the role of the type/strength of noncovalent interaction on surface patterning efficiency. The SRG studies were conducted in spin-coated thin films containing a relatively small amount of the azobenzenes (10 mol%) in poly(4-vinyl pyridine) (P4VP), denoted as P4VP(**x**)$_{0.1}$, where **x** refers to the azobenzene molecule in question (**1–5**) and the subscript to the stoichiometry used. P4VP is a popular choice when constructing supramolecular polymeric complexes based on hydrogen bonding [45] and it also functions as a halogen-bond acceptor [46]. In the chromophore design, the unique possibility provided by halogen bonding to fine-tune the nature and strength of the polymer–dye interaction by single halogen atom mutation was exploited. Molecule **1** acts as a "reference" molecule, incapable of forming a halogen bond, but the acidic hydrogen can participate in weak (3.9 kcal/mol) hydrogen bonding. Molecules **2** and **3** contain bromine and iodine atoms as halogen-bond-donors, respectively, and their interaction strengths with pyridine units develop in the order **2** (3.5 kcal/mol) < **3** (5.1 kcal/mol) [11].

SRG formation on polymer–azobenzene complexes containing **1–3** was followed by in situ light-diffraction measurements (Fig. 4a) and ex situ atomic-force microscope observation (Fig. 4b), based on which the SRG formation efficiency strongly depends on the bond-donor unit: Both the diffraction efficiency of the gratings and the achieved modulation depth develop in the order **3** > **2** > **1**, i.e., I > Br > H. This suggests that (1) in the halogen-bonded complexes (**2** vs **3**) the surface patterning efficiency increases with the polymer-dye interaction strength and (2) halogen bonding, presumably caused by its higher directionality, is remarkably efficient in promoting the light-induced surface patterning process (**1** vs **2**) [11]. Thus, halogen bonding appears as a highly promising new tool for enhancing light-induced macroscopic movements in azopolymers, and, equally important, provides us with fundamental tools which are not apparent in more conventional polymer systems.

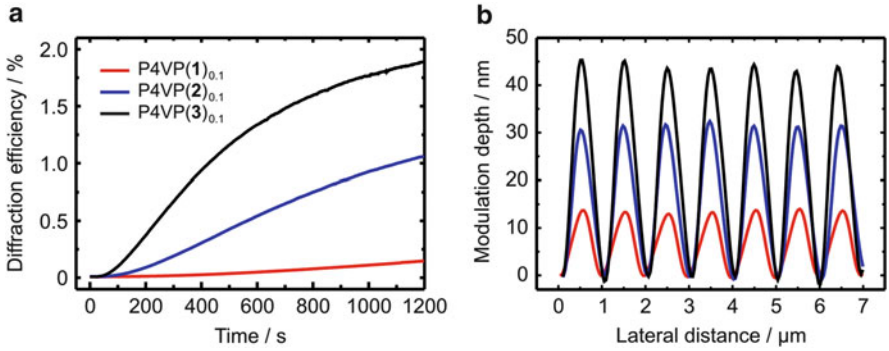

Fig. 4 Comparison between (**a**) the kinetics of the first-order diffraction efficiency and (**b**) the surface profiles of thin films of P4VP(**1**)$_{0.1}$, P4VP(**2**)$_{0.1}$, and P4VP(**3**)$_{0.1}$. The samples were spin-coated on silicon substrates and their thickness was 90 ± 5 nm. Redrawn with permission from Priimagi et al. [11]. Copyright 2012, Wiley

In Saccone et al. [43] the study was extended to compare the SRG formation driven by halogen bonding and strong (11.8 kcal/mol) hydrogen bonding in structurally similar perfluorinated azobenzenes (**3** vs **4**), and to compare the SRG formation triggered by different halogen-bond-donor motifs (**3** vs **5**). The single crystal X-ray characterization of trimeric 2:1 complexes of **4** and **5** with 1,2-bis (4-pyridyl)ethylene, used as a model compound for P4VP, nicely illustrates the structural features of the halogen- and hydrogen-bonded complexes (Fig. 5). Whereas the halogen-bonded trimers are highly linear, the hydrogen-bonded trimers adopt a zig-zag arrangement featuring extremely short O–H···N hydrogen bonds (the O···N distance is 2.556 Å, comparable to the shortest O–H···N hydrogen bond for which an O···N distance of 2.515 Å has been reported [47]) and arene-perfluoroarene quadrupolar interactions. These latter interactions may cause aggregation when **4** is complexed to P4VP, limiting its applicability, while they are not present in the halogen-bonded complex.

The diffraction efficiency curves for P4VP(**3**)$_{0.1}$ vs P4VP(**4**)$_{0.1}$, and for P4VP (**5**)$_{0.1}$ are shown in Fig. 6a. Two important conclusions can be drawn. First, although the final diffraction efficiency (and modulation depth) of the **3**- and **4**-based complexes are approximately equal, the diffraction efficiency rise is much faster for the halogen-bonded complex. This is despite the fact that the interaction strength is much weaker. Given that the chemical structures of the dyes are very similar, this is an unambiguous proof of the potential of halogen bonding in SRG formation. An inspection of the molecular electrostatic potential (MEP) surfaces of the compounds (Fig. 6b) supports the hypothesis that directionality is the distinctive feature responsible for the success of halogen bonding. Although the positive value of the MEP is much higher on the phenolic hydrogen of **4**, compared to that on the σ-hole of **3** and **5** (**4** > **5** > **3**), the positive area is spread out in **4**, while it is narrowly focused on the extension of the C–I bond in **3** and **5**. Second, there is a clear increase of the diffraction efficiency if **5** is used in place of **3**. This is presumably because of

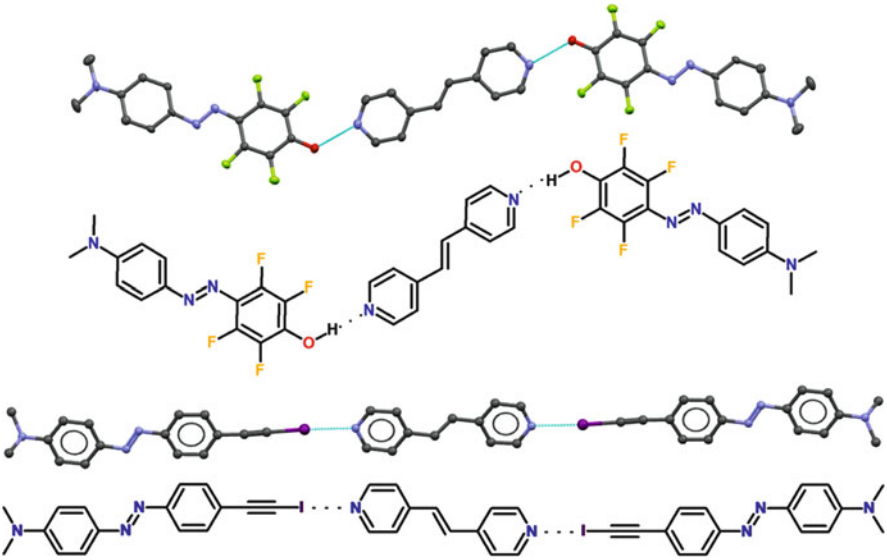

Fig. 5 Supramolecular trimers formed by **4** (*top*) and **5** (*bottom*) with 1,2-bis(4-pyridyl)ethylene as found by single crystal X-ray diffraction. The trimers are undulated for the hydrogen-bonded complex and linear for the hydrogen-bonded complex. Redrawn with permission from Saccone et al. [43]. Copyright 2014, Royal Society of Chemistry

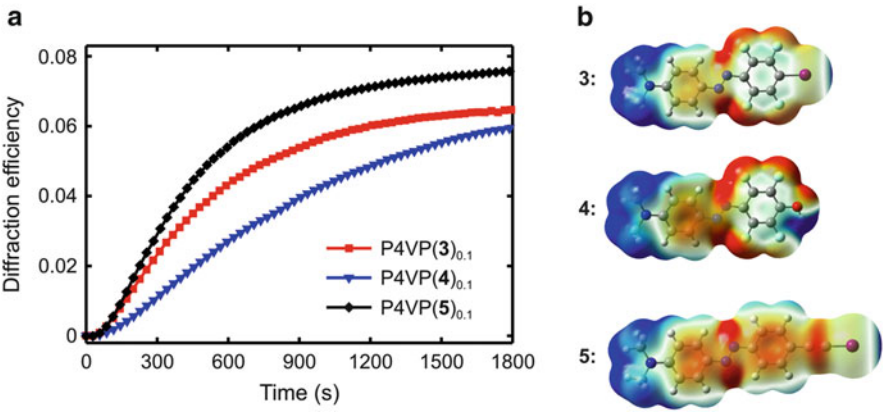

Fig. 6 (**a**) Diffraction efficiency curves for P4VP(**3**)$_{0.1}$ vs P4VP(**4**)$_{0.1}$, and for P4VP(**5**)$_{0.1}$. (**b**) Plots of the electrostatic potential of compounds **3**, **4**, and **5** computed at PBE0/6-311++G(d,p) level in vacuo. Potentials are mapped on the respective isosurfaces (0.001 a.u.) of electron density. Values of electrostatic potential range from −0.03 (*red*) to 0.03 (*blue*) a.u. Atom color scheme: C, *gray*; H, *light gray*; N, *dark blue*; O, *red*; F, *sky blue*, I, *magenta*. Redrawn with permission from Saccone et al. [43]. Copyright 2014, Royal Society of Chemistry

the more favorable photochemical properties of **5** compared to **3** [43]. We believe the directionality of halogen bonding provides a more rigid junction between the photoactive units and the polymer backbone, which in turn enhances the light-induced macroscopic motions in the system. These conclusions are relevant for both the halogen-bonding and SRG communities as they point out that the iodine attached to the acetylene moiety is a very reliable and strong halogen bonding donor, even stronger than that bound to a perfluorobenzene ring [48]. Furthermore, the use of a non-fluorinated dye to produce efficient optical response in supramolecular polymers may bring the advantage of avoiding aggregation and phase separation which may occur more easily when a significant fraction of the fluorinated dye is complexed to the P4VP.

4 Photoactive Halogen-Bonded Liquid Crystals

Liquid-crystal (LC) phases induced by halogen bonding were first reported in 2002 for supramolecular side-chain polymers [46] and were extended to thermotropic small-molecule complexes in 2004 [49]. The field has expanded over the years, as has also been reviewed recently [50]. The majority of halogen-bonded LCs are assembled by combining alkoxystilbazoles, widely used promesogenic molecules [51], with halogen-bond donors such as iodoperfluorobenzenes [52], iodoperfluoroalkanes [53], iodoacetylenes [54], and molecular iodine [55]. From these examples, one could argue that very strong halogen-bond donors are required to stabilize the high-temperature mesophases, and that only molecules containing highly electrophilic iodine atoms are suitable for the task. Indeed, this was demonstrated in Nguyen et al. [49] by showing that when complexing iodo- and bromopentafluorobenzene with alkoxystilbazoles, only the former exhibited LC behavior. This observation also demonstrates that quadrupolar interactions between benzene and perfluorobenzene rings are not responsible for the stability of the mesophases, but they are truly driven by halogen bonding. In the same paper it was also shown that the stability of the halogen-bond-driven LC phases is similar to those induced by hydrogen bonding [49].

The first example of halogen-bonded liquid crystal with additional functional properties appeared in 2012 when an azobenzene-based system capable of combining a high degree of photoinduced anisotropy and exceptionally efficient SRG formation was reported [12]. The structure of the complex is shown in Fig. 7. The design is rather unusual because of the lack of flexible alkyl chains, which have been reported to suppress the formation of SRGs in LC polymers [56].

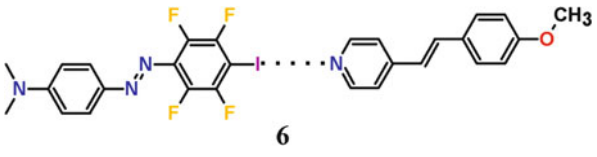

6

Fig. 7 Chemical structure of the halogen-bonded complex **6**

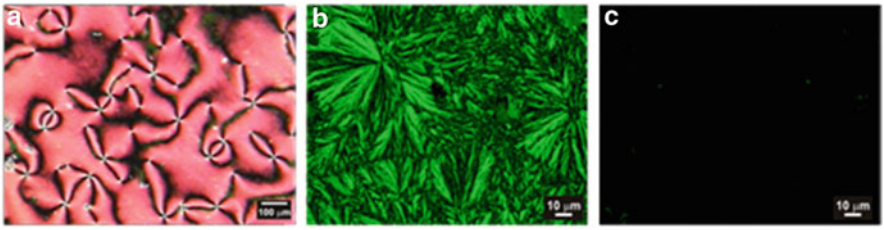

Fig. 8 (**a**) POM image of the nematic LC phase shown by **6** on cooling from the isotropic state. (**b**) POM image of a spin-coated (crystalline) thin film of **6**. (**c**) Upon irradiation with circularly polarized light (488 nm, 30 s, 100 mW/cm^2) the crystal structure is destroyed and the film becomes opaque when imaged between crossed polarizers. Redrawn with permission from Priimagi et al. [12]. Copyright 2012, Wiley

The azobenzene compound used also promotes efficient SRG formation because of the presence of the dimethylamino group [57]. The rod-like dimeric complex, formed thanks to a highly directional halogen bond, indeed exhibited a high-temperature monotropic nematic LC phase (I 405 N 387 K; see Fig. 8a), which in turn should promote photoalignment [58, 59]. The existence of halogen bonding was confirmed by X-ray diffraction and infrared and X-ray photoelectron spectroscopies [12]. Interestingly, when the same stilbazole molecule was complexed with 4-hydroxy-4′-dimethylaminoazobenzene, the noncovalent interaction being stronger but less directional, no LC phase was formed. Hence, it seems that the light-functional behavior of the complex is truly enabled by halogen bonding and cannot easily be obtained in complexes driven by other non-covalent interactions.

The light-responsive behavior of **6** was studied in non-annealed spin-coated thin films (thickness ca. 250 nm). The films were crystalline at room temperature (Fig. 8b), and exhibited relatively high optical scattering, which was strongly reduced even upon short irradiation with a 488-nm laser beam (30 s, 100 mW/cm^2, circular polarization; the wavelength was chosen to induce both *trans–cis* and *cis–trans* photoisomerization of the azobenzene). Such "pre-irradiation" transformed the pristine crystalline film (Fig. 8b) into an amorphous film (Fig. 8c). Upon irradiating the isotropic thin films with linearly polarized light (488 nm, 100 mW/cm^2) at room temperature, they became highly anisotropic (Fig. 9). Irradiation for 2 min led to a 49% decrease in the absorbance parallel to the polarization direction of the excitation beam, and a 38% increase in the absorbance in the perpendicular direction. This result is clear evidence of a photoinduced reorientation of the supramolecular complex **6**. Prior to irradiation, the molecular alignment is random, but excitation with linearly polarized light causes the molecules to align preferentially in the direction perpendicular to the polarization plane, which is seen as an increase in $A\perp$. The efficient photoalignment of **6** can be attributed to its high-temperature liquid crystallinity [59]. As mentioned above, the halogen-bonded supramolecular complex **6** exhibits not only efficient photoalignment capability, but is also able to form SRGs upon interference irradiation [12]. The gratings were inscribed on the same 250-nm film used for photoalignment studies, and, based on the AFM images

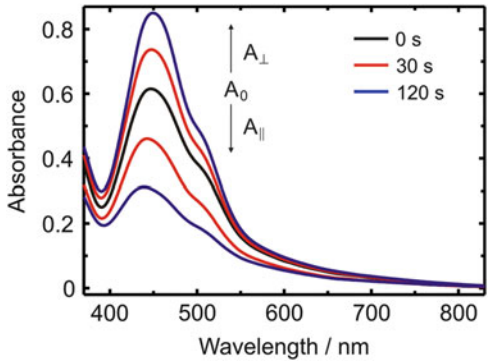

Fig. 9 Selected polarized absorption spectra of a spin-coated thin film of **6** after irradiation with linearly polarized light (488 nm, 100 mW/cm^2). *Black curve*: initial spectrum (same for both polarizations). The *red* and *blue curves* correspond to the polarized absorption spectra in the directions parallel ($A\| < A_0$) and perpendicular ($A\perp > A_0$) to the polarization plane, taken after 30 and 120 s of irradiation time, respectively. Redrawn with permission from Priimagi et al. [12]. Copyright 2012, Wiley

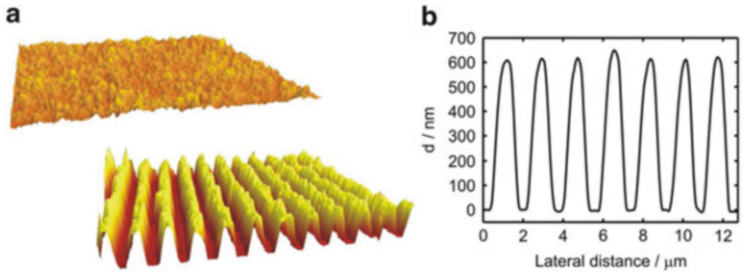

Fig. 10 (**a**) Atomic-force microscope views of the spin-coated thin film of **6** before (*top*) and after (*bottom)* SRG inscription (5 min, 300 mW/cm^2). (**b**) The surface-modulation depth of the grating shown in (**a**). Redrawn with permission from Priimagi et al. [12]. Copyright 2012, Wiley

of Fig. 10a, the troughs of the grating appear to be flat. The AFM surface profile of Fig. 10b shows that the modulation depth of the grating was 600 nm, 2.4 times higher than the initial film thickness. This is a clear indication that all material is removed from the troughs of the grating, and that the light-induced mass-transport efficiency of this halogen-bonded complex is exceptionally high. We refer the reader to Park et al. [60] for another example of a crystalline material with highly efficient grating formation ability.

Another example of photoresponsive liquid crystalline material based on halogen bonding appeared recently [61]. The idea here was to extend the concept of photoinduced order–disorder phase transition (Fig. 1c) from "conventional" photoresponsive LCs to halogen-bonded supramolecular complexes. To do this, the authors complexed azopyridines (AzPy) and molecular dihalogens (Fig. 11) in a

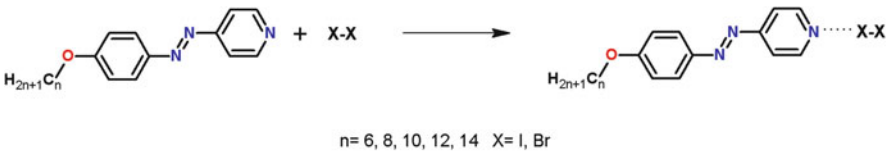

Fig. 11 Chemical structures of the halogen-bonded complexes used in Chen et al. [61]

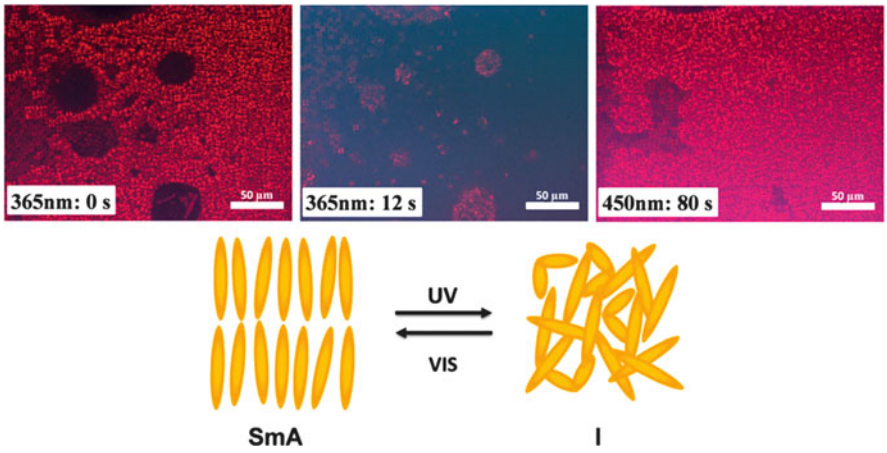

Fig. 12 Polarized light optical microscope observation of I_2-AzPy C12 at its LC phase upon UV irradiation. The *right picture* was obtained after irradiation with visible light for 80 s. Reproduced with permission from Chen et al. [61]. Copyright 2014, Royal Society of Chemistry

1:1 ratio. These adducts are closely related to those obtained by using alkoxystilbazoles and I_2 [55]. They were characterized by several techniques, Raman spectroscopy being particularly useful in identifying the complex formation. The stretching peak of the molecular iodine at 185 cm^{-1} moved to 159 cm^{-1} upon complexation, which is a clear sign of halogen bonding with the azopyridine. Polarized-optical microscopy revealed the presence of enantiotropic smectic A phases for all the Br_2-based complexes and for some of the I_2-based ones. It should be noted that the Br_2-complexes are the first halogen-bonded liquid crystals in which the bromine atom acts as a halogen-bond donor. In order to study the LC-to-isotropic phase transition, the complexes were irradiated with UV light at a temperature where the complexes exhibited LC phase. As shown in Fig. 12 for the complex I_2-AzPy having a C_{12} alkyl chain (I_2-AzPyC_{12}), the liquid crystallinity quickly disappeared upon photoirradiation, as evidenced by disappearance of the birefringent LC texture. This is a clear sign of photoinduced phase transition caused by *trans–cis* isomerization. The initial LC texture was recovered after the isotropic sample was irradiated with visible light or by thermal treatment. The highlighted studies provide valuable knowledge on the use of halogen bonding in the design and manipulation of functional supramolecular materials for photonic applications.

5 Halogen-Bonded Crystals That Move

One of the most intriguing features of azobenzene solids is the production of three-dimensional movements upon light irradiation (Fig. 1e). This photomechanical effect has been studied in several different systems and has led to a new category of photomobile smart materials which are attracting increasing attention for applications as light-driven actuators and micromachines [18, 36, 62]. The photoisomerization of azobenzenes has also recently been studied in crystalline materials despite the fact that the stereochemical change from the *trans* to the *cis* form and vice versa could be hindered in crystals. Single crystals of azobenzene indeed allow photoisomerization, and, when the crystals are sufficiently thin, they may give rise to rapid and, in some cases, reversible photomechanical effects [63, 64]. Very recently it has been argued [65] that, if kinetically persistent *cis*-azobenzenes could be synthesized, a *cis* → *trans* crystal-to-crystal isomerization (i.e., isomerization from the pristine crystalline form to the other stereoisomeric form without amorphization) could be achieved. Such compounds were reported in Bushuyev et al. [65]. In the material design, useful suggestions given in Bléger et al. [66] were taken into account, as it was found that extremely long *cis*-isomer half-lives are characteristic of *o*-fluorinated azobenzenes. Symmetrically substituted 4-haloperfluoro azobenzenes were thus prepared (Fig. 13a).

The half-lives of the compounds shown in Fig. 13a in a CH_2Cl_2 solution were found to be in the order of 2 months, which enabled the isolation of **7** and **8** in both *trans* and *cis* forms for structural characterization by single crystal X-ray diffraction (Fig. 13b). The photomechanical studies were performed using small (10–20 μm) crystals irradiated with a 457-nm laser beam, and revealed a fast and irreversible bending, with the tip of the crystal reaching angles up to 180° (Fig. 13c) [65]. The more efficient crystal packing of the *trans* form was the proposed explanation for the permanent bending. Powder X-ray diffraction studies confirmed the concomitant disappearance of the reflections of the *cis* form of the azodyes and the appearance of those corresponding to the *trans* form; moreover, the photoisomerization was also confirmed by single crystal X-ray diffraction on *post*-irradiated crystals.

In the above work, the photoinduced bending was studied in the pure compounds **7** and **8**, despite the fact that the perfluoroiodobenzene rings of **8** certainly act as halogen-bond donors potentially to form photomobile co-crystals. Such halogen-bonded azobenzene cocrystals have been studied now in two instances [67, 68]. In Saccone et al. [67], **8** was co-crystallized with a series of halogen-bond acceptors. As an example, Fig. 14 presents the crystal structure of the adduct (**8**):$(StOMe)_2$, where StOMe is the halogen-bond acceptor molecule shown in Fig. 7. Because StOMe is a monodentate halogen-bond acceptor, a trimeric adduct was obtained upon slow evaporation from THF. As expected, the main structure-driving factor is the N···I halogen bonding between the iodines of **8** and the pyridine nitrogens of StOMe. Interestingly, the iodotetrafluorobenzene and pyridyl rings of the (**8**):$(StOMe)_2$ trimers are not coplanar, and thus arene-perfluoroarene quadrupolar

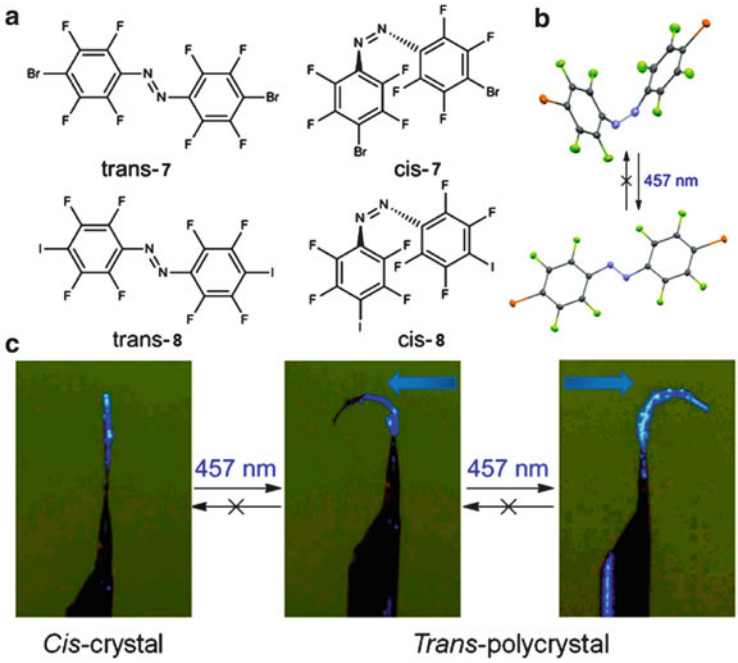

Fig. 13 (**a**) *cis* and *trans* forms of **7** and **8**. (**b**) *cis–trans* isomerization of **7** depicted with structures based on single crystal X-ray diffraction. (**c**) Irreversible bending of a thin crystal of *cis*-**7** by 457 nm light, with the *arrow* at the top of the figures indicating the direction of irradiation. Redrawn with permission from Bushuyev et al. [65]. Copyright 2013, American Chemical Society

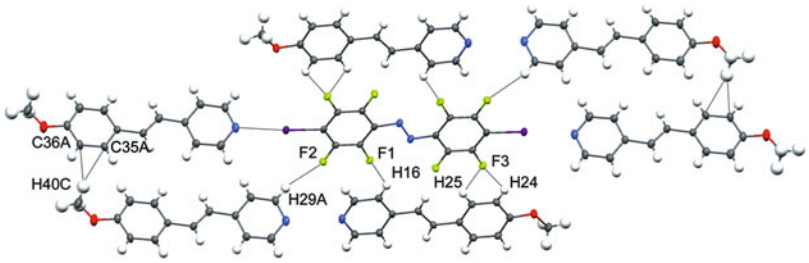

Fig. 14 Hydrogen bonds and C–H···π contacts in (**8**):$(StOMe)_2$. The disorder of the StOMe molecule has been omitted. Reproduced with permission from Saccone et al. [67]. Copyright 2014, Wiley

interactions [69] do not take place. In terms of distances and angles between the halogen-bond donor and acceptor, the (**8**):$(StOMe)_2$ trimer shares strong similarities with the compounds reported in Bruce et al. [52] but, interestingly, it is not liquid crystalline. The most important conclusion of this study was to assess the reliability of **8** as a halogen-bond donor capable of constructing various

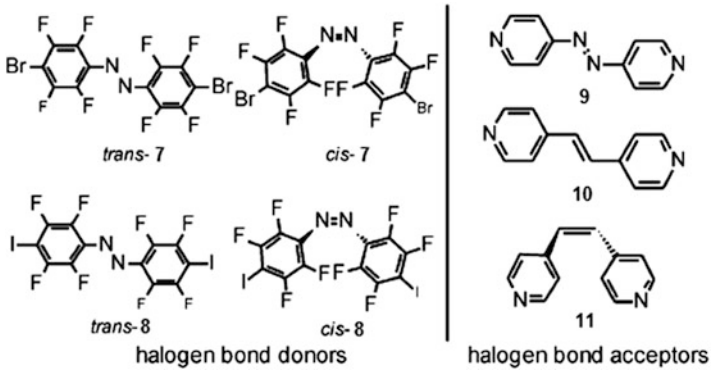

Fig. 15 The compounds used in Bushuyev et al. [68]

supramolecular structures in the solid state, a fact which could pave the way to the assembly of the first photoactive co-crystals.

The first halogen-bonded photomechanical cocrystals were published in 2014, employing materials shown in Fig. 15 [68]. They comprise compounds **7** and **8**, also used in Bushuyev et al. [65] and Saccone et al. [67], which function as halogen-bond donors, and the dipyridine derivatives (**9**, **10**, and **11**), one containing the *trans*-azo link, and the other two having the *trans* and *cis* C=C links, respectively. Co-crystals were obtained by slow evaporation of a concentrated 1:1 solution of the halogen-bond donor and acceptor, and the structural characterization revealed some of the features already observed in the co-crystals of **8** with other halogen-bond acceptors [67] (Fig. 16).

As anticipated, thanks to the directionality of halogen bonding, the geometry of the synthons involved in the non-covalent interaction is translated in the geometry of the final supramolecular structure [4]. This is clearly evident in the crystal packing of (*cis*-**7**)(**10**) and (*trans*-**7**)(**10**). In the latter, the linear structure of the tectons is maintained in the crystal, in which infinite chains are held together by Br···N halogen bonds and π–π stacking, while the V-shape of the *cis* form of **7** imposes a zigzag geometry (Fig. 16a, b). It should be noted that in the "all-*cis*" co-crystal (*cis*-**8**)(**11**), no π–π stacking interactions are present (Fig. 16d). All the co-crystals containing the *cis* form of **7** and **8** exhibit a photomechanical behavior which is very sensitive to the differences in crystal packing. For example, the irradiation power required for the crystal to bend as well as the deflection angle of the crystal seem to follow the efficiency of the crystal packing, given as calculated volume per non-hydrogen atom in a unit cell. The already mentioned "all-*cis*" co-crystal (*cis*-**8**)(**11**) requires a low irradiation power of 5 mW cm^{-2} to bend, and the deflection angle exceeds 90°, while it exhibits the least efficient crystal packing with a volume per non-hydrogen atom in a unit cell of 16.6 $Å^3$. The mixed *cis–trans* co-crystals, including **7** and **8** with **10**, display a denser packing than the former co-crystal and, as a consequence, the

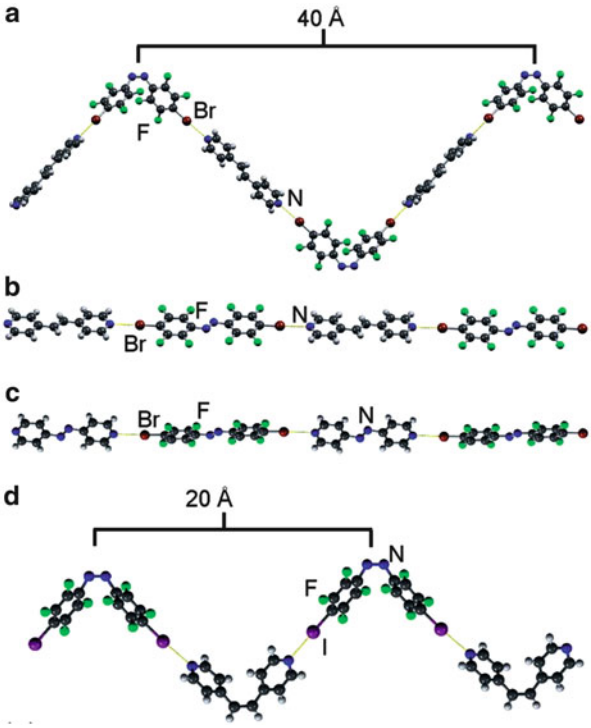

Fig. 16 (**a**) Zigzag structure of a chain in the (*cis*-**7**)(**10**) cocrystal. Linear structure of supramolecular chains: (**b**) in the (*trans*-**7**)(**10**) cocrystal and (**c**) in the (*trans*-**7**)(**9**) cocrystal. (**d**) Zigzag structure of a (*cis*-**8**)(**11**) chain. Redrawn with permission from Bushuyev et al. [68]. Copyright 2014, Royal Society of Chemistry

Table 1 Photomechanical behavior of the co-crystals studied in Bushuyev et al. [68]

Cocrystal	Irradiation power ($mW \cdot cm^{-2}$)	Deflection angle (°)	Volume per non-H atom in the unit cell ($Å^3$)	Volume per non-H atom in the unit cell for corresponding cocrystal of *trans*-**7** or -**8** ($Å^3$)
(*cis*-**8**)(**11**)	5	>90	16.6	16.1
(*cis*-**8**)(**10**)	60	10	15.8	15.1
(*cis*-**7**)(**10**)	60	9	15.4	15.0
(*cis*-**8**)(**9**)	200	4	15.4	15.4
(*cis*-**7**)(**9**)	200	3	14.8	14.8

bending of the crystals is less efficient (lower deflection) and requires higher irradiation power (60 mW cm^{-2}). The most efficient packing is held by the co-crystals containing the **9** molecule which bends only very slightly with high power (Table 1).

As discussed in Bushuyev et al. [65], single-crystal X-ray diffraction on irradiated samples revealed the occurrence of the *cis–trans* isomerization within

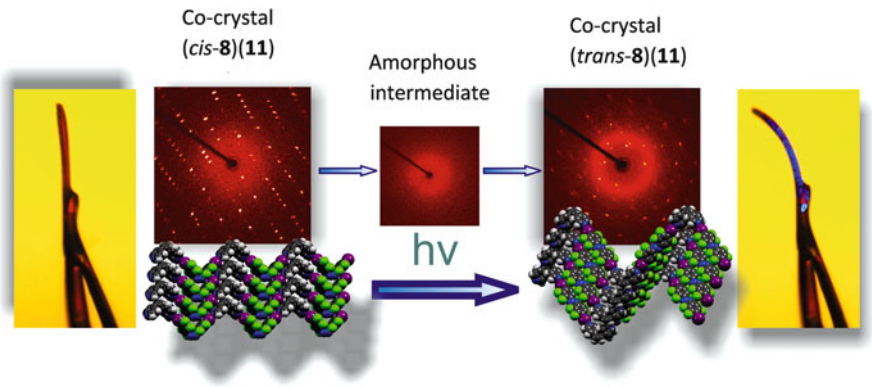

Fig. 17 Photoinduced bending of halogen-bonded cocrystals, followed by in situ X-ray diffraction reveals that the transition from the unbent *cis* single crystal to the bent polycrystalline *trans* state proceeds through an amorphous intermediate phase. Reproduced with permission from Bushuyev et al. [68]. Copyright 2014, Royal Society of Chemistry

the crystal, in this case (*cis*-**8**)(**11**). Surprisingly, the crystal remained of high quality even after irradiation, enabling the structure determination. Furthermore, for the first time, the isomerization process was followed by probing the changes in the X-ray diffraction pattern of the co-crystals. Disappearance of reflections of the (*cis*-**8**)(**11**) co-crystal and appearance of those of the *trans*-**8** product suggest a transformation mediated by an amorphization process followed by recrystallization (Fig. 17). The *cis–trans* isomerization and bending of the co-crystal (*cis*-**8**)(**11**) were also probed with differential scanning calorimetry and hot-stage microscopy, the latter revealing a slight mechanical bending upon reaching the temperature at which the isomerization took place [68].

6 Conclusions

We have brought out the potential of halogen bonding in the field of photoresponsive azobenzene-containing materials through several examples employing polymeric, liquid crystalline, and crystalline materials. Clearly the well-established key features of halogen bonding, namely strength and directionality, are responsible for the great performances of the halogen-bond-driven adducts. In the case of photoactive polymers, these two features ensure a rigid and linear polymer-dye junction which allows for high performance in terms of light-induced surface patterning efficiency [11, 43]. The directionality of halogen bonding is responsible for the self-assembly of a highly photoresponsive liquid-crystalline complex, capable of combining exceptionally efficient surface-relief

grating formation and a high degree of photoalignment [12]. The strength of halogen bonding provides rigid mesogenic complexes which undergo photoinduced phase transitions from liquid-crystalline to amorphous phase and vice versa by light irradiation [61]. Last but not least, the ubiquitous presence of perfluorinated synthons in halogen bonding structures [65, 67] has allowed the production of photoresponsive molecules with very long *cis–trans* half-lives, suitable for the self-assembly of the first photomobile co-crystals [68]. Although the first photoactive halogen-bonded materials were reported only in 2012, the field has already proved to be interesting and there are plenty of other directions to be investigated. For example, the concepts of multivalency and cooperativity [69] have been poorly exploited with halogen bonding [70] compared to other specific interactions such as hydrogen bonding [71] or metal coordination [72]. These concepts proved to be useful for the self-assembly of efficient supramolecular materials and nanomachines [69] and hopefully are soon to be exploited in the field of halogen bonding. Many other interesting properties of halogen-bonded photoresponsive materials are, therefore, expected to be revealed in the near future.

References

1. Desiraju GR, Ho PS, Kloo L, Legon AC, Marquardt R, Metrangolo P, Politzer P, Resnati G, Rissanen K (2013) Pure Appl Chem 85:1711–1713
2. Clark T (2013) WIRES Comput Mol Sci 3:13–20
3. Legon AC (1999) Angew Chem Int Ed 38:2686–2714
4. Saccone M, Cavallo G, Metrangolo P, Pace A, Pibiri I, Pilati T, Resnati G, Terraneo G (2013) CrystEngComm 15:3102–3105
5. Metrangolo P, Meyer F, Pilati T, Resnati G, Terraneo G (2008) Angew Chem Int Ed 47:6114–6127
6. Wilcken R, Zimmermann MO, Lange A, Joerger AC, Boeckler FM (2013) J Med Chem 56:1363–1388
7. Ding X, Tuikka M, Haukka M (2012) Halogen bonding in crystal engineering. In: Benedict JB (ed) Recent advances in crystallography. InTech, New York, pp 143–168
8. Scholfield MR, Vander Zanden CM, Carter M, Ho PS (2013) Protein Sci 22:139–152
9. Priimagi A, Cavallo G, Metrangolo P, Resnati G (2013) Acc Chem Res 46:2686–2695
10. Meyer F, Dubois P (2013) CrystEngComm 15:3058–3071
11. Priimagi A, Cavallo G, Forni A, Gorynsztejn-Leben M, Kaivola M, Metrangolo P, Milani R, Shishido A, Pilati T, Resnati G, Terraneo G (2012) Adv Funct Mater 22:2572–2579
12. Priimagi A, Saccone M, Cavallo G, Shishido A, Pilati T, Metrangolo P, Resnati G (2012) Adv Mater 24:OP345–OP352
13. Kravchenko A, Shevchenko A, Ovchinnikov V, Priimagi A, Kaivola M (2011) Adv Mater 23:4174–4177
14. Dhammika Bandara HM, Burdette SC (2012) Chem Soc Rev 41:1809–1825
15. Mativetsky JM, Pace G, Elbing M, Rampi MA, Mayor M, Samorì P (2008) J Am Chem Soc 130:9192–9193
16. Ceroni P, Credi A, Venturi M (2014) Chem Soc Rev 43:4068–4083
17. Yu H, Ikeda T (2011) Adv Mater 23:2149–2180
18. Mahimwalla Z, Yager KG, Mamiya J, Shishido A, Priimagi A, Barrett CJ (2012) Polym Bull 69:967–1006

19. Natansohn A, Rochon P (2002) Chem Rev 102:4139–4175
20. Ikeda T (2003) J Mater Chem 13:2037–2057
21. Wiswanathan NK, Kim DY, Bian S, Williams J, Liu W, Li L, Samuelson L, Kumar J, Tripathy SK (1999) J Mater Chem 9:1941–1955
22. Ikeda T, Mamiya JI, Yu Y (2007) Angew Chem Int Ed 46:506–528
23. Dumont M, El Osman A (1999) Chem Phys 245:437–462
24. Yaroshchuk O, Reznikov Y (2012) J Mater Chem 22:286–300
25. Seki T, Nagano S, Hara M (2013) Polymer 54:6057–6072
26. Priimagi A, Kaivola M, Virkki M, Rodriguez FJ, Kauranen M (2010) J Nonlinear Opt Phys 19:57–73
27. Aissou K, Shaver J, Fleury G, Pécastaings G, Brochon C, Navarro C, Grauby S, Rampnoux JM, Dihaire S, Hadziioannou G (2013) Adv Mater 25:213–217
28. Rochon P, Batalla E, Natansohn A (1995) Appl Phys Lett 66:136–138
29. Kim DY, Tripathy SK, Li L, Kumar J (1995) Appl Phys Lett 66:1166–1168
30. Laugugné Labarthet F, Buffeteau T, Sourisseau C (1998) J Phys Chem B 102:2654–2662
31. Priimagi A, Shevchenko A (2014) J Polym Sci B Polym Phys 52:163–182
32. Lee S, Kang HS, Park JK (2012) Adv Mater 24:2069–2103
33. Zettsu N, Ogasawara T, Mizoshita N, Nagano S, Seki T (2008) Adv Mater 20:516–521
34. Priimagi A, Barrett CJ, Shishido A (2014) J Mater Chem C 2:7155–7162
35. White TJ, Tabiryan NV, Serak SV, Hrozhyk UA, Tondiglia VP, Koerner H, Vaia RA, Bunning TJ (2008) Soft Matter 4:1796–1798
36. Yamada M, Kondo M, Mamiya JI, Yu Y, Kinoshita M, Barrett CJ, Ikeda T (2008) Angew Chem Int Ed 47:4986–4988
37. Cheng F, Yin R, Zhang Y, Yen CC, Yu Y (2010) Soft Matter 6:3447–3449
38. Shields Z, Murray JS, Politzer P (2010) Int J Quantum Chem 110:2823–2832
39. Politzer P, Murray JS, Clark T (2013) Phys Chem Chem Phys 15:11178–11189
40. Corradi E, Meille SV, Messina MT, Metrangolo P, Resnati G (2000) Angew Chem Int Ed 39:1782–1786
41. Chudzinski MG, McClary CA, Taylor MS (2011) J Am Chem Soc 133:10559–10567
42. Voth AR, Khuu P, Oishi K, Ho PS (2009) Nat Chem 1:74–79
43. Saccone M, Dichiarante V, Forni A, Goulet-Hanssens A, Cavallo G, Vapaavuori J, Terraneo G, Barrett CJ, Resnati G, Metrangolo P, Priimagi A (2014) J Mater Chem C. doi:10.1039/C4TC02315C
44. Vapaavuori J, Valtavirta V, Alasaarela T, Mamiya JC, Priimagi A, Shishido A, Kaivola M (2011) J Mater Chem 21:15437–15441
45. Brinke GT, Ikkala O (2004) Chem Rec 4:219–230
46. Bertani R, Metrangolo P, Moiana A, Perez E, Pilati T, Resnati G, Rico-Lattes I, Sassi A (2002) Adv Mater 14:1197–1201
47. Steiner T, Majerz I, Wilson CC (2001) Angew Chem Int Ed 40:2651–2654
48. Aakeröy CB, Baldrighi M, Desper J, Metrangolo P, Resnati G (2013) Chem Eur J 19:16240–16247
49. Nguyen HL, Horton PN, Hursthouse MB, Legon AC, Bruce DW (2004) J Am Chem Soc 126:16–17
50. Bruce DW (2012) Liquid crystals formed from specific supramolecular interactions. In: Gale PA, Steed JW (eds) Supramolecular chemistry: from molecules to nanomaterials. Wiley, Chichester
51. Bruce DW (2001) Adv Inorg Chem 52:151–204
52. Bruce DW, Metrangolo P, Meyer F, Präsang C, Resnati G, Terraneo G, Whitwood AC (2008) New J Chem 32:477–482
53. Metrangolo P, Präsang C, Resnati G, Liantonio R, Whitwood AC, Bruce DW (2006) Chem Commun 3290–3292
54. González L, Gimeno N, Tejedor RM, Polo V, Ros MB, Uriel S, Serrano JL (2013) Chem Mater 25:4503–4510

55. McAllister LJ, Präsang C, Wong JPW, Thatcher RJ, Whitwood AC, Donnio B, O'Brien P, Karadakov PB, Bruce DW (2013) Chem Commun 49:3946–3948
56. You F, Paik MY, Häckel M, Kador L, Kropp D, Schmidt HW, Ober CK (2006) Adv Funct Mater 16:1577–1581
57. Zhang Q, Wang X, Barrett CJ, Bazuin CG (2009) Chem Mater 21:3216–3227
58. Zakrevskyy Y, Stumpe J, Faul CFJ (2006) Adv Mater 18:2133–2136
59. Kreger K, Wolfer P, Audorff H, Kador L, Stingelin-Stutzmann N, Smith P, Schmidt HW (2010) J Am Chem Soc 132:509–516
60. Park JW, Nagano S, Yoon SJ, Dohi T, Seo J, Seki T, Park SJ (2014) Adv Mater 26:1354–1359
61. Chen J, Yu H, Zhang L, Yang H, Lu Y (2014) Chem Commun 50:9647–9649
62. van Oosten CL, Bastiaansen CWM, Broer DJ (2009) Nat Mater 8:677–682
63. Koshima H, Ojima N, Uchimoto H (2009) J Am Chem Soc 131:6890–6891
64. Bushuyev OS, Singleton TA, Barrett CJ (2013) Adv Mater 25:1796–1800
65. Bushuyev OS, Tomberg A, Friščić T, Barrett CJ (2013) J Am Chem Soc 135:12556–12559
66. Bléger D, Schwarz J, Brouwer AM, Hecht S (2012) J Am Chem Soc 134:20597–20600
67. Saccone M, Terraneo G, Pilati T, Cavallo G, Priimagi A, Metrangolo P, Resnati G (2013) Acta Cryst B 70:149–156
68. Bushuyev OS, Corkery TC, Barrett CJ, Friščić T (2014) Chem Sci 5:3158–3164
69. Badjić JD, Nelson A, Cantrill SJ, Turnbull WB, Stoddart JF (2005) Acc Chem Res 38:723–732
70. Voth AR, Hays FA, Ho PS (2007) Proc Natl Acad Sci U S A 104:6188–6193
71. Prins LJ, Reinhoudt DN, Timmerman P (2001) Angew Chem Int Ed 40:2383–2426
72. Cotton FA, Lin C, Murillo CA (2001) Acc Chem Res 34:759–771

Top Curr Chem (2015) 359: 167–204
DOI: 10.1007/128_2014_552

Published online: 1 October 2014

Halogen Bonds in Organic Synthesis and Organocatalysis

S. Schindler and Stefan M. Huber

Abstract In contrast to hydrogen bonding, halogen bonding has so far found very little use in organic synthesis and organocatalysis. Although there are multiple reports on the use of elemental iodine in a wide range of organic reactions, the understanding of the actual mode of activation in these cases is very rudimentary. Recently, first proof-of-principle reactions have been established towards the use of carbon-based halogen-bond donors as activators or organocatalysts. These halogen-based Lewis acids offer more structural variety and potential than elemental iodine itself, and the mode of activation is better understood. Yet, the reported cases still only cover simple benchmark reactions, and there is a clear need for further and more complex applications.

Keywords Halogen bonding · Noncovalent interactions · Organocatalysis · Supramolecular chemistry

Contents

S. Schindler and S.M. Huber (✉)
Ruhr-University Bochum, Universitätsstraße 150, 44801 Bochum, Germany
e-mail: stefan.m.huber@rub.de

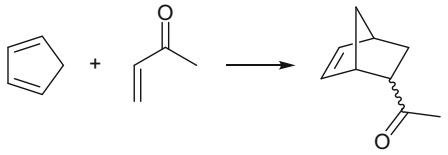

Scheme 1 Typical Diels–Alder reaction

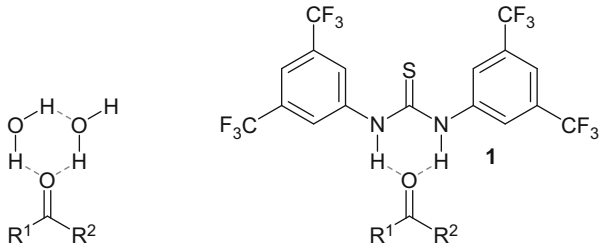

Fig. 1 Carbonyl activation by water and thiourea derivative **1**

1 Hydrogen Bonding in Non-covalent Organocatalysis

Hydrogen bonds are ubiquitous in nature. As arguably the most important type of non-covalent interactions, hydrogen bonds are crucial for various processes of life and also allow for the specific binding of substrates in enzyme pockets [1]. Consequently, generations of researchers have mimicked nature to develop applications of hydrogen bonds in chemistry with ever-increasing complexity and control [2, 3].

The effect of hydrogen bonding on the rate of a chemical reaction is best illustrated by the Diels–Alder reaction between cyclopentadiene and an α,β-unsaturated carbonyl compound (Scheme 1).

This reaction is more than two orders of magnitude faster in water than when using isooctane as solvent [4]. Jorgensen rationalized this effect by the coordination of two water molecules to the oxygen atom of the carbonyl group (Fig. 1, left) [5, 6].

Hine [7] and Kelly [8] were the first to prepare synthetic equivalents of this bidentate motif, using biphenylene diols as catalysts. Shortly after Etter had studied the hydrogen bonding patterns in supramolecular assemblies of various carbonyl compounds [9, 10], Curran introduced diarylurea derivatives as further bidentate organocatalysts [11, 12]. This interplay between supramolecular chemistry and non-covalent catalysis has turned out to be very fruitful ever since [13–15]. Schreiner subsequently showed that thioureas are also potent organocatalysts, which offer several advantages compared to urea derivatives, e.g., better solubility [13, 16]. In a proof-of-principle study, thiourea derivative **1** (Fig. 1, right) was used to catalyze the Diels–Alder reaction shown in Scheme 1 [16].

The first *enantioselective* transformation catalyzed by chiral hydrogen-bond donors was reported by Jacobsen et al. in 1998 [17]. His group demonstrated that

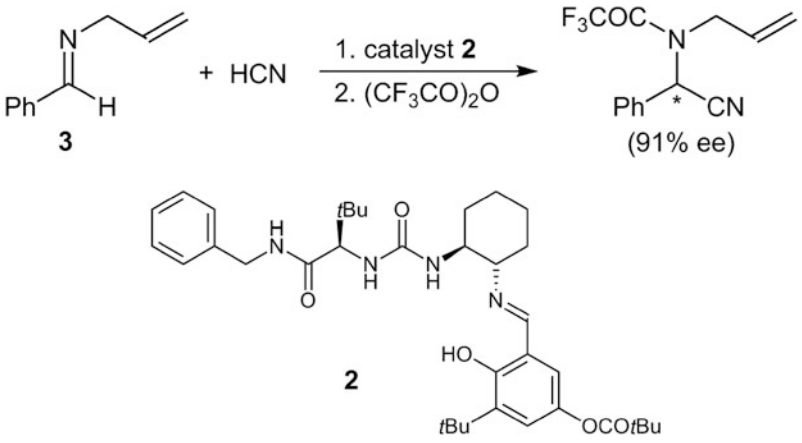

Scheme 2 Strecker reaction with catalyst **2** [17]

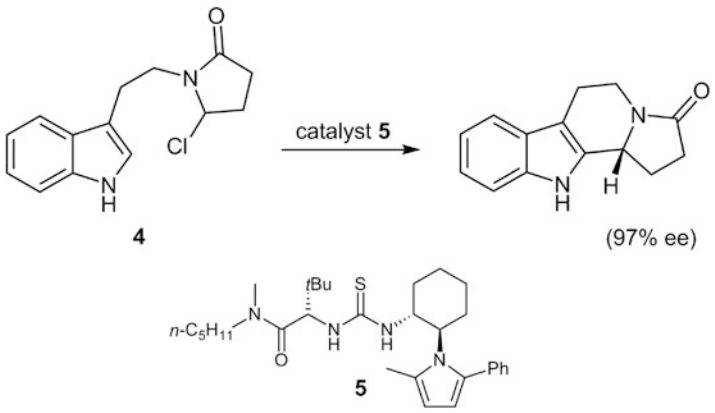

Scheme 3 Pictet–Spengler reaction catalyzed by **5** [23]

urea derivatives like **2** induce high enantioselectivity (91% *ee*) in the Strecker reaction shown in Scheme 2. Initially, it was proposed that the urea binds in a bidentate fashion to the nitrogen atom of imine **3** [18]. Later, the mechanism was revised and it was shown that in fact the urea coordinates to the cyanide anion of HCN, directing its attack towards the imine [19]. This reaction thus classifies as a variant of asymmetric counterion-directed catalysis [20–22].

Subsequently, this anion-binding-based mechanism was transferred to various other anions and reactions [20–22]. In 2007, Jacobsen reported the organocatalytic enantioselective Pictet–Spengler cyclization shown in Scheme 3 [23]. In the course of the reaction, thiourea derivative **5** binds to chloride liberated from intermediate **4** (which is generated in situ from the corresponding hydroxylactam). This

represented the first case in which the binding of an organocatalyst to a halide was exploited [14].

By now, thiourea derivatives and other hydrogen-bond donors are well established as non-covalent organocatalysts for the activation of neutral substrates or for anion-binding-based transformations, and numerous further examples have been reported for both variants [13–15, 24, 25].

2 Halogen Bonding in Organic Synthesis and Non-covalent Organocatalysis

2.1 Further Directional Interaction: Halogen Bonding

As described above, non-covalent organocatalysis has so far been almost exclusively based on hydrogen bonding. There are, however, alternative weak but directional interactions which may also be used in this area. Most notably this applies to halogen bonding ("XB"), i.e., the interaction between a Lewis base and an electrophilic halogen substituent (Fig. 2) [26–32]. Even though this kind of adduct formation can, energetically, be as favorable as a medium-strength hydrogen-bond [33], the interaction was all but ignored [27, 28, 34, 35] until the 1990s [36–46].

Strong halogen-bond donors R–X (halogen-based Lewis acids) typically rely on highly electronegative – either perfluorinated or cationic – backbones R [26, 29–31]. Alternatively, strong halogen-bond donors are also obtained for highly polarizable substituents R, as in the case of elemental iodine [47–50]. The directionality of halogen bonds is even stronger than that of hydrogen bonds, with R–X–LB angles typically very close to 180°. This illustrates that halogen bonding is not merely a weak van-der-Waals type interaction, but rather one which also comprises contributions from electrostatic [51, 52] and $n \rightarrow \sigma^*$ charge-transfer interaction terms [28, 53–56]. The degree to which electrostatic and charge-transfer terms contribute to the overall interaction energy depends on the actual halogen-bond donor and Lewis base under consideration, but it is noteworthy that the high directionality of the interaction seems to be best explained by charge-transfer contributions ([57] and references cited therein) (arising from the donation of electron density from the lone pair of the Lewis base into the σ* orbital of the R–X bond).

As weak non-covalent interactions are best observed in crystal structures, it is not surprising that halogen bonding was at first mainly explored in the solid state, where it now constitutes a reliable design principle for crystal engineering [26, 29, 58–61]. In contrast, applications in solution have been relatively sparse until a few years ago, with one notable exception being the work of Sandorfy in the 1970s [62]. In recent years, however, the number of applications in the liquid phase has seen a steady increase [63, 64]. This especially concerns the development of

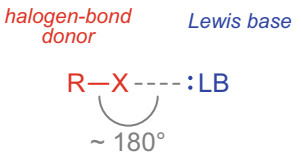

Fig. 2 Halogen bonding between halogen-bond donor and Lewis base

halogen-bond-based anion receptors, with important contributions by the groups of Resnati/Metrangolo [42], Beer [45, 46], and Taylor [43, 44].

These anion receptors also point towards a potential use of halogen-bonds in organocatalysis, based on the fact that successful hydrogen-bond-based non-covalent organocatalysts like thioureas are typically also powerful anion receptors [13, 14]. A demonstrative indication that the comparison with hydrogen-bond donors is valid was reported in 2000, when Resnati, Metrangolo et al. could show that the formation of polymeric non-covalent networks between diamines and polyfluorinated halogen-bond donors may outcompete the adduct formation with hydrogen-bond donors like diphenols [33] – especially since the latter constitute an early class of noncovalent organocatalysts [8]. In light of all this, it is somewhat surprising that halogen bonding has so far found very little use in organic synthesis and organocatalysis, as will be discussed in more detail below.

Compared to hydrogen bonds, which are already well established in this field, halogen bonds feature some distinct differences which are of direct relevance to the aspired applications. First, as already mentioned, the directionality is markedly higher for halogen bonds. As a consequence, the margin of error in the design of multidentate Lewis acids is much lower for the halogen-based variants. In the long term, however, this might also constitute an advantage, as the selectivity of multidentate halogen-bond donors towards different substrates might likewise be higher. Second, polyfluorinated backbones which are often the basis of strong halogen-bond donors are much lower in polarity compared to typical functional groups forming the basis of hydrogen bond donors (amides, ureas, alcohols) and thus at least the polyfluorinated types of halogen-bond donors could be considered as the "hydrophobic" counterparts to the rather hydrophilic hydrogen-bond donors [65, 66]. Accordingly, the solubility of halogen-based Lewis acids in apolar solvents will likely be advantageous. Finally, and most obviously, halogen bonding is based on a different type of interacting atoms. As there are several halogens, the interaction can be tuned by the substitution of one halogen substituent (e.g., iodine) by another (e.g., bromine). More importantly, halogens are more polarizable and bigger in size than hydrogen. In the context of the hard and soft acids and bases (HSAB) theory [67, 68], halogen-bond donors would be qualified as "softer" Lewis acids compared to hydrogen-bond donors – which should have consequences for the substrate preference of future halogen-based organocatalysts.

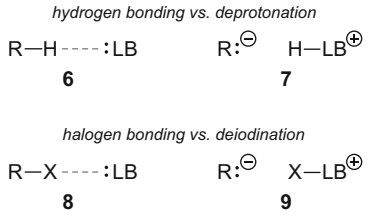

Fig. 3 Non-covalent adducts vs atom transfer

2.2 Overview and Scope

In the following we will summarize the reported cases in which halogen bonding has been utilized as a non-covalent interaction in organic synthesis. Given that halogen substituents play an important role in organic chemistry and are involved in a multitude of chemical reactions, it is important to define precisely the boundaries of halogen bonding in this context, which will also delineate the scope of this review.

A hydrogen-bond adduct between a Lewis base and a hydrogen-bond donor could also be considered as a "frozen deprotonation": the Lewis base donates electron density into the σ* orbital of the R–H bond and thus typically weakens and elongates the bond, but not to the point of an actual cleavage of the R–H bond. The hydrogen-bonded complex **6** is then a stable, thermodynamic minimum (Fig. 3). If, however, a (stronger) Lewis base donates sufficient electron density into the σ* orbital to actually cleave the R–H bond, deprotonation occurs and the product **7** consists of two fragments, $R^{(-)}$ and $H\text{-}LB^{(+)}$. In the latter case, **6** is not a stable minimum, but resembles or equals the transition state of the deprotonation **7**.

This differentiation, which is certainly simplified to some degree, applies in a very analogous fashion to halogen bonding: if the interaction between the halogen-bond donor and the Lewis base becomes too strong, the result will not be a stable non-covalent adduct like **8**, but the products of a dehalogenation reaction **9**. In the latter case, the halogen bonding between R–X and LB has merely transient character.

One typical example of the occurrence of "halogen bonding" in a *transient* species is the bromination of alkenes: its textbook description involves a non-covalent precursor complex **10**, in which the Br–Br – alkene angle is linear (Scheme 4). Subsequently, the Br–Br bond is broken, and a bromonium intermediate **11** is created. The latter process could also be described as a debromination of the strong halogen-bond donor dibromine by the alkene, or as an "X-philic" [69] S_N2-type reaction at bromine.

Similarly, intermediates which may be described as halogen-bond-based adducts play an important role in halogen–metal exchange reactions (Scheme 5) [70].

Scheme 4 Bromination of alkenes

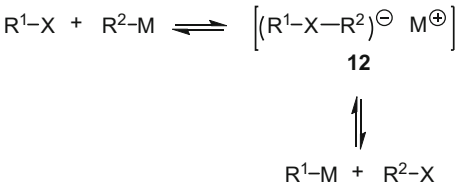

Scheme 5 Halogen-metal exchange reaction with intermediate **12**

Reaction of a metallated carbon nucleophile R′–M with an organohalogen compound R–X leads to an "ate complex" **12** [71, 72], the relevance of which in lithium–halogen exchange reactions was postulated as early as 1958 by Wittig [71]. Experimental evidence for this intermediate was subsequently obtained by Reich [73, 74], and in 1986 Farnham reported the first isolation of such an (iodine-based) 10-I-2 [75] ate complex [76]. In 1998, Hoffmann reported a related ate complex as an observable intermediate in an iodine–magnesium exchange reaction [77]. In the further course of the reaction, these intermediates are converted to the end products R′–X and R–M [78].

There are numerous other cases in organic synthesis in which a transition state or a transient local minimum involves (what is nowadays called) [32, 79, 80] halogen bonding, but in which ultimately the R–X bond of the (original) halogen-bond donor is cleaved. This literature is much too extensive to include in this review.

In the following, we will instead focus (almost) exclusively on applications of halogen bonding in organic synthesis, in which the R–X bond of the halogen-bond donor stays intact over the course of the complete reaction. In these cases, the halogen-bond donor forms a stable adduct R–X – LB with the Lewis base, featuring a "covalent" R–X bond and a markedly weaker "non-covalent" X – LB bond. The presented literature covers papers up until late 2013 and is comprehensive to the best of our knowledge, although the search in the early literature is somewhat complicated by the fact that the term "halogen bonding" was introduced relatively late [35, 79–81].

The subsequent chapters are ordered according to the nature of the halogen-bond donor used, starting with solely halogen-based Lewis acids and then turning towards nitrogen- and especially carbon-based halogen-carrying backbones.

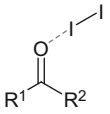

Fig. 4 Postulated non-covalent activation of carbonyl compounds by iodine [106]

2.3 Solely-Halogen-Based Halogen-Bond Donors

Halogen atoms themselves are also very suitable backbones R to form strong halogen bond donors R–X. Out of the many feasible combinations which would generate potent Lewis acids, very few have actually seen use in organic synthesis in a (possibly) "non-covalent" fashion as defined above.

2.3.1 Elemental Halogens[1]

Concerning the elemental halogens, fluorine and chlorine are only slightly electrophilic if at all, but are very reactive, and so they do not form "non-covalent" adducts in the sense mentioned in the Sect. 2.2. The same is true, to a lesser extent, for elemental bromine. Although it is known, for instance, from the side-on complexes of bromine with benzene derivatives that bromine may act as a halogen-bond donor [82–85], these kinds of adducts are typically of a pre-reactive nature and lead to bromination of the substrates by Br–Br bond cleavage (see also Scheme 4) [82].

Strong halogen-bond donors R–X are not only obtained for very electronegative backbones R, but also for strongly polarizable ones [47–49]. Thus, elemental iodine is a strong halogen-bond donor, and its binding constants with various Lewis bases have been determined in solution [50].

There is also ample literature on the use of elemental iodine – either in stoichiometric or catalytic amounts – in organic synthesis. This chemistry has been covered in two reviews from 2006 and 2011 [86–88], and a multitude of further cases of iodine-mediated or iodine catalyzed transformations have been published since then [89–104]. Lately, two more specialized reviews on the use of iodine in protection/deprotection reactions [105] and in reactions involving oxygen-containing functional groups [88] have appeared.

Some of the reported reactions, especially those involving stoichiometric amounts of iodine, are clearly based on modes of action not related to halogen bonding, e.g., utilizing the oxidation potential of iodine or introducing an iodine substituent in the final product. In numerous cases, however, the activity of iodine is postulated to be based on its Lewis acidity, e.g., its interaction with carbonyl compounds as Lewis bases (Fig. 4) [86–88, 107].

[1] We will not consider here the formation of (inter)polyhalogen compounds like tribromide or triiodide as side- or by-products, e.g., in halogenation reactions.

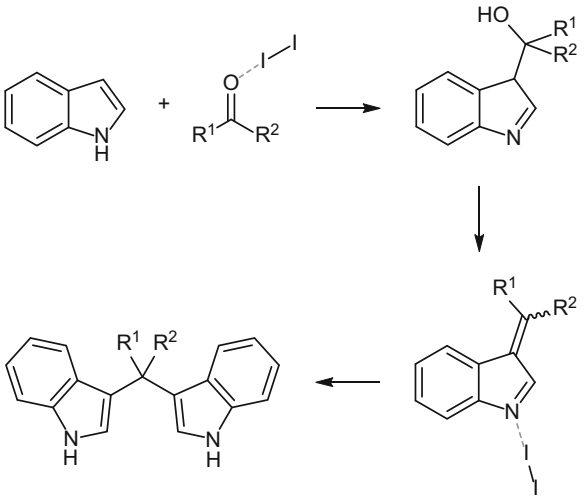

Scheme 6 Iodine-catalyzed addition of indole to ketones

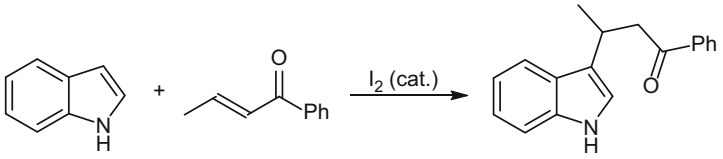

Scheme 7 Iodine-catalyzed Michael addition

Examples for which this type of activation by iodine has been postulated cover a wide variety of organic transformations, including, e.g., Strecker-type reactions [108], acetal formation and cleavage [105], imine formation [86–88], and Michael additions [86–88]. Two representative reactions are shown in Scheme 6 (nucleophile addition to ketones) [106] and Scheme 7 (Michael addition) [89].

The use of elemental iodine in organic synthesis suffers from two drawbacks, however: first, there is obviously no possibility to modify the catalyst, e.g., to obtain a chiral variant, and second, it is often very difficult to elucidate the exact mode of action of iodine in the respective reaction. In a review from 2011 [88], Jereb et al. state that "there is an open debate about the nature of the actual catalyst in I_2-catalyzed reactions, particularly when conducted in protic solvents. There are a plethora of papers, but very little mechanistic explanation is given. (. . .) A large majority of the publications have operated with tentative schemes; many have speculated about HI or ROI formation as the driving force." Similarly, in a review from 2006 [87], Togo et al. conclude that "in all these reactions (. . .) a small amount of hydrogen iodide formed through the reaction of iodine with the substrate or solvent is a key species for the reaction." Indeed, it is well known that iodine may form hydrogen iodide in solvents like methanol [109].

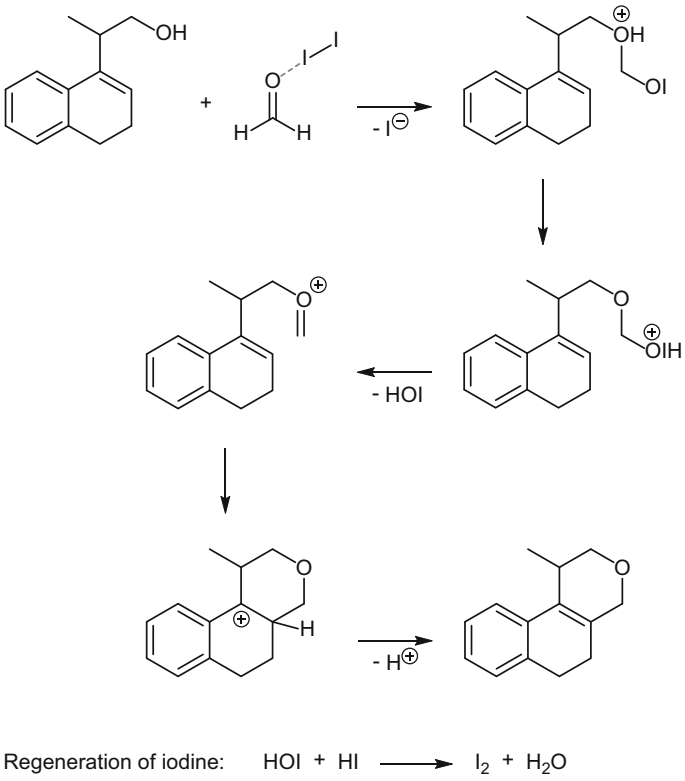

Scheme 8 Postulated mechanism for iodine-catalyzed reaction

To complicate things further, some iodine-catalyzed reactions which seem to operate via a non-covalent activation may in fact involve an I–I cleavage step, with subsequent regeneration of the (only seemingly unaffected) catalyst [102, 110, 111]. One such postulated example is given in Scheme 8 [110].

Thus, at the moment it is difficult to say whether (or to which extent) the type of activation depicted in Fig. 4 is indeed relevant for the reported cases of iodine catalysis. Although no conclusive mechanistic studies have been published, in a few cases it could be shown by comparison experiments that hydrogen iodide is less active than iodine in the respective reaction (for an example, see Scheme 7) [89, 90]. While this rules out hidden acid catalysis, there is clearly a need for further detailed mechanistic investigations of iodine-catalyzed reactions.

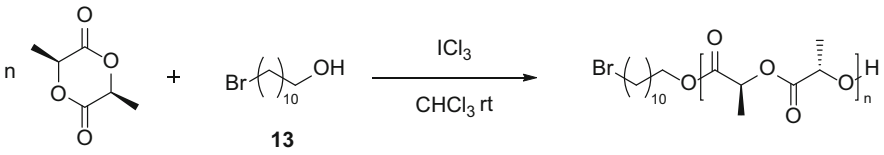

Scheme 9 Polymerization of L-lactide to poly(L-lactide) with ICl_3

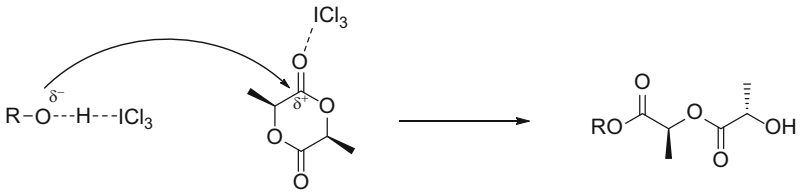

Scheme 10 Proposed mechanism of the twofold activation

2.3.2 Interhalogen Compounds

To the best of our knowledge, there is only one case in which an interhalogen compound has been used as a halogen bonding[2] catalyst. Coulembier et al. reported that iodine trichloride (ICl_3) catalyzes the ring-opening polymerization of L-lactide [112]. Using different spectroscopic methods, they found that the iodine(III) compound activates both the monomer L-lactide and the initiator **13** (11-bromo-1-undecanol) via halogen and hydrogen bonding respectively (Scheme 9).

More specifically, a significant shift of the C=O vibrational band in FT-IR spectroscopy occurred when titrating L-lactide with ICl_3. Increased equivalents of the XB donor induced a shift towards higher wavenumbers. This trend matches the theory of halogen bonding, being considered as a charge transfer from oxygen to iodine. Furthermore, NMR titration of L-lactide and ICl_3 in a 1:1 ratio led to a second set of signals shifted to the low field region in the carbon spectrum. As for the initiator, a significant shift of the hydroxylic proton after addition of ICl_3 points towards the formation of a hydrogen bond between the two compounds. Based on these observations, the mechanism of the polymerization seems to proceed via an activation of both initiator **13** and monomer by HB and XB, respectively (Scheme 10). The elucidation of the reaction mechanism faces a similar challenge to that of the reactions catalyzed by elemental iodine; however, it is very difficult to determine whether and to what extent acid traces also play a role in the activation, especially since it is known that iodine trichloride hydrolyzes to give HCl and HIO_3

[2] This example involves an iodine(III) species as halogen-bond donor R–X. The recent IUPAC definition of halogen bonding (2013, Pure Appl Chem 85:1711) states that "X may be covalently bound to more than one group".

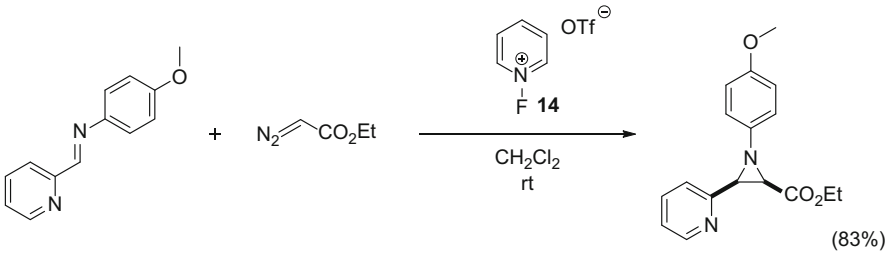

Scheme 11 Aziridine synthesis in the presence of N–F compound **14**

[113]. It is also uncertain whether more than one molecule of ICl_3 is necessary to cleave the L-lactide.

Using a monomer/initiator/catalyst ratio of 174/1/15, 86% conversion of the L-lactide was observed. The resulting poly(L-lactide) chains showed a molecular weight of 21,600 g/mol and a degree of polymerization of ca. 150. An advantage of this reaction is the fact that no additional activator for the initiator is necessary, as ICl_3 acts as a twofold initiator.

2.4 N–X-Based Halogen-Bond Donors

Owing to the relatively high electronegativity of nitrogen, N–X compounds also constitute strong halogen-bond donors. Some applications of N–X-based halogen bond donors have been postulated to include halogen bonding as a mode of activation. More precisely, there is one report on an N–F-based organocatalyst, and several papers involving reactions of *N*-halosuccinimides.

Concerning the first variant, Bew et al. reported the use of *N*-fluoropyridinium triflate as an "F^+ organocatalyst" for the aziridine synthesis from imines and ethyl diazoacetates [114]. Catalytic amounts of the fluorinated pyridinium salt **14** are claimed by the authors to function as a source for the fluorenium cation F^+ which presumably activates the imine component, thus facilitating the following nucleophilic attack of ethyl diazoacetate leading to the aziridine system (Scheme 11).

The mechanism of activation could either involve formal F^+ transfer from the pyridinium salt to the imine, or the formation of a halogen bond between the N–F reagent and the imine. While organic compounds with fluorine substituents generally do not act as electrophilic halogen bond donors, several exceptions have been reported [115].

N-Halosuccinimides with chlorine, bromine, or iodine substituents at the nitrogen are well-known electrophilic halogenating reagents in organic chemistry [116, 117]. Their mode of action likely involves the formation of a halogen-bond-like transient species similar to those described above (Fig. 3). Some publications mention that the NXS compound (X=Br, I) can be activated by the addition of a

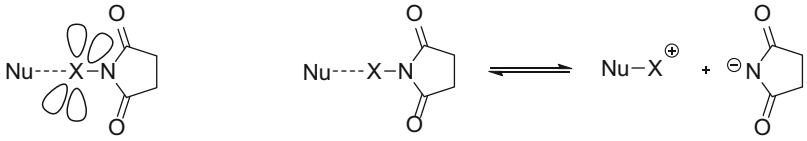

Scheme 12 Activation of NXS by nucleophile (Nu)

nucleophile [118–120]. Halogen bonding adducts of the type shown in Scheme 4 have indeed been characterized structurally for *N*-iodosuccinimide complexes [121]. However, it is implausible that these complexes constitute the actual "activated species" which is responsible for the halogenation. Since the nucleophile complexes the halogen atom from the opposite direction of the X–N bond, the halogen atom is surrounded by two of its lone pairs and two substituents, but lacks any electrophilic region (see Scheme 12, left).

Instead, it is more likely that the N–X-bond is cleaved heterolytically, resulting in an equilibrium with the adduct $[Nu–X]^+$ (Scheme 12, right; Nu=nucleophilic activator). The latter then reacts with the nucleophilic compound to be halogenated. As the N–X bond is likely broken, these reactions are not directly relevant in the specific context introduced above, and only a few illustrative cases will be mentioned (for recent events: [122]). One impressive example is the enantioselective halocyclization of polyprenoids which is carried out under addition of 1 equiv. of a chiral nucleophilic phosphoramidite. This nucleophilic phosphoramidite abstracts halenium ions from NIS or NBS via the phosphor atom to form a tight ion pair which then initiates the cyclization reaction by coordination to a double bond in the substrate [123].

A reaction mixture of DBU and NBS was also shown to promote several amination and imidation reactions, such as the α-imidation of ketones in an one-pot reaction, the β-amination of chalcones and allylic aminations [118–120]. All these reactions proceed via a bromenium transfer from NBS to DBU to form the actual reactive species, as described in Scheme 12.

2.5 C–X-Based Halogen-Bond Donors

2.5.1 Monodentate Halogen-Bond Donors

As carbon is less electronegative than nitrogen, C–X-based halogen-bond donors are less Lewis acidic than N–X-based ones, but at the same time also more stable towards C–X bond cleavage than the latter. In this chapter we will focus on monodentate C–X-based halogen-bond donors, i.e., halogen-based Lewis acids that may only form one halogen bond to a substrate (irrespective of their number of halogen substituents).

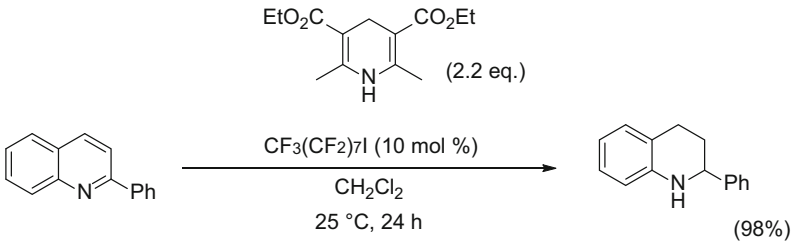

Scheme 13 Reduction of 2-phenylquinoline in the presence of 1-iodoperfluorooctane

The first case in which organocatalysis by halogen bonding was postulated, a report by Bolm et al. in 2008 [124], in fact involves C–X-based halogen-bond donors. As a test reaction, the reduction of quinoline derivatives by a Hantzsch Ester was chosen. Previously, this type of reaction had been reported to proceed enantioselectively with Ir[COD]Cl_2/(*S*)-SegPhos or chiral Brønsted acids (Scheme 13) [125].

While no appreciable formation of the reduced product was observed without addition of a catalyst, yields increased to up to 98% with the addition of various halogen bond donors. XB donors employed in this series of experiments were terminally mono-brominated or mono-iodinated perfluoroalkanes. Brominated catalysts showed lower conversions of 2-phenylquinoline than iodinated ones (at comparable alkane chain lengths). This observation is consistent with the order of XB strength for different halogen substituents (I > Br > Cl) [26]. Furthermore, a trend towards higher yields for longer perfluoroalkane chain length could be observed. This effect is also in accordance with XB theory, as a more electron-withdrawing group R usually leads to a stronger XB donor R–X.

Further evidence that the activation is based on halogen bonding was obtained via NMR spectroscopy. While no signal shifts could be observed in the proton spectra, the carbon and fluorine spectra turned out to be more helpful. Significant shifts were detected for quinoline carbon atoms and all fluorine atoms, especially the CF_2I-group. These kinds of shifts had been observed in the context of halogen bond formation before [126]. Thus, it was postulated that a halogen bond is formed between the iodine atom of the catalyst and the quinoline nitrogen, which activates the substrate for reduction by the Hantzsch ester. Comparison experiments with non-iodinated compounds or traces of acid were not performed [64]. The substrate scope of the reaction was expanded towards several 2- and 6-substituted quinolines, and it was shown that electron-poor quinolines are reduced more readily.

Apart from the interaction between catalyst and substrate, halogen bonds can also be used in other aspects of organic synthesis. For example, Legros et al. employed a perfluorinated XB donor to facilitate the recycling of the actual organocatalyst of the reaction. This application was based on the concept to non-covalently tag the catalyst with perfluorinated alkane chains (“pony tailing”) [127], so that the resulting fluorophilic complex readily precipitates from some

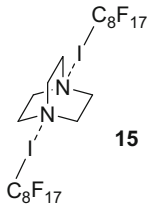

Fig. 5 Halogen-bond based complex **15** of DABCO and 1-iodoperfluorooctane

organic solvents and can be separated by a simple filtration from the reaction mixture. Due to the comparably weak strength of non-covalent halogen bonds, the catalyst can subsequently easily be recovered.

More specifically, Legros et al. used 1-iodoperfluorooctane to recycle the organocatalyst DABCO (1,4-diazabicyclo[2.2.2]octane) after it had promoted a Morita–Baylis–Hillman reaction [128]. Preliminary ^{19}F-NMR experiments showed a strong shift of the CF_2I group of 5.15 ppm towards higher field upon addition of 0.5 equiv. of DABCO. Once again, this is a good indication of halogen bond formation between iodine and nitrogen, presumably leading to a 2:1 complex (see Fig. 5).

The catalyst was added as adduct **15** to the reaction mixture of 2,4-dichlorobenzaldehyde and methyl acrylate in methanol, and the Morita–Baylis–Hillman product **16** was obtained in 90% yield. After completion of the reaction, the catalyst complex could be precipitated from the reaction mixture by addition of dichloromethane and acetonitrile (Scheme 14).

The catalyst recycled by this protocol could be reused in up to five consecutive runs. Recovery rates for **15** lay between 91% and 77% whereas yields of product **16** gradually dropped from 90% in the first cycle to 64% in the fifth. Thus, by recovering and recycling the catalyst, the amount of chemical waste can be diminished, which is an important aspect of green chemistry.

Another application of halogen bonding in organic synthesis concerns the ligand arrangement of metal-organic catalysts.

Charette et al. examined a Rh(II)-carboxylate catalyst with four amino acid derived *N*-phthaloyl ligands [129]. This catalyst has seen widespread use, for example in the cyclopropanation of alkenes with diazo compounds. Depending on the orientation of these ligands (up or down), four different symmetries are possible. Previous studies were unable to clarify which is the enantioselectively active one (Scheme 15).

While low enantiomeric excesses (2–43%) were obtained with the *N*-phthaloyl species (i.e., **17** and **19**), the tetrachlorinated analogues **18** and **20** had considerably higher enantioselectivities (80–93% *ee*). Crystal structures of **17** and **18** revealed that the C_4 symmetry ("all-up") is predominant for both cases in the solid phase. Furthermore, the distance between the phthaloyl moieties is somewhat shorter in the case of **18**. Distances between chlorine atoms and oxygen atoms of the adjacent phthaloyl group range from 3.21 to 3.84 Å and are even shorter for tetrabrominated

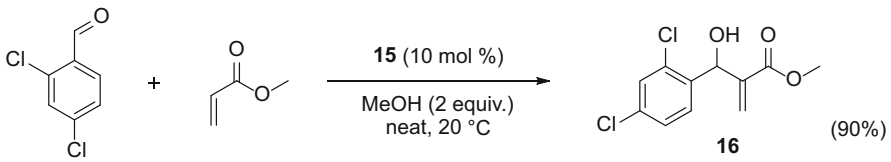

Scheme 14 Morita–Baylis–Hillman reaction catalyzed by adduct **15**

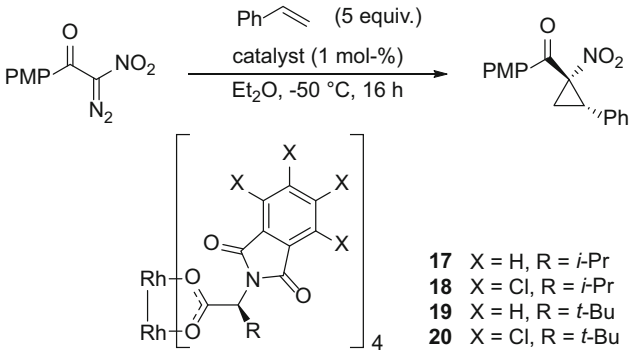

Scheme 15 Cyclopropanation reaction with different Rh catalysts

ligands (3.08–3.78 Å). These short distances are an indication of the formation of halogen bonds.

To determine whether the catalyst remains in this conformation in solution, ^{1}H-^{13}C heteronuclear NOESY experiments were set up. If one of the ligands flips, nOe (nuclear Overhauser effect) contacts between the side chain protons and the phthaloyl carbons should be visible. No cross peaks were detected in the case of **20**, meaning that the all-up conformation is also predominant in solution, whereas cross peaks in the spectrum of **19** indicated that the C_4 symmetry is not maintained in solution. Variable temperature NMR experiments with **20** confirmed this, as the aromatic carbon atoms give rise to two singlets at room temperature, which merge into one broad singlet at higher temperatures (comparable to the spectrum of **19** at room temperature).

In conclusion, the "all-up" conformation appears to be the one leading to high enantioselectivities. One side of the metal center is shielded by the side chains of the amino acids, whereas the other forms part of the tight reactive pocket created by the ligands. Most importantly, in the case of the polychlorinated ligands, this favorable conformation is likely supported by halogen bonding.

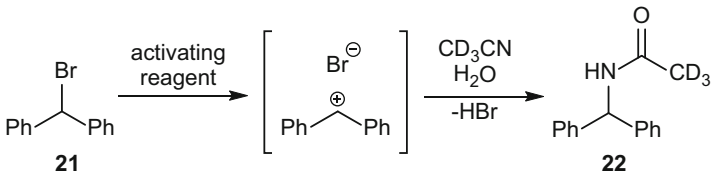

Scheme 16 Solvolysis of benzhydryl bromide as test reaction

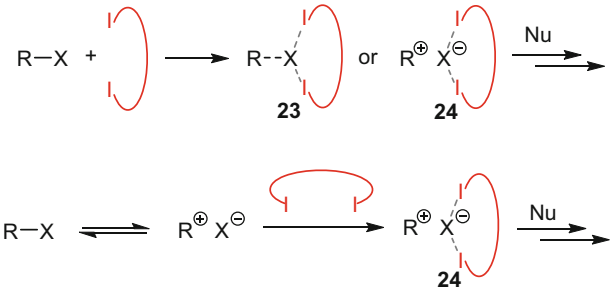

Scheme 17 Possible modes of activation of XB donors (shown in *red*) and halogenated substrates

2.5.2 Multidentate Halogen-Bond Donors

Proof-of-Principle Reaction

Inspired by the pioneering work on halogen-based multidentate anion receptors [42–46, 130], our group aspired to use multidentate halogen-bond donors as activators or catalysts in organic synthesis. Since it is also well known from crystallographic studies that halides are very potent halogen-bond acceptors (Lewis bases), our first goal was to use halogen-based Lewis acids in formal halide abstraction reactions. In these cases, a comparatively weak carbon–halogen bond is cleaved in solution to enable subsequent S_N1-type reactivity. The halogen-bond donor either binds to a halide which is liberated in equilibrium from the substrate or coordinates to the C–X bond of the substrate, weakens it, and thus actively abstracts the halogen anion. Similar applications based on hydrogen-bond donors, mainly thiourea derivatives, are already known [13, 14, 20–22].

In a first proof-of-principle study, we chose benzhydryl bromide **21** as a test substrate, since this compound features a relatively weak C–Br bond. If the corresponding benzhydryl carbocation is formed (see Scheme 16) and no further nucleophiles are added, the solvent (acetonitrile) will attack the cation and form a nitrilium ion intermediate. Finally, traces of water in the solvent will hydrolyze this species to from *N*-benzhydryl acetamide **22** in an overall Ritter-like reaction. The formation of this product from benzhydryl bromide can easily be followed by ^{1}H-NMR spectroscopy.

As already indicated, the halogen-bond donor may act via several different mechanisms, which may also occur in parallel (see Scheme 17). By coordinating

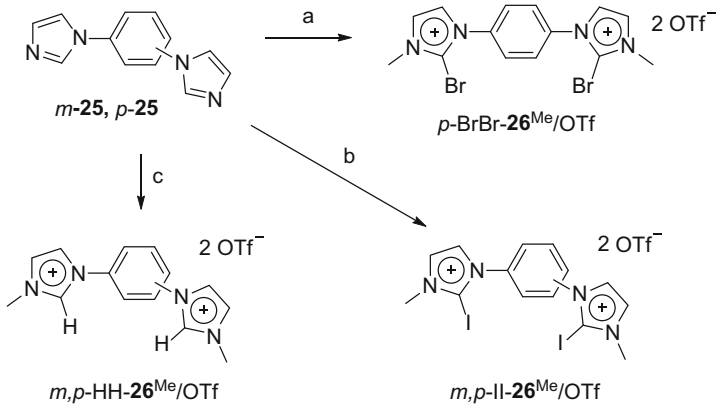

Scheme 18 Synthesis of bis(imidazolium)-based XB donors and reference compounds. (Path a) 1. *n*-BuLi (2.3 equiv.), THF, −78°C; CBr_4 (2.0 equiv.), THF, −78°C; 2. MeOTf (5.6 equiv.), CH_2Cl_2. (Path b) 1. *n*-BuLi (2.6 equiv.), THF, −78°C; I_2 (2.4 equiv.), THF, −78°C; 2. MeOTf (4 equiv.), CH_2Cl_2; c) MeOTf (4 equiv.), CH_2Cl_2

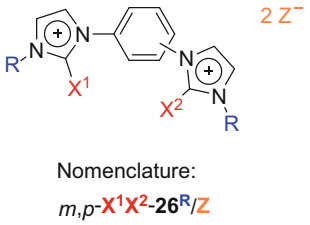

Fig. 6 Nomenclature for bis(imidazolium) compounds

to the bromine atom of the C–Br bond, the Lewis acid would polarize the bond further and weaken it, facilitating the following S_N2-type attack of the nucleophile (see **23** in Scheme 17). Alternatively, and much more likely for this kind of substrate, is an S_N1-type reactivity where the C–Br bond is broken to form a carbocation **24** as intermediate. This cation may also form in solution in a heterolysis equilibrium, from which the halogen-bond donor would remove the halide by complexation. Currently, there is insufficient data to discern between the latter two mechanistic pathways.

The halogen-bond donors applied in this test reaction consist of a benzene core with two halogenated imidazolium moieties. The synthesis started with literature-known bis(imidazoles) **25** in *meta* or *para* configuration which were first treated with base (*n*-BuLi) and then brominated or iodinated using CBr_4 or iodine, respectively. Subsequent *N*-methylation with methyl triflate gave the bis(imidazolium) activator as triflate salt in good overall yield. The non-halogenated compound for reference experiments could be obtained by direct methylation of **25** (Scheme 18).

To simplify and structure the nomenclature of the bis(imidazolium) compounds, the abbreviation system given in Fig. 6 is used.

The solvolysis of benzhydryl bromide did not proceed without addition of activator under the chosen reaction conditions. Traditional monodentate XB donors such as 1,4-diiodoperfluorobenzene and 1,3,5-triiodoperfluorobenzene did not increase yields of **22**. Bidentate cationic XB donors *m*,*p*-II-**26**^{Me}/OTf based on the imidazolium motif, however, lead to a yield of more than 80% of **22** under otherwise unaltered reaction conditions.

As mentioned earlier, in catalyses by elemental iodine or perfluorinated iodoalkanes [86–88, 124] it is sometimes difficult to rule out that traces of acid contribute at least partially to the observed reactivity. Thus, in this study our goal was to show as unambiguously as possible that halogen bonding is indeed responsible for the activation of the substrate. In the solvolysis reaction of benzhydryl bromide, accidental acid catalysis by impurities can safely be ruled out as the use of even 1 equiv. of the strong acid HOTf (trifluoromethanesulfonic acid) yields only 25% of **22** under otherwise identical conditions. Furthermore, trace amounts of acid can be quenched by the addition of 10 mol% of pyridine to the reaction, whereas the effect of the bis(iodoimidazolium) activators is only marginally affected by this additional component.

As it is conceivable that the activation by the halogen-bond donors may also be based on acidic protons at the imidazolium backbones, or other interactions apart from halogen bonding, a further comparison experiment was performed with the analogous non-iodinated species. As these compounds *m*-HH-**26**^{Me}/OTf and *p*-HH-**26**^{Me}/OTf lead to only about 7% product formation, however, strong indications point towards halogen bonding as the actual mode of activation.

Furthermore, 2 equiv. of the mono-iodinated analogue *p*-HI-**26**^{Me}/OTf give a 49% yield of **22**, as opposed to 80% in case of the di-iodinated analogue. As the number of electrophilic halogen centers in solution is identical in both cases, this finding points towards a bidentate coordination of the bis(imidazolium) halogen-bond donors towards the substrate, as anticipated.

Brominated analogue *p*-BrBr-**26**^{Me}/OTf showed lower conversions than iodinated activators, which is in accordance with XB theory since iodine features a better polarizability. Furthermore, X-ray- and NMR-data support the formation of halogen bonds. Single crystals of *p*-II-**26**^{Me}/OTf already show a contact between iodine and oxygen from the weakly coordinating counterion triflate with an O–I distance of 2.84 Å, significantly shorter than the sum of the van der Waals radii (3.50 Å) [131]. In addition to that, X-ray structural analysis of a cocrystal of *m*-II-**26**^{Me}/BPh_4 with TBA bromide reveals a bidentate binding of the bromide to the halogen-bond donor with I–Br distances of 3.12 and 3.23 Å (Fig. 7). In both crystals the angle C–I $\cdots$ X is close to 180°, which is another characteristic of halogen bonds [26, 57].

Apart from these observations in the solid phase, indications for halogen bonding were also obtained in the liquid phase. First, NMR-experiments were conducted with regard to the chemical shift of the imidazolium carbon atom bearing the iodine. The singlet shifts from $\delta = 102.4$ ppm by about 9 ppm towards the downfield upon treatment with 1 equiv. of tetrabutylammonium bromide. A downfield-shift of this proportion is in agreement with halogen bond theory and the donation of

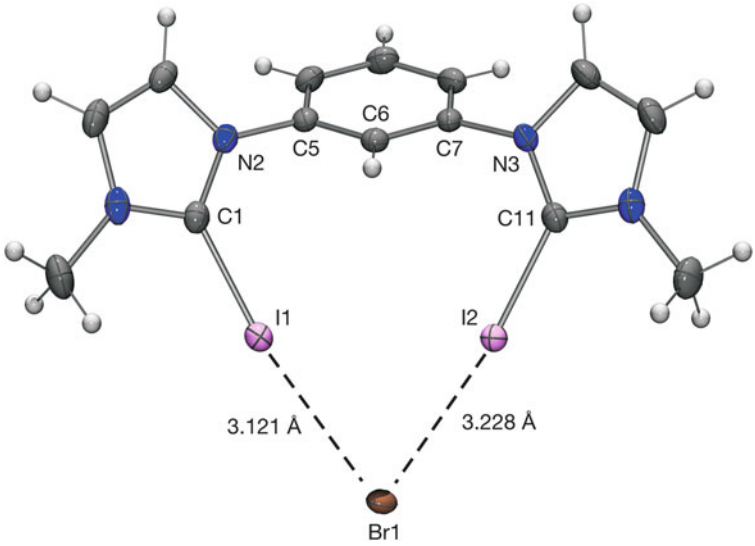

Fig. 7 X-Ray structural analysis of the complex of bromide with *m*-II-**26**^{Me}/BPh_4 (anion omitted for clarity; ellipsoids at 50% probability); selected bond lengths [Å] and angles [°]: C1–I1 2.090, C11–I2 2.083, C11–I2–Br1 170.5, C1–I1–Br1 172.1, C11–N3–C7–C6 54.4, C6–C5–N2–C1 −60.0 [132]

electron density from bromide to the σ* orbital of the C–I bond. When examining the carbon spectrum of the benchmark reaction mixture after 4 days, the signal stemming from the iodine-carrying carbon is shifted to a similar position ($\delta = 110.2$ ppm). Thus, XB donors seem to bind bromide in the course of the reaction. When, instead of stoichiometric amounts, only 20 mol% of activator were used in the reaction, the yield dropped to 28% under otherwise identical conditions. This finding indicates that the binding of bromide to the halogen-bond donor is strong enough to prevent the Lewis acid from activating further substrate.

Since a contact between an oxygen atom of the triflate anion and an iodine substituent of the Lewis acid can be detected in the solid phase, it is conceivable that the anion also partially blocks the binding sites in solution. Thus, the activity of the halogen-bond donor in the test reaction might be reduced by a competition between triflate and liberated bromide for the electrophilic center. A possible means to avoid this deactivating effect might be to exchange the anion for a less nucleophilic and thus less coordinating one. Consequently, the analogous tetrafluoroborate salt of halogen-bond donor *p*-II-**26**^{Me}/BF_4 was prepared by alkylation of the neutral intermediate with Me_3OBF_4. Test runs with this Lewis acid gave higher yields (97%) of the solvolysis product under similar reaction conditions, further illustrating the importance of the counterion for the activity of the halogen-bond donors.

Isothermal Calorimetric Titrations

Apart from the studies of performance of aforementioned XB donors in test reactions, further information on the nature of halogen bonding (and thus valuable indications for the design of future activators) was also obtained by thermodynamic measurements [132]. The thermodynamics of binding events were measured by isothermal titration calorimetry (ITC), in which the bisimidazolium salt is titrated with a tetrabutylammonium halide and the heat of binding is detected. This allows the determination of all relevant binding parameters, such as enthalpy, entropy, free energy, and stoichiometry coefficient, in a single measurement. The most important finding of these titrations, which will be discussed in more detail below, is the fact that the entropic term contributed considerably (more than 50%) to the overall free energy of binding – in contrast to the thermodynamic binding parameters involving neutral halogen-bond donors [48, 50, 132, 133].

In a first round of experiments, XB donors *m*-II-**26**^{Me}/OTf and *p*-II-**26**^{Me}/OTf were titrated with tetrabutylammonium chloride, bromide, and iodide in acetonitrile at room temperature. For the *meta*-substituted Lewis acid, binding constants of 2.5–5.2 $\times$ 10^5 M^{-1} were found, with the association strength decreasing from the chloride to the iodide complex. These overall relatively similar binding energies of -31.4 to -33.2 kJ M^{-1} (from iodide to chloride complex), however, result from a compensation of enthalpic and entropic trends: from chloride to iodide the enthalpic contribution to the overall binding free energy increases, while the entropic part decreases. In all cases, stoichiometry coefficients of one were found, indicating a bidentate coordination of the halides to the XB donor.

The *para*-substituted analogue, on the other hand, showed a 2:1 binding in the complex with TBA chloride. Here, the bite angle appears to be too large to favor a bidentate binding. Accordingly, compared to the *meta* compound, binding constants are reduced by about one order of magnitude for the same halides. The main reason for the different binding energies is a decrease of the enthalpy term.

While the outcome of comparison experiments in the test reaction mentioned above with brominated and non-halogenated analogues has already provided strong indications for halogen bonding, further examination of this aspect by ITC measurements could support the formation of XBs between the Lewis acids and the halides. For example, the binding strength of *m*-BrBr-**26**^{Me}/OTf to bromide was determined to be significantly lower (-17.5 kJ/mol) than that of the iodinated analogue, with an association constant reduced by two orders of magnitude. Furthermore, no heat response (indicative of halide binding) could be detected when titrating *m*-HH-**26**^{Me}/OTf with bromide. Thus, strong binding of the halides to the backbone protons at the 4- and 5-position of the imidazolium moiety of *m*-II-**26**^{Me}/OTf can be excluded. Similarly, the bis-methylated comparison compound *m*-MeMe-**26**^{Me}/OTf did not lead to any detectable heat response upon halide addition.

A more detailed comparison of the iodinated and the brominated Lewis acids reveals that the decreased binding energy of the latter is primarily due to a smaller contribution of the entropy. One possible explanation for this is the assumption that less solvent molecules are bound in solution to the bromine substituent of **26** due to

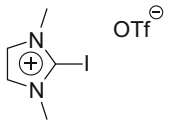

27

Fig. 8 Iodinated monomeric imidazolium reference compound

its smaller surface and σ-hole. Consequently, binding of a halide would release less solvent molecules and the entropy change would be less pronounced (Fig. 8).

An ITC examination of the mono-iodinated bisimidazolium XB donor *m*-HI-**26**^{Me}/OTf gave results which are in accordance with its performance in the benzhydryl bromide solvolysis test reaction. The binding constant was comparable to the di-iodinated *para* compound *p*-II-**26**^{Me}/OTf, and thus significantly higher than that of the monomeric imidazolium salt **27**. The higher halide binding strength of *m*-HI-**26**^{Me}/OTf compared to that of **27** indicates the contribution of a secondary activation from the non-halogenated imidazolium moiety, induced either by a hydrogen bond from the hydrogen atom at C2 or by the positive charge of the second ring system.

The temperature dependency of the halogen-bond-based binding events is somewhat counter-intuitive. The unexpectedly high contribution of the entropic term to the overall free energy of binding already indicates that the overall association strength between the halogen-bond donor and the halide should become stronger at higher temperatures. Indeed, this trend was confirmed by a series of ITC titrations of TBA bromide with *m*-II-**26**^{Me}/OTf at temperatures between 10°C and 50°C, in which the binding strength (ΔG^0) increased steadily. This behavior is in contrast to that of neutral XB donors (complexes of C_6F_5I with metal fluorides), for which a decrease of the free energy of binding at higher temperatures was observed [134, 135].

The effect of structural variations of the halogen-bond donors on the binding parameters was investigated by exchange of their counterions with less nucleophilic ones as well as by a variation of the alkyl side chain bound to the imidazolium nitrogen. Halogen-bond donors with triflate, tetrafluoroborate, hexafluorophosphate, and tetraphenylborate anions gave rather similar binding energies to halides, with only slightly stronger binding for the latter two counterions. Compared to the N-methylated analogues, the N-octylated XB donors *m*-II-**26**^{Oct}/OTf and *m*-II-**26**^{Oct}/BPh_4 showed a minor increase of binding strength, which is due to an increase of the entropic part for the former and an increase of the enthalpic part for the latter compound. These findings render an interpretation and analysis of the overall trend rather difficult. More importantly, however, the introduction of the octyl chain also leads to a higher solubility of the halogen-bond donors and thus broadens the range of applicable solvents. While the N-methylated compounds were limited to acetonitrile, acetone (with comparable binding parameters to acetonitrile), ethanol, water/methanol 1/9, and DMSO (with no detectable heat response for the latter three), the octylated compound *m*-II-**26**^{Oct}/OTf is also soluble in less polar solvents. As most (polar) hydrogen-bonding solvents are generally

unsuitable for the formation of strong halogen bonds [48], the availability of further less polar solvents is very important for future applications, especially since stronger binding may be expected in these solvents. The ITC titrations of *m*-II-**26**^{Oct}/OTf in THF and DCM confirmed this assumption, most notably the comparatively high binding constant to bromide of 3.3×10^6 M^{-1} in THF.

Halopyridinium-Based Halogen-Bond Donors as Activators

In order to broaden the scope of bidentate XB donors available for application in organic synthesis, further scaffolds were developed and tested. In a first approach, the halopyridinium motif was selected due to previously reported short contacts of such compounds to halides in X-ray structural analyses [136–143]. An azo bridge was chosen as a synthetically readily available linker for two halopyridinium moieties. The syntheses of the corresponding bidentate halogen-bond donors like **29** start with an azo-coupling of two 4-aminopyridines derivatives **28** which bear either bromine or iodine substituents in the 3- and/or 5-position of the pyridine. NaOCl or $PhI(OAc)_2$ as coupling reagents gave only low yields, necessitating the use of the strong oxidant $PhIL_2(OTf)_2$ (L=DMAP) [55]. Subsequent N-methylation with MeOTf or Me_3OBF_4 yields the dicationic halogen-bond donors as triflate or tetrafluoroborate salts. According to NMR data, all compounds were obtained as single isomers, and X-ray structural analyses identified them as *trans* isomers. Although irradiation of the neutral intermediates resulted in partial isomerization and formation of the respective *cis* isomers, the latter converted back to the more stable *trans* form within a few minutes and could not be isolated (Scheme 19).

The X-ray structural analysis of **29a** showed an almost perpendicular arrangement of the two pyridinium groups. Furthermore, a coordination of triflate anions (via one of their oxygen atoms) to all four iodine substituents of the XB donor was found, with O–I distances which are significantly below the sum of the van-der-Waals radii (2.90 vs 3.48 Å) [131]. In the case of the brominated analogue **29b**, only weak contacts of the bromine substituents to the fluorine atoms of triflate were found (Fig. 9).

In order to assess the activating ability of these azobis(halopyridinium) compounds, they were tested in the previously described solvolysis reaction of benzhydryl bromide (see above for blank reaction as well as results for HOTf and pyridine additives). In the presence of 20 mol% of pyridine to quench traces of acid, stoichiometric amounts of halogenated activators **29a** and **29b** gave 75% and 82% yield of solvolysis product **22** after 36 h of reaction time, respectively. In contrast, the non-halogenated analogue **29d** produced only traces of amide **22**. In a first assessment this seemed to confirm the activation of benzhydryl bromide by halogen bonding. However, the non-halogenated pyridinium salt **29d** gave a 69% yield of amide **22** after 36 h in the absence of 20 mol% pyridine. This finding cannot be explained by traces of acid, but instead hints at the presence of another mode of activation which further complicates the evaluation of the reaction.

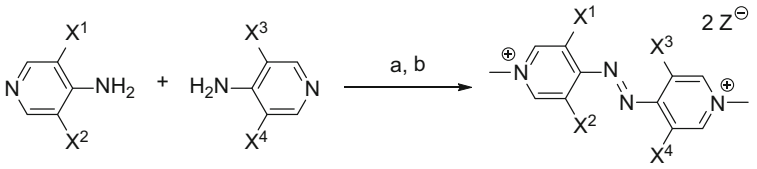

28a (X^1,X^2 = I)
28b (X^1,X^2 = Br)
28c (X^1 = H; X^2 = I)
28d (X^1,X^2 = H)

29a (X^1 - X^4 = I) (Z=OTf)
29a'(X^1 - X^4 = I) (Z=BF_4)
29b (X^1 - X^4 = Br) (Z=OTf)
29c (X^1,X^3 = I; X^2,X^4 = H) (Z=OTf)
29d (X^1 - X^4 = H) (Z=OTf)
29e (X^1,X^2 = I; X^3,X^4 = H) (Z=OTf)

Scheme 19 Synthesis of 4,4′-azobis(pyridinium)-based XB donors and reference compounds

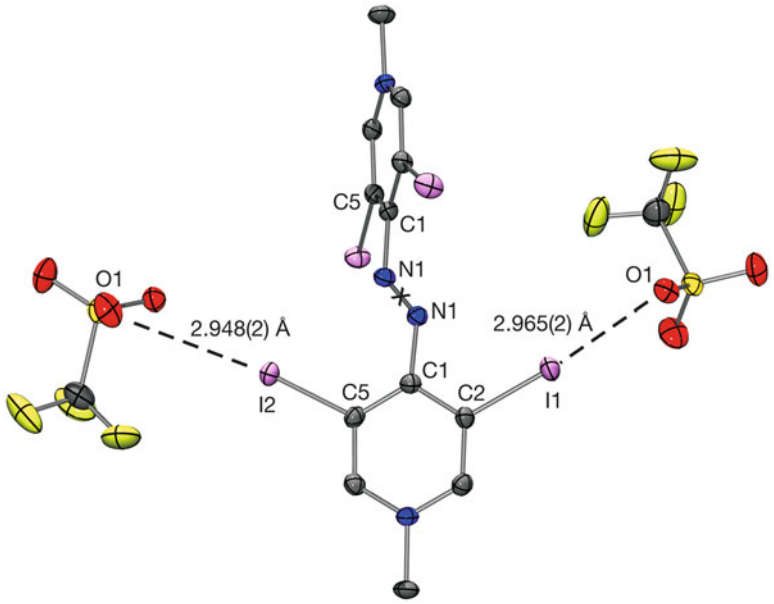

Fig. 9 X-Ray structural analysis of XB-donor **29a** (ellipsoids at 50% probability; only two of the four XBs per dication are shown); selected bond lengths [Å] and angles [°]: N1–N1 1.242(3), C5–I2 2.089(3), C2–I2 2.090(3), C2–I1–O1 176.37(9), C5–I2–O1 169.82(8), C5–C1–N1–N1 −58.8 (3), C2–C1–N1–N1 127.2(2), C5–C1–C1–C2 −115.7(3); x=center of inversion [136]

As a first step towards the identification of this second activation mechanism, single crystal structures involving bisiodinated halogen-bond donor **29a** were obtained directly from the reaction mixture. X-Ray analysis revealed a complex of **29a** with Br_4^{2-}. The distances between the four bromine atoms hint at the presence of one molecule of elemental bromine (2.43 Å) which is coordinated to

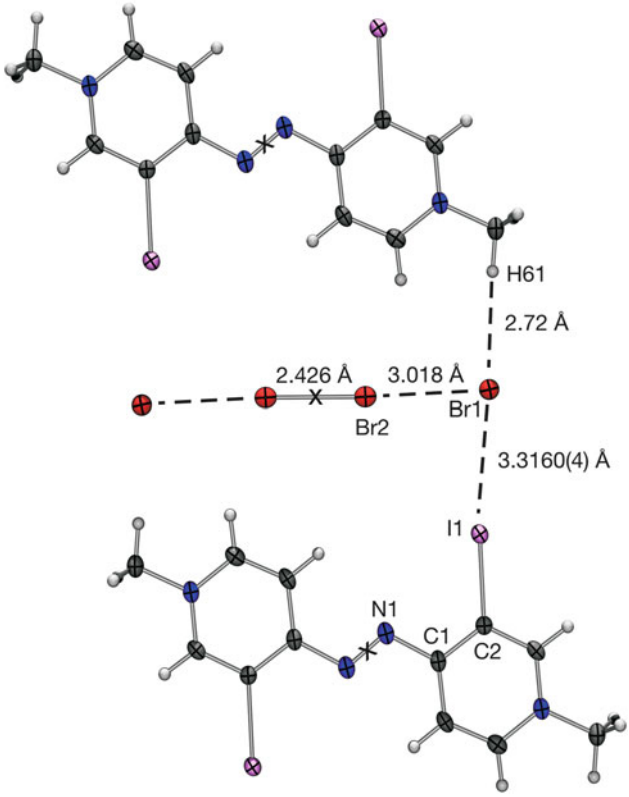

Fig. 10 X-Ray structural analysis of a complex of the dication of **29c** with (formally) Br_4^{2-} (ellipsoids at 50% probability); selected bond lengths [Å] and angles [°]: N1–N1′ = 1.238(5), C2–I1 = 2.100(4), C2–C1–N1–N1′ = 180.0, C2–C1–C1′–C2′ = 180.0; exact distances within Br_4^{2-}: Br2–Br2 = 2.4257(6), Br1–Br2 = 3.0185(6); x = centers of inversion [136]

two bromide anions via halogen bonding (3.02 Å). This adduct forms a complex with **29a** by halogen bonds of the terminal bromine atoms towards the iodine moiety as well as by hydrogen bonds of the same atoms towards the methyl group of **29a** (Fig. 10).

A series of comparison experiments subsequently established that elemental bromine is formed by oxidation of HBr (which is formed during the reaction) by the halogen-bond donors and that elemental bromine is also a very potent activator for the test reaction. Gratifyingly, addition of 1 equiv. of cyclohexene completely quenches the activity of elemental bromine and thus enables an undisturbed assessment of the activation potential of the halopyridinium-based activators. Thus, in the presence of 1 equiv. of cyclohexene and 10 mol% of pyridine, iodinated activator **29a** gave a yield of 93% of the solvolysis product after 36 h, whereas the analogous non-halogenated compound gave only negligible yield. Compared to **29a**, the yield was considerably lower for the brominated halogen-bond donor **29b** (76% after

36 h) which is in agreement with the theory of halogen bonding. Interestingly and in contrast to the findings with imidazolium-based halogen-bond donors, the tetrafluoroborate salt of **29a′** produced lower yields of **22** compared to the triflate salt.

In addition, partly iodinated compounds **29c** and **29e** were synthesized and employed in the test reaction. Yet both yielded, apart from the amide **22**, non-negligible amounts of the hydrolysis products benzhydrol and dibenzhydryl ether. The fact that these side products are observed in the presence of **29c** and **29e**, but not in the presence of **29a** and **29b** cannot be satisfactorily explained at the moment.

As the above-mentioned multidentate halogen-bond donors are intended to complement hydrogen-bond-based compounds in organocatalysis, a comparison with a prototypical hydrogen bonding organocatalyst was also performed. Addition of 1 equiv. of thiourea derivative **1** [14] to the reaction mixture did not result in a significant increase in the yield of **22** compared to the blank reaction. Instead, about 40% of benzhydryl bromide were consumed in a side reaction which is believed to originate from nucleophilic attack of the thiourea to substrate **21**.

Triazolium-Based Halogen-Bond Donors as Activators

As shown in the cases of the bisimidazolium-based activators, the denticity of the halogen-bond donor has a strong influence on the binding strength towards the XB acceptor [144]. For the synthesis of tri- or multidentate halogen-bond donors, a robust and mild protocol for the introduction of halogen-bonding moieties to a central core will be necessary, which should also allow systematic variations of the activator structure. All these requirements are met by 5-halo-1,2,3-imidazolium moieties, which can be introduced via a Cu(I)-catalyzed 1,3-dipolar Huisgen cycloaddition [145] reaction between azides and iodoalkynes (and subsequent N-methylation). The suitability of these compounds as potent halogen-bond donors had already been established by Beer et al. [36, 146].

As a backbone structure, a *meta*-substituted benzene core was chosen, since this motif had been shown to allow a favorable bite angle for two five-membered-ring derived halogen-bond donors towards halides before (see above). Hence, the synthesis of the bidentate target compounds **30** proceeded by a Cu(I)-catalyzed cycloaddition reaction of *n*-octyl azide, benzyl azide, or (*R*)-1-ethylphenyl azide with 1,3-bis(iodoalkynyl)benzene. The following N-methylation proceeded regioselectively at the nitrogen atom closest to the benzene core [147]. Just as for the bisimidazolium compounds, X-ray structural analysis of 1,3-I-**30**-^{Bn}/OTf showed short contacts between the iodine atoms and an oxygen atom of the triflate counterion. The analogous tridentate (and tricationic) compound could be obtained starting from 1,3,5-tris(iodoalkynyl)benzene, but only benzyl azide as coupling partner lead to appreciable triazole ring formation. Methylation of the intermediate with MeOTf afforded 1,3,5-I-**30**-^{Bn}/OTf in good yield (Scheme 20).

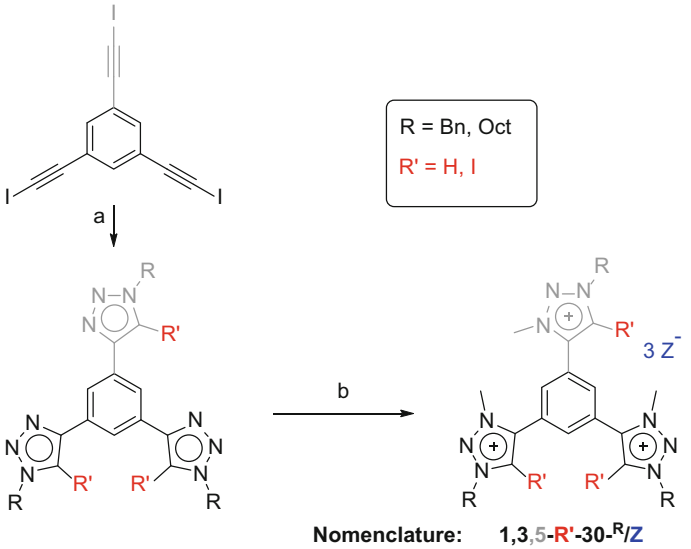

Scheme 20 Synthesis of triazolium XB donors. (Path a) CuI/TBTA (10 or 20 mol%), azide (2 or 3 equiv.), THF, rt, 18 h. (Path b) MeOTf (4 or 6 equiv.), DCM, rt, 2d. Anion exchange: $NaPF_6$ (3 or 4.5 equiv.), MeOH, rt, 2d

The performance of these iodotriazolium-based compounds as XB donors in organic synthesis was once again tested in the halide abstraction benchmark reaction involving benzhydryl bromide (see above). Again, 10 mol% of pyridine were included in all experiments to inhibit an activation by possible traces of acid. To check for activating effects arising from the backbones of the halogen-bond donors, the non-halogenated compounds were tested as well, but all gave only a comparatively low yield of the solvolysis product **22** after 96 h (7% for 1,3-H-**30**-^{Bn}/OTf, 11% for 1,3-H-**30**-^{Oct}/OTf, and 15% for the potentially tridentate 1,3,5-H-**30**-^{Bn}/OTf). The iodinated bidentate analogues, in contrast, give rise to yields of the product of 78% (1,3-I-**30**-^{Bn}/OTf) and 62% (1,3-I-**30**-^{Oct}/OTf) in the same reaction time. An explanation for the reduced activity of 1,3-I-**30**-^{Oct}/OTf could not be found. Anion metathesis towards the less coordinating hexafluorophosphate was possible in case of the *N*-benzylated compound 1,3-I-**30**-^{Bn}/OTf, but yields of **22** did not change drastically with this XB donor (82% after 96 h). 1,3,5-I-**30**-^{Bn}/OTf turned out to promote the reaction far better, yielding >95% of **22** even after only 48 h. Thus, the action of the activator indeed seems to evoke a tridentate binding mechanism. Surprisingly, the analogous hexafluorophosphate salt 1,3,5-I-**30**-^{Bn}/PF_6 produced only a 73% yield after 48 h (and 92% after 96 h). This is somewhat unexpected, as hexafluorophosphate is expected to coordinate less to the iodine centers compared to triflate, and should thus enhance the reactivity of the XB donor.

Polyfluorinated Azo-Bridged Halogen-Bond Donors

So far, all XB donors discussed in this chapter as activators in organic synthesis have been of ionic nature, as the iodine (or bromine) substituents were bound to a cationic core structure [148]. While the cationic backbone induces a larger polarization of electron density at the halogen atom and thus increases its Lewis acidity, it also bears some disadvantages. For instance, the low-to-medium solubility of the salt-like structures in apolar solvents will likely restrict their application in certain organic reactions. In addition, the alkylation step which is required at some point in the synthesis will limit the range of accessible bifunctional halogen-bond donors. Also, the presence of anions brings with it several potential complications, most importantly the detrimental binding to the electrophilic halogen centers. As a result, neutral multidentate XB donors would constitute a highly desirable complement to cationic activators.

As indicated in the introduction, poly- or perfluorinated backbones are usually necessary to obtain a sufficiently electron-withdrawing effect. Since monodentate polyfluorinated halogen-bond donors like 1,3,5-triiodoperfluorobenzene and 1,4-diiodoperfluorobenzene did not show any activity in test reactions, our group focused on the design and synthesis of multidentate variants. The azo-bridge had already been introduced as a suitable linker for two *ortho*-halogenated six-membered ring systems [136] and was therefore chosen as a first core structure for the bidentate XB donor **31**. The similarity of the backbone structures of the neutral halogen-bond donor **31** and the dicationic Lewis acid **29a** is also of advantage in another respect: it allows one to compare directly the performance of polyfluorinated vs cationic halogen-bearing moieties with an identical geometrical arrangement of the electrophilic halogen centers (Scheme 21).

The synthesis of **31** and **32** starts with the iodination or bromination of 3,4,5-trifluoroaniline in the 2- and 6-positions with a mixture of potassium iodide and potassium iodate in methanol or *N*-bromosuccinimide in dichloromethane, respectively. The subsequent linkage of two aniline derivatives via an azo bridge is achieved with the hypervalent iodine reagent $PhIL_2(OTf)_2$ (L=DMAP) in moderate yield (Fig. 11).

The X-ray structural analysis of single crystals of **31** showed an almost perpendicular arrangement of both aryl moieties to each other, in a similar fashion to that observed with **29a**. In contrast to the latter, the iodine centers undergo a different coordination due to the absence of anions as Lewis basic centers. Instead, each molecule of **31** forms a complex with a second one, featuring noticeably short intermolecular I–I contacts (3.79 and 3.88 Å). This is in line with the ambiphilic nature of the iodine substituents, which feature an electrophilic σ-hole in the elongation of the C–I bond [26], but also a nucleophilic belt of electron density perpendicular to the C–I bond axis. Thus, the ideal coordination angle for C–I···I–C contact should be close to 90°. The solid-state structure of **31** features angles of 76° and 69°, indicating that the first I–I contact is likely to be a halogen bond, while the second is at least partly also a van-der-Waals-based interaction.

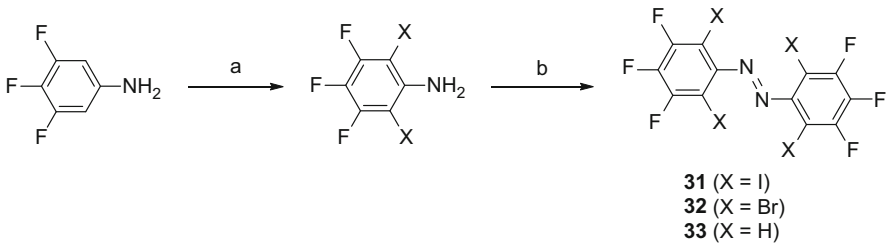

Scheme 21 Synthesis of polyfluorinated halogen-bond donors **31** and **32**. (Path a) KI, KIO_3, HCl, MeOH (X=I) or *N*-bromosuccinimide, CH_2Cl_2 (X=Br). (Path b) $PhIL_2(OTf)_2$ (L=4-dimethylaminopyridine), CH_2Cl_2

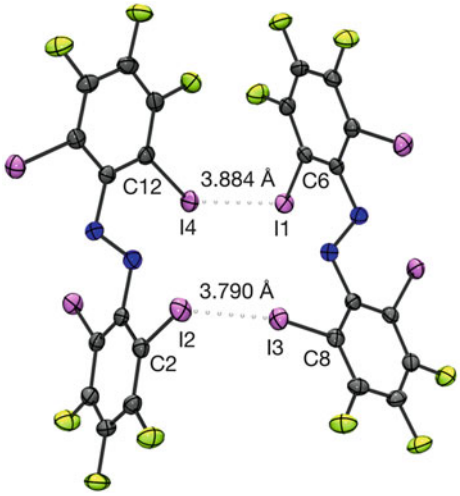

Fig. 11 Intermolecular halogen-bonds formed in the crystal packing of **31**; selected angles [°]: C12–I4···I1 = 68.67(6), C6–I1···I4 = 146.91(7), C8–I3···I2 = 76.13(6), C2–I2···I3 = 166.18(6). In the crystal structure of compound **31**, each of the four iodine substituents is connected to neighboring molecules by one of the two kinds of halogen-bonds shown in this figure [148]

The performance of the neutral bidentate halogen-bond donors in a halide abstraction reaction was once again evaluated by the solvolysis of benzhydryl bromide in acetonitrile (including 10 mol% of pyridine). In the presence of activator **31**, the yields of amide **22** were only marginally increased when compared to the blank reaction, if at all. Even after 25 days (!) of reaction time, the yield of the solvolysis product amounted to no more than 27% in the presence of **4a**, compared to 18% in the background reaction. While this slight activation was reproduced several times, it may still be within the margin of error of the experiment. The brominated and non-halogenated analogues **32** and **33** gave yields which were virtually identical to those of the blank reaction. In direct comparison to the

dicationic activator **29a** (almost quantitative yield of **22** after 36 h), it is obvious that this neutral activator is far less active. As the orientation of the iodine substituents in space is identical for both **31** and **29a**, this difference in reactivity vividly illustrates that cationic backbones are much more effective for the design of potent halogen-bond donors than polyfluorinated backbones.

Polyfluorinated Halogen-Bond Donors as Organocatalysts

Despite the disappointing performance of the azo-bridged neutral XB donors, activators based on neutral scaffolds remained an intriguing topic, due to the various advantages mentioned above [133]. In order to achieve stronger binding strength, a more rigid backbone as linker was needed, and quantum-chemical calculations indicated that arene linkers would satisfy this criterion. To avoid atropisomers, the symmetrically substituted 2,6-diiodo-3,4,5-trifluorophenyl group was chosen as halogen-bonding moiety (Fig. 12).

The synthesis of the target molecules *p*-**34** and *m*-**35** posed major challenges, however. The presence of iodine substituents excluded or severely limited the application of cross-coupling reactions. In addition, the multiple fluorine substituents rendered the benzene cores very electron-deficient and thus impeded iodination reactions. The eventually successful synthetic route involves an initial Suzuki-type cross-coupling step to build up the polyfluorinated polyaryl backbone [149] and consecutive iodination with *N*-iodosuccinimide in triflic acid [150]. With this protocol it was also possible to obtain the potentially tridentate compound **39** in respectable overall yield (Scheme 22).

X-Ray structural analysis of the co-crystal of *p*-**34** with tri(dimethylamino) cyclopropenium chloride showed several halogen bonds to the halide. Most importantly, a bidentate coordination to chloride is observed for one side of the halogen-bond donor. As this induces a slight distortion of the central aryl backbone, the distance between the iodine atoms on the other side of the XB donor is elongated, and two monodentate halogen-bonds to chloride are found on this side (Fig. 13).

To test the possibility of using these neutral Lewis acids in organic synthesis, again a benchmark reaction was used. In all the previous cases presented above, stoichiometric amounts of the halogen-bond donor needed to be used, as the latter apparently bound too strongly to the halide and was thus not available for further activation. To be able to use catalytic amounts of the halogen-bond donor, an internal recycling of the Lewis acids is thus necessary. As a consequence, a different test reaction (instead of the solvolysis of benzhydryl bromide) was chosen to evaluate the potential of *p*-**34**, *m*-**35**, and **39**: Jacobsen et al. had already shown that the reaction of 1-chloroisochroman with silyl ketene acetals (see Scheme 23) can be catalyzed by (chiral) hydrogen-bond donors [151]. It was anticipated that the silyl group released during the reaction scavenges the liberated chloride and thus enables the halogen-bond donor to abstract chloride more than once, i.e., to act in a catalytic manner.

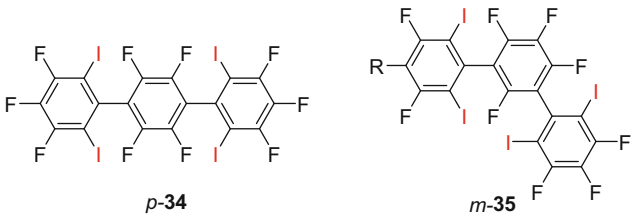

Fig. 12 Neutral XB donors *p*-**34** and *m*-**35** as target molecules

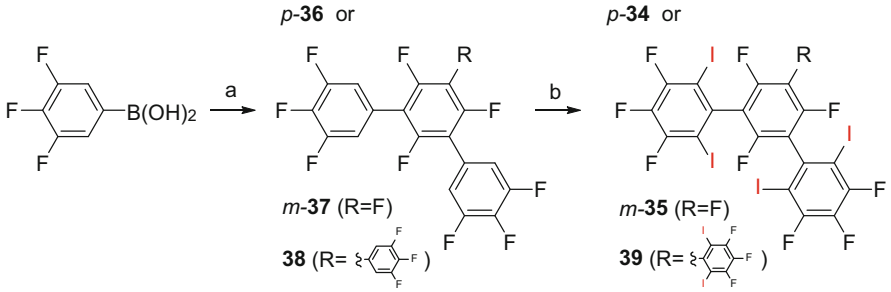

Scheme 22 Synthesis of neutral halogen-bond donors. (Path a) 1,4-$C_6F_4I_2$ (0.5 equiv.) or 1,3-$C_6F_4I_2$ (0.5 equiv.), XPhos (5 mol%), $Pd_2(dba)_3$ (1 mol%), Na_2CO_3 (*p*-**36**,*m*-**37**), 1,3,5-$C_6F_3I_3$ (0.11 equiv.), XPhos (1 mol%), $Pd_2(dba)_3$ (0.1 mol%), Na_2CO_3 (0.33 equiv.) (**38**), toluene/THF/H_2O, 95°C. (Path b) *N*-Iodosuccinimide (NIS) (13 equiv.) (*p*-**34**, *m*-**35**) or NIS (20 equiv.) (**39**), HOTf, 0°C to rt

No product formation was observed under the selected reaction conditions (12 h at −78°C) [151] in the absence of any catalyst. Likewise, the non-halogenated compounds **36** and **38** did not induce a significant yield of **40**. In stark contrast, the presence of 10 mol% of the analogous iodinated XB donors *p*-**34** or **39** leads to a yield of **40** of 37% and 91%, respectively. Since the compounds *p*-**36**/*p*-**34** and **38**/**39** only differ in the presence or absence of iodine substituents, halogen bonding seems to be the basis for this activation. This reasoning is supported by the fact that a monodentate variant (1,3,5-triiodo-2,4,6-trifluorobenzene) and the *meta*-substituted compound *m*-**35** induced little or no yields of the product, further emphasizing the importance of the number and relative orientation of the iodine substituents. The fact that these results were achieved with only 10 mol% of halogen bond donor and an increase to 20 mol% led to considerably higher yields shows that a catalytic activation mode takes place. Hidden acid catalysis can safely be ruled out in this reaction as well, since addition of 1 mol% or 10 mol% of the strong acid HOTf leads to only 14% or 27% yield of **40**, lower than observed for XB donors *p*-**34** and **39**. Further evidence for the important role of the halogen-bond donors is the fact that the activity of these Lewis acids is completely quenched by the addition of 20 mol% of tetrabutylammonium chloride. This confirms that binding of anions is part of the mode of activation of the halogen-based Lewis

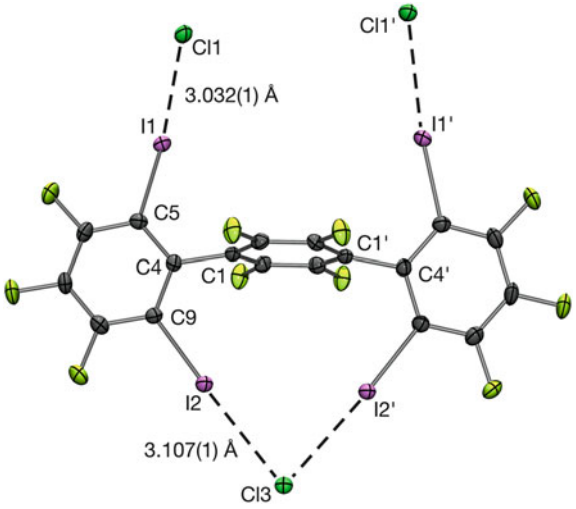

Fig. 13 Part of the crystal structure of the adduct of *p*-**34** with tris(dimethylamino)cyclopropenium chloride (ellipsoids at 50% probability). Cations have been omitted for clarity. Chloride anions Cl1 form additional halogen-bonds with further molecules of *p*-**34**. Selected bond distances [Å] and angles [°]: C5–I1 = 2.110(3), C9–I2 = 2.112(3), I2–I2′ = 4.1121(4), I1–I1′ = 6.7302(5), C1′–C1–C4 = 170.54(2), C5–I1–Cl1 = 173.84(9), C9–I2–Cl3 = 172.19(9) [133]

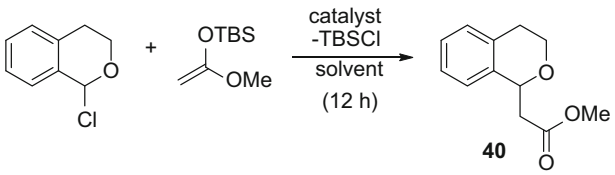

Scheme 23 Selected test reaction of 1-chloroisochromane to ester **40**

acids. To compare the halogen-bond-based catalysis with that by a hydrogen-bond donor, the reaction was performed with 10 mol% of Schreiner's thiourea catalyst **1** under otherwise identical reaction conditions, leading to a yield of product **40** of 12%. Similar results were obtained in methyl-*tert*-butylether. This demonstrates the significant potential of halogen bonding in organocatalysis.

Finally, the binding strengths of XB catalysts *p*-**34** and *m*-**35** as well as thiourea derivative **1** to chloride and bromide were determined by isothermal titration calorimetry. At the measuring temperature of 30°C, the hydrogen bond donor showed a binding constant of 2.9×10^5 mol^{-1} (corresponding to $\Delta G^0 = -31.7$ kJ/mol) towards both anions. The *para*-substituted XB donor bound less strongly to both anions ($\Delta G^0 = -28.3$ kJ/mol for chloride, $\Delta G^0 = -27.8$ kJ/mol for bromide), and the complexes with the *meta*-substituted variant *m*-**35** were again slightly less stable ($\Delta G^0 = -24.7$ kJ/mol for chloride, $\Delta G^0 = -23.9$ kJ/mol for bromide). While the latter trend is in agreement with the findings in the catalysis study, the strong binding

by the thiourea seems to contradict the experimental results. Yet, while the entropic contribution to the overall binding free energy is almost negligible for the halogen-bond donors, it is very significant for the hydrogen-bond donor. Consequently, the latter will bind less strongly to halides at low temperatures like the one employed for the catalysis reaction (−78°C), reconciling catalysis and ITC studies. Overall, these investigations demonstrate that halogen-bond donors can be as potent in anion-binding catalyses as the well-established hydrogen-bond donors.

3 Summary and Outlook

Neglected for a long time, halogen bonding has by now been established as a reliable motif in crystal engineering. In contrast to the increasing experience gained in these solid-state investigations, the development of halogen-bond-based applications in solution has lagged behind considerably. The scarce and isolated work of earlier decades on this topic was mainly concerned with the detection of these interactions in solution and very fundamental studies of their behavior. The last few years have seen a marked increase in solution-based studies and applications of halogen bonding [63, 64]. In parallel, the halogen-bond donors employed have become more sophisticated, which is most strikingly exemplified by the development of several multidentate halogen-bond-based anion receptors [42–46]. Multidenticity allows for a stronger and more ordered binding of Lewis bases and thus represents a crucial step towards the application of halogen bonding in organic synthesis.

Compared to hydrogen-bond organocatalysts like thiourea derivatives, the use of halogen-bond donors as noncovalent activators or organocatalysts is still at a very early stage. On the one hand, there are now a variety of applications of elemental iodine in a wide range of organic transformations. Unfortunately, the mechanistic understanding of the actual mode of activation is – at the moment – only rudimentary. Only in very few cases could hidden acid catalysis be ruled out. Nevertheless, it seems very plausible that iodine may activate organic substrates via its Lewis acidity, and further investigations will hopefully shed more light on the underlying mechanisms. On the other hand, first proof-of-principle reactions have been established regarding the use of carbon-based halogen-bond donors in organocatalysis. These halogen-based Lewis acids obviously offer much more structural variety and potential than elemental iodine itself, and the mode of activation is better understood. Yet the reported cases still only cover simple benchmark reactions, and there is a clear need for further [152] and more complex applications. At this early stage, the challenge also remains for new applications to show with reasonable certainty that halogen bonding is indeed the dominant mode of activation.

Just as has been the case for hydrogen bonding, the interplay between supramolecular studies and actual organocatalytic applications will also be crucial for halogen bonding. Further multidentate halogen-bond-based receptors and

organocatalysts will prove helpful in studying fundamental effects of halogen bonding in solution. Clearly, one important long-term goal is enantioselective organocatalysis by halogen bonding. The rational development of such applications is certainly not trivial, as suitable structural motifs still have to be identified and synthesized. The success story of hydrogen-bond-based catalysts, though, will serve as a major inspiration for these endeavors.

References

1. Jeffrey GA (1997) An introduction to hydrogen bonding. Oxford University Press, Oxford
2. Steed JW, Atwood JL (2009) Supramolecular chemistry, 2nd edn. Wiley, Chichester
3. Pihko PM (ed) (2009) Hydrogen bonding in organic synthesis. Wiley, Weinheim
4. Gholami MR, Talebi BA (2003) J Phys Org Chem 16:79–83
5. Blake JF, Jorgensen WL (1991) J Am Chem Soc 113:7430–7432
6. Blake JF, Lim D, Jorgensen WL (1994) J Org Chem 59:803–805
7. Hine J, Linden SM, Kanagasabapathy VM (1985) J Am Chem Soc 107:1082–1083
8. Kelly TR, Meghani P, Ekkundi VS (1990) Tetrahedron Lett 31:3381–3384
9. Etter MC, Panunto TW (1988) J Am Chem Soc 110:5896–5897
10. Etter MC (1990) Acc Chem Res 23:120–126
11. Curran DP, Kuo LH (1994) J Org Chem 59:3259–3261
12. Curran DP, Kuo LH (1995) Tetrahedron Lett 36:6647–6650
13. Schreiner PR (2003) Chem Soc Rev 32:289–296
14. Zhang Z, Schreiner PR (2009) Chem Soc Rev 38:1187–1198
15. Doyle AG, Jacobsen EN (2007) Chem Rev 107:5713–5743
16. Wittkopp A, Schreiner PR (2003) Chem Eur J 9:407–414
17. Sigman MS, Jacobsen EN (1998) J Am Chem Soc 120:4901–4902
18. Vachal P, Jacobsen EN (2002) J Am Chem Soc 124:10012–10014
19. Zuend SJ, Jacobsen EN (2009) J Am Chem Soc 131:15358–15374
20. Mahlau M, List B (2013) Angew Chem Int Ed 52:518–533
21. Brak K, Jacobsen EN (2013) Angew Chem Int Ed 52:534–561
22. Beckendorf S, Asmus S, Mancheno OG (2012) ChemCatChem 4:926–936
23. Raheem IT, Thiara PS, Peterson EA, Jacobsen EN (2007) J Am Chem Soc 129:13404–13405
24. Taylor MS, Jacobsen EN (2006) Angew Chem Int Ed 45:1520–1543
25. Malerich JP, Hagihara K, Rawal VH (2008) J Am Chem Soc 130:14416–14417
26. Metrangolo P, Meyer F, Pilati T, Resnati G, Terraneo G (2008) Angew Chem Int Ed 47:6114–6127
27. Hassel O, Roemming C (1962) Quart Rev 16:1–18
28. Bent HA (1968) Chem Rev 68:587–648
29. Fourmigue M (2009) Curr Opin Solid State Mater Sci 13:36–45
30. Legon AC (2010) Phys Chem Chem Phys 12:7736–7747
31. Lu Y, Wang Y, Zhu W (2010) Phys Chem Chem Phys 12:4543–4551
32. Desiraju GR, Ho PS, Kloo L, Legon AC, Marquardt R, Metrangolo P, Politzer P, Resnati G, Rissanen K (2013) Pure Appl Chem 85:1711–1713
33. Corradi E, Meille SV, Messina MT, Metrangolo P, Resnati G (2000) Angew Chem Int Ed 39:1782–1786
34. Weiss R, Miess GE, Haller A, Reinhardt W (1986) Angew Chem Int Ed 25:103–104
35. Legon AC (1999) Angew Chem Int Ed 38:2687–2714
36. Kilah NL, Wise MD, Serpell CJ, Thompson AL, White NG, Christensen KE, Beer PD (2010) J Am Chem Soc 132:11893–11895
37. Vargas Jentzsch A, Emery D, Mareda J, Metrangolo P, Resnati G, Matile S (2011) Angew Chem Int Ed 50:11675–11678

38. Hardegger LA, Kuhn B, Spinnler B, Anselm L, Ecabert R, Stihle M, Gsell B, Thoma R, Diez J, Benz J, Plancher J-M, Hartmann G, Banner DW, Haap W, Diederich F (2011) Angew Chem Int Ed 50:314–318
39. Carlsson A-CC, Graefenstein J, Budnjo A, Laurila JL, Bergquist J, Karim A, Kleinmaier R, Brath U, Erdelyi M (2012) J Am Chem Soc 134:5706–5715
40. Raatikainen K, Rissanen K (2012) Chem Sci 3:1235–1239
41. Meazza L, Foster JA, Fucke K, Metrangolo P, Resnati G, Steed JW (2013) Nat Chem 5:42–47
42. Mele A, Metrangolo P, Neukirch H, Pilati T, Resnati G (2005) J Am Chem Soc 127:14972–14973
43. Sarwar MG, Dragisic B, Sagoo S, Taylor MS (2010) Angew Chem Int Ed 49:1674–1677
44. Dimitrijevic E, Kvak O, Taylor MS (2010) Chem Commun 46:9025–9027
45. Caballero A, White NG, Beer PD (2011) Angew Chem Int Ed 50:1845–1848
46. Zapata F, Caballero A, White NG, Claridge TDW, Costa PJ, Felix V, Beer PD (2012) J Am Chem Soc 134:11533–11541
47. Huber SM, Jimenez-Izal E, Ugalde JM, Infante I (2012) Chem Commun 48:7708–7710
48. Sarwar MG, Dragisic B, Salsberg LJ, Gouliaras C, Taylor MS (2010) J Am Chem Soc 132:1646–1653
49. Cabot R, Hunter CA (2005–2007) Chem Commun 2009
50. Laurence C, Graton J, Berthelot M, El Ghomari MJ (2011) Chem Eur J 17:10431–10444
51. Politzer P, Murray JS, Clark T (2010) Phys Chem Chem Phys 12:7748–7757
52. Clark T (2013) Wiley Interdiscip Rev Comput Mol Sci 3:13–20
53. Karpfen A (2003) Theor Chem Acc 110:1–9
54. Hassel O (1970) Science 170:497–502
55. Weiss R, Rechinger M, Hampel F (1994) Angew Chem Int Ed 1893–1995
56. Weiss R, Schwab O, Hampel F (1999) Chem Eur J 5:968–974
57. Huber SM, Scanlon JD, Jimenez-Izal E, Ugalde JM, Infante I (2013) Phys Chem Chem Phys 15:10350–10357
58. Rissanen K (2008) CrystEngComm 10:1107–1113
59. Brammer L, Espallargas GM, Libri S (2008) CrystEngComm 10:1712–1727
60. Bertani R, Sgarbossa P, Venzo A, Lelj F, Amati M, Resnati G, Pilati T, Metrangolo P, Terraneo G (2010) Coord Chem Rev 254:677–695
61. Cavallo G, Metrangolo P, Pilati T, Resnati G, Sansotera M, Terraneo G (2010) Chem Soc Rev 39:3772–3783
62. Di Paolo T, Sandorfy C (1974) Can J Chem 52:3612–3622
63. Erdelyi M (2012) Chem Soc Rev 41:3547–3557
64. Beale TM, Chudzinski MG, Sarwar MG, Taylor MS (2013) Chem Soc Rev 42:1667–1680
65. Vargas Jentzsch A, Matile S (2013) J Am Chem Soc 135:5302–5303
66. Vargas Jentzsch A, Emery D, Mareda J, Nayak SK, Metrangolo P, Resnati G, Sakai N, Matile S (2012) Nat Commun 3:905
67. Pearson RG (1963) J Am Chem Soc 85:3533–3539
68. Mayr H, Breugst M, Ofial AR (2011) Angew Chem Int Ed 50:6470–6505
69. Zefirov NS, Makhon'kov DI (1982) Chem Rev 82:615–624
70. Bailey WF, Patricia JJ (1988) J Organomet Chem 352:1–46
71. Wittig G, Schollkopf U (1958) Tetrahedron 3:91–93
72. Wittig G (1958) Angew Chem Int Ed 70:65–71
73. Reich HJ, Phillips NH, Reich IL (1985) J Am Chem Soc 107:4101–4103
74. Reich HJ, Green DP, Phillips NH (1989) J Am Chem Soc 111:3444–3445
75. Perkins CW, Martin JC, Arduengo AJ, Lau W, Alegria A, Kochi JK (1980) J Am Chem Soc 102:7753–7759
76. Farnham WB, Calabrese JC (1986) J Am Chem Soc 108:2449–2451
77. Schulze V, Bronstrup M, Bohm VPW, Schwerdtfeger P, Schimeczek M, Hoffmann RW (1998) Angew Chem Int Ed 37:824–826
78. Hoffmann RW, Broenstrup M, Mueller M (2003) Org Lett 5:313–316

79. Metrangolo P, Pilati T, Resnati G (2006) CrystEngComm 8:946–947
80. Dumas JM, Peurichard H, Gomel M (1978) J Chem Res (S) 54–55
81. Legon AC (1998) Chem Eur J 4:1890–1897
82. Rosokha SV, Kochi JK (2002) J Org Chem 67:1727–1737
83. Hassel O, Stromme KO (1958) Acta Chem Scand 12:1146
84. Hassel O, Stroemme KO (1959) Acta Chem Scand 13:1781–1786
85. Vasilyev AV, Lindeman SV, Kochi JK (2001) Chem Commun 909–910
86. Banerjee AK, Vera W, Mora H, Laya MS, Bedoya L, Cabrera EV (2006) J Sci Ind Res 65:299–308
87. Togo H, Iida S (2006) Synlett 2159–2175
88. Jereb M, Vrazic D, Zupan M (2011) Tetrahedron 67:1355–1387
89. Banik BK, Fernandez M, Alvarez C (2005) Tetrahedron Lett 46:2479–2482
90. Yadav JS, Reddy BVS, Reddy MS, Prasad AR (2002) Tetrahedron Lett 43:9703–9706
91. Das B, Chowdhury N, Damodar K (2007) Tetrahedron Lett 48:2867–2870
92. Das B, Balasubramanyam P, Krishnaiah M, Veeranjaneyulu B, Reddy GC (2009) Synthesis 3467–3471
93. Reddy BVS, Divyavani C, Yadav JS (2010) Synthesis 1617–1620
94. Das B, Kumar JN, Kumar AS, Kanth BS (2010) Synthesis 3113–3116
95. Boens B, Faugeras P-A, Vergnaud J, Lucas R, Teste K, Zerrouki R (2010) Tetrahedron 66:1994–1996
96. Batchu H, Bhattacharyya S, Batra S (2012) Org Lett 14:6330–6333
97. Singh N, Singh KN (2012) Synlett 23:2116–2120
98. Xu W, Kloeckner U, Nachtsheim BJ (2013) J Org Chem 78:6065–6074
99. Rai VK, Sharma N, Kumar A (2013) Synlett 24:97–101
100. Chen D-S, Li Y-L, Liu Y, Wang X-S (2013) Tetrahedron 69:7045–7050
101. Bhunia N, Das B (2013) Synthesis 45:1045–1050
102. Figueiredo CAM, Reddy KRKK, Monteiro PA, de Carvalho JE, Ruiz ALTG, Silva LF Jr (2013) Synthesis 45:1076–1082
103. Yan R, Kang X, Zhou X, Li X, Liu X, Xiang L, Li Y, Huang G (2014) J Org Chem 79:465–470
104. Huang H-M, Li Y-J, Ye Q, Yu W-B, Han L, Jia J-H, Gao J-R (2014) J Org Chem 79:1084–1092
105. Das S, Borah R, Devi RR, Thakur AJ (2008) Synlett 2741–2762
106. Bandgar BP, Shaikh KA (2003) Tetrahedron Lett 44:1959–1961
107. Parvatkar PT, Parameswaran PS, Tilve SG (2012) Chem Eur J 18:5460–5489
108. Alcaide B, Almendros P, Cabrero G, Ruiz MP (2008) Synthesis 2835–2839
109. Cruickshank FR, Benson SW (1969) J Phys Chem 73:733–737
110. Silva LF Jr, Quintiliano SA (2009) Tetrahedron Lett 50:2256–2260
111. Yang F-L, Wang F-X, Wang T-T, Wang Y-J, Tian S-K (2014) Chem Commun 50:2111–2113
112. Coulembier O, Meyer F, Dubois P (2010) Polym Chem 1:434–437
113. Holleman A, Wiberg N (2007) Lehrbuch der Anorganischen Chemie, 102nd edn. de Gruyter, Berlin, p 461
114. Bew SP, Fairhurst SA, Hughes DL, Legentil L, Liddle J, Pesce P, Nigudkar S, Wilson MA (2009) Org Lett 11:4552–4555
115. Metrangolo P, Murray JS, Pilati T, Politzer P, Resnati G, Terraneo G (2011) Cryst Growth Des 11:4238–4246
116. Virgil SC (1995) In: Paquette LA (ed) Encyclopedia of reagents for organic synthesis. Wiley, New York, p 768
117. Fieser LF, Fieser M (1998) Reagents for organic synthesis 12. Wiley, New York, p 79
118. Wei Y, Lin S, Liang F (2012) Org Lett 14:4202–4205
119. Wei Y, Lin S, Liang F, Zhang J (2013) Org Lett 15:852–855
120. Wei Y, Liang F, Zhang X (2013) Org Lett 15:5186–5189
121. Castellote I, Moron M, Burgos C, Alvarez-Builla J, Martin A, Gomez-Sal P, Vaquero JJ (2007) Chem Commun 1281–1283
122. Denmark SE, Kuester WE, Burk MT (2012) Angew Chem Int Ed 51:10938–10953

123. Sakakura A, Ukai A, Ishihara K (2007) Nature 445:900–903
124. Bruckmann A, Pena MA, Bolm C (2008) Synlett 900–902
125. Zhou Y-G (2007) Acc Chem Res 40:1357–1366
126. Metrangolo P, Panzeri W, Recupero F, Resnati G (2002) J Fluorine Chem 114:27–33
127. Gladysz JA (1994) Science 266:55–56
128. Dordonne S, Crousse B, Bonnet-Delpon D, Legros J (2011) Chem Commun 47:5855–5857
129. Lindsay VNG, Lin W, Charette AB (2009) J Am Chem Soc 131:16383–16385
130. Walter SM, Kniep F, Herdtweck E, Huber SM (2011) Angew Chem Int Ed 50:7187–7191
131. Bondi A (1964) J Phys Chem 68:441–451
132. Walter SM, Kniep F, Rout L, Schmidtchen FP, Herdtweck E, Huber SM (2012) J Am Chem Soc 134:8507–8512
133. Kniep F, Jungbauer SH, Zhang Q, Walter SM, Schindler S, Schnapperelle I, Herdtweck E, Huber SM (2013) Angew Chem Int Ed 52:7028–7032
134. Beweries T, Brammer L, Jasim NA, McGrady JE, Perutz RN, Whitwood AC (2011) J Am Chem Soc 133:14338–14348
135. Libri S, Jasim NA, Perutz RN, Brammer L (2008) J Am Chem Soc 130:7842–7844
136. Kniep F, Walter SM, Herdtweck E, Huber SM (2012) Chem Eur J 18:1306–1310
137. Freytag M, Jones PG, Ahrens B, Fischer AK (1999) New J Chem 23:1137–1139
138. Brammer L, Espallargas GM, Adams H (2003) CrystEngComm 5:343–345
139. Logothetis TA, Meyer F, Metrangolo P, Pilati T, Resnati G (2004) New J Chem 28:760–763
140. Espallargas GM, Brammer L, Sherwood P (2006) Angew Chem Int Ed 45:435–440
141. Awwadi FF, Willett RD, Twamley B (2009) J Mol Struct 918:116–122
142. Minguez Espallargas G, Zordan F, Arroyo Marin L, Adams H, Shankland K, van de Streek J, Brammer L (2009) Chem Eur J 15:7554–7568
143. Raatikainen K, Cametti M, Rissanen K (2010) Beilstein J Org Chem 6(4)
144. Kniep F, Rout L, Walter SM, Bensch HKV, Jungbauer SH, Herdtweck E, Huber SM (2012) Chem Commun 48:9299–9301
145. Hein JE, Tripp JC, Krasnova LB, Sharpless KB, Fokin VV (2009) Angew Chem Int Ed 48:8018–8021
146. Kilah NL, Wise MD, Beer PD (2011) Cryst Growth Des 11:4565–4571
147. Mullen KM, Mercurio J, Serpell CJ, Beer PD (2009) Angew Chem Int Ed 48:4781–4784
148. Walter SM, Jungbauer SH, Kniep F, Schindler S, Herdtweck E, Huber SM (2013) J Fluorine Chem 150:14–20
149. Tannaci JF, Noji M, McBee JL, Tilley TD (2008) J Org Chem 73:7895–7900
150. Olah GA, Wang Q, Sandford G, Surya Prakash GK (1993) J Org Chem 58:3194–3195
151. Reisman SE, Doyle AG, Jacobsen EN (2008) J Am Chem Soc 130:7198–7199
152. Jungbauer SH, Walter SM, Schindler S, Rout L, Kniep F, Huber SM (2014) Activation of a carbonyl compound by halogen bonding. Chem Commun 50:6281–6284

Index